A STUDY OF THE PROMPT AND DELAYED GAMMA-RAYS FOLLOWING THERMAL NEUTRON CAPTURE IN ^{107}Ag AND ^{109}Ag

A thesis submitted for the award of the
degree of Doctor of Philosophy of
the University of London

by

MYINT THEIN
M.Sc. (London).

University of London Reactor Centre
Department of Mechanical Engineering
Imperial College of Science & Technology
LONDON, SW7 2AZ

May 1977

နမောတဿဘဂဝတော အရဟတော သမ္မာသမ္ဗုဒ္ဓဿ။

DEDICATED TO

MY PARENTS

AND TEACHERS.

သဗ္ဗသတ္တာ အဝေ ရာဟန္တု

LOVE AND PEACE TO ALL BEINGS. (BUDDHA)

A B S T R A C T

This thesis presents the results of a comprehensive study of the prompt and delayed gamma radiation following neutron irradiation of silver isotopes.

The gamma radiation emitted, following the thermal neutron capture in ^{107}Ag and ^{109}Ag was studied using natural and ^{107}Ag enriched silver samples. The measurements were performed at the University of London Reactor Centre, England, and the FRJ-2 DIDO Reactor, Julich - F.R. Germany, with external-target-geometry. Energies and relative intensities of low-energy gamma rays were determined by means of a Compton-Suppression Spectrometer and various Ge(Li) detectors. The high energy (n,γ) spectrum was studied with a specially-designed pencil-shaped Ge(Li) detector.

To extend our knowledge of the ^{108}Ag level scheme, γ-γ coincidence measurements in $^{107}Ag(n,\gamma)^{108}Ag$ reaction were carried out using two Ge(Li) detectors. The present data, when combined with a previous (n,γ) study with a curved crystal spectrometer, (d,p) studies and $(p,n\gamma)$ measurements, allow a level scheme to be constructed. The energies of 50 excited states below 1.3 MeV and the gamma transitions between them were determined and spin-parity assignments are discussed. A value of (7269.85 ± 0.32) keV was determined for the neutron binding energy of ^{108}Ag. A further 59 levels above 1.3 MeV are tentatively proposed and could form a basis for further study.

The γ-transitions in $^{109}Ag(n,\gamma)^{110}Ag$ were identified from the comparison of the spectra obtained by using enriched ^{107}Ag and natural silver targets. A level scheme for ^{110}Ag is proposed.

The gamma-ray energies and intensities following the decays of $^{108m,g}Ag$, $^{110m,g}Ag$ and ^{133g}Ba isotopes have been measured and the level schemes are discussed. In addition, the gamma energies and intensities in ^{226}Ra are presented.

ACKNOWLEDGEMENTS

The author would like to express his gratitude and sincere thanks to his supervisor, Dr. T.D. Mac Mahon for his guidance, invaluable help and advice (scientifically and socially), and effort during the course of this research.

I would like also to thank Mr. M. Kerridge, Director of the University of London Reactor Centre, and Dr. J.G. Williams for their help and guidance. Also most sincere thanks are due to all other members of the staff of the University of London Reactor Centre; in particular Mr. T.C. Jones, Mr. E.A.Y. Caesar, Mr. J.W. Brown, Mr. G.D. Burholt, Mr. J.G. Sanderson, Mr. J.H. Roberts and Mrs. W. Carder, without whose help and assistance this project would not have been completed.

Professor Dr. O.W.B. Schult, Head of the Department, Institut fur Kernphysik, K.F.A.-Julich, F.R. Germany,and Dr. H.Seyfarth whose continued interest, many helpful discussions have been invaluable, I acknowledge very gratefully. I am also indebted to the authorities for their financial support. I am also grateful to Mr. N. Wust, Mr. Ermer and other members of the staff of the FRJ-2 DIDO Reactor and Computer Centre at KFA for their help and very good co-operation.

Thanks must also go to Dr. P. Rice-Evans, Mr. R.N. Thomas, Mr. Yusoff Sulaiman (Bedford College), Mr. R.A.J. Taylor (Imperial College) and friends at U.L.R.C. and Imperial College Field Station.

I am grateful to the Ministry of Education, Socialist Republic of the Union of Burma, and the British Council for awarding a Colombo Plan Scholarship, and to my friends and colleagues at the Physics Department, Rangoon University.

I owe a special tribute to the patient effort of Mrs. J. Vine for typing an almost illegible manuscript and transforming it into a presentable form.

My special thanks and gratitude to Ma Yi Yi Myint for her help, assistance and support. Last, but not least, I thank my wife, Ma Mya Shwe, and parents for their encouragement, help, patience and sacrifices during my research work.

TABLE OF CONTENTS

		Page
	TITLE PAGE	
	ABSTRACT	1.
	ACKNOWLEDGEMENTS	3.
	TABLE OF CONTENTS	5.
	LIST OF FIGURES	10.
	LIST OF TABLES	13.
1.	INTRODUCTION	16.
1.1	Some Aspects of Neutron-Capture Gamma-Ray Spectroscopy	16.
1.1.1	Major Features of Neutron Capture	16.
1.1.2	Experimental Technique	20.
1.1.3	Recent Technical Developments	22.
1.1.4	Gamma-Gamma Coincidence Techniques	25.
1.2	Ge(Li) Detectors in (n,γ) Measurements	28.
1.2.1	Types of Ge(Li) Detectors	28.
1.2.2	A Ge(Li) Detector Spectrum	30.
1.2.3	Compton Scattering Process	30.
1.2.4	Compton Suppression Spectrometer	32.
1.2.5	Pair Spectrometer	33.
1.2.6	Multiple-Compton-Interaction Spectrometers	34.
1.3	(n,γ) Reaction Mechanisms	35.

			Page
2.	PRELIMINARY MEASUREMENTS		44.
	2.1	A study of some Neutron Scattering Properties of High Density Polythene and Graphite.	44.
		2.1.1 Introduction	44.
		2.1.2 Scattering from the surface of a high density polythene block as a function of the angle-of-incidence	45.
		2.1.3 Neutron scattering from a cylindrical block of graphite	46.
		2.1.4 Extrapolation of the results of the Time-of-Flight Beam Tube Experiments to the 0^{o} Through Tube	49.
		2.1.5 Predicted flux at (n,γ) target position using polythene scatterer in the centre of the 0^{o} Through Tube	51.
		2.1.6 Predicted flux at the (n,γ) target position using a graphite scatterer	52.
		2.1.7 Summary	54.
	2.2	^{133g}Ba and ^{226}Ra as calibration standards for Ge(Li) detectors	62.
		2.2.1 Introduction	62.
		2.2.2 Experimental arrangement and calibration	63.
		2.2.3 Gamma energies and intensities	64.

			Page
	2.2.4	Results and Discussion	64.
	2.2.4(a)	The Decay of ^{133g}Ba	64.
	2.2.4(b)	The Decay of ^{226}Ra	69.
3.	DECAY SCHEMES OF Ag ISOTOPES		82.
	3.1	Decay of ^{108m}Ag	82.
	3.1.1	Introduction	82.
	3.1.2	Experimental procedures	83.
	3.1.3	Results and Discussion	83.
	3.1.4	Decay scheme of ^{108m}Ag	84.
	3.2	The Decay of ^{108g}Ag	88.
	3.2.1	Introduction	88.
	3.2.2	Experimental procedures	89.
	3.2.3	Results and Discussion	90.
	3.3	The Decay of ^{110g}Ag	96.
	3.3.1	Introduction	96.
	3.3.2	Experimental Method and Results	97.
	3.4	Gamma Transitions in ^{110}Cd Following the Decay of ^{110m}Ag	100.
	3.4.1	Introduction	100.
	3.4.2	Experimental Procedures	101.
	3.4.3	Gamma Energies and Intensities	102.
	3.4.4	Internal Conversion Coefficients	105.
	3.4.5	The Decay Scheme of ^{110m}Ag → ^{110}Cd	107.
	3.4.6	Discussion	109.

			Page
4.	DESCRIPTION OF (n,γ) EXPERIMENT APPARATUS		125.
	4.1	Thermal Neutron Beam Facility	125.
		4.1.1 Thermal Neutron Beam Tube	125.
		4.1.2 Beam Tube Collimator	125.
		4.1.3 Shutter Assembly	126.
		4.1.4 Shielding	127.
		4.1.5 Neutron Beam Stop	127.
		4.1.6 Thermal Neutron Beam Profiles	128.
	4.2	Detector Assembly	129.
		4.2.1 Ge(Li) Detector Specifications	129.
		4.2.2 Resolution of the Ge(Li) Detectors	130.
	4.3	Compton-Suppression Spectrometer System	131.
		4.3.1 Electronics and NC-26 Time Analyser	132.
		4.3.2 Performance of the Compton Suppression Spectrometer System	135.
5.	GAMMA RAYS FROM THE THERMAL-NEUTRON CAPTURE IN NATURAL AND ^{107}Ag ENRICHED SILVER		150.
	5.1	Low Energy (n,γ) Measurements	150.
	5.2	Analysis of the Low-Energy Measurements	151.
		5.2.1 Energy and Efficiency Calibration	151.
		5.2.2 Gamma Energies and Relative Intensities in ^{107}Ag(n,γ)^{108}Ag and ^{109}Ag(n,γ)^{110}Ag Reactions	152.

Page

5.2.3 Background Radiations at ULRC 153.

5.3 High Energy $^{107}Ag(n,\gamma)^{108}Ag$ Measurements 155.

6. MEASUREMENT OF γ-γ COINCIDENCES IN THE REACTION $^{107}Ag(n,\gamma)^{108}Ag$ 184.

6.1 Introduction 184.

6.2 Apparatus 184.

6.3 Electronics 186.

6.3.1 Detection and Selection of Events 187.

6.3.2 Reduction and Storage of the Data 188.

6.3.3 Controlling and Monitoring the Measurement 188.

6.4 Evaluation of the Data 189.

7. RESULTS AND DISCUSSION 195.

7.1 Level Scheme of ^{108}Ag 195.

7.2 Level Scheme of ^{110}Ag 214.

REFERENCES 227.

LIST OF FIGURES

		Page
1.1	Differential cross-section as a function of the scattering angle for a variety of energies.	42.
1.2	Varieties of construction of a guard scintillator.	42.
1.3	Six different experimental arrangements for Compton-Scattering Spectrometers.	43.
2.1	Neutron scattering experimental arrangements. A. Polythene Scatterer. B. Graphite Scatterer.	59.
2.2	Polythene Scatterer Results.	60.
2.3	Graphite Scatterer Results.	61.
2.4	^{133g}Ba Spectrum with Compton Suppression.	80.
2.5	Proposed Disintegration Scheme for ^{133g}Ba.	81.
3.1	^{108m}Ag Spectrum with Compton Suppression.	94.
3.2	Decay Scheme of ^{108}Ag.	95.
3.3	^{110m}Ag Spectrum with Compton Suppression.	119.
3.4	^{110m}Ag Decay Scheme.	120.

		Page
3.5	Background-Corrected ^{110m}Ag Coincidence Spectra.	
	A. Ungated Spectrum.	121.
	B. 657.76 keV Gated Spectrum.	122.
	C. 706.70 keV Gated Spectrum.	123.
	D. 763.91 keV Gated Spectrum.	124.
4.1	General Layout of 0° Face at ULRC.	138.
4.2	Neutron Beam Stop.	139.
4.3	Thermal Neutron Beam Profiles.	
	A. At Target Position.	140.
	B. At Beam Stop Position.	140.
4.4	(n,γ) Apparatus with shielding.	141.
4.5	NaI(Tl) Annulus Ring.	142.
4.6	Block Diagram for Compton Spectrometer.	143.
4.7	Simplified NC 26 Internal Block Diagram.	144.
4.8	T A C Logic Diagram.	144.
4.9	Singles and Compton Suppressed Spectra of ^{137}Cs.	145.
4.10	A. ^{60}Co Decay Spectrum (First Section) .	146.
	B. ^{60}Co Decay Spectrum (Second Section).	147.
4.11	A. ^{152g}Eu Decay Spectrum with Compton Suppression.	148.
	B. ^{152g}Eu Decay Spectrum without Compton Suppression.	149.

		Page
5.1	Sample holder and Pencil-Shaped Ge(Li) Detector.	164.
5.2	Efficiency of Compton Suppression Spectrometer.	165.
5.3	Efficiency of Vertical Ge(Li) Detector.	166.
5.4	Low Energy ^{107}Ag (n, γ) ^{108}Ag Spectrum.	167.
5.5	Low Energy natural Ag (n, γ) Spectrum.	168.
5.6	Relative Double Escape Peak Efficiency.	169.
5.7	$^{107}Ag(n,\gamma)$ ^{108}Ag Spectra with Pencil Shaped Detector.	
	A. 0.0 – 1.5 MeV Region.	170.
	B. 1.5 – 4.5 MeV Region.	171.
	C. 4.5 – 7.5 MeV Region.	172.
6.1	Beam tube system and measuring equipment on the top of the F R J – 2 DIDO Reactor at Julich,F.R.Germany.	192.
6.2	Target holder and shielding of the external beam.	193.
6.3	Peak and Background Regions in Coincidence Matrix.	194.
6.4	Block Diagram of Electronics.	195.
7.1	Primary Gamma Transitions in $^{107}Ag(n,\gamma)$ ^{108}Ag Reaction.	222.
7.2	Proposed Partial Level Scheme of ^{108}Ag.	223.
7.3	Preliminary Level Scheme of ^{110}Ag.	226.

LIST OF TABLES

		Page
2.1	Polythene Scatterer Results.	56.
2.2	Graphite Scatterer Results (Experiment).	57.
2.3	Graphite Scatterer Results.	58.
2.4	Photon energies in ^{133g}Ba Decay.	71.
2.5	Absolute photon intensity values in ^{133g}Ba Decay.	72.
2.6	Relative photon intensities in ^{133g}Ba Decay.	73.
2.7	Internal Conversion Coefficients.	74.
2.8	E C Branching Ratios and log ft Values.	75.
2.9	Deduced Properties in ^{133g}Ba Decay.	76.
2.10	Gamma Ray energies and absolute intensities in ^{226}Ra.	77.
2.11	Relative gamma ray intensities of the strong transitions in ^{226}Ra Decay.	79.
3.1	Gamma Ray energies and relative intensities of transitions in the decay of ^{108m}Ag to ^{108}Pd Levels.	86.

		Page
3.2	Conversion Coefficients and Multipolarities in ^{108m}Ag Decay.	87.
3.3	Gamma Ray energies and relative intensities of transitions in the decay of 2.41 min ^{108g}Ag.	92.
3.4	β^+,EC and β^-Branching to Levels in ^{108}Pd.	93.
3.5	Gamma Ray Energies and Intensities in the decay of ^{110g}Ag.	99.
3.6	Gamma Transition Energies in ^{110m}Ag Decay.	111.
3.7	Relative Gamma Intensities in ^{110m}Ag Decay.	112.
3.8	Weak Gamma Transitions in ^{110m}Ag Decay.	113.
3.9	Internal Conversion Coefficients and Multipolarities in ^{110m}Ag Decay.	114.
3.10	Beta Branching Ratio and log ft Values.	116.
3.11	Energies and Absolute Intensities of Gamma Rays in ^{110m}Ag Decay.	117.
3.12	Gamma-Gamma Coincidence Data.	118.
4.1	^{60}Co gamma ray energies and intensities.	137.
5.1	Isotopic Compositions and Relative Contributions of Ag and Ge Samples.	157.

		Page
5.2	Low Energy Gamma Rays and Relative Intensities in $^{107}Ag\ (n,\gamma)\ ^{108}Ag$ Reaction.	158.
5.3	Low Energy Gamma Rays and Relative Intensities in $^{109}Ag\ (n,\gamma)\ ^{110}Ag$ Reaction.	160.
5.4	Background Radiation at ULRC.	161.
5.5	High Energy Gamma Rays and Relative Intensities in $^{107}Ag\ (n,\gamma)\ ^{108}Ag$ Reaction.	162.
5.6	Thermal Neutron Capture Gamma Rays from the $^{107}Ag\ (n,\gamma)\ ^{108}Ag$ Reaction obtained with a Curved Crystal Spectrometer at RISO and the Transitions in ^{108}Ag Levels.	173.
7.1	Energy Levels in ^{108}Ag ($E_x \lesssim 1300$ keV).	216.
7.2	Possible p-n Configurations of the ^{108}Ag and ^{110}Ag Levels.	218.
7.3	Binding Energy of ^{108}Ag.	219.
7.4	Further Suggested Levels in ^{108}Ag ($1.3\ MeV \lesssim E_x \lesssim 2.0\ MeV$).	220.
7.5	Further Suggested Levels in ^{108}Ag above 2.0 MeV.	221.

1. INTRODUCTION

1.1 Some Aspects of Neutron-Capture Gamma-Ray Spectroscopy

Soon after the discovery of the neutron, the importance of neutron capture was recognised and this study continues to offer an interesting and theoretical challenge today. Studies of neutron capture γ-rays have contributed to our knowledge of neutron separation energies, γ-transition probabilities, decay schemes and properties of nuclear energy levels. They have also shed light on a number of other aspects of the broad problem of nuclear structure. It is a well known fact that these studies of the radiation from neutron capture, when combined with the complementary information obtained from other types of studies such as (d,p) reaction, conversion electrons, γ-γ coincidence, angular correlation and life-time studies of the excited states, yield a wealth of spectroscopic information for nuclear structure.

1.1.1 Major Features of Neutron Capture

The process involves the capture of a neutron by a target nucleus to form a compound state which decays to the ground state or to one or more isomeric states of a residual nucleus by means of electromagnetic transitions including internal conversion and internal pair formation. In a few cases (which include Li, B and N) the nucleus may disintegrate with the emission of a proton or an α-particle. Mostly the emission of a charged particle is not energetically possible in thermal neutron

capture or is retarded by the coulomb barrier when the disintegration energy is insufficient to overcome it. So the most probable mode of de-excitation is then the emission of electromagnetic radiation.

The energy balance of the system[1] is simply

$$S_n + E_c = E_o$$

where S_n = the neutron binding energy corresponding to the difference in masses of the initial and final states.

E_c = neutron kinetic energy in centre-of-mass system.

E_o = excitation energy of the compound nucleus.

The energy E_o is rarely emitted in one transition, $E_{\gamma o}$, to the ground state, more often several cascade transitions pass through lower states. The gamma transitions $E_{\gamma j}$, originating from the compound state are called the primary transitions and those resulting in decay of these populated states, $E_{\gamma j}$ are called secondary.

For thermal capture, the neutron energy is negligibly small ($E_c \simeq 0$) but a correction (ε) must be included for the recoil of the compound nucleus following γ-emission,

$$\varepsilon \simeq \frac{E_\gamma^2}{2M_{A+1}C^2} \simeq 5.0 \times 10^{-7} \frac{E_\gamma^2}{A+1} \text{ keV}$$

Therefore the energy balance for thermal neutron capture becomes

$$S_n = E_{\gamma o'} + \varepsilon_{o'} = (E_{\gamma j'} + \varepsilon_{j'}) + (E_{\gamma j} + \varepsilon_j)$$

This energy sum should include corrections for the internally converted transitions when appropriate. Even in thermal capture the prompt or sufficiently short-lived state secondary transitions are Doppler shifted as a result of the nuclear recoil from the primary radiation. But the average energy is unchanged.

At low bombarding energies (thermal capture), because of the centrifugal barrier for the high angular momenta, neutron capture proceeds almost entirely by s-wave. The ratio of s-wave to p-wave penetrabilities for neutron[2] can be given as:

$$P_s/P_p = 1 + 1/(KR)^2$$

where K = the wave number of the neutron

R = the effective interaction radius from the target nucleus.

For thermal neutron energies and medium weight nuclei this ratio is $\simeq 10^7$ and p-wave capture is completely negligible. The penetrabilities, P_s and P_p become comparable when KR is unity, which

in medium weight nuclei occurs for neutrons of about 100 keV energy.

In high energy neutron capture, the average primary radiation energy $E_{\gamma j}$, is larger by

$$E_c = E_n \cdot \frac{M_A}{M_n + M_A}$$

where E_n is the laboratory neutron energy.

In the case of s-wave neutron capture

I_t ; π_t = the spin and the parity states of the target nuclei

$I_c = I_t \pm \frac{1}{2}$; $\pi_c = \pi_t$ = the spin and the parity states of the compound state.

Both spin states are formed to some degree in the capture process except where $I_t = 0$. The states populated by dipole primary transitions, $E_{\gamma j}$, have spins

$\left|I_c - 1\right|$,----------,(I_c+1) which for s-wave capture is equivalent to

$\left|I_t - \frac{3}{2}\right|$,--------$(I_t + \frac{3}{2})$ and parity π_t for magnetic dipole and $-\pi_t$ for electric dipole transitions.

$$I_j = (I_t \pm \tfrac{1}{2}) \text{ and } (I_t \pm \tfrac{3}{2}) \text{ for } I_t > \tfrac{3}{2} .$$

1.1.2 Experimental Technique

Neutron capture γ-rays were first observed in 1934 by Lea who appeared to have detected the γ-ray produced by capture of neutrons in hydrogen and by Amaldi who detected capture in other elements.[3] But the following fifteen years brought little more knowledge about this radiation other than some coarse determination of the maximum energy emitted. Work during this period was virtually impossible because of the lack of strong neutron sources and of efficient γ-ray detectors with adequate resolution. The situation was drastically improved when nuclear reactors provided source strengths many orders of magnitude greater.

The broadest features of the experimental approaches are considered with respect to three categories: neutron source, detector and data recording system. The important neutron source characteristics are the intensity, energy distribution, irradiation geometry and environment of the target, and the neutron and γ-ray background. For detector parameters, greatest demands are placed on the resolution attainable. Data recording is also not a simple procedure.

Reactors provide not only the strongest sources for thermal capture but also the most practical and widespread. Although the accelerators can provide sufficient source strength for some arrangements using thermal neutrons, the cost of operation is usually prohibitive in comparison with a reactor facility.

The neutron capture experiments using reactors can be classified according to whether the target is internal or external to the reactor shielding.

Internal Target Geometry

The target is placed in the high flux region within the reactor shielding, and then an opening through the shielding is provided to allow the γ-rays to be studied. This geometry can provide enough counting rate for insensitive instruments and to study low cross-section materials. The signal-to-background ratio can be highly improved by taking advantage of a highly collimated beam. Therefore high resolution spectrometers with less efficiency become feasible. But there are certain disadvantages as well. It is impossible to carry out coincidence experiments. It is also inconvenient to change the sources due to the high radiation-background from the reactor core and surrounding materials. Neutron absorbers and scatterers, which are usually used in the collimator to minimize the neutron flux in the γ-ray beam for health and background control, attenuate low energy γ-rays and result in reduced sensitivity.

External Target Geometry

A neutron beam is extracted from the reactor by the use of a neutron collimator and the target is irradiated in this beam external to the reactor shielding. A well collimated thermal neutron beam with reasonable collimation of the γ-ray and fast neutron components permits the detector system to be located quite near to the target so that a maximum solid angle is obtained. This is a primary requisite for coincidence measurements in order to maximize the true to accidental coincidence ratio. Targets can be easily changed for all purposes. A serious disadvantage is that shielding must be provided for both scattered neutrons and γ-radiation. It is possible to reduce the fast neutron and γ-ray components with only a small sacrifice of thermal neutron intensity by the use of bismuth or quartz crystal filters. This external geometry is the only possibility for coincidence measurements.

1.1.3 Recent Technical Developments

Progress in the study of neutron-capture γ-rays seems to depend on technical developments to a greater extent than in most areas of nuclear physics. Almost every known method of detecting and measuring γ-rays has been employed, namely, Geiger counters, cloud chamber, emulsion, ion chamber, single NaI crystal spectrometer, 2-crystal compton spectrometer, 3-crystal pair spectrometer, 180^{o} magnetic spectrometer, magnetic lens spectrometer and crystal diffraction spectrometer.[1-10]

The technical development that is still of central importance for capture γ-ray spectroscopy is the Ge(Li) detector, since it has a very much higher detection efficiency than any other high-resolution γ-ray spectrometers. Powerful reactors have been put into operation, the neutron beams have been optimized, Germanium detectors of various sizes with almost their ideal resolution are commercially available and other detection devices have been improved, not to mention the tremendous development regarding the systems in use for the recording and handling of the data. One possibility for the future is the production of extremely large Germanium detectors and it would be a major advance for the study of resonance-capture spectra where higher counting rates are badly needed. Another possibility is that a new detector material with a lower band gap can be developed into a detector with a better energy resolution than Ge(Li). Although at least one material of this kind (Cd Te) is being actively tested at this time in several laboratories, the resolutions obtained to date are discouragingly poor - no better than for NaI (Tl) scintillators.[10)]

There are also continuing notable improvements in the performance of the curved crystal diffraction spectrometers. Ways to reduce the mosaic spread in the diffraction crystal caused by bending have been discovered. At Leningrad[11)] and Risø[12)], a procedure is used to bend the crystal along a plane that minimizes the distortion of the reflection planes. At Argonne[13)], thinner crystals have been used. These developments are making the diffraction spectrometer steadily more competitive

in comparison with the Ge(Li) detectors. At present time, the energy at which the two systems have equal resolution is as high as 2 MeV for some measurements.

The Risø spectrometer[12,13], often operated at high energies in the fifth order of reflection, has allowed observations with a resolution of 17 eV at 90 keV and 0.43 keV at 900 keV. The general resolution function is

$$\Delta E = \frac{2.5E^2}{10^6 n}$$

where E = energy in keV

n = order of the reflection

and ΔE = the full width at half-maximum.

The accuracy of a measurement is approximately 16% of this value. These spectrometers provide the most detailed and precise γ-ray spectra for low energy region.

The performance of the internal-conversion spectrometers is also ever progressing. At Argonne[15] a super-conducting solenoid is used to funnel the conversion electrons onto a solid-state detector

that is some distance from the (n,γ) target. The effective solid angle of the detector is large for the conversion electrons and small for γ-rays. In addition, the principal virtues of the system are that it records a wide range of energies simultaneously (unlike a magnetic spectrometer) and that it can be used for coincidence measurements. A second high-sensitivity internal-conversion spectrometer system at Grenoble[16,17] has an (n,γ) target inside the reactor and a magnetic spectrograph outside. Although the basic principle is the same as others, it provides an instrument of exceptionally high efficiency and good energy resolution because of the high flux of the reactor and a careful suppression of background radiations.

1.1.4 Gamma-Gamma Coincidence Techniques

The outstanding precision and wide dynamic range of bent-crystal spectrometers make them most valuable tools for the study of the low energy secondary transitions. They allow the observation of more, and weaker low energy γ-rays than Ge(Li) detectors do. However, despite the precise high-resolution determination of a wealth of low energy γ-ray information, the data obtained with these instruments, even when combined with those of the less precise high energy primary γ-ray information of Ge(Li) detectors are still not sufficient to determine the level structure and decay pattern of the low-lying excited states as completely and unambiguously as could be hoped. As is unavoidable, the use of these instruments, in the construction of the level scheme of the low-lying excited states often must depend upon confidence that the statistical expectation for

accidental energy balances is extremely small. However, since the (n,γ) reaction populates a myriad of low-lying excited states, there are often several pairs of levels between which a given transition can be placed.[17] This is not the fault of the bent-crystal spectrometer, since the high-resolution of this device is supreme in the ability to minimise such accidental energy balances. Indeed, it is the plethora of excited states and low energy γ-rays that is at fault. In other words, the nucleus itself is the guilty party.

The coincidence technique can provide unequivocal data concerning the sequential time ordering of transitions, information on the life-time of some excited states, γ-γ and γ-e angular correlations and directional polarization correlations. γ-γ coincidence studies between high energy primary and low energy secondary transitions permit a simple study of the population of particular states by the primary events and the subsequent population of lower excited states which are not directly populated by primary transitions from the capture state. The neutron binding energy can be established from these results. Coincidences among low energy secondary transitions can complement and extend our knowledge of the low-lying level structure provided by the high-low coincidence data. Delayed coincidences, while perhaps not as generally useful as prompt coincidence, can determine life-times for some nuclear states and show a time relationship between members of cascades which relate to these decay modes. Moreover the coincidence data provides the missing link in the interpretation of the combined data of bent-crystal electron studies, primary transition investigations and charged-

particle data to establish a rather complete level scheme.

For the gamma-gamma coincidence work , the NaI-Ge(Li) and Ge(Li)-Ge(Li) systems have been used. Despite the higher detection efficiency of a NaI(Tl)-Ge(Li) coincidence system, the poor resolution of the scintillator minimizes its value and an all-Ge(Li) system is still immeasurably superior. Also Ge(Li)-Si(Li) systems are now in operation to study (γ,e) coincidences.

1.2 Ge(Li) Detectors in (n,γ) Measurements

The field of thermal neutron capture γ-ray spectroscopy has developed and matured enormously over the past decade due to significant developments and improvements in experimental technique. The most outstanding technical advance has been brought about by the use of solid-state high-resolution detectors - principally the Ge(Li) spectrometer. The Ge(Li) detector has enlarged the scope, accuracy and quantitative significance of studies in the (n,γ) field. Despite the parallel improvements in bent-crystal spectrometers, whose energy resolution is superior to that of Ge(Li) detectors, the fine resolution capabilities of the latter devices, coupled with their superior γ-ray detection efficiency, has led to their widespread use in studies of low energy spectra. In addition these detectors are playing a major role in almost every other branch of natural science such as activation analysis, biomedical and environmental studies, criminology and geophysics.

1.2.1 Types of Ge(Li) Detectors

There are primarily four types of Ge(Li) detectors in use,[18,19] namely the thin window X-ray detectors, the planar detector, the cylindrically symmetric or true coaxial detector and the single open-ended or trapezoidal detector.

The thin-window X-ray detector is made from a rectangular or circular insert of p-type germanium with a few millimetres thickness. The Li ions are diffused to a depth of from 0.1 to 1 mm to form the n-type junction and then drifted by means of an applied bias voltage. A thin metallic gold window is alloyed to provide both the second junction and the thin entrance window. These detectors are usually small in size to minimize capacitance, hence allowing the highest possible resolution. It is normally used for low energy (< 1 MeV) γ-ray detection because efficiency decreases sharply toward higher energies.

The standard planar detector is made from either a circular or rectangular ingot of p-type germanium from 10 to 20 mm thick. The drifting is ended before punch-through, leaving a thin region (0.5 to 2 mm) of original p-type germanium to serve as the second junction.

In true coaxial detectors, Li ions are diffused into its circumference, forming a skin of over-compensated n-type germanium from 0.4 to 1.0 mm thick. The drifting proceeds radially and then is terminated before reaching the centre, leaving a fairly uniform cylindrical core of p-type material.

In the single open-ended circular or trapezoidal detector Li ions are diffused into both the ingot circumference and one of the ends. Drifting proceeds towards the open end and is then terminated when a small core remains as observed from the open end. The p-type core extends part way into the interior and is usually not uniform. This type of detector yields a higher efficiency than the true coaxial detector for the same ingot size and depletion depth.

1.2.2 A Ge(Li) Detector Spectrum

The prominent features of the pulse height spectrum of a gamma ray with energy < 3 MeV are the peaks corresponding to absorption in the detector of the full energy and the broad continuum. The continuum distribution is a sum of many different kinds of events, primarily Compton scattering of the γ-ray in or out of detector. If the γ-ray energy exceeds the electron-positron pair production threshold value, additional peaks appear in the spectrum at one (single-escape peak) and two (double-escape peak) electron masses below the full energy peak, corresponding to the escape of one and two annihilation quanta, respectively.

1.2.3 Compton Scattering Process[18)]

In the energy range from 100 keV to 3 MeV, the interaction between γ-ray and Ge takes place mainly through Compton scattering.

If an incident γ-ray with energy E collides with an electron (assumed free and at rest) of a scattering medium, the energy of the scattered γ-ray can be given as:

$$E' = E\, m_o C^2/\{E\,(1 - \cos\theta) + m_o C^2\}$$

where θ = scattering angle

The kinetic energy which is transferred to the recoil electron and absorbed in the Ge crystal lattice by secondary processes is

$$T = \frac{E^2(1 - \cos\theta)}{E(1 - \cos\theta) + m_o C^2}$$

So the backscatter peak from γ-rays scattered by surrounding materials, (i.e. $\theta = 180^o$) occurs with energy $\frac{1}{2}\ m_o C^2/(1 + m_o C^2/2E)$. The recoil electrons have a continuous energy distribution below the 'Compton edge' at $E/(1 + m_o C^2/2E)$.

Klein-Nishina formula[20] for the differential cross section can be presented as:

$$\frac{d\sigma}{d\Omega} = \frac{r_o^2}{2}\ Z\ (\frac{E'}{E})^2\ (\frac{E'}{E} + \frac{E}{E'} - \sin^2\theta)$$

Where $r_o^2 = \frac{e^2}{m_o C^2}$ = classical electron radius

Z = atomic number (32 for Ge)

Differential cross section as a function of the scattering angle for a variety of energies is given in Fig.1.1.

1.2.4 Compton Suppression Spectrometer[18,19,20]

In this system, a Ge(Li) detector is surrounded by a guard scintillator (NaI or plastic) which is as large as possible. The Compton interaction, which produces the pulse in the Ge(Li) detector, must be accompanied by recording of a scattered γ-ray in the guard scintillator. Such events are eliminated by means of a prohibition signal from anticoincidence circuit. The principal merit of the method is that it retains the efficiency of the full-energy peaks. The guard scintillator suppresses not only the Compton distribution but also the external background and cosmic radiation. A variety of guard scintillators are displayed in Fig.1.2 . As shown in Fig.1.1 it is quite clear that for energies above 200 keV the scattering occurs more strongly in forward direction. Therefore the arrangement of Fig.1.2(b) seems better than other conventional anti-Compton arrangements.

1.2.5 Pair Spectrometer[18,19,21]

Electron-positron pair production is one of the three ways γ-rays interact with matter. For γ-ray energies above 1.02 MeV (threshold energy for pair production) a γ-ray can be transformed into an electron-positron pair and these electrons share the kinetic energy equal to the difference between the γ-energy and threshold energy for pair production. The most prominent feature of the spectrum of a high energy (> 3 MeV) γ-ray measured by a Ge(Li) detector is the peaks which appear at positions 1022 keV and 511 keV below the full-energy position correspondong to a pair-production interaction in the detector followed by escape of the positron-electron annihilation quanta.

The two 511 keV quanta result from subsequent annihilation of the positron and these two quanta, at 180^{o} with respect to each other, can be used to signify the occurence of pair production. Most experimental arrangements used to suppress the Compton distribution can also be used as pair spectrometers. The annihilation -quanta, which are scattered in opposite directions, are usually recorded by two optically independent halves of a NaI(Tl) crystal which surrounds a central Ge(Li) detector. Under these conditions the electronic equipment ensures analysis of pulses from the Ge(Li) detector only in the case of triple coincidences between two halves of the crystal and the central detector. Generally a single channel

analyser (SCA) is set up with a window in the 511 keV region in each half of the NaI(Tl) crystal. Then the spectrum obtained from the Ge(Li) detector contains principally double escape peaks.

1.2.6. Compton Scattering Spectrometers or Multiple-Compton-Interaction Spectrometers[18,19)]

It is a well known fact that the γ-rays in the energy range from 0.1 to 3 MeV interact in germanium principally via Compton scattering. Multiple Compton interactions of the γ-ray take place in various sectors of the detector. If the detector could be partitioned in such a way that each separate interaction was noted and only coincidences of several interactions were to be recorded, then the continuous distribution can be suppressed strongly, while the total-absorption peak would consist solely of events of Multiple Compton Interaction

Several experimental set-ups have been developed using combined or composite Ge(Li) detectors, in such detectors only double coincidences are required in order to establish that multiple Compton interaction has occurred. Fig.1.3 illustrates six variations of the Compton scattering spectrometer system.

1.3 (n,γ) REACTION MECHANISMS

There are three main regions of interest in (n,γ) spectra (1) a high-energy region (> 4 MeV) in which individual well-resolved γ-rays are observed, (2) an intermediate energy region (2.5 $<E_\gamma<$ 4 MeV) in which a broad maximum is produced by a myriad of unresolved γ-ray lines, and, (3) a low-energy region consisting of individual and usually resolvable γ-ray lines. The shape of the capture γ-ray spectrum is determined in detail by the energies, spins, and parities of the levels between the capture-state and the ground state, and by the γ-ray transition probabilities which depend not only on energy and multipolarity but also on the detailed structure of the states.

The neutron separation energy of a particular nucleus may be obtained directly from the energy of the ground state γ-ray, or from the sum of the energies of the γ-rays in a competing cascade, with the usual corrections for nuclear recoil. Values for neutron separation energies determined from the (n,γ) reaction are complementary to those obtained from mass differences and the (γ,n), (d,p) and other reactions.[22,23]

$$S_n(n,\gamma) = Q(d,p) + |\varepsilon|$$

where S_n = neutron separation energy in (n,γ) reaction

Q = Q-value in (d,p) reaction

$|\varepsilon|$ = deuteron binding energy ≃ 2.223 MeV

The absolute intensity I_γ (i.e. photons per capture) of a capture γ-ray may be determined if the radiative capture cross-section σ of the target nucleus A is known, using the following equation:

$$I_\gamma \sigma = C_\gamma / N_A \eta_\gamma \phi$$

where C = counting rate

N_A = total number of target atoms

η_γ = absolute γ-detector efficiency

ϕ = thermal neutron flux

The radiative widths for E1, M1 and E2 γ-rays of energy E_γ emitted in transitions from the capture state may be written in the following approximate forms which are derived from expressions given by Blatt and Weisskopf:[24,25]

$$\Gamma_{\gamma if}(E1) = 6.8 \times 10^{-2}\ E_\gamma^3\ A^{2/3}\ D_i/D_o$$

$$\Gamma_{\gamma if}(M1) = 2.1 \times 10^{-2}\ E_\gamma^3\ D_i/D_o$$

$$\Gamma_{\gamma if}(E2) = 4.9 \times 10^{-8}\ E_\gamma^5\ A^{4/3}\ D_i/D_o$$

where A = mass number

D_i = the spacing at the separation energy of levels having the same spin and parity as the capture state

D_o = the single-particle level spacing for states of the same spin and parity

E_γ, D_i, D_o = in MeV

Γ_γ = in eV

The primary high-energy transitions, since low-energy primary transitions are too weak to be observed, provide the information about the mechanism for the (n,γ) process. The energy distribution of the primary γ-rays is obtained by multiplying the above radiation widths by the density of final states denoted by $D_f(E_i-E_f)^{-1}$. The result for radiation of multipole order 1 is

$$N_1(E_i-E_f) = C_1.(E_\gamma)^{2l+1}.\ D_f(E_i-E_f)^{-1}$$

where C_1 is independent of E_γ.[26] The factor $(E_\gamma)^{2l+1}$ favours the emission of radiation with higher energy. However, since the levels become more and more closely spaced as one moves from the ground state to the capture state the factor $D_f(E_i-E_f)^{-1}$ favours emission of quanta of low energy. With existing state densities and energy differences in medium to heavyweight nuclei, the primary transitions are more likely to be of high energy to states near the ground state.[26] The low-energy primary transitions to a state near the capture state would be weak because of the dominance of the energy term $(E_\gamma)^{2l+1}$ and also the subsequent secondary transition strengths would be shared among several transitions of most probably high energies. The net result is to make these secondary high-energy events unobservable. This leads to the general rule that any transition observed with an energy > 75% of the binding-energy is a primary transition to a low-energy state of the product nucleus.

It is obvious that by observing primary (high-energy) radiation, the energies of many of the low-lying states of the product nuclei may be determined, provided that the binding energy of the neutron in the product nucleus is known. Since E1 radiation is the strongest radiation among observed transitions, the spins and parities of the final states for the strong transitions can be determined or limited provided the spin and parity of the capture state is known. Furthermore, a weak transition may be a strong M1 or E2 transition or a weak E1 transition. Therefore the spin may be limited for the states to which weak primary transitions are observed.

A procedure by which neutron capture γ-ray intensities in odd-odd nuclei may be used for predicting the spins J of the various levels of the multiplet formed by coupling the odd proton (spin j_p) to the odd neutron (spin j_n) has been discussed by Varshalovich.[27] It is assumed that the nucleus is well represented by the shell model and that residual interactions which split the multiplet are small compared to single-particle excitation energies. Assuming that γ-ray transitions from the capture state J_c to a level of the multiplet involve only the single-neutron jump $j_{n1} \rightarrow j_{n2}$, the ratio of reduced transition probabilities for γ-rays feeding any two members of the multiplet may be written:

$$\frac{B(L,J_c \rightarrow J_1)}{B(L,J_c \rightarrow J_2)} = \frac{(2J_1 + 1) \cdot W^2(j_{n1}J_c j_{n2}J_1, j_p L)}{(2J_2 + 1)\ W^2(j_{n1}J_e j_{n2}J_2, j_p L)}$$

where W(abcd,ef) are Racah coefficients.[28]

One of the most interesting characteristics of the high-energy transitions is the distribution of radiation widths (transition probabilities) for a given multipole transition.[10,24] Three kinds of statistical laws are expected to apply. First, the intensity of transitions from various initial states to a single final state is a random variable with a very broad distribution. Porter-Thomas distribution[29] of reduced neutron widths indicates that the wide

fluctuation observed in the reduced widths is the result of the complexity of the wave functions of the highly excited states formed in neutron capture. After making some reasonable assumptions about the statistical nature of these states it says that for a reaction which proceeds by way of a single exit channel the distribution of widths is

$$P_{(x)} = x^{-\frac{1}{2}} e^{-x/2},$$

where x is the ratio of the reduced neutron width for a given resonance to the average neutron width overall resonance $(\Gamma/\bar{\Gamma})$. This distribution belongs to the class of chi-squared distribution with v degrees of freedom, i.e. a distribution of the form

$$P(x,v) = \frac{v}{2} \left|\Gamma\left(\frac{v}{2}\right)\right|^{-1} \left|\frac{vx}{2}\right|^{\left(\frac{v}{2} - 1\right)} e^{-vx/2},$$

where $\Gamma(v/2)$ is the usual mathematical gamma function and v is the number of degrees of freedom, i.e. the number of exit channels and x is defined as above. Large fluctuations in radiation widths are experimentally observed for most nuclei, and for most of them the measured distribution of widths is consistent with the Porter-Thomas form i.e. $v = 1$. But there still may be individual nuclei where nuclear structure effects will dominate over the statistical nature of a resonance and may cause the Porter-Thomas distribution to be violated.[24] There have been reports of a failure of the Porter-Thomas distribution for some

nuclei such as ^{142}Pr.[10] However these are still open to question until more extensive investigations are completed. As thermal neutron capture is dominated by one or two resonances, the radiation width to a given level may or may not be large enough to allow the observation of transitions to the level even if spin and parity selection rules are satisfied. Bollinger and Thomas[30,31] used the average-resonance irradiation technique and found consistency with the spins and parities of all of the levels shown.

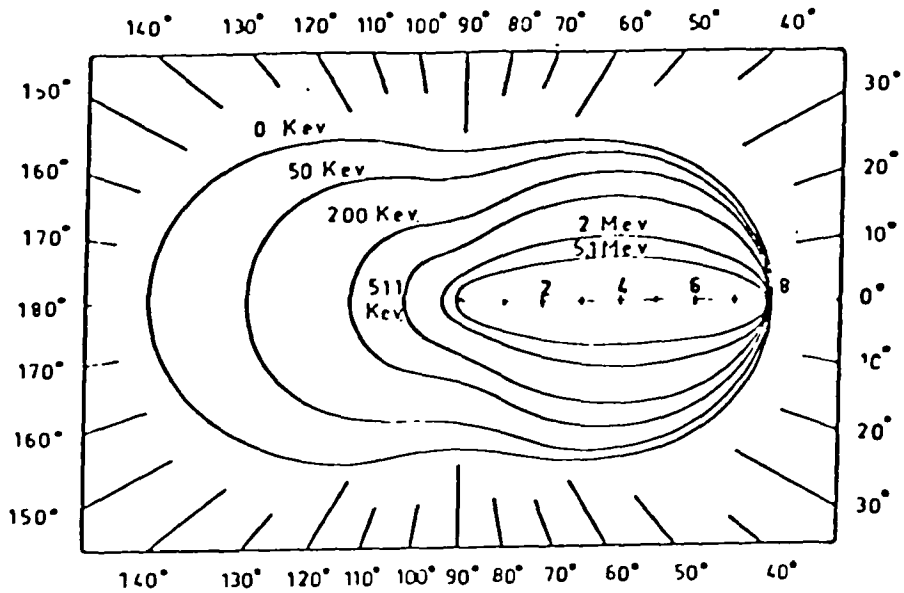


Figure 1.1 Differential cross-section as a function of the scattering angle for a variety of energies.

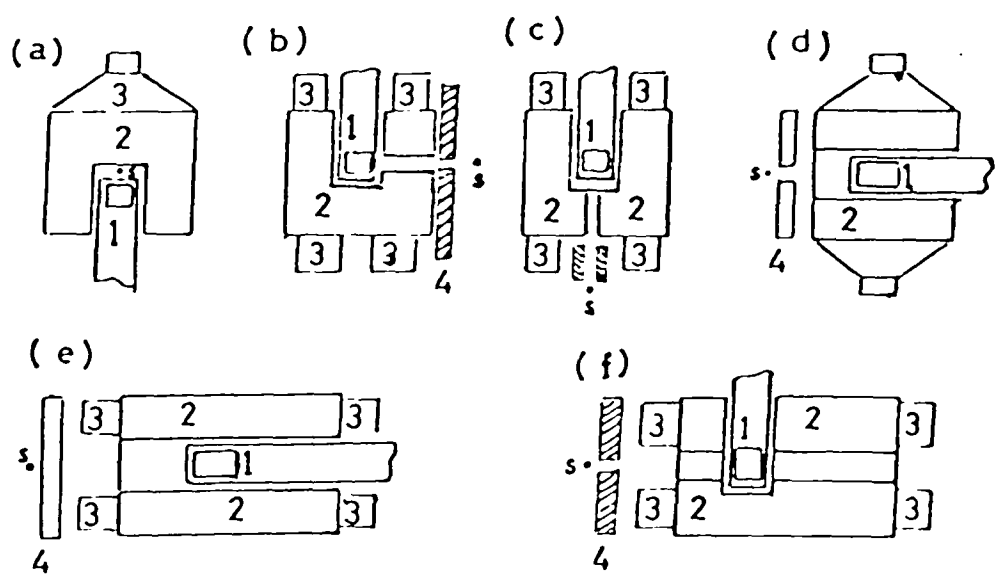


Figure 1.2 Varieties of construction of a guard scintillator (Reference 19)

1. Semiconductor Detector
2. Guard scintillator
3. Photomultiplier
4. Lead collimator
5. Source

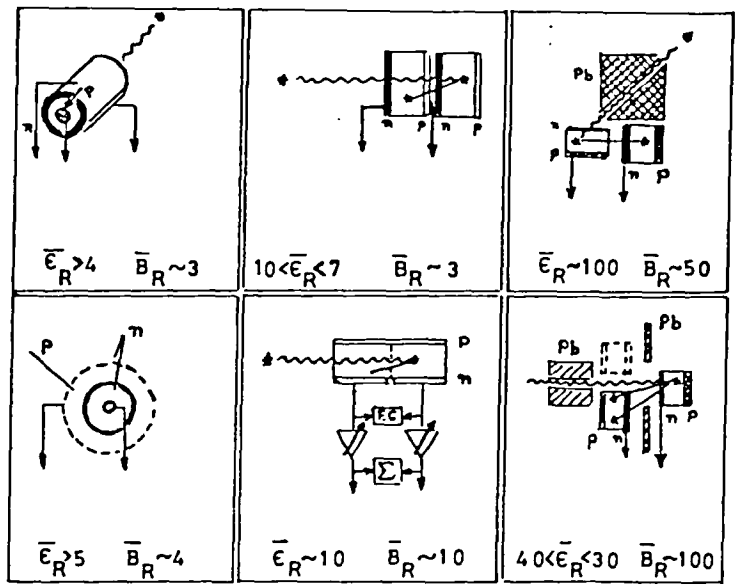


Fig. 1.3. Six different experimental arrangements for Compton-Scattering Spectrometers which are discussed in Ref. (18).

$\bar{\epsilon}_R$ = The mean efficiency reduction factor for the ^{137}Cs to ^{60}Co region in the sum coincidence mode relative to the singles mode.

$\bar{B}_R$ = The net background reduction factor.

= Ratio of the peak to Compton edge in the singles mode.

2. PRELIMINARY MEASUREMENTS

2.1 A Study of some Neutron Scattering Properties of High Density Polythene and Graphite

2.1.1 INTRODUCTION

The capture gamma ray experiment makes use of the 0^{o} - 180^{o} through tube which passes through the graphite of the 270^{o} thermal column at a distance of approximately 50 cm. from the centre of the core*. Therefore it was essential to put a neutron scatterer in the thermal column to get a reasonable neutron flux at the target position which would be outside the reactor shielding. There were two choices of neutron scatterers i.e. high density polythene and graphite. The aim of this experiment was to provide data to help in the choice of scattering block. The neutron flux scattered through 90^{o} from the 135^{o} neutron beam was measured, using two BF_3 counters, as a function of angle-of-incidence on a block of high density polythene. The second part of the experiment examined the scattering and diffusion of neutrons in a block of graphite.

The experiment is carried out at the 135^{o} (Time-of-Flight) neutron beam (Fig. 2.1) where the thermal neutron flux at the position of the scatterer is $\sim 2 \times 10^{4}$ neutrons $cm^{-2}.s^{-1}$.

*See Fig. 4.1.

2.1.2 Scattering from the surface of a high density polythene block as a function of the angle-of-incidence

Predicted flux at the position of the detectors assuming isotropic scattering from a point source

Since the distance between the neutron detectors and the neutron beam is large compared with the diameter of the neutron beam we shall assume that the neutrons are being scattered from a point source; in this case the neutron flux at the detectors, to a first approximation, is given by

$$\Phi_p = \frac{N}{4\pi d^2}$$

where N is the total number of neutrons per second striking the polythene (= area of beam X neutron flux)

and d is the distance from the centre of the beam to the detectors

$N = 2.59 \times 10^5 \ s^{-1}$

$d = 96.5$ cm.

$\Phi_p = 2.21 \ cm^{-2}s^{-1}$

Measured count rate as a function of angle

The count rates N_p as a function of θ, the angle of incidence of the neutron beam on the polythene block, has been measured and is shown in Table 2.1.

A parameter of $f_p(\theta)$ is defined as follows:-

$$f_p(\theta) = \frac{N_p(\theta)}{\Phi_p} = 0.452 \times N_p(\theta)$$

This parameter $f_p(\theta)$ represents a combination of the neutron detector efficiency and the non-isotropy of the neutron scattering from the polythene block. This parameter will be used in section 2.1.5 below to estimate the neutron flux from the 0^o through tube.

2.1.3 Neutron Scattering from a Cylindrical Block of Graphite

A cylindrical graphite block (diameter 7.6 cm.) is placed in the neutron beam with its axis horizontal and perpendicular to the neutron beam. The count rate is measured as a function of the length L of graphite between the centre of the neutron beam and the detectors (see Fig.2.1.B).

Predicted neutron flux at the detector position assuming isotropic scattering from a point source

If N = total number of neutrons falling on the graphite cylinder per second,

x = average path length of the neutrons in the graphite block,

and Σ_s = macroscopic neutron scattering cross-section of graphite.

then the number of neutrons scattered from the neutron beam per second is

$$N(1 - e^{-\Sigma_s x})$$

If these neutrons are scattered isotropically then the resultant flux at the detectors would be given by

$$\frac{N\,(1 - e^{-\Sigma_s x})}{4\pi d^2}$$

Taking into account the loss of neutrons due to absorption and scattering in that part of the graphite block between the neutron beam and the detectors, the predicted flux at the detectors becomes

$$\Phi_g = \frac{N\,(1 - e^{-\Sigma_s x})}{4\pi d^2} \cdot e^{-(\Sigma_a + \Sigma_s)\,L}$$

where L is the distance from the centre of the neutron beam to the face of the graphite nearest the detectors.

Σ_a = $10^{-5} cm^{-1}$

Σ_s = $0.385\ cm^{-1}$

N = $2.59 \times 10^5 s^{-1}$

x = 7.48 cm.

d = 99 cm.

$\Phi_g(L) = 1.98e^{-0.385L}$

Measured count rate as a function of L

The measured count rate as a function of L is shown in Table 2.2 .

By using a computer exponential fitting program, a semi-empirical formula for count rate as a function of L can be given as

$$N_g(L) = 12.81e^{-0.1085L} \ s^{-1}$$

Values of $N_g(L)$ obtained from the above equation are also listed in Table 2.2 and agree with the measured count rates to within 2.3%.

A parameter $f_g(L)$ is defined as

$$f_g(L) = \frac{N_g(L)}{\Phi_g(L)}$$

$$= \frac{12.81e^{-0.1085L}}{1.98\ e^{-0.385L}}$$

$$= 6.47\ e^{0.276L}$$

This parameter can then be used to estimate the neutron flux obtainable using a graphite scatterer in the through-tube.

2.1.4 Extrapolation of the Results of the Time-of-Flight Beam Tube Experiments to the 0° Through Tube

Neutron Flux distribution in the thermal column at the position of the 0° through tube

It can be shown that the neutron flux in a rectangular slab of moderating material with effective dimensions a,b,c, in the x,y,z, directions respectively, and with neutrons diffusing into it through the base plane z = o, is given by:-[32,33]

$$\Phi(x,y,z) = \sum_{m,n} A_{mn} \cos\left(\frac{m\pi x}{a}\right) \cos\left(\frac{n\pi y}{b}\right) \sinh \nu_{mn} (c-z)$$

where $\nu_{mn}^2 = \left(\frac{m\pi}{a}\right)^2 + \left(\frac{n\pi}{b}\right)^2 + \frac{1}{L^2}$

L being the neutron diffusion length = 48.5 cm in graphite

The constants A_{mn} may be evaluated by applying the boundary condition:-

$$\Phi = \Phi_o \quad \text{at} \quad z = o$$

then $A_{mn} = \left(\frac{4}{\pi}\right)^2 \frac{\Phi_o}{mn \sinh \nu_{mn} C}$

At large distances from the source we need consider only the first harmonic:-

$$\Phi(x,y,z) = \left(\frac{4}{\pi}\right)^2 \Phi_o \cos\left(\frac{\pi x}{a}\right) \cos\left(\frac{\pi y}{b}\right) e^{-\nu_{11} z}$$

In the reactor thermal column we assume:-

$\Phi_o = 10^{12}$ cm^{-2}s^{-1}

a = 85.2 cm (vertical dimension)

b = 103 cm (horizontal dimension)

$\nu_{11} = 0.0479$ cm^{-1}

At the 0^o through tube x = 33 cm and z = 14 cm

$$\Phi(y) = 2.87 \times 10^{11} \cos\left(\frac{\pi y}{103}\right) \text{ cm}^{-2}\text{s}^{-1}$$

The average flux in the 0^o through tube is given by

$$\bar{\Phi}(y) = \frac{\int \Phi(y)\, dy}{\int dy} = 1.90 \times 10^{11} \text{cm}^{-2}\text{s}^{-1}$$

2.1.5 Predicted flux at (n,γ) target position using the polythene scatterer in the centre of the 0° through tube

If, to a first approximation, we assume isotropic scattering from the surface of the polythene then the flux at the (n,γ) target position would be given by

$$\Phi_{pp}(d) = \frac{N}{4\pi d^2} \quad cm^{-2}s^{-1}$$

where N is the total number of neutrons falling on the polythene surface per second, and d is the distance from the centre of the 0° through tube to the (n,γ) target position (356 cm.).

$$N = \int \Phi\,(y)\, dA$$

where A is the elliptical surface of the polythene scatterer viewed from the reactor core.

$$N = \int_0^{R\tan\theta} 2.87\times10^{11} \cos\left(\frac{\pi y}{103}\right).2 \cot\Phi \,.\, (R^2\tan^2\theta - y^2)^{\frac{1}{2}}\, dy \; s^{-1}$$

$$= 1.41 \times 10^{14} \sin(0.145 \tan\theta)\; s^{-1}$$

and $\Phi_{pp}(d) = 8.85 \times 10^{7} \sin(0.145 \tan\theta)\; cm^{-2}s^{-1}$

Now using the factor $f_p(\theta)$ determined experimentally in paragraph 2.1.3 above, and assuming we used the same detectors in the (n,γ) target position we can predict their neutron count rate as

$$N_{pp}(\theta) = \Phi_{pp}(d) \times f_p(\theta)$$

The estimated count rates as a function of angle-of-incidence are given in Table 2.1 , and plotted in Fig. 2.8.2.

2.1.6 Predicted flux at the (n,γ) target position using a graphite scatterer

If we treat each 5 cm length of the graphite scatterer separately (5 cm being the width of the Time-of-Flight neutron beam) then we can use the same equation as in section 2.1.3 above, i.e.

$$\Phi_{pg} = \sum_{i=1}^{20} \frac{N_i(1-e^{-\Sigma_s x})}{4\pi d_i^2} e^{-(\Sigma_a + \Sigma_s)L_i}$$

where Σ_a, Σ_s and x are as given in section 2.1.3 and d_i is the distance from the centre of the i^{th} section to the (n,γ) target position.

d_i = (408.5 - 5i) cm

N_i = is the number of neutrons per second falling on the i^{th} section.

$$N_i = \int_{5i-55}^{5i-50} \Phi(y)\ 2R\ dy$$

where R is the radius of the graphite = 4.76 cm

$$N_i = 8.96 \times 10^{13} \sin \frac{\pi y}{103} \Big|_{5i-55}^{5i-50}$$

L_i = is the distance from the centre of the i^{th} block to the end of the graphite scatterer nearer the (n,γ) target position

L_i = (102.5 - 5i) cm (if the graphite completely fills the hole in the thermal column).

Now using the factor $f_g(L)$ obtained in 2.1.3 above and again assuming we used the same detectors in the (n,γ) target position we can predict their neutron count rate as

$$N_{pg} = \sum_{i=1}^{20} N_{pgi}$$

where $N_{pgi} = \Phi_{pgi} \times f_g(L_i)$

$$= \frac{N_i(1-e^{-\Sigma_s x})}{4\pi d_i^2} \times 6.47e^{(0.276-\Sigma_a-\Sigma_s)L_i}$$

$$= 6.63 \times 10^{12} \frac{e^{-0.109L_i}}{d_i^2} \mathrm{Cos}(0.153i - 1.601)$$

Values of N_{pgi} and N_{pg} are given for various total lengths of graphite absorber in Table 2.3 ; N_{pg} is plotted in Fig. 2.3 as a function of length of the graphite scatterer.

2.1.7 SUMMARY

The highest predicted count rate using a polythene scatterer in the 0^o through tube is

$$2.2 \times 10^8 \ s^{-1}$$

with an angle of incidence of 82.5^o.

With a graphite scatterer, the maximum count rate is obtained with a block of graphite terminating about 10-15 cm from the centre of the thermal column. The predicted count rate is then

$9.2 \times 10^7 \ s^{-1}$

It would appear therefore that the polythene scatterer would be more effective by a factor of about 2.

TABLE 2.1

POLYTHENE SCATTERER

$f_p(\theta) = 0.452\ N_p(\theta)$

$N_{pp}(\theta) = \Phi_{pp}(d) \times f_p(\theta)$

$\Phi_{pp}(d) = 8.55 \times 10^7 \sin(0.145 \tan \theta)\ cm^{-2}\ s^{-1}$

θ (deg)	$N_p(\theta)$	$f_p(\theta)$	$\Phi_{pp}(d) \times 10^{-7}$	$N_{pp}(d,\theta) \times 10^{-8}$
85	5.222	2.3603	8.83	2.08
82.5	6.107	2.7604	7.92	2.19
80	6.849	3.0957	6.51	2.02
75	8.618	3.8953	4.58	1.78
70	10.258	4.6366	3.45	1.60
65	11.827	5.3458	2.72	1.45
60	13.366	6.0414	2.21	1.34
55	15.075	6.8139	1.83	1.25
52.5	16.104	7.2790	1.67	1.22
50	17.473	7.8978	1.53	1.21
47.5	17.886	8.0845	1.40	1.13
45	18.597	8.4058	1.28	1.08
40	19.720	8.9134	1.08	0.963
35	21.171	9.5693	0.901	0.862
30	22.428	10.1375	0.743	0.753
25	22.973	10.3838	0.601	0.624
22.5	23.311	10.5366	0.534	0.563
20	23.580	10.6582	0.469	0.500
17.5	23.220	10.4954	0.406	0.426
15	23.146	10.4620	0.345	0.361
10	22.851	10.3287	0.277	0.234

TABLE 2.2.

GRAPHITE SCATTERER (EXPERIMENT)

$N_g(L)$ = Experiment count rate

N_{FIT} = Computer fitted values

= $12.81 \exp(-0.1085L)\ s^{-1}$

L (cm)	$N_g(L)$ per 1000 secs	N_{FIT} x 1000	DEVIATION %
2.54	9725	9724	0
3.81	8510	8473	+ 0.43
5.08	7299	7382	1.14
6.35	6503	6432	1.09
7.64	5583	5604	- 0.38
8.89	4802	4883	- 1.69
10.16	4242	4254	- 0.28
11.43	3754	3706	1.28
12.70	3201	3229	- 0.87
13.97	2878	2814	2.22
15.24	2430	2452	- 0.91

TABLE 2.3. GRAPHITE SCATTERER

$$N_{pgi} = 6.63 \times 10^{12} \cdot \frac{e^{-0.109 L_i}}{(408.5-5i)^2} \cdot \cos(0.153i-1.601)$$

	i	L_i=102.5-5i	L_i=87.5-5i	L_i=77.5-5i	L_i=72.5-5i	L_i=67.5-5i	L_i=62.5-5i	L_i=57.5-5i
- 47.5	1	0.00120	0.00616	0.01833	0.03161	0.05451	0.09401	0.16213
- 42.5	2	0.00473	0.02427	0.07218	0.12448	0.21468	0.37025	0.63853
- 37.5	3	0.01279	0.06558	0.19505	0.33639	0.58014	1.00052	1.72550
- 32.5	4	0.02991	0.15342	0.45632	0.78697	1.35722	2.34067	4.03675
- 27.5	5	0.06461	0.33141	0.98571	1.69997	2.93180	5.05620	8.71996
- 22.5	6	0.13240	0.671915	2.01998	3.48367	6.00797	10.36140	17.86935
- 17.5	7	0.26095	1.33855	3.98120	6.86602	11.84119	20.42141	35.21895
- 12.5	8	0.49848	2.55693	7.60501	13.11566	22.61937	39.00956	67.27621
- 7.5	9	0.92704	4.75523	14.14336	24.39176	42.06624	72.54779	125.11654
- 2.5	10	1.68276	8.63163	25.67283	44.27557	76.35802	131.68769	227.10968
+ 2.5	11	2.98477	15.31026	45.53692	78.53335	135.43929	233.57972	402.83355
7.5	12	5.17338	26.53667	78.92734	136.11876	234.75155	404.85449	
12.5	13	8.75227	44.89443	133.52836	230.28414	397.14996		
17.5	14	14.41648	73.94874	219.94381	379.31695			
22.5	15	23.01700	118.06478	351.15702				
27.5	16	35.34725	181.31220					
32.5	17	51.50250	264.17940					
37.5	18	69.29944						
42.5	19	80.74018						
47.5	20	64.55838						
TOTAL		3.59406×10^7	7.42789×10^7	8.84243×10^7	9.19365×10^7	9.31372×10^7	9.21324×10^7	8.90707×10^7

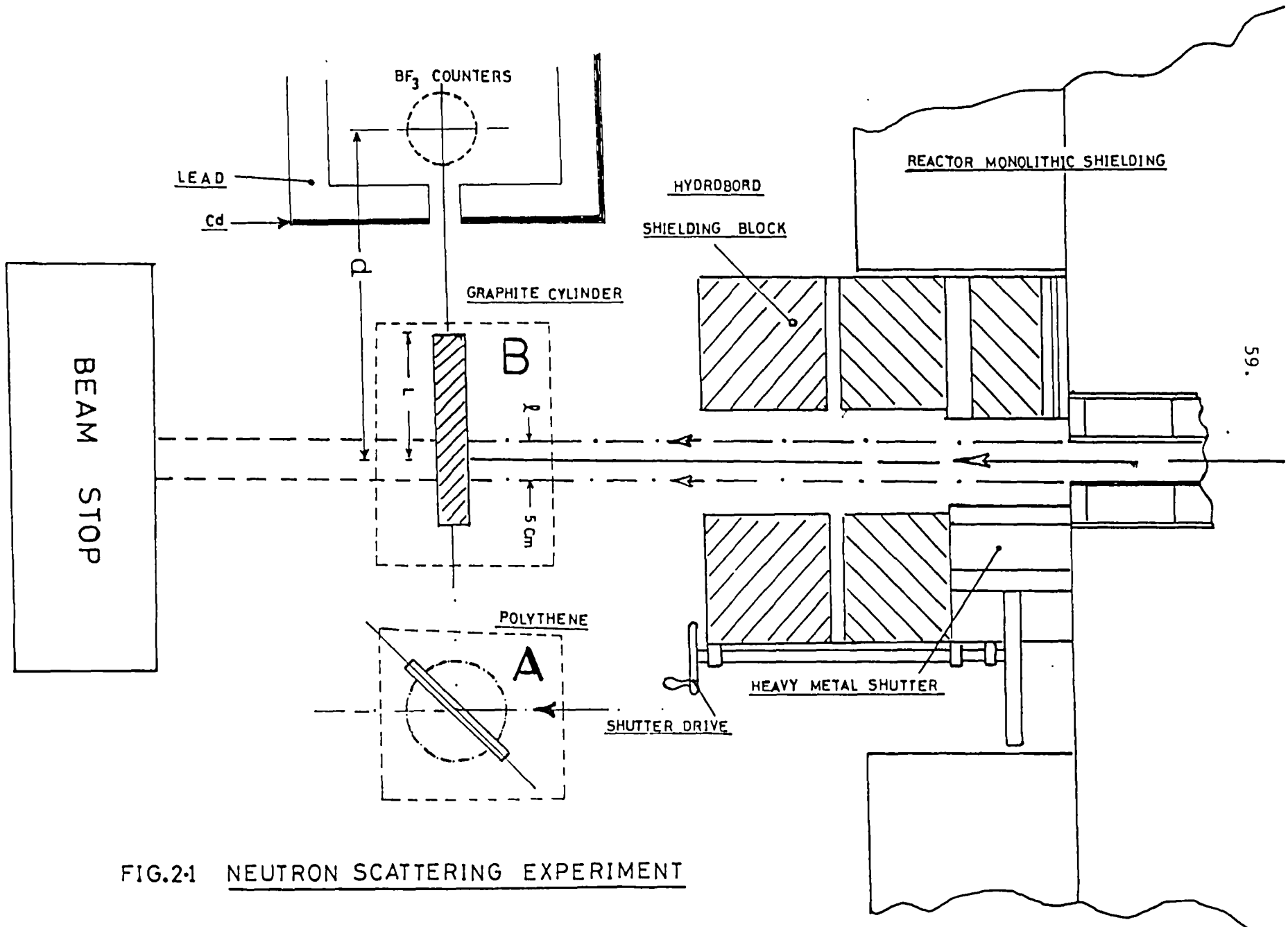


FIG.2·1 NEUTRON SCATTERING EXPERIMENT

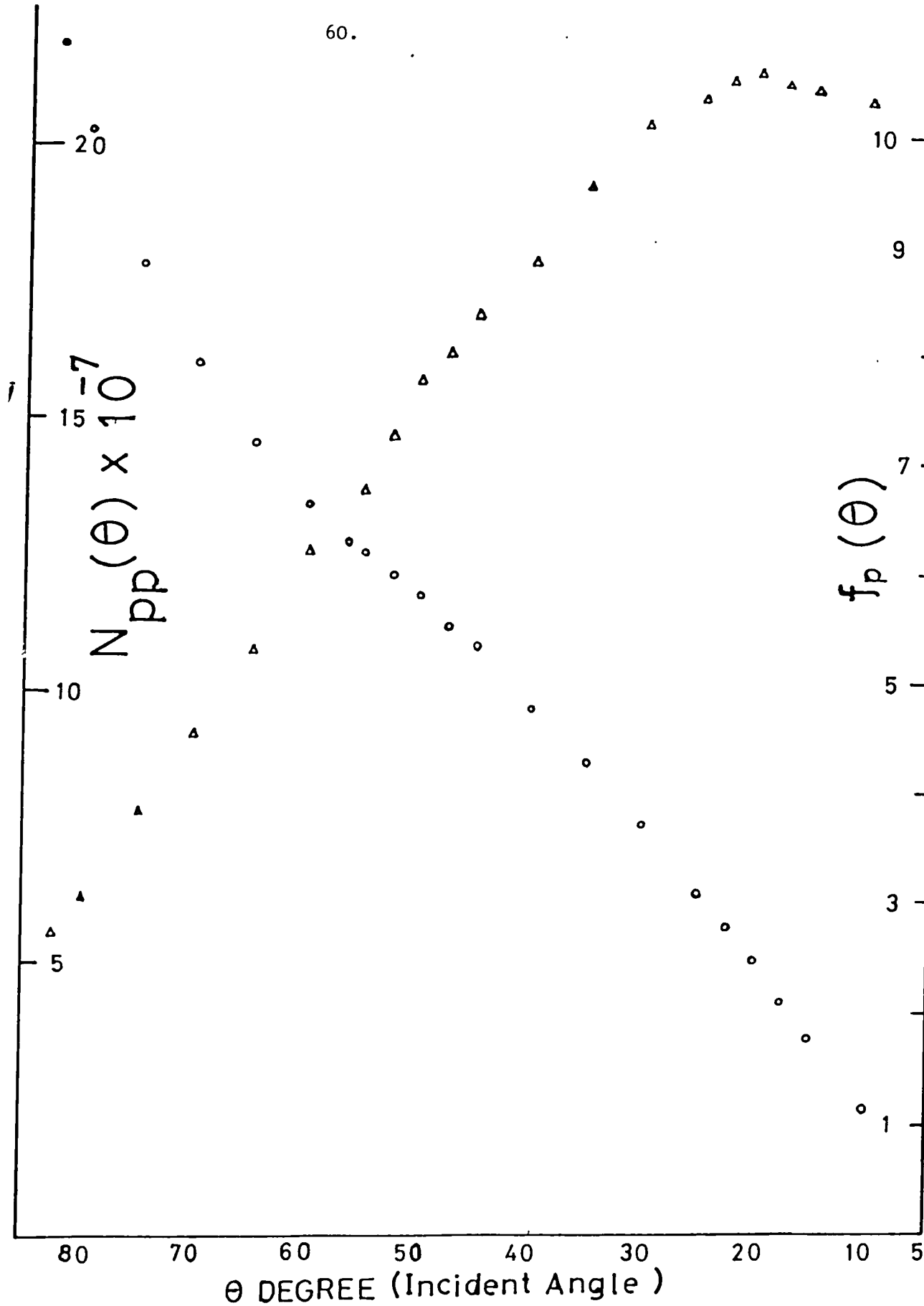
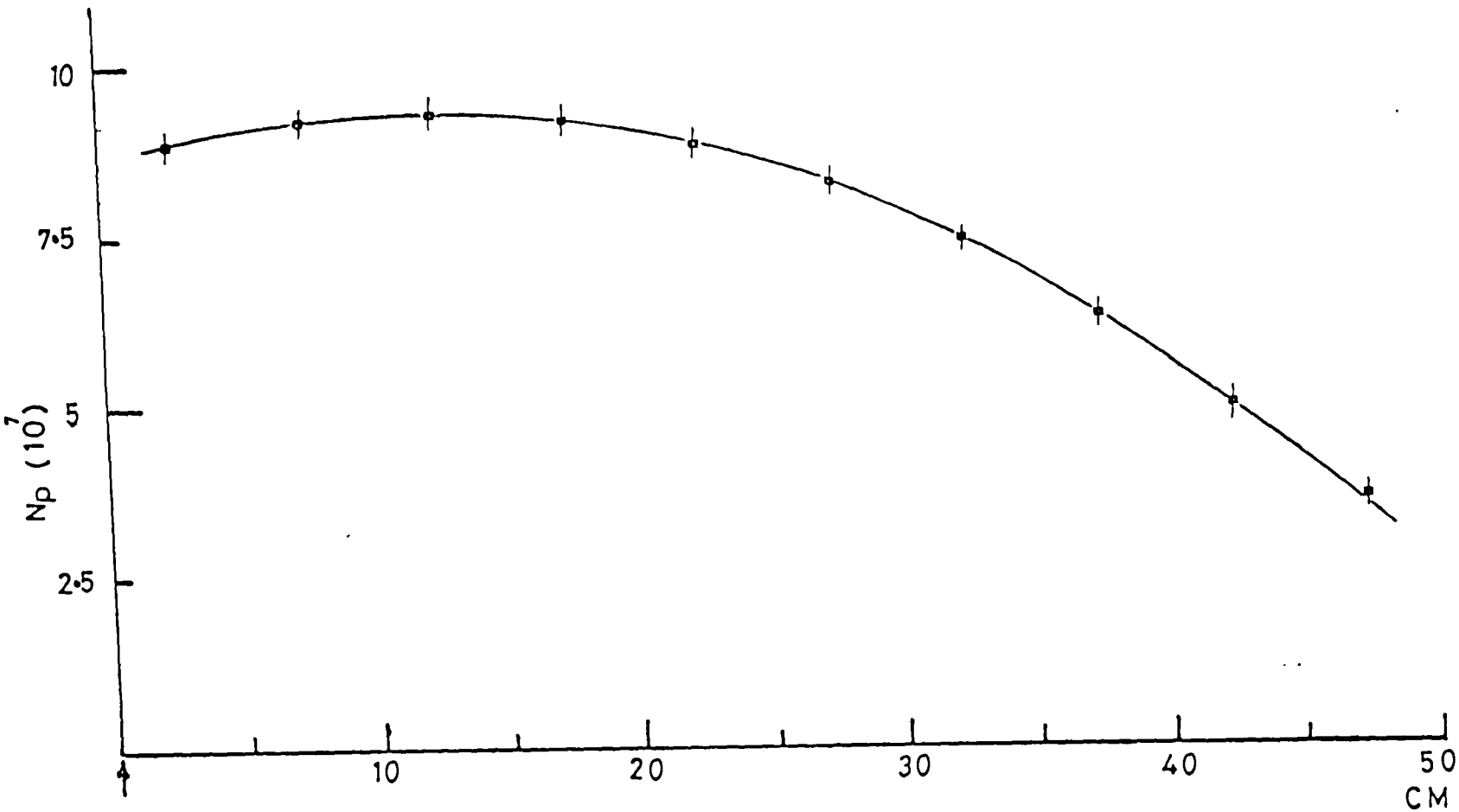


FIG.(2·2) POLYTHENE SCATTERER

FIG.(2·3) GRAPHITE SCATTERER



2.2 ^{133g}Ba and ^{226}Ra AS CALIBRATION STANDARDS FOR Ge(Li) DETECTORS

2.2.1 INTRODUCTION

Ge(Li) detectors are calibrated for energy and intensity measurements of gamma rays by using calibrated sources which emit one or more gamma rays of accurately known energy and intensity. This requires several radioactive sources.

^{133}Ba is an important reference gamma ray source since it has nine gamma rays in the energy range 50 - 400 keV, and has a comparatively long half-life of 10.5 years.[34] There are however certain inconsistencies in previously published gamma ray intensities in ^{133}Ba decay (Henry 1974[34]; Schmidt-Ott and Fink 1972[35]; Bosch et al. 1968[36]; Alexander and Lau 1968[37]; Notea and Gurfinkel 1968[38]).

The isotope ^{226}Ra is a remarkable calibration source because of its value for efficiency calibration of Ge(Li) detectors. ^{226}Ra ($T_{\frac{1}{2}}$ = 1600 y) in equilibrium with its decay products, emits at least 60 gamma rays with energies in the range 180 to 2500 keV.[39] But the intensities of the major gamma rays, based on the conversion electron measurements of Dzelepow et al (1958)[40] are reported by several authors (Ewan et al 1964[41]; Walford et al 1968[42]) as giving systematic errors in the efficiency curves of various Ge(Li) detectors. Although Robert (1968)[43] and Wallace et al (1969)[44] have measured the gamma-ray intensities directly from the gamma-ray spectra, all these values appear to differ systematically from each other.

In view of these discrepancies and the importance of these isotopes as calibration sources the gamma ray spectra of ^{133g}Ba and ^{226}Ra have been carefully studied using high resolution Ge(Li) detectors.

2.2.2 Experimental Arrangement and Calibration

The Ge(Li) Detectors

The gamma ray spectra in this experiment were measured using two coaxial Ge(Li) detectors having active volumes of 20 cc and 33 cc together with a Canberra 1417B amplifier and a Laben 8000 multichannel analyser system. The resolutions (FWHM) of the detectors are 2.5 keV and 2.2 keV at 1.33 MeV respectively.

Energy and Efficiency Calibration

The standard sources ^{22}Na, ^{54}Mn, ^{57}Co, ^{60}Co, ^{88}Y, ^{241}Am (Martin and Blichert-Toft 1970)[39], ^{137}Cs, ^{203}Hg (Valivaara et al 1970)[45], ^{152g}Eu (Aubin et al 1969)[46] and ^{56}Co (Martin et al 1970[39], Aubin et al 1969)[46] are used for energy and efficiency calibrations of the detectors.

The SAMPO computer program (Routti 1969[47], Routti & Prussin 1969)[48] is used throughout the experiment to determine peak positions and areas.

2.2.3 Gamma Energies and Intensities

With the aid of the precisely known energies of the calibrated sources and the SAMPO computer program, the gamma ray energies of ^{133g}Ba and ^{226}Ra decays were determined. Several experimental runs were taken for periods ranging from 2 to 10 hours measuring the spectra of the sources under study independently as well as combined with standard sources. The weighted average values are taken as final results, and are listed in Tables 2.4 and 2.10.

The absolute intensity values are measured with two Ge(Li) detectors at various source-detector distances, using a 0.4 MBq (± 1.6% standard deviation) calibrated ^{138g}Ba source supplied by the Radiochemical Centre, Amersham, England. The weighted average intensities are taken as final results and are listed in Table 2.5. Intensity uncertainties listed in these Tables include statistical uncertainties in the peak areas, as well as a 2% uncertainty established for the efficiency curves. The weighted average intensities for ^{226}Ra are given in Tables 2.10 and 2.11.

2.2.4 Result and Discussion

2.2.4(a) The Decay of ^{133g}Ba

The 437 keV peak is a sum peak arising mainly from the 356 and 81 keV cascade. This was proved both by counting the source at different distances from the detectors and by suppressing the 81 keV

gamma using a lead absorber of 2 mm thickness. The gamma energies determined in the present work agree well with the values adopted by Henry (1974)[34] except for the 81 keV gamma, and are in reasonable agreement with other previously published results. Previously reported gamma rays at 35 and 391 keV (Paradellis et al 1968)[49] are not confirmed.

The absolute intensity of 356 keV gamma in the present work is in excellent agreement with the value given by Henry (1974) but differs from those given by Bosch et al (1968) and Notea and Gurfinkel (1968).

Relative intensities derived from the absolute intensities are listed in Table 2.6 together with earlier results.

Internal Conversion Coefficients

As an excellent data on the relative electron intensity values are available, the internal conversion coefficients are calculated using the gamma ray intensities determined in the present work in conjunction with relative conversion electron intensities adopted by Henry (1974)[34]. The following formula is used for K-electron internal conversion coefficient values.

$$\alpha_K(X) = \alpha_K(356) \cdot \frac{I_e(X)}{I_e(356)} \cdot \frac{I_\gamma(356)}{I_\gamma(X)}$$

I_e = Relative K-conversion intensity

I_γ = Relative (or absolute) gamma intensity

α_K = K-electron internal conversion coefficient

$\alpha_K(356)$ = 0.0211 [34]

The total conversion coefficient α is then calculated from α_K by employing the (K+L+M+---/K) conversion electron intensity ratio (Henry 1974)[34]. The internal conversion coefficients obtained in the present calculation and the previously published values are given together in Table 2.7.

Examining the present α_K values, it is clear that M1 multipolarity is dominant for 53, 80, 81 and 303 keV transitions. Any contributions of E2 multipolarity is limited to a few percent. Equal contributions of E2 and M1 is possible for 161 keV transition. The 276, 356 and 384 keV transitions have pure E2 character. Our values for α_K support this assignment.

The decay scheme of ^{133g}Ba

The Electron-Capture Branching Ratios

The spins and parities of the ground states of ^{133}Ba and ^{133}Cs are $\frac{1}{2}^+$ and $\frac{7}{2}^+$ respectively. If an electron capture branch

existed, it would be therefore of a unique second forbidden type and may be neglected. Other transitions are at most second forbidden.

Using the absolute gamma intensities measured in the present work and the electron intensities from Henry (1974), the branching ratios were calculated and are shown in Table 3.10 where they are compared to earlier results. It is quite clear that the feeding is mainly towards the two high levels (384 and 437 keV). Only upper limits can be given regarding the branchings to the 81 and 161 keV levels.

The Log ft Values

The logarithmic values of comparative half-lives (log ft) are calculated using the following equation as suggested by Lederer et al. (1967)[50]:

$$\log ft = \log(f_o t) + \log(C) - \log(p)$$

where f_o is a function of the disintegration energy for EC (or the maximum kinetic energy of the particle in $\beta^{\pm}$ emission) and the total half life, C is a function of atomic number and p is the branching ratio.

The log ft values of the present work are given in Table 2.8. with other published data. The EC branches leading to the 437 and 384 keV levels may be classified as allowed transitions with ($\Delta I = 0, 1$) although our log ft values are rather high for allowed transitions but not unreasonable. The EC branches leading to the 81 and 161 keV levels are classified as second-forbidden transitions with ($\Delta I = 2$).

Transition Rates

The estimated transition probabilities are calculated using the Weisskopf formula.[25] It should be noted that these theoretical estimates are crude and are not expected to represent accurately transitions in actual nuclei. Experimental gamma decay half-life ($T_{\frac{1}{2}\gamma}$) for M1 and E2 are also calculated and presented in Table 2.9 together with Weisskopf single proton estimation values.

The multipolarity mixing ratios (δ^2) from previously reported internal conversion work were used to calculate M1 retardation and E2 enhancement factors over the single proton estimates of Weisskopf for all transitions in ^{133}Cs. Columns 7 and 8 of Table 6 give M1-retardation and E2-enhancement factors. The ^{133}Ba decay scheme is summarized in Fig. 2.5.

Discussion

Bosch et al. (1968)[36] have compared the experimental levels in ^{133}Cs with the predictions of the pairing-plus-quadrupole model and with calculations based on extended quasiparticle phonon-coupling theory for odd-mass spherical nuclei. However, none of these theories provides a good fit to the sequence of levels in ^{133}Cs. Particularly, these calculations account for only one low lying $\frac{5}{2}^+$ state, whereas two such states have been observed in ^{133}Cs.

Winn and Sarantites (1970)[51] have applied the observed E2-enhancement and M1-retardation factors to point out some differences in the structure of the two $\frac{5}{2}^+$ states. They have decided that the 161 keV state is more strongly phonon-mixed than 81 keV state. Our M1-retardation and E2-enhancement factors support their conclusion.

2.2.4(b) Decay of ^{226}Ra

The radium source had an activity of 0.37 ± 1% MBq and was encapsulated in platinum - 10% iridium metal 0.5 mm ± 5% thick. The gamma spectra were measured at two different source-detector distances (20 cm and 30 cm) so that it could be regarded as a point source. In the calculation of the attenuation of the gamma rays in the wall of the source it was assumed that the wall was pure platinum. The error introduced by this was smaller than the error in efficiency calibration.

The weighted average values of energy and intensity are given in Table 2.10 and Table 2.11 in comparison with previous results.

The energies obtained in this work agree well with previous results. The relative intensities reported by Wallace[44] are higher at low energy region (< 700 keV) and slightly lower at high energy region (700 - 1800 keV). Recently Hachem (1974)[52] has reported the energies and intensities for the gamma rays with energy greater than 1.1 MeV and Zobel et al (1977)[53] have given the energy and relative intensity values for 17 prominent gamma rays. The recent publication of Nuclear Data Sheets[54] should also be noted. These latest results are in reasonable agreement with the present work. However, a radium source in equilibrium with its decay products provides a cheap and rapid method for the calibration of Ge(Li) detectors, but it would be more advantageous to have available calibrated radium sources encapsulated in a low atomic number material for a minimum loss of gamma rays in the wall of the capsule.

TABLE 2.4

PHOTON ENERGIES IN ^{133g}Ba DECAY

Present Work	Henry (1974)	Schmidt-Ott and Fink (1972)	Greenwood (1970)	Bosch et al. (1968)	Notea and Gurfinkel (1968)	Thun et al. (1966)
53.14 ± 0.06	53.155 ± 0.016	53.16 ± 0.05		53.40 ± 0.06	53.42 ± 0.25	53.17 ± 0.04
79.65 ± 0.03	79.621 ± 0.011	79.67 ± 0.08		79.70 ± 0.05	-	79.60 ± 0.05
81.03 ± 0.03	80.997 ± 0.005	81.04 ± 0.06	80.998 ± 0.008	80.94 ± 0.05	81.15 ± 0.26	80.997± 0.006
160.63 ± 0.03	160.60 ± 0.04	160.50 ± 0.07		160.64 ± 0.07	160.58 ± 0.27	160.66 ± 0.06
223.16 ± 0.03	223.11 ± 0.04	223.10 ± 0.05		223.14 ± 0.07	223.21 ± 0.45	223.43 ± 0.26
276.41 ± 0.03	276.397 ± 0.012	276.38 ± 0.05	276.397 ± 0.012	276.54 ± 0.05	276.50 ± 0.32	276.43 ± 0.26
302.87 ± 0.03	302.851 ± 0.015	302.71 ± 0.05	302.851 ± 0.015	302.84 ± 0.05	302.00 ± 0.63	303.09 ± 0.21
356.03 ± 0.03	356.005 ± 0.017	356.04 ± 0.10	356.005 ± 0.017	356.24 ± 0.05	356.32 ± 0.48	356.26 ± 0.15
383.87 ± 0.03	383.851 ± 0.020	383.83 ± 0.10	383.851 ± 0.020	383.78 ± 0.05	384.13 ± 0.42	384.09 ± 0.20

TABLE 2.5

ABSOLUTE PHOTON INTENSITY VALUES (%) IN ^{133}Ba DECAY

keV	Present Work	Notea and Gurfinkel (1968)	Bosch et al. (1968)	*Henry (1974)
53.14	2.21 ± 0.04	1.96 ± 0.22	2.48 ± 0.12	2.20 ± 0.03
79.65	2.54 ± 0.12	2.54 ± 0.41	2.36 ± 0.24	2.43 ± 0.12
81.03	34.31 ± 1.65	30.9 ± 5.0	34.34 ± 0.89	32.75 ± 0.62
160.63	0.72 ± 0.03	0.626 ± 0.074	0.76 ± 0.06	0.72 ± 0.02
223.16	0.45 ± 0.02	0.416 ± 0.051	0.48 ± 0.06	0.47 ± 0.01
276.41	7.33 ± 0.26	6.01 ± 0.67	7.1 ± 0.3	7.29 ± 0.12
302.87	18.40 ± 0.65	15.39 ± 0.17	17.9 ± 0.7	18.62 ± 0.19
356.03	62.27 ± 1.68	51.7 ± 5.7	59. ± 1.	62.27
383.87	8.81 ± 0.25	7.34 ± 0.82	8.4 ± 0.4	8.84 ± 0.12

*The absolute photon intensity for 383.87 keV is given as 0.6227 by Henry (1974). Absolute intensities are calculated by using this value with adopted relative intensities.

TABLE 2.6

RELATIVE PHOTON INTENSITIES IN ^{133}Ba DECAY

keV	Present Work	Henry (1974)	Schmidt-Ott and Fink (1972)	Bosch et al (1968)	Notea and Gurfinkel (1968)	Alexander and Lau (1968)
53.14	3.55 ± 0.06	3.54 ± 0.05	3.54 ± 0.05	4.2 ± 0.2	3.78 ± 0.09	3.3 ± 0.05
79.65	4.07 ± 0.19	3.9 ± 0.2	3.9 ± 0.2	4.0 ± 0.4	4.90 ± 0.59	(11 ± 4
81.08	54.99 ± 2.65	52.6 ± 1.0	52.6 ± 1.0	58.2 ± 1.5	59.8 ± 7.2	65.9±3.9((55
160.63	1.15 ± 0.04	1.15 ± 0.04	1.16 ± 0.05	1.07 ± 0.05	1.21 ± 0.05	1.20 ± 0.06
223.16	0.73 ± 0.03	0.75 ± 0.02	0.74 ± 0.04	0.78 ± 0.06	0.803± 0.042	0.74 ± 0.06
276.41	11.77 ± 0.32	11.7 ± 0.2	11.4 ± 0.3	11.8 ± 0.3	11.61 ± 0.17	12.0 ± 0.4
302.87	29.55 ± 0.84	29.9 ± 0.3	30.2 ± 0.6	29.8 ± 0.8	29.75 ± 0.29	30.6 ± 0.9
356.03	100	100	100	100	100	100
383.87	14.19 ± 0.40	14.2 ± 0.2	14.4 ± 0.3	14.3 ± 0.3	14.18 ± 0.26	14.2 ± 0.5

TABLE 2.7

INTERNAL CONVERSION COEFFICIENTS

Transition energy keV	Present Work		Henry (1974)		Notea and Gurfinkel (1968)		Theory (Hager & Seltzer, 1968)	
	α_K	α	α_K	α	α_K	α	α_K(M1)	α_K(E2)
53	4.8 ± 0.011	5.7 ± 1.2	4.8 ± 1.1	5.7 ± 1.1	4.65 ± 0.91	5.2 ± 1.0	4.84	6.66
80	1.5 ± 0.2	1.7 ± 0.3	1.5 ± 0.2	1.7 ± 0.3	1.25 ± 0.19	1.43 ± 0.22	1.50	2.41
81	1.40 ± 0.06	1.61 ± 0.08	1.46 ± 0.05	1.75 ± 0.05	1.19 ± 0.15	1.44 ± 0.18	1.43	2.30
161	0.204 ± 0.11	0.252 ± 0.012	0.204 ± 0.008	0.253 ± 0.010	0.295± 0.084	0.35 ± 0.10	0.207	0.268
223	0.091 ± 0.005	0.100 ± 0.008	0.085 ± 0.003	0.097 ± 0.011	0.076± 0.008	0.087 ± 0.010	0.0844	0.0918
276	0.047 ± 0.002	0.571 ± 0.0029	0.0469 ± 0.0015	0.0571 ± 0.0024	0.048± 0.010	0.058 ± 0.012	0.0479	0.0462
303	0.037 ± 0.002	0.044 ± 0.002	0.0374 ± 0.0011	0.0481 ± 0.0015	0.034± 0.006	0.039 ± 0.007	0.0377	0.0347
356	0.0211	0.0256	0.0211	0.0256	0.021	0.024	0.0248	0.0211
384	0.017 ± 0.001	0.021 ± 0.002	0.0172 ± 0.0008	0.0205 ± 0.0008	0.018± 0.004	0.021 ± 0.005	0.0205	0.0169

TABLE 2.8

ELECTRON-CAPTURE BRANCHING RATIOS AND log ft VALUES IN ^{133}Ba DECAY

Energy levels in ^{133}Cs (keV)	Present work		Henry (1974)		Bosch et al. (1968)		Notea and Gurfinkel (1968)		Mann and Chaturvedi (1963)		Schmidt-Ott and Fink (1972)
	I_{ec}	log ft									I_{ec}
437.01	86.0 ± 1.7	6.5	86.0	6.7	82 ± 3	6.5	71.6 ± 8.6	6.35	88 ± 5	6.3	85.5 ± 1.5
383.87	13.9 ± 0.7	8.1	14	8.1	11 ± 2	8.0	22.0 ± 2.4	7.71	12 ± 8	7.7	14.5 ± 0.5
160.63	<0.1	>10.5	-	-	<3	>9.6	0.58 ± 0.70	10.0	0.3 ± 3	10.6	<1
81.03	<1.6	>10.0	-	-	7 ± 3	≳9.5	5.8 ± 11	9.3	0		<2

TABLE 2.9

Deduced Properties : a, δ, λ, Partial $T_{\frac{1}{2}\gamma}$, M1 Retardation, E2 Enhancement

E_γ	Branching Ratio a	$\lvert\delta\rvert$	λ (E2)	λ (M1)	Partial $T_{\frac{1}{2}\gamma}$(M1)	Partial $T_{\frac{1}{2}}(M1)_{sp}$	Partial $T_{\frac{1}{2}\gamma}$(E2)	Partial $T_{\frac{1}{2}}(E2)_{sp}$	M1 Retardation	E2 Enhancement
53	0.171 ± 0.029	.093± .020	0.009	0.991	<5.88ns	0.159ns	<0.68μs	32.5μs	<37	>48
80	0.884 ± 0.093	.131±0.017	0.017	0.983	297 ps	47.2 ps	17.3 ns	4.31μs	6.3	249
81	1.0	.169± .003	0.029	0.971	17.8ns	45.0 ps	0.627μs	3.96μs	396	6.3
161	0.116 ± 0.007	1.04 ±0.06	0.519	0.481	2.06ns	5.78 ps	1.90ns	129	356	68
223	0.011 ± 0.001	<0.44	<0.170	>0.830	<1.99ns	>2.15 ps	8.9ns	24.9ns	<926	<2.8
276	0.090 ± 0.004		1.0				<1.78ns	8.55ns		>4.8
303	0.593 ± 0.051	0.11^{+7}_{-11}	0.012	0.988	42.5 ps	0.86 ps	3.55 ns	5.42 ns	49	1.5
356	0.739 ± 0.014		1.0				<0.208 ns	2.42 ns		>11.6
384	0.397 ± 0.016		1.0				0.087 ns	1.65 ns		19

δ, $T_{\frac{1}{2}\gamma}$ - adopted from Henry (1974)

λ - M1 and E2 content for each transition

TABLE 2.10

γ-Ray Energies (keV) and Absolute Intensities in ^{226}Ra Decay

keV		Absolute Intensity	
Present Work	Nucl. Data Tables (1970)	Present Work	Nucl. Data Sheet (1970)
186.14 ± 0.03	186.0 ± 0.1	3.87 ± 0.12	3.3 ± 0.1
242.01 ± 0.03	241.92 ± 0.03	7.67 ± 0.23	7.4 ± 0.6
258.63 ± 0.03	258.8 ± 0.1	0.60 ± 0.02	0.56 ± 0.09
274.68 ± 0.03	274.8 ± 0.1	0.48 ± 0.02	0.48 ± 0.09
295.01 ± 0.03	295.22 ± 0.04	18.35 ± 0.50	18 ± 1
351.69 ± 0.03	351.99 ± 0.06	36.01 ± 0.93	35 ± 3
405.65 ± 0.03	405.9 ± 0.4	0.17 ± 0.01	0.15 ± 0.04
454.83 ± 0.04	455.0 ± 0.3	0.29 ± 0.02	0.29 ± 0.05
461.90 ± 0.05	462.1 ± 0.2	0.20 ± 0.01	0.21 ± 0.05
469.96 ± 0.04	470.0 ± 0.3	0.14 ± 0.01	0.13 ± 0.04
480.28 ± 0.03	480.5 ± 0.2	0.32 ± 0.02	0.34 ± 0.07
486.92 ± 0.02	487.2 ± 0.2	0.42 ± 0.01	0.41 ± 0.08
533.68 ± 0.04	533.8 ± 0.2	0.16 ± 0.01	0.17 ± 0.04
580.08 ± 0.03	580.3 ± 0.2	0.35 ± 0.01	0.33 ± 0.06
609.24 ± 0.02	609.4 ± 0.2	44.26 ± 0.82	43 ± 3
665.42 ± 0.02	665.6 ± 0.2	1.49 ± 0.03	1.5 ± 0.2
703.16 ± 0.03	703.1 ± 0.2	0.46 ± 0.02	0.48 ± 0.06
719.87 ± 0.03	719.9 ± 0.2	0.36 ± 0.02	0.42 ± 0.05
752.88 ± 0.03	753.0 ± 0.3	0.14 ± 0.02	0.11 ± 0.08
768.41 ± 0.03	768.4 ± 0.2	4.65 ± 0.09	5.0 ± 0.5
785.98 ± 0.03	786.0 ± 0.2	1.08 ± 0.03	1.18 ± 0.09
806.25 ± 0.03	806.2 ± 0.2	1.25 ± 0.03	1.2 ± 0.2
821.28 ± 0.03	821.2 ± 0.3	0.19 ± 0.03	0.16 ± 0.04
826.08 ± 0.03	826.0 ± 1.0	0.21 ± 0.03	0.13 ± 0.06
839.12 ± 0.03	839.1 ± 0.2	0.60 ± 0.02	0.59 ± 0.08
934.20 ± 0.03	934.1 ± 0.2	3.09 ± 0.06	3.1 ± 0.3
964.29 ± 0.03	964.2 ± 0.3	0.38 ± 0.02	0.39 ± 0.05
1052.18 ± 0.04	1052.0 ± 0.3	0.32 ± 0.02	0.35 ± 0.04
1070.65 ± 0.06	1070.0 ± 0.3	0.27 ± 0.01	0.27 ± 0.04
1104.40 ± 0.04	1104.0 ± 0.4	0.15 ± 0.01	0.16 ± 0.03
1120.48 ± 0.04	1120.4 ± 0.2	15.03 ± 0.30	14.0 ± 0.8
1133.72 ± 0.04	1133.8 ± 0.3	0.24 ± 0.02	0.25 ± 0.05
1155.36 ± 0.04	1155.3 ± 0.3	1.67 ± 0.04	1.7 ± 0.2
1207.88 ± 0.04	1207.7 ± 0.3	0.50 ± 0.02	0.52 ± 0.06
1238.31 ± 0.04	1238.2 ± 0.3	6.09 ± 0.12	6.4 ± 0.6
1281.54 ± 0.04	1281.1 ± 0.2	1.53 ± 0.04	1.6 ± 0.2
1304.03 ± 0.08	1303.8 ± 0.4	0.12 ± 0.01	0.14 ± 0.03
1377.81 ± 0.04	1377.8 ± 0.2	4.16 ± 0.09	4.6 ± 0.4
1385.47 ± 0.05	1385.4 ± 0.2	0.91 ± 0.03	1.03 ± 0.08
1401.65 ± 0.04	1401.7 ± 0.3	1.47 ± 0.03	1.7 ± 0.3
1408.12 ± 0.04	1408.0 ± 0.2	2.63 ± 0.05	2.8 ± 0.3
1509.26 ± 0.04	1509.5 ± 0.3	2.17 ± 0.05	2.2 ± 0.2
1538.67 ± 0.06	1538.8 ± 0.3	0.45 ± 0.02	0.53 ± 0.04
1543.40 ± 0.07	1543.4 ± 0.4	0.29 ± 0.02	0.40 ± 0.04
1583.35 ± 0.04	1583.5 ± 0.3	0.71 ± 0.04	0.77 ± 0.06
1594.89 ± 0.05	1594.9 ± 0.4	0.30 ± 0.02	0.34 ± 0.03
1599.54 ± 0.06	1599.6 ± 0.4	0.35 ± 0.02	0.40 ± 0.07

TABLE 2.10

γ-Ray Energies (keV) and Absolute Intensities in ^{226}Ra Decay (cont'd)

keV		Absolute Intensity	
Present Work	Nucl. Data Tables (1970)	Present Work	Nucl. Data Sheet (1970)
1661.35 ± 0.04	1661.5 ± 0.2	1.06 ± 0.04	1.16 ± 0.07
1684.19 ± 0.04	1684.2 ± 0.3	0.24 ± 0.02	0.26 ± 0.02
1729.87 ± 0.04	1729.9 ± 0.2	3.22 ± 0.07	3.2 ± 0.2
1764.55 ± 0.04	1764.7 ± 0.2	15.96 ± 0.38	16.6 ± 0.8
1838.60 ± 0.12	1838.6 ± 0.3	0.36 ± 0.02	0.36 ± 0.03
1847.65 ± 0.04	1847.7 ± 0.3	2.04 ± 0.06	2.2 ± 0.2
1873.43 ± 0.04	1873.6 ± 0.3	0.20 ± 0.01	0.23 ± 0.02
1896.81 ± 0.06	1896.8 ± 0.4	0.15 ± 0.01	0.17 ± 0.03
2118.69 ± 0.04	2118.9 ± 0.3	1.32 ± 0.03	1.30 ± 0.09
2204.26 ± 0.04	2204.5 ± 0.3	5.09 ± 0.13	5.4 ± 0.5
2293.56 ± 0.07	2293.7 ± 0.3	0.33 ± 0.03	0.35 ± 0.03
2447.89 ± 0.04	2448.0 ± 0.3	1.68 ± 0.04	1.77 ± 0.09

TABLE 2.11

RELATIVE GAMMA INTENSITIES OF THE STRONGER TRANSITIONS IN ^{226}Ra DECAY

keV	Present Work	Dzelepow et al (1958)	Robert (1968)	Wallace et al (1969)	Mowatt (1970)
186.14	8.74 ± 0.27	8.48	-	9.91 ± 0.31	8.20 ± 0.12
242.01	17.33 ± 0.52	22.26	17.16 ± 0.64	19.33 ± 0.30	16.1 ± 0.21
295.01	41.46 ± 1.13	40.0	43.1 ± 2.6	47.84 ± 0.91	41.45 ± 0.56
351.69	81.36 ± 2.10	80.0	85.4 ± 2.6	87.2 ± 1.9	79.7 ± 1.1
609.24	100	100	100	100	100
768.41	10.51 ± 0.20	11.22	-	9.90 ± 0.21	
934.20	6.98 ± 0.14	7.00	7.94 ± 0.57	6.26 ± 0.18	
1120.48	33.96 ± 0.68	35.2	35.9 ± 1.8	31.90 ± 0.73	34.9 ± 0.7
1238.31	13.76 ± 0.27	12.72	13.3 ± 1.3	12.77 ± 0.12	
1377.81	9.40 ± 0.20	10.02	8.98 ± 0.51	8.70 ± 0.48	
1385.47	2.06 ± 0.07	-	-		
1729.87	7.27 ± 0.16	5.09	7.44 ± 0.38	6.94 ± 0.20	
1764.55	36.06 ± 0.86	34.6	39.2 ± 1.5	35.34 ± 0.10	

Nucl. Inst. Methods. 74 (1969) 353-354

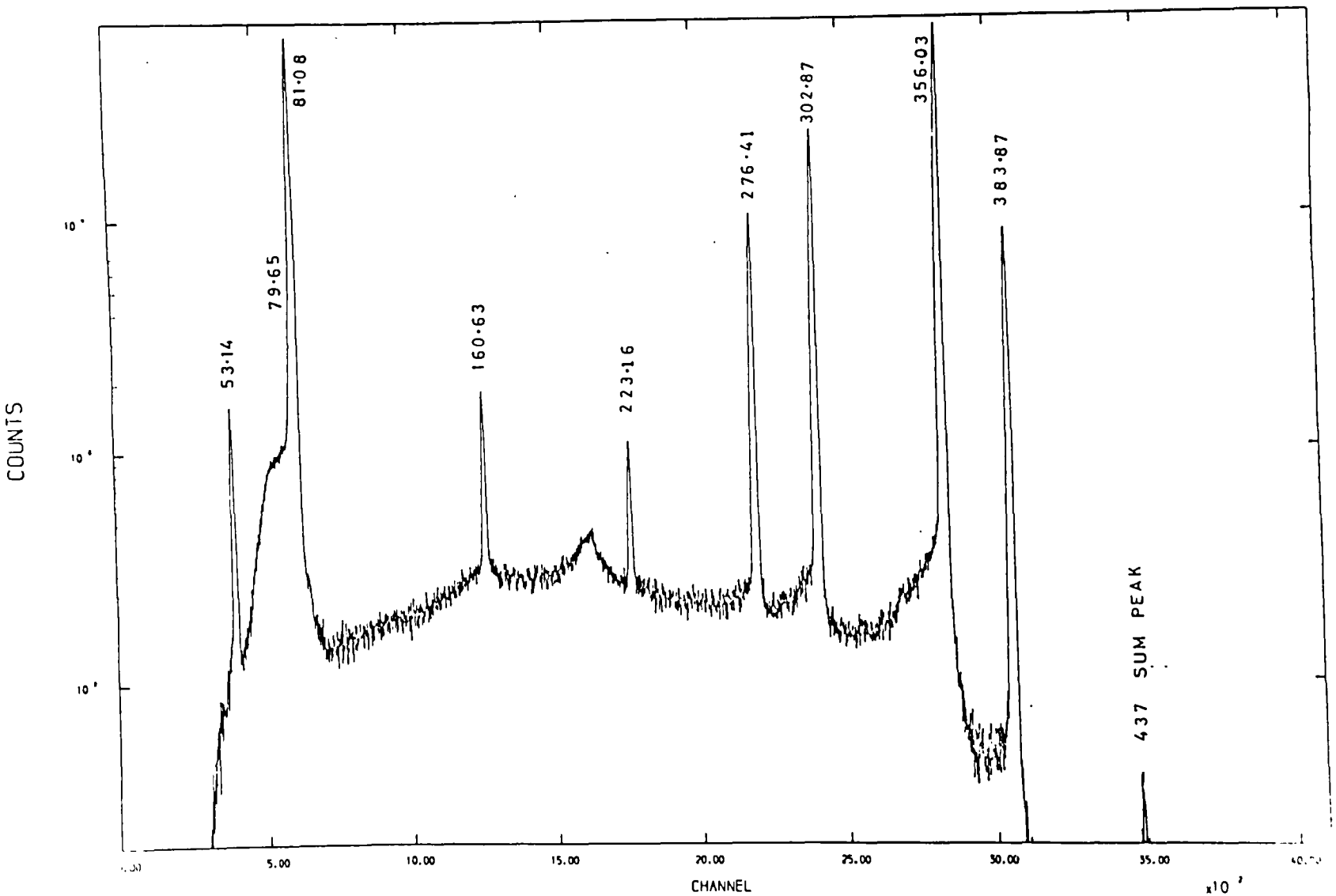


FIGURE 2.4 ••••• BA 133G DECAY 0.0-0.5 MEV WITH COMPTON SUPPRESSION •••••

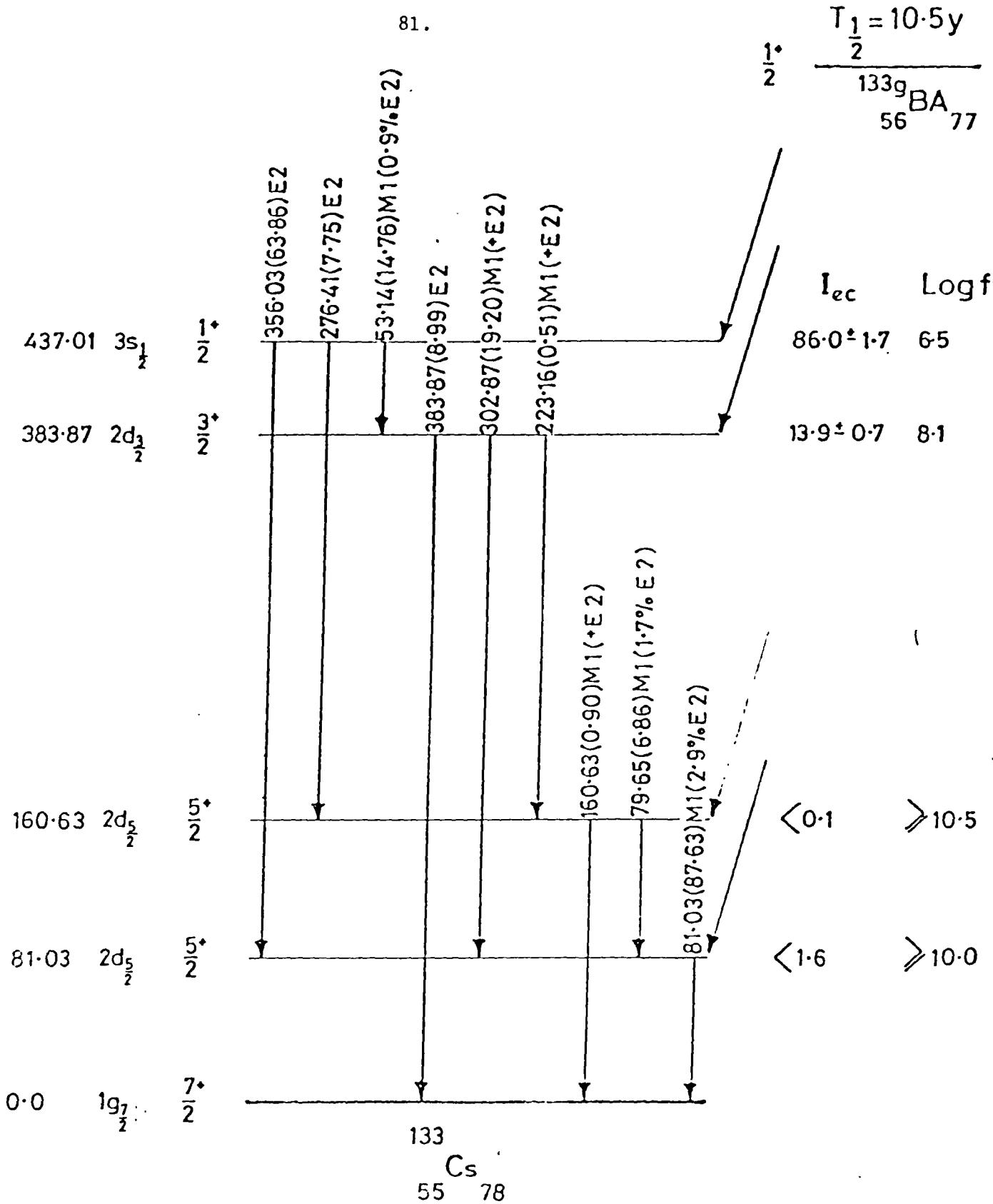


FIG.2.5. PROPOSED DISINTEGRATION SCHEME FOR ^{133g}BA

The numbers in parentheses indicate absolute γ+ce per 100 decays

3. DECAY SCHEMES OF Ag ISOTOPES

3.1. DECAY OF ^{108m}Ag

3.1.1 INTRODUCTION

The existence of a long-lived isomer of ^{108}Ag was first reported by Wahlgren et. al. (1960)[55]. They reported that this isomer decays with a half-life of > 5 years. The principal mode of decay was by electron capture to a level at 1772 keV in ^{108}Pd which de-excited via a triple cascade of γ-rays (722, 616 and 434 keV) to the ground state. An 81 keV γ-ray was tentatively assigned to be in cascade with an unobserved isomeric transition in ^{108}Ag. Later γ-γ angular correlation measurements were carried out on all γ-ray pairs in EC branch, and a 30 keV isomeric transition in coincidence with the 81 keV γ-ray was established (Funk et al 1961[56]; Kistner et al 1962[57]). Kistner and Sunyar (1966)[58] reported the results of the magnetic spectrometer studies of conversion electron spectra in both the EC and the isomeric internal transition branches of the ^{108m}Ag decay. Harbottle (1970)[59] has also determined the half-life of ^{108m}Ag as (127 ± 7) years using a 'Nucleometer' internal source methane-flow proportional counter. Hamilton et al (1971)[60] and Kracikova et al (1968)[61] have reported the weak transitions in ^{108m}Ag decays measured with semi conductor detectors. All these measurements were performed with irradiated natural silver samples in which most of the ^{110m}Ag activity had been allowed to decay. In the present work the gamma ray spectrum of ^{108m}Ag is re-investigated using a silver foil enriched to 99.6% in ^{107}Ag and high resolution Ge(Li) detectors.

3.1.2 EXPERIMENTAL PROCEDURES

A 10 mg silver foil enriched in ^{107}Ag was irradiated at Consort II reactor for ten days with the thermal neutron flux of $\simeq 1.7 \times 10^{11} n.cm^{-2}sec^{-1}$. The sample was left for two days so that all short-lived isotopes (2.4 min ^{108g}Ag and 24 secs ^{110g}Ag) should decay. The singles gamma spectra (*) were measured with the Compton Suppression spectrometer, the details of which are given in Chapter 4.

3.1.3 RESULTS AND DISCUSSION

Energies and Intensities of Gamma Rays

The γ-ray spectra were analyzed using the SAMPO computer program for energy and intensity determinations. The usual standard sources, ^{152}Eu and ^{226}Ra sources were used for energy and efficiency calibrations. Singles runs were taken for periods of 10, 20 and 48 hours to search for the weak transitions. The present sample has the activity ratio of ^{108m}Ag : ^{110m}Ag as 1 : 13. Unambiguous assignments of the lines of ^{108m}Ag were possible because of former studies of ^{110m}Ag decay and $^{107}Ag(n,\gamma)$ measurements. The sum peaks were identified by taking a singles run with a 2 mm thick lead absorber between the source and the detector. The energy of the 79.14 keV transition was determined from (n,γ) work.

The weighted average values of energy and intensity are presented in Table 3.1 together with previous results. Only the upper limits can be given for intensities of 837 and 1020 keV gamma rays. The intensity value of the 406 keV transition in the present work is much higher than others.

(*) See Figure 3.2

3.1.4 Decay Scheme of ^{108m}Ag

The internal conversion coefficients are calculated using the relative gamma ray intensities determined in the present work in conjunction with relative conversion electron intensities of Kistner et al (1966) and by assuming that the 434 keV ($2^+ \rightarrow 0^+$) E2 transition has the theoretical value 7.8×10^{-3} for its K-shell internal conversion coefficient.[62] The fraction of ^{108m}Ag decays which proceeds in the isomeric branch was determined from the 79 to 434 keV gamma ray ratio as (8.1 ± 0.6)%. This value is in good agreement with the previous result of (8.5 ± 0.8)%.[58]

The spins and parities of the ground state (1^+), the 79 keV state (2^-) and the isomeric state 109.43 keV (6^+) in ^{108}Ag have been established by Kistner and Sunyar (1966).[58] This group and Estulin et al (1966)[63,121] have discussed the configuration of these states. The ground state configuration for ^{108}Ag is either $[\pi(g_{9/2}^{-3})_{7/2}, \nu(d_{5/2}^{-1})]_{1^+}$ or $[\pi\, g_{9/2}^{-1}, \nu\, g_{7/2}^{-1}]_{1^+}$ as inferred from allowed β-decay to even parity levels in ^{110}Cd and from nuclear magnetic dipole moment measurements.[64] The 79 keV state (2^-) is obtained by coupling of $P_{\frac{1}{2}}$ odd proton and $d_{5/2}$ odd neutron. It was confirmed in ^{107}Ag(d,p) measurements of Brient (1972).[65]

The 931, 1048 and 1053 keV levels in ^{108}Pd are two phonon triplet and 434 keV is a one phonon state. Therefore 614-434 keV cascade is a $4^+ \rightarrow 2^+ \rightarrow 0^+$ quadrupole-quadrupole cascade. The conversion coefficients of 614 and 723 keV transitions are consistent with M1, E2 or a mixture of M1 and E2.(TABLE 3.2)

Kistner et al (1966)[58] have shown that the half-life of 79 keV level ^{108}Ag is $< 10^{-9}$ sec. Estulin (1967)[63] has reported as $T_{\frac{1}{2}} < 7 \times 10^{-10}$ sec from delayed coincidence measurements. The most complete data on ^{108m}Ag decay has been compiled by Bertrand[66].

TABLE 3.1.

Energies and Relative Intensities of transitions in the decays of ^{108m}Ag to ^{108}Pd levels

Present Work		Hamilton et al (1971)		Kracikova et al (1968)		Kistner et al (1966)	
keV	I_γ	keV	I_γ	keV	I_γ	keV	I_γ
406.28 ± 0.05	10.56 ± 0.29	405.7	<0.011	405.7 ± 1.0	0.8 ± 0.4	-	-
433.99 ± 0.03	100	434.00 ± 0.10	100	433.7 ± 0.5	100	433.6 ± 0.5	100
614.34 ± 0.09	99.76 ± 3.67	614.37 ± 0.10	99.1 ± 2.4	613.5 ± 0.4	105 ± 10	613.9 ± 0.6	103 ± 3
633.05 ± 0.09	< .3(^{108}Cd)	632.89 ± 0.12	0.16 ± 0.02	633.0 ± 1.0	0.18 ± 0.07	-	-
722.91 ± 0.04	98.30 ± 3.15	722.95 ± 0.08	99.1 ± 2.4	722.6 ± 0.5	102 ± 10	722.7 ± 1.0	102 ± 2
836.5 ± 0.6	<0.08	836.5 ± 0.04	0.005 ± 0.003	836.5 ± 1.0	0.06 ± 0.04	-	-
1020	<0.08	1020	<0.003	1020 ± 3	1.0 ± 0.5	-	-

TABLE 3.2.

Conversion Coefficients and Multipolarities in ^{108m}Ag Decay

Transition (keV)	Relative gamma intensity	Conversion Shell	Relative c.e. intensity	Conversion Coefficients	Theoretical Conversion Coefficient			Multipolarity
					E1	M1	E2	
79.14	6.62 ± 0.90	K	2.04 ± 0.10	0.24 ± 0.05	0.27	0.71	2.40	E1
		L	0.25 ± 0.02	0.030 ± 0.006	0.034	0.091	0.81	
		M, N,---	0.061 ± 0.013	0.007 ± 0.002	-	-	-	
434.0	100	K	1.00	-	-	-	7.8×10^{-3}	E2 (Assumed)
		L, M,---	0.148 ± 0.023	$(1.15 \pm 0.18)\times10^{-3}$	-	-	-	
614.3	99.76 ± 3.67	K	0.37 ± 0.03	$(2.89 \pm 0.26)\times10^{-3}$	1.04	3.00	2.92	M1, E2, M1 + E2
		L, M,---	0.051 ± 0.016	$(0.40 \pm 0.13)\times10^{-3}$	-	-	-	
722.9	98.30 ± 3.15	K	0.250 ± 0.016	$(1.98 \pm 0.14)\times10^{-3}$	0.73×10^{-3}	2.05×10^{-3}	1.91×10^{-3}	M1, E2, M1 + E2
		L, M,---	0.046 ± 0.008	$(0.37 \pm 0.07)\times10^{-3}$	-	-	-	

3.2 THE DECAY OF ^{108g}Ag

3.2.1 INTRODUCTION

The decay of ^{108g}Ag($T_{\frac{1}{2}}$=2.4 min) has been studied by several groups*) using scintillation detectors and Ge(Li) detectors in the singles and coincidence modes. ^{108g}Ag decays by electron capture and positron emission to levels in ^{108}Pd and by negatron emission to levels in ^{108}Cd.[66] There are considerable discrepancies in the reported branching to these levels in ^{108}Pd due to different γ-ray intensities.[50,55,67-72] In addition, a state at 1473 keV in ^{108}Cd which decays to 642 keV state with 841 keV γ-ray is reported only by Frevert (1962)[67] and a state at 1440 keV in ^{108}Pd was first reported by Taylor et al (1964).[72] The latter group also pointed out that there is feeding to a level at about 940 keV and that the 511 keV photons observed are from the depopulation of this level as well as from annihilation radiation. In coulomb excitation experiments on Cd isotopes by Milner et al (1969),[73] a 970 ± 1 keV line has been assigned as the transition from a second 2^+ state in ^{108}Cd lying at 1603 keV. Recently Johnson et al (1971)[70] reported that the 841 keV transition in ^{108}Cd was not observed. In addition, this group and Okano et al[71] (1970) showed that there is no evidence for the existence of a 1603 keV (2^+) state in ^{108}Cd. This is not surprising since this state is very near to the Q-value (1.63 MeV) for negatron decay. Even if it exists,

* REFERENCES: 55,67-69

the population of the two-photon states in ^{108}Cd in the decay of ^{108}Ag must be very weak. Because of these uncertainties, it was considered important to recheck carefully the gamma spectrum of ^{108g}Ag using a high resolution Ge(Li) detector.

3.2.2 EXPERIMENTAL PROCEDURES

Sources of about 1 mg each were prepared from a sample of 99.6% enriched ^{107}Ag metal purchased from the Stable Isotope Unit, A.E.R.E., Harwell. The samples were irradiated in the In-Core Irradiation System (I.C.I.S.) which provides for the fast transfer of samples in and out of the reactor core for either single or cyclic irradiation. The transfer tube is mounted inside an aluminium tube which passes from the reactor top through the centre of the core. The neutron flux is $\simeq 2 \times 10^{12} n.cm^{-2}s^{-1}$ and the irradiation periods varied from 20 secs. to 30 secs. Irradiated samples were then transferred pneumatically to the radiochemical laboratory. A 30 cc true-coaxial Ge(Li) detector of resolution 2.2 keV at 1.33 MeV was used in conjunction with a Laben 8000 multichannel analyser and Magnetic Tape System to record the γ-ray spectra. Each singles measurement, which lasted for a period of 5 mins, was begun about 100 secs. after irradiation to allow for the decay of the 24 sec. ^{110g}Ag impurity. Long-lived background contributions were determined by counting the samples about one hour after irradiation.

The measurements were repeated when Compton Suppression spectrometer was available. ^{107}Ag sample was placed in the thermal neutron beam of flux $2 \times 10^6 n.cm^{-2}sec^{-1}$, and the irradiation periods varied from 10 minutes to 30 minutes. The Compton Suppression spectrometer consists of a 72 cc true-coaxial Ge(Li) detector surrounded by a 20 cm diameter x 20 cm length NaI annulus. The details of this system are mentioned in Chapter 4. The procedure is the same as mentioned before.

3.2.3 Results and Discussion

The γ-ray spectra were analyzed using SAMPO program for energy and intensity determinations. The usual standard sources were used for energy and efficiency calibrations. The energies and intensities are presented in Table 3.3.

The energy values of 433.985 ± 0.008, 618.913 ± 0.027 and 633.067 ± 0.016 were taken from the results of $^{107}Ag(n,\gamma)^{108}Ag$ (Breitig et al 1974)[74,75] since it was impossible to measure the energies so accurately in this experiment. The intensity values, in the present work agree well with previously published results. The 510.8 keV gamma ray may be the composite of annihilation radiation and a weak gamma ray. So the intensity for the 510.8 could be somewhat low since no special effort was made to annihilate all of the positrons at the source. The error assigned does not take this into

consideration. The 841 keV γ-ray was reported by Frevert (1962)[67] and Okano et al (1971)[71]. Although this γ-ray was observed in the present measurement, only an upper limit for its intensity could be given. The 388 keV γ-ray is reported only by Okano et al (1971) and it was not seen in this work. An upper limit for its intensity is given. Most (if not all) of the intensity of 1052.1 keV γ-ray may result from true summing of the 433.99 and 618.91 keV γ-rays. Positron, electron capture, and beta branching to levels in ^{108}Pd and ^{108}Cd from the decay of ^{108}Ag as reported in the literature are given in Table 3.4 . The decay scheme of 2.41 min ground state of ^{108}Ag is given in Fig. 3.1 .

TABLE 3.3.

GAMMA RAY ENERGIES AND RELATIVE INTENSITIES OF TRANSITIONS IN THE DECAY OF 2.41 min ^{108}Ag

keV Present Work	Present Work	Okano et al (1971)	Johnson et al (1970)	Perlman et al (1953)	Wahlgren et al (1960)	Taylor et al (1964)	Frevert (1962)
433.985 ± 0.008	27.08 ± 1.02	100	26.6 ± 0.6	35	32	29	25.0
497.1 ± 0.5	0.06 ± 0.03	0.25 ± 0.09	0.07 ± 0.04	-	-		
510.8 ± 0.4	18.98 ± 1.24	-	25.7 ± 0.6	35	37	~ 34	32.4
618.913 ± 0.027	14.45 ± 0.92	54.1 ± 2.4	14.6 ± 0.4	27.5	22	)	15.0
633.067 ± 0.016	100	355.1 ±14.9	100	100	100	} 115	100
880.2 ± 0.4	0.12 ± 0.02	0.65 ± 0.03	0.12 ± 0.02				~ 1.2
930.8 ± 0.7	0.024 ± 0.013	0.091± 0.016	0.025± 0.012				
1006.8 ± 0.5	0.75 ± 0.05	2.71 ± 0.11	0.79 ± 0.08				
1052.6 ± 0.4	0.091 ± 0.011	-	0.13 ± 0.03				
1105.8 ± 0.5	0.091 ± 0.011	0.26 ± 0.02	0.13 ± 0.01				
1441.1 ± 0.4	0.13 ± 0.02	0.56 ± 0.04	0.14 ± 0.02				
1540.0 ± 0.5	0.05 ± 0.02	0.20 ± 0.02	0.040± 0.015				
388	<	< 0.2	-				
840	< 0.03	< 0.1	< 0.04				

TABLE 3.4.

POSITRON, ELECTRON CAPTURE AND BETA BRANCHING TO LEVELS IN ^{108}Pd AND ^{108}Cd FROM THE DECAY OF ^{108}Ag AS REPORTED IN THE LITERATURE

Level populated	FEEDING IN % PER DECAY			
	Perlman (1953)	Wahlgren (1960)	Frevert (1962)	Frevert (1965)
β^- ^{108}Cd ground	97.3	93.8	95.0 ± 0.3	95.9 ± 0.3
β^- ^{108}Cd 632.9 keV	0.8	1.9	1.73 ± 0.10	1.75 ± 0.10
β^- ^{108}Cd 1473 keV	-	-	~ 0.02	~ 0.02
β^+ ^{108}Pd ground	0.14	0.36	0.28 ± 0.02	0.28 ± 0.02
EC ^{108}Pd ground	1.5	3.35	2.49 ± 0.25	1.73 ± 0.12
EC ^{108}Pd 434 keV	0.06	0.18	0.19 ± 0.03	0.19 ± 0.03
EC ^{108}Pd 1053 keV	0.22	0.42	0.26 ± 0.03	0.27 ± 0.03

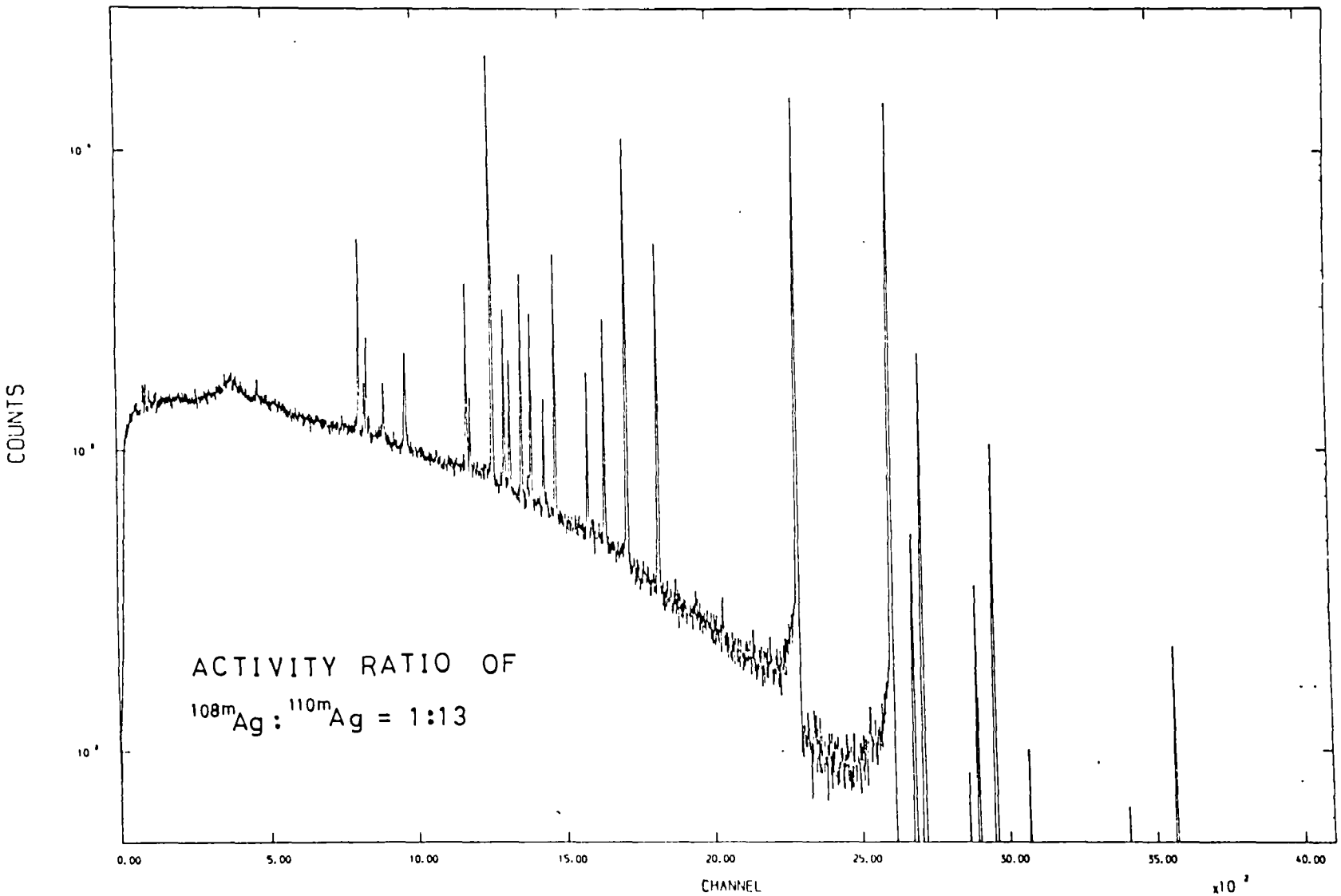


FIG. 3.2 ••••• SILVER 108M DECAY WITH COMPTON SUPPRESSION •••••

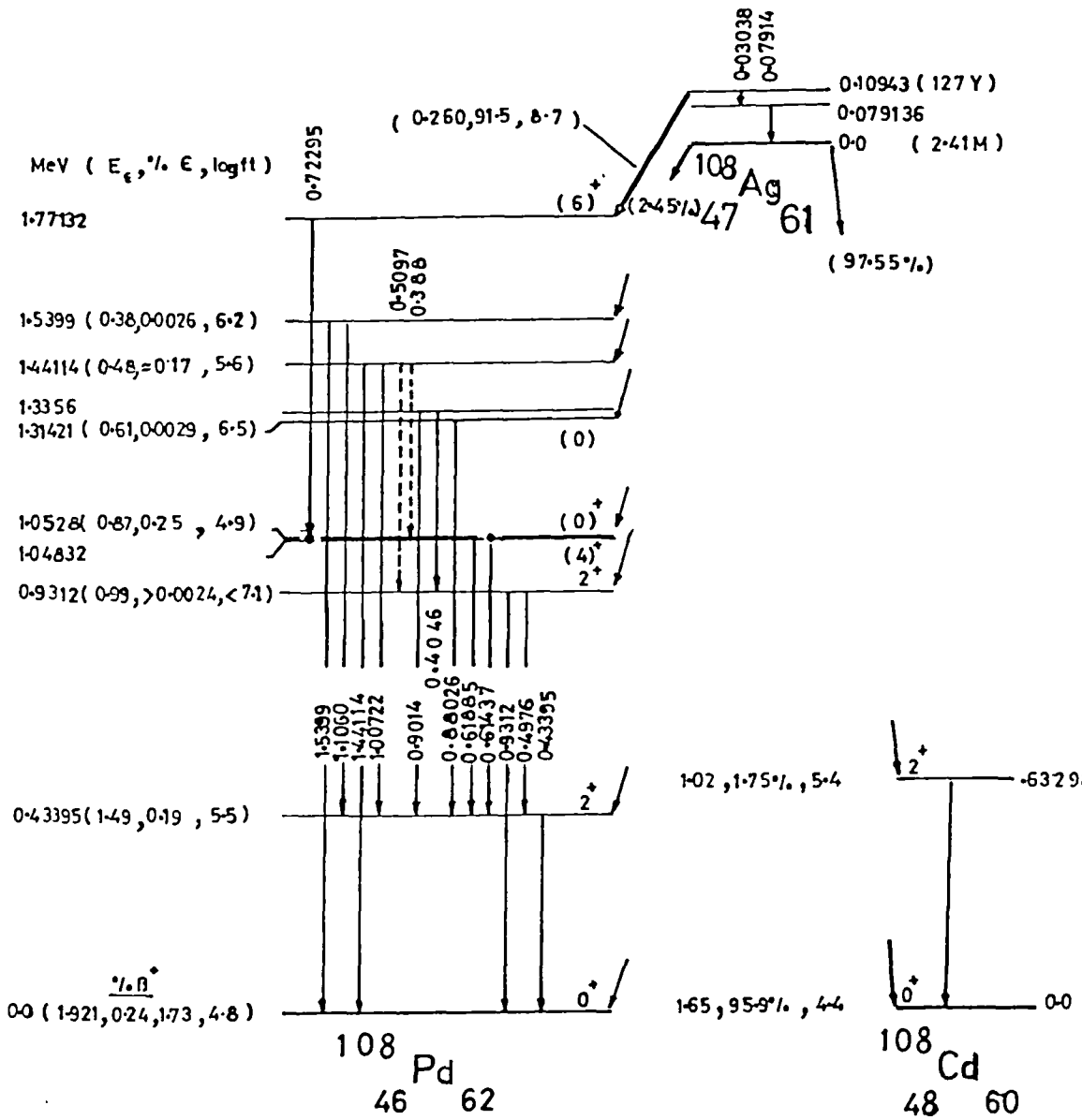


FIG. 3·1 DECAY SCHEME OF ^{108}Ag (Reference 81)

3.3. THE DECAY OF ^{110g}Ag

3.3.1 INTRODUCTION

In an earlier investigation of ^{110g}Ag decay, Boley (1954)[76] has reported γ-rays with energies of 660, 720, 810, 880 and 940 keV. Frevert et al (1963) then reported as finding only the 660 keV γ-ray and some evidence for a 1480 keV γ-ray. Later Moragues et al (1967)[77] reported evidence for the existence of γ-rays at 658, 770, 818, 950, 1130 and 1476 keV. More recently Van Hise et al (1970)[78] reported γ-rays with energies of 657.8, 815.6, 1125.9, 1186.4, 1421.8, 1475.8, 1630.0, 1674.2 and 1783.3 keV. They also reported evidence for the existence of a new level at 1473.2 keV, a few keV lower than a level at 1475.8 keV, which was observed for the $2^+ \rightarrow 2^+$ transition in the decay of ^{110m}Ag. The spin and parity of ^{110g}Ag is 1^+, which favours the depopulation to 0^+ states. The low-lying states of adjacent medium-weight nuclei (such as ^{108}Pd, ^{108}Cd) show collective motions many of which may be described by the quadrupole vibrator model. Although 2^+ and 4^+ members of the expected triplet of levels are frequently observed, the 0^+ member seems much more elusive and has less collective behaviour. Detailed information of the decay of ^{110g}Ag would, therefore, help in the formulation of a more meaningful theoretical description of two-phonon states.

3.3.2 Experimental Method and Results

Sources of about 1 mg each were prepared from a sample of metallic natural silver with 99.999% purity and sealed in polythene capsules. Each was irradiated for five to ten seconds in a thermal neutron flux of 2×10^{12} n-cm^{-2}sec^{-1} in the ICIS system. In addition, an empty polythene capsule was irradiated and measured to identify background γ-rays. Each singles measurement, which lasted for a period of 100 secs, was begun about one minute after irradiation. The γ-rays of the ^{110g}Ag decay can be distinguished from those of ^{108g}Ag using the knowledge gained in the study of the decay of ^{108g}Ag.

The energies and intensities obtained in the present work are shown in Table 3.5 . In addition to the data from the present measurements, the energies for the 657.76, 818.04 and 1475.75 keV transitions are taken from the previous ^{110m}Ag decay scheme measurements since these γ-rays are common in both decays. It was possible to determine the energies of these transitions in the decay of ^{110m}Ag with good accuracy, because of the absence of the problems associated with measurements on the very short-lived ^{110g}Ag.

The previously reported γ-ray at 770 keV was observed in present work as 771.2 keV, but only an upper limit could be given for its intensity. The 1630 keV γ-ray was not observed in the present work so that only an upper limit for its intensity is given. The 815 keV γ-ray energy agrees well with the value of Van Hise et al (1970)[78]. They have interpreted the new level at 1473.2 keV (which decays to 657.7 keV level through 815.5 keV γ-transition) as the 0^+ member of a two phonon-triplet. The 815 keV and 818 keV γ-rays were well resolved in this measurement since the energy gain was about 0.5 keV per channel.

TABLE 3.5.

GAMMA RAY ENERGIES AND INTENSITIES IN THE DECAY OF ^{110g}Ag

keV		Relative Intensity	
Present Work	Van Hise et al (1970)	Present Work	Van Hise et al
657.76 ± 0.03	657.8 ± 0.2	100	100
815.12 ± 0.16	815.5 ± 0.3	0.87 ± 0.15	0.79 ± 0.12
818.04 ± 0.04	817.8 ± 1.2	0.23 ± 0.10	0.19 ± 0.09
1126.05 ± 0.19	1125.9 ± 0.3	0.35 ± 0.04	0.36 ± 0.03
1186.6 ± 0.5	1186.4 ± 0.7	0.063± 0.020	0.056 ± 0.020
1421.5 ± 1.5	1421.8 ± 1.3	0.052± 0.025	0.044 ± 0.030
1475.75 ± 0.05	1475.8 ± 1.3	0.13 ± 0.04	0.11 ± 0.05
-	1630.0 ± 1.2	< 0.05	0.048 ± 0.030
1674.9 ± 1.3	1674.2 ± 0.9	0.17 ± 0.05	0.15 ± 0.06
1783.78 ± 0.20	1783.3 ± 1.3	0.17 ± 0.08	0.17 ± 0.09
771.2 ± 1.5	-	< 0.05	

3.4 Gamma Transitions in ^{110}Cd Following the Decay of ^{110m}Ag

3.4.1 Introduction

The primary features of the decay scheme of ^{110m}Ag were well established by 1964. All of the available data to that date were incorporated in the decay scheme given by Newbolt and Hamilton (1964)[79]. Several inconsistencies in the low energy beta branching ratios determined from beta spectra measurements and gamma ray intensities were also pointed out by those authors. With the availability of Ge(Li) detectors, the decay scheme of ^{110m}Ag was reinvestigated in order to measure the γ-ray energies and intensities more precisely and to clarify such questions. The 1967 edition of the Table of Isotopes (Lederer et al 1967)[50] contains the decay scheme of ^{110m}Ag. All of the available data to the year 1971 have been compiled by Bertrand and Raman (1971)[80]. More recently, however, it was revised by Horen et al (1973)[81].

In addition to accurately measuring γ-ray energies and intensities for the well established transitions in the ^{110m}Ag decay,[80] careful searches for several weak transitions (< 1%) have been reported by various authors.

Kracikova and Kracik (1967)[82] introduced nine new weak transitions. Brahmavar et al (1969)[83] tried to measure those weak transitions without success, but they observed three new weak transitions. However, Kracikova (1970)[84] again observed 23 weak transitions besides the 15 strong transitions. Also Phillips et al (1972)[85] could establish 18 weak transitions in their reinvestigation of ^{110m}Ag decay. A study of the reaction ^{109}Ag(^{3}He,d)^{110}Cd by Auble et al (1972)[86] has resulted in the observation of several new transitions in ^{110}Cd. They asked for a revised level diagram for this isotope. Pratt (1974)[89] has also recently reported a study of the radioactive decay of ^{110m}Ag. Several new weak transitions were observed.

The above situation prompted the present work on additional precise gamma ray energy and intensity measurements in the ^{110m}Ag decay. Accurate data on the transitions in the decay of ^{110m}Ag could also serve as convenient energy and intensity calibration standards as 15 transitions have an intensity greater than 1% and cover an energy range from 400 to 1600 keV. This reaction includes a resume of recent work on the γ-ray energies, intensities, beta branching ratios and log ft values to provide useful calibration standards.

3.4.2. EXPERIMENTAL PROCEDURES

The ^{110m}Ag($T_{\frac{1}{2}}$ = 250.4d) was prepared at the ULRC Consort 100 kW research reactor. Natural silver (99.999% purity) was irradiated in a thermal neutron flux of 10^{12}cm^{-2}s^{-1}. The thermal neutron capture cross

sections of ^{107}Ag and ^{109}Ag leading to $^{108g}Ag(T_{\frac{1}{2}} = 2.42$ min), $^{108m}Ag(T_{\frac{1}{2}} = 127$ y), $^{110g}Ag(T_{\frac{1}{2}} = 24.4$ s) and $^{110m}Ag(T_{\frac{1}{2}} = 250.4$ d) are (37.2 ± 1.2 b), (3.0 ± 1.5 b), (89 ± 4 b) and (4.5 ± 0.2 b) respectively. The sample was then allowed to cool for 2 days after irradiation so that any short lived impurities such as $^{108g-110g}Ag$ had decayed. A small contribution from ^{108m}Ag was observed.

A 33cc coaxial Ge(Li) detector was used with a Canberra 1412 research amplifier and a Laben 8000 multichannel analyser system. A resolution of 2.2 keV was obtained at 1.33 MeV gamma energy. The gamma-gamma coincident experiments were performed using 33 cc and 60 cc coaxial Ge(Li) detectors.

The calibrated standard sources (^{241}Am, ^{133}Ba, ^{57}Co, ^{60}Co, ^{137}Cs, ^{152}Eu, ^{22}Na and ^{88}Y) were used for the energy and efficiency calibrations.

3.4.3 GAMMA ENERGIES AND INTENSITIES IN ^{110m}Ag DECAY

Gamma Energies

Spectra, accumulated for periods ranging from 3 to 15 hours, were obtained of ^{110m}Ag alone, standard sources alone, and ^{110m}Ag together with standard sources. The background runs were also taken

at identical equipment settings as the singles runs to identify and eliminate transitions due to naturally occurring radioisotopes. Peak channel positions were determined using the SAMPO computer program. The peak positions and energies were fitted to a third order polynomial. The weighted average values are taken as final result and shown in Table 3.6.

Gamma Intensities

The singles spectra of ^{110m}Ag were taken at three different source-detector distances (5 cms, 10 cms and 15 cms). The area under the photopeak and efficiency calibrations were performed using the SAMPO program. Efficiency fittings were performed in two different energy regions (50 - 300 keV and 200 - 2000 keV) because of the shape of the efficiency curve of the Ge(Li) detectors.

The weighted average intensities are taken as final results and shown in Table 3.7. Intensity uncertainties include statistical uncertainties in the peak areas as well as a 2% uncertainty established for the efficiency curve.

Weak Transitions

One of the aims of this work was to search for weak transitions. Several experimental runs ranging 15 - 30 hours were carried

out with the Ge(Li) detector at different source-detector positions. Several sum peaks were observed in the high energy region. The single spectra were taken with lead absorber (2mms. thick) between source and detector. By analysing the changes in above spectra, sum peaks were identified.

Results and Discussion

The energies and relative intensities of the 15 well established gamma rays were shown in Tables 3.6 and 3.7 respectively in comparison with the previous published values. The present values are in reasonable agreement with those values.

The energies and relative intensities for the weak transitions obtained in the present work are shown in Table 3.8 together with the previous results by Pratt (1974)[89], Kracikova (1970)[84] and Phillips et al (1972)[85]. The present energies agree with those values given by Phillips. Although there are differences within one standard deviation for low energy region, the present values are in reasonable agreement with the values of Pratt. The energies given by Kracikova differ from the others by more than one standard deviation.

The present relative intensities of weak transitions agree well with the values given by Phillips[85].

3.4.4. INTERNAL CONVERSION COEFFICIENTS

The K-Electron Internal Conversion Coefficients

The gamma-ray relative intensities measured in the present work combined with published values of the K-shell internal conversion electron relative intensities were used to calculate K-electron internal conversion coefficients (ICC). The most precise values of K-conversion electron relative intensities were adopted from Newbolt and Hamilton (1964)[79] and Moragues (1967)[77]. Using the well known fact that the 657.76 keV ($2^+ \rightarrow 0^+$) transition has a pure E2 character, the theoretical value of $\alpha_K(657.8) = 2.75 \times 10^{-3}$ (Hager & Seltzer 1968)[90] was taken to bind the gamma ray and K-converted electron relative intensities. The K-electron ICC obtained and the theoretical values for α_K of pure E2 and M1 multipolarities calculated by interpolation between the values given by Hager and Seltzer (1968)[90] are presented in Table 3.9. The multipole assignments, made on the basis of the experimental data, are also included in the table.

It is easily seen that the present values of α_K for the 677.6 and 818.0 keV transitions indicate dominant E2 multipolarity with a few percent of M1 multipolarity. For 1384.3, 1505.1 and 1562.30 keV transitions, M1 multipolarity is dominant.

The experimental α_K for the 706.70 keV transition agrees with the theoretical α_K for M1 multipolarity. However, in view of the large experimental error, a small contribution of E2 to a mixture E2 + M1 is possible.

The experimental α_K values for the 446.8, 620.3 and 687.0 keV transitions are lower than the theoretical ones for both E2 and M1, which are relatively close to each other. From the spins and parities of the levels between which the transitions take place, it is concluded that a mixture of E2 + M1 is possible.

The 657.8, 744.3, 763.9, 884.7, 937.52 and 1475.8 keV transitions have a pure E2 character. Our values for α_K strengthen this assignment.

Internal Conversion Coefficients

Internal conversion coefficients α may be calculated from the K-electron ICC, by employing $(K + L + M + ---/K)$ as the conversion intensity ratio:

$$\alpha = \alpha_K (K + L + M + ---/K)$$

The ICC values for different shells, used in the present work, are given in Table 3.9 together with the internal conversion coefficients obtained.

3.4.5. THE DECAY SCHEME OF $^{110m}Ag \rightarrow ^{110}Cd$

The Beta Branching Ratios

The decay scheme of ^{110m}Ag composed of the 15 strong transitions has been well established for some time.[*] The present task is to place as many of the new weak transitions in the decay scheme as possible and to work out level energies in ^{110}Cd, β^- branching ratios, absolute gamma ray intensities and log ft values on the basis of the decay scheme mentioned by Horen et al (1973).[81]

In Fig.3.4 is presented a scheme for the decay of ^{110m}Ag to levels of ^{110}Cd which incorporates in a consistent manner the data of the present work as well as those of earlier investigators.

The ^{110m}Ag with the half-life of (250.4 d) de-excites to the ground state of $^{110}Ag(T_{\frac{1}{2}} = 24.42 \pm 0.14$ s) and depopulates by β^- decay to the levels of ^{110}Cd. The level energies, shown in Fig.3.4 are based on the gamma ray transition energy balance for each level.

From the internal conversion coefficients and the relative intensities of the gamma transitions, the β^- branching ratios and the absolute gamma ray intensities were calculated by employing the feeding and depopulation of the levels. Denoting the β^- branching

[*] REFERENCE: 46, 79-89, 92, 93

ratios to 2926.75, 2876.79, 2659.81, 2561.10, 2539.58, 2479.95, 2220.04, 2162.76 and 1542.43 keV levels by A, B, C, D, E, F, G, H, and I respectively and X as a factor for converting from gamma ray relative units to absolute gammas per disintegration, the following results are obtained:

$$A = 68.70 \pm 1.94\%$$

$$B = 0.398 \pm 0.105\%$$

$$C = 0.027 \pm 0.007\%$$

$$E = 0.114 \pm 0.027\%$$

$$F = 30.70 \pm 0.96\%$$

$$I < 0.040 \%\ ;\ D = G = H \simeq 0$$

$$X = 0.9430 \pm 0.0233$$

The beta branching ratios, obtained in the present work, are shown in Table 3.10 together with the previously published results.

Absolute Gamma-Ray Intensities

The absolute gamma ray intensities were calculated from the relative intensities by multiplying with the factor X = 0.9430 ± 0.0233. The results in units of gammas per hundred disintegrations are given in Table 3.11. The absolute intensity for 567.76 keV (the reference gamma for ^{110m}Ag) agree well with that value given by the Nuclear Data Group.[80] The two results are presented.

The log ft Values

The beta energy leading to the 2927 keV level is 83 keV (Horen, Bertrand and Auble 1973). This implies that the β^- energies to the 2877, 2660, 2540, 2480 and 1542 keV levels should be 133, 350, 470, 530 and 1468 keV respectively. The log ft values were calculated according to the method suggested by Table of Isotopes. The values obtained are given in Table 3.10 with other published data.

3.4.6 Discussion

The level scheme presented in Fig. 3.4 essentially coincides with the one proposed by W.W. Pratt (1974) and confirmed by many other investigators.

The gamma-gamma coincidence data are thoroughly covered for 15 strong lines by separate coincidence measurements using 33 cc and 60 cc Ge(Li) detectors together with the Dual parameter data collection coincidence system (Yusof Sulaiman and Thomas) with time resolution of 80 ns. Fig. 3.5 displays some of the coincidence spectra. Coincidence results are given in Table 3.12. Present results are in good agreement with Krane et al (1970).

The 2881 keV level This level is in agreement with a level established by A.W. Sunyar et al (1971). The J^π value is assigned as 7^-.

The 2662 keV level This level is reported in $^{108,110}Cd(^3He,d)$ reactions. The J^π value is assigned as $(0-2)^+$.

The 2465 and 2332 keV levels These two levels are simply taken from Cd(t,d) reaction investigations to fit the weak gamma transition energies. The J^{π} value for the latter level is given as $(0^+ - 2^+)$.

The 2251 keV level This level is introduced for weak gamma transitions. Energy-wise, the 626 and 229 keV transitions fit very well between this level and 2877 and 2480 levels respectively.

The 1784 keV level This level is reported by several investigators[78,85,96] for both ^{110g}Ag and ^{110m}Ag decays. The former work established this as a $(2,1)^+$ level which decays by the 1784 keV transition to the ground state of ^{110}Cd and by the 1126 keV transition to the 658 keV level. The adopted relative intensities values of these transitions in ^{110g}Ag decay are 0.17 ± 0.09 and 0.36 ± 0.03 respectively. As pointed out by Phillips et al (1972)[85], in the decay of ^{110m}Ag only 1.4% of the decay is to the ground state of ^{110}Ag. Bearing in mind the experimental relative intensities as 0.012 and 0.032, it would indicate that this level must also be populated by gamma decay which follows the beta decay of ^{110m}Ag.

TABLE 3.6

GAMMA TRANSITION ENERGIES IN ^{110m}Ag DECAY

PRESENT WORK	LAVI	HAMILTON	LEGRAND	AUBIN	KRACIKOVA	KERN
446.80 ± 0.03	446.60 ± 0.20	446.78 ± 0.04	446.89 ± 0.16	446.89 ± 0.08	446.8 ± 0.6	446.79 ± 0.02
620.33 ± 0.03	620.18 ± 0.10	620.24 ± 0.03	620.45 ± 0.16	620.36 ± 0.08	620.2 ± 0.5	620.31 ± 0.02
657.76 ± 0.03	657.70 ± 0.11	657.72 ± 0.03	657.76 ± 0.04	657.72 ± 0.04	657.7 ± 0.4	657.72 ± 0.02
677.59 ± 0.03	677.57	677.56 ± 0.03	677.71 ± 0.12	677.61 ± 0.05	677.5 ± 0.5	677.58 ± 0.03
686.96 ± 0.03	686.71 ± 0.20	686.83 ± 0.03	687.06 ± 0.16	686.96 ± 0.05	686.8 ± 0.5	686.95 ± 0.03
706.70 ± 0.03	706.78 ± 0.20	706.66 ± 0.04	706.64 ± 0.06	706.68 ± 0.05	706.5 ± 0.5	706.65 ± 0.02
744.30 ± 0.03	744.33 ± 0.09	744.20 ± 0.04	744.32 ± 0.12	744.27 ± 0.07	744.0 ± 0.5	744.26 ± 0.02
763.91 ± 0.03	763.81 ± 0.18	763.88 ± 0.04	763.90 ± 0.06	763.93 ± 0.05	763.5 ± 0.5	763.92 ± 0.03
818.04 ± 0.03	818.25 ± 0.20	818.01 ± 0.04	818.05 ± 0.08	818.00 ± 0.06	818.0 ± 0.5	818.00 ± 0.03
884.67 ± 0.04	884.22 ± 0.08	884.66 ± 0.04	884.66 ± 0.04	884.61 ± 0.05	884.5 ± 0.5	884.65 ± 0.03
937.45 ± 0.04	937.42 ± 0.10	937.47 ± 0.04	937.46 ± 0.06	937.40 ± 0.05	937.5 ± 0.5	937.45 ± 0.03
1384.32 ± 0.05	1383.85 ± 0.20	1384.22 ± 0.04	1384.35 ± 0.06	1384.30 ± 0.05	1384.0 ± 0.5	1384.24 ± 0.04
1475.75 ± 0.05	1475.42 ± 0.16	1475.75 ± 0.04	1475.81 ± 0.08	1475.77 ± 0.07	1475.5 ± 0.6	1475.71 ± 0.04
1504.95 ± 0.05	1504.65 ± 0.29	1504.91 ± 0.08	1505.11 ± 0.14	1504.94 ± 0.07	1505.0 ± 0.6	1504.95 ± 0.04
1562.10 ± 0.05	1561.92 ± 0.20	1562.23 ± 0.06	1562.37 ± 0.12	1562.17 ± 0.08	1561.5 ± 0.7	1562.26 ± 0.05

TABLE 3.7

RELATIVE GAMMA INTENSITIES IN ^{110m}Ag DECAY

keV	PRESENT WORK	LAVI	HAMILTON	LEGRAND	AUBIN	KRACIKOVA
446.80 ± 0.03	3.67 ± 0.14	3.57 ± 0.71	3.5 ± 0.2	3.6 ± 0.2	3.73 ± 0.14	3.0 ± 0.3
620.33 ± 0.03	2.98 ± 0.07	2.79 ± 0.06	2.7 ± 0.2	2.5 ± 0.2	2.88 ± 0.14	2.7 ± 0.3
657.76 ± 0.03	100	100	100	100	100	100
677.59 ± 0.03	11.45 ± 0.32	11.93 ± 0.41	11.5 ± 0.4	10.4 ± 0.4	11.77 ± 0.31	13.9 ± 1.5
686.96 ± 0.03	6.95 ± 0.19	7.25 ± 0.33	7.1 ± 0.3	6.7 ± 0.3	7.15 ± 0.22	7.5 ± 1.0
706.70 ± 0.03	17.57 ± 0.41	17.15 ± 0.85	17.2 ± 0.4	17.2 ± 0.3	17.60 ± 0.40	16.6 ± 1.5
744.30 ± 0.03	5.03 ± 0.12	4.43 ± 0.13	4.7 ± 0.3	5.3 ± 0.3	4.75 ± 0.20	4.1 ± 0.6
763.91 ± 0.03	23.94 ± 0.62	23.73 ± 0.72	23.9 ± 0.9	24.1 ± 1.0	23.82 ± 0.61	22.6 ± 2.0
818.04 ± 0.04	7.87 ± 0.22	7.81 ± 0.39	7.7 ± 0.3	7.4 ± 0.3	7.75 ± 0.25	7.6 ± 0.7
884.67 ± 0.04	78.46 ± 1.94	80.28 ± 4.01	78.0 ± 1.6	76.0 ± 0.6	77.85 ± 1.55	81.1 ± 8.0
937.45 ± 0.04	36.50 ± 0.80	37.31 ± 1.42	36.3 ± 0.8	35.9 ± 0.5	36.30 ± 0.80	36.5 ± 3.0
1384.32 ± 0.05	27.65 ± 0.64	28.26 ± 1.42	27.6 ± 0.6	27.2 ± 0.6	27.41 ± 0.62	29.8 ± 2.0
1475.75 ± 0.05	4.65 ± 0.11	4.44 ± 0.16	4.6 ± 0.2	4.6 ± 0.2	4.51 ± 0.18	5.2 ± 0.5
1504.95 ± 0.05	14.74 ± 0.44	15.19 ± 0.49	14.7 ± 0.4	14.6 ± 0.4	14.75 ± 0.30	16.2 ± 2.0
1562.10 ± 0.05	1.36 ± 0.04	1.40 ± 0.09	1.34 ± 0.07	1.5 ± 0.4	1.25 ± 0.10	1.4 ± 0.1

TABLE 3.8

ENERGIES AND RELATIVE INTENSITIES OF WEAK GAMMA TRANSITIONS IN ^{110m}Ag DECAY

PRESENT WORK		PRATT		PHILLIPS		TRANSITIONS IN ^{110m}Cd
E_γ	I_γ	E_γ	I_γ	E_γ	I_γ	
120.22 ± 0.14	0.016 ± 0.005			120.0 ± 0.1	< 0.015	2659.8 - 2539.6
133.40 ± 0.04	0.079 ± 0.005	133.0 ± 0.3	0.056 ± 0.010	133.2 ± 0.2	0.09 ± 0.02	2465.2 - 2331.8
219.25 ± 0.10	0.035 ± 0.009	219.0 ± 0.4	0.041 ± 0.010	219.7 ± 0.3	0.13 ± 0.03	2880.6 - 2662.
220.75 ± 0.10	0.005 ± 0.009	220.6 ± 0.4	0.041 ± 0.010	221.4 ± 0.3	0.11 ± 0.03	2880.6 - 2659.8
229.35 ± 0.16	0.0290± 0.010		< 0.015	229.0 ± 0.3	0.052 ± 0.015	2479.9 - 2250.5
266.49 ± 0.07	0.044 ± 0.007		< 0.020	266.4 ± 0.2	0.05 ± 0.01	2926.8 - 2659.8
365.03 ± 0.06	0.118 ± 0.012	365.3 ± 0.3	0.090 ± 0.020	365.1 ± 0.1	0.11 ± 0.02	2926.8 - 2561.1
386.95 ± 0.11	0.047 ± 0.016		< 0.030	386.6 ± 0.2	0.043 ± 0.009	2926.8 - 2539.6
396.75 ± 0.10	0.041 ± 0.015		< 0.015	396.7 ± 0.3	0.036 ± 0.008	2876.8 - 2479.9
626.26 ±	0.215 ± 0.014	626.4 ± 0.3	0.140 ± 0.030	626.1 ± 0.1	0.19 ± 0.03	2876.8 - 2250.5
997.15 ± 0.12	0.137 ± 0.017	996.8 ± 0.3	0.135 ± 0.025	997.1 ± 0.1	0.14 ± 0.02	2539.6 - 1542.4
1018.67 ± 0.15	0.030 ± 0.005		< 0.012	1018.7 ± 0.4	0.03 ± 0.01	2561.1 - 1542.4
1085.35 ± 0.11	0.070 ± 0.012	1085.4 ± 1.0	0.072 ± 0.020	1085.7 ± 0.3	0.058 ± 0.008	2561.1 - 1475.8
1117.38 ± 0.05	0.057 ± 0.016	1117.3 ± 1.0	0.038 ± 0.015	1117.4 ± 0.3	0.039 ± 0.007	2659.8 - 1542.4
1126.03 ± 0.12	0.032 ± 0.08		< 0.022	1125.7 ± 0.3	0.026 ± 0.006	1783.8 - 657.8
	< 0.025		< 0.040	1252.0 ± 1.5	0.058 ± 0.019	-
1334.44 ± 0.06	0.166 ± 0.011	1334.5 ± 0.6	0.111 ± 0.015	1334.4 ± 0.2	0.16 ± 0.03	2876.8 - 1542.4
1783.78 ± 0.20	0.012 ± 0.003	1783.7 ± 0.6	0.007 ± 0.002	1783.8 ± 1.0	0.010 ± 0.004	1783.8 - 0
1903.48 ± 0.10	0.017 ± 0.004	1903.5 ± 0.6	0.016 ± 0.005	1903.2 ± 0.3	0.017 ± 0.004	2561.1 - 657.8

TABLE 3.9

INTERNAL CONVERSION COEFFICIENTS AND TRANSITION MULTIPOLARITIES OF ^{110m}Ag DECAY

Gamma Ray Energy keV	Gamma Ray Relative Intensity	Conversion Shell	Relative Electron Intensity(a)	Experimental $\alpha_K(x10^3)$	*Theoretical $\alpha_K(x10^3)$ M1	E2	Experimental $\alpha_K(x10^3)$	Transition Multipolarity
446.80	3.67 ± 0.14	K	9.2 ± 1.0(b)	6.89 ± 0.79	7.84	8.21	6.89 ± 0.79	M1 + E2
620.33	2.78 ± 0.07	K	3.2 ± 0.3	3.16 ± 0.29	3.48	3.20	3.16 ± 0.29	M1 + E2
657.76	100	K L M + N	100	2.75	3.03	2.75	3.17	E2
677.59	11.45 ± 0.32	K L	10.9 ± 0.8 1.2 ± 0.3	2.62 ± 0.21	2.83	2.54	2.91 ± 0.23	M1 + E2
686.96	6.95 ± 0.19	K L M + N	6.0 ± 0.5 0.7 ± 0.2 0.11 ± 0.05	2.37 ± 0.21	2.74	2.45	2.63 ± 0.23	M1 + E2
706.70	17.57 ± 0.41	K L M + N	16.0 ± 0.9 1.80 ± 0.15 0.33 ± 0.07	2.50 ± 0.15	2.57	2.29	2.84 ± 0.17	M1
744.30	5.03 ± 0.12	K L M + N	3.6 ± 0.3 0.3 ± 0.1 0.11 ± 0.05	1.97 ± 0.17	2.27	2.00	2.19 ± 0.19	E2
763.91	23.94 ± 0.62	K L) M + N)	16.5 ± 0.5(b) 2.3 ± 0.5	1.90 ± 0.08	2.14	1.88	2.16 ± 0.09	E2
818.04	7.87 ± 0.22	K L	4.7 ± 0.3 0.4 ± 0.1	1.64 ± 0.11	1.83	1.59	1.78 ± 0.12	M1 + E2

TABLE 3.9 (continued)

INTERNAL CONVERSION COEFFICIENTS AND TRANSITION MULTIPOLARITIES OF ^{110m}Ag DECAY

Gamma Ray Energy keV	Gamma Ray Relative Intensity	Conversion Shell	Relative Electron Intensity(a)	Experimental $\alpha_K(x10^3)$	*Theoretical $\alpha_K(x10^3)$ M1	E2	Experimental $\alpha_K(x10^3)$	Transition Multipolarity
884.67	78.46 ± 1.94	K L	37.6 ± 1.0 4.1 ± 0.4	1.32 ± 0.05	1.53	1.32	1.46 ± 0.03	E2
937.45	36.50 ± 0.80	K L + M + N	15.5 ± 1.0 2.2 ± 0.2	1.17 ± 0.08	1.34	1.15	1.33 ± 0.09	E2
1384.32	27.65 ± 0.64	K L + M + N	5.6 ± 0.4 0.72 ± 0.06	0.56 ± 0.04	0.58	0.50	0.63 ± 0.05	M1 + E2
1475.75	4.65 ± 0.11	K	0.68 ± 0.08	0.40 ± 0.05	0.50	0.44	0.40 ± 0.05	E2
1504.95	14.74 ± 0.44	K L + M + N	2.4 ± 0.2 0.31 ± 0.08	0.45 ± 0.04	0.48	0.43	0.51 ± 0.05	M1 + E2
1562.10	1.36 ± 0.04	K	0.22 ± 0.03	0.44 ± 0.05	0.45	0.39	0.44 ± 0.05	M1 + E2

(a) From Moragues (1967)

(b) From Newbolt (1964)

* Hager et al (1968) can be applied as well

TABLE 3.10

BETA BRANCHING RATIOS (%) AND LOG (ft) VALUES

Level in ^{110}Cd (MeV)	β^--energy (MeV)	Present Work		Nucl. Data Sheets		KRACIKOVA		PHILLIPS		TYPE
		B.R.	log ft	B.R.	log ft	B.R.	log ft	B.R.	log ft	
2.927	0.083	68.70 ± 0.96	5.4	68.1	5.4	65	5.4	67.8	5.4	Allowed (GT)
2.877	0.133	0.398 ± 0.105	8.2	0.36	8.3	-	-	-	-	Allowed (F + GT)
2.660	0.350	0.027 ± 0.007	10.8	0.04	10.6	-	-	-	-	1st Forbidden (F + GT)
2.540	0.470	0.114 ± 0.027	10.6	0.13	10.5	-	-	-	-	1st Forbidden (F + GT)
2.480	0.530	30.70 ± 0.96	8.3	34.2	8.2	33	8.3	30.9	8.2	Allowed (F + GT)
1.542	1.468	<0.04	>12.8	-	-	0.04	11	0.2	12.1	Forbidden

TABLE 3.11

ENERGIES AND ABSOLUTE INTENSITIES
OF GAMMA-RAYS IN ^{110m}Ag DECAY

keV	I_γ% (Present Work)	I_γ% (Nucl. Data Sheets)
120.22 ± 0.14	0.015 ± 0.005	?
133.40 ± 0.04	0.074 ± 0.005	-
219.25 ± 0.10	0.033 ± 0.009	-
220.75 ± 0.10	0.033 ± 0.009	-
229.35 ± 0.16	0.028 ± 0.010	-
266.49 ± 0.07	0.041 ± 0.007	0.05
365.03 ± 0.06	0.111 ± 0.012	0.10
386.95 ± 0.11	0.044 ± 0.016	-
396.75 ± 0.10	0.039 ± 0.015	0.034
446.80 ± 0.03	3.46 ± 0.13	3.3
620.33 ± 0.03	2.81 ± 0.07	2.6
626.26 ± 0.08	0.203 ± 0.014	-
657.76 ± 0.03	94.30 ± 2.33	94.3
677.59 ± 0.03	10.80 ± 0.30	10.8
686.96 ± 0.03	6.55 ± 0.18	6.7
706.70 ± 0.03	16.57 ± 0.39	16.2
744.30 ± 0.03	4.74 ± 0.11	4.4
763.91 ± 0.03	22.57 ± 0.58	22.5
818.04 ± 0.03	7.42 ± 0.21	7.3
884.67 ± 0.04	73.98 ± 1.83	73.6
937.45 ± 0.04	34.42 ± 0.75	34.2
997.15 ± 0.12	0.129 ± 0.017	0.13
1018.67 ± 0.15	0.028 ± 0.005	0.03
1085.35 ± 0.11	0.066 ± 0.012	0.055
1117.38 ± 0.05	0.054 ± 0.016	0.037
1126.03 ± 0.12	0.030 ± 0.008	-
1334.44 ± 0.06	0.157 ± 0.011	0.14
1384.32 ± 0.05	26.07 ± 0.60	26.0
1475.75 ± 0.05	4.38 ± 0.10	4.3
1504.95 ± 0.05	13.90 ± 0.42	13.9
1562.10 ± 0.05	1.28 ± 0.04	1.3
1783.78 ± 0.20	0.011 ± 0.003	-
1903.48 ± 0.10	0.016 ± 0.004	0.016

TABLE 3.12

Gamma-Gamma Coincident Data

E_γ	Gating Transition				
	0.658	0.764	0.885	0.937	0.707
0.447	√	–	√	√	–
0.620	√	√	√	–	–
0.658	–	√	√	√	√
0.678	√	–	√	–	√
0.687	√	√	–	–	–
0.707	√	–	√	–	–
0.744	√	–	–	–	√
0.764	√	–	√	–	–
0.818	√	√	–	–	√
0.885	√	√	–	√	√
0.937	√	–	√	–	–
1.384	√	–	√	–	–
1.476	–	√	–	–	√
1.505	√	√	–	–	–
1.562	√	–	–	–	√

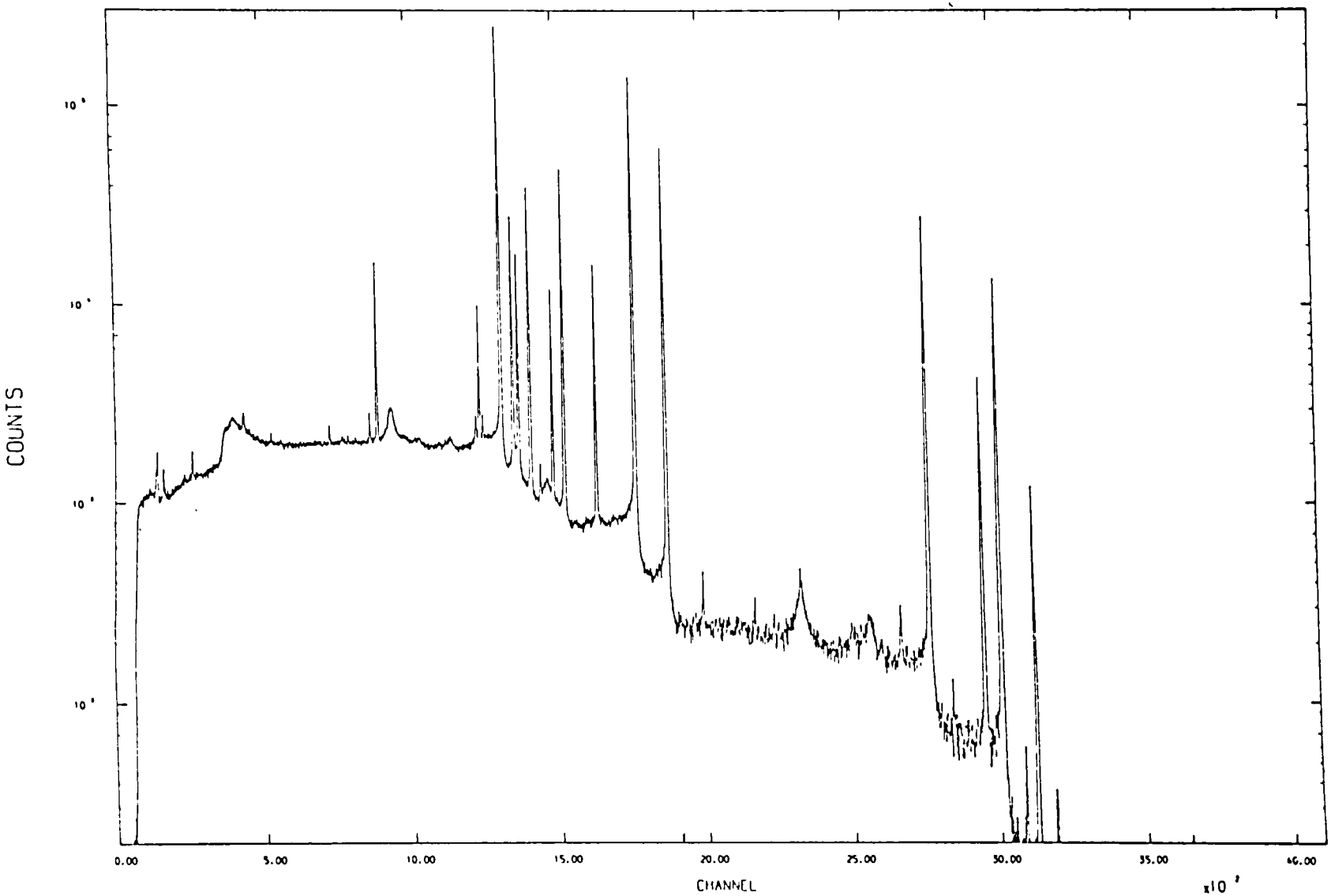


FIG.3.3 ••••• SILVER 110M DECAY SPECTRUM WITH COMPTON SUPPRESSION •••••

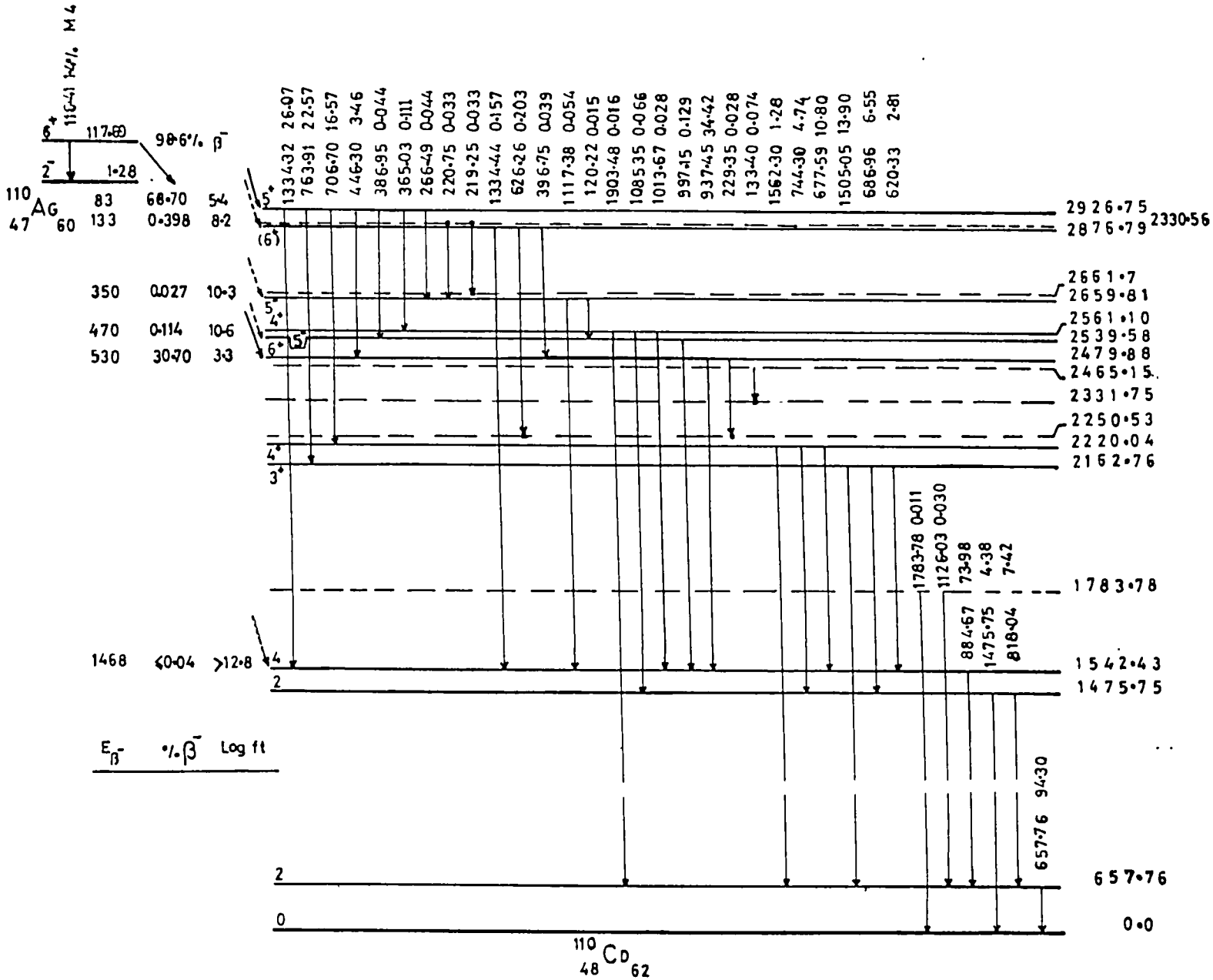
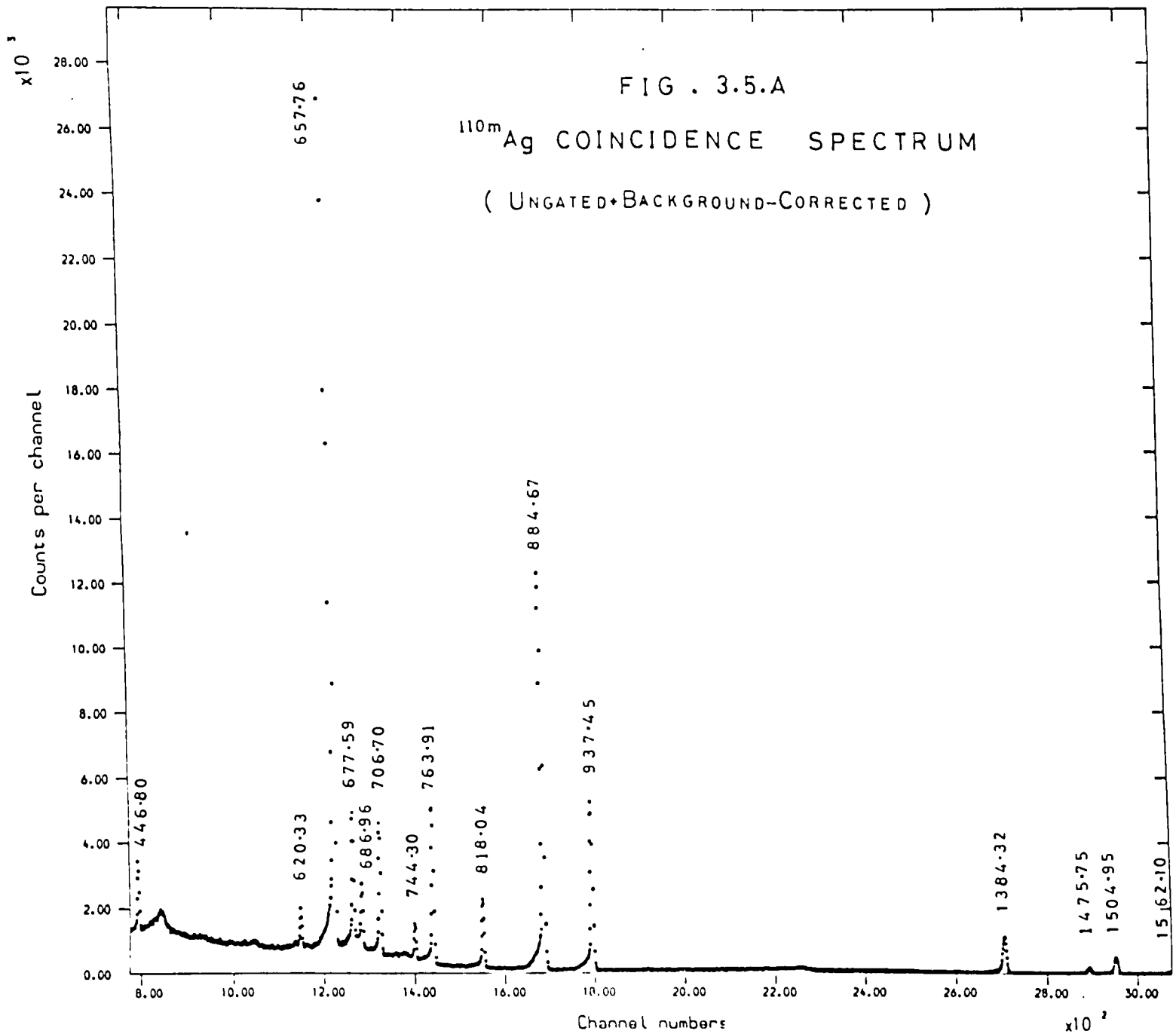
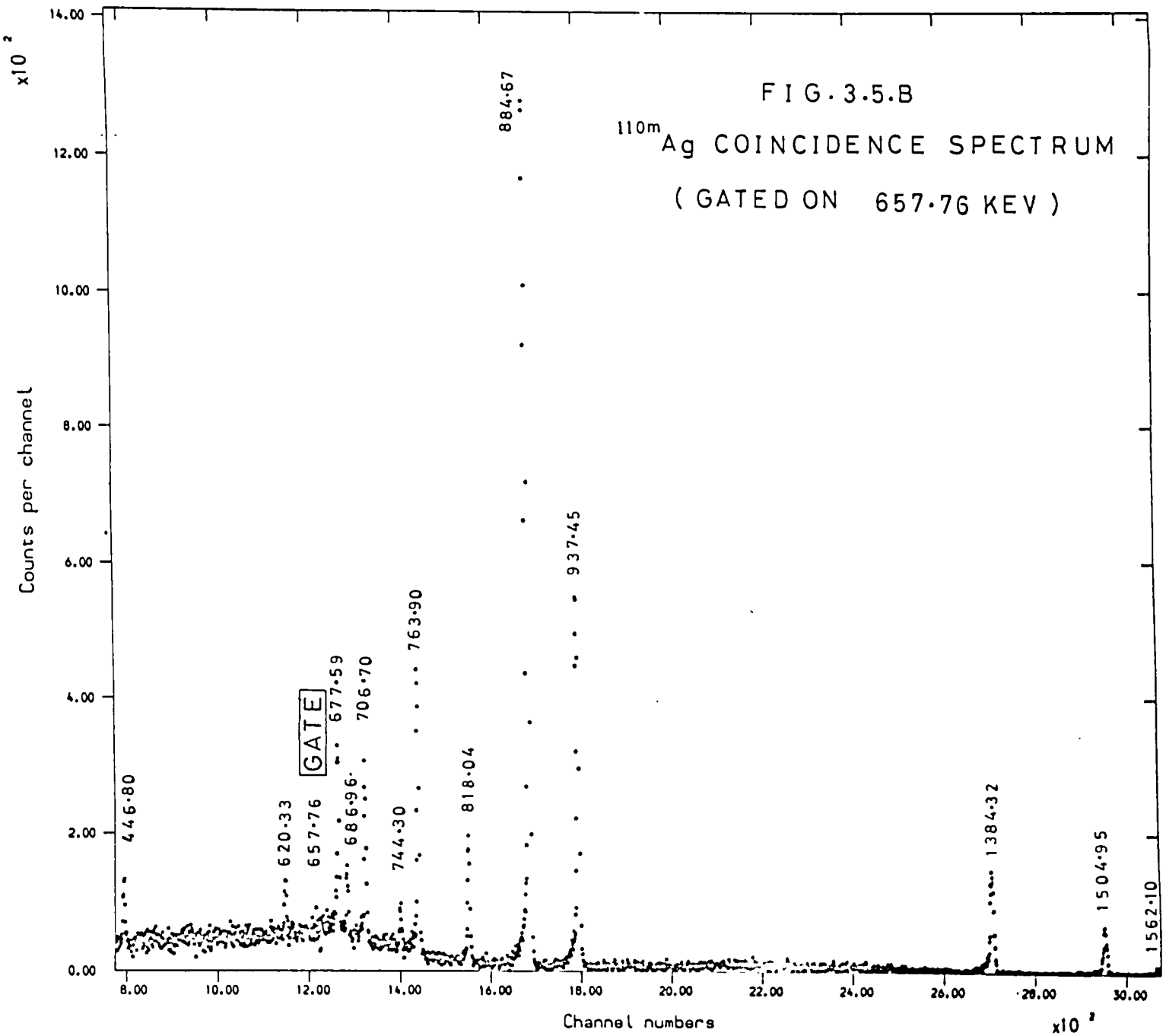
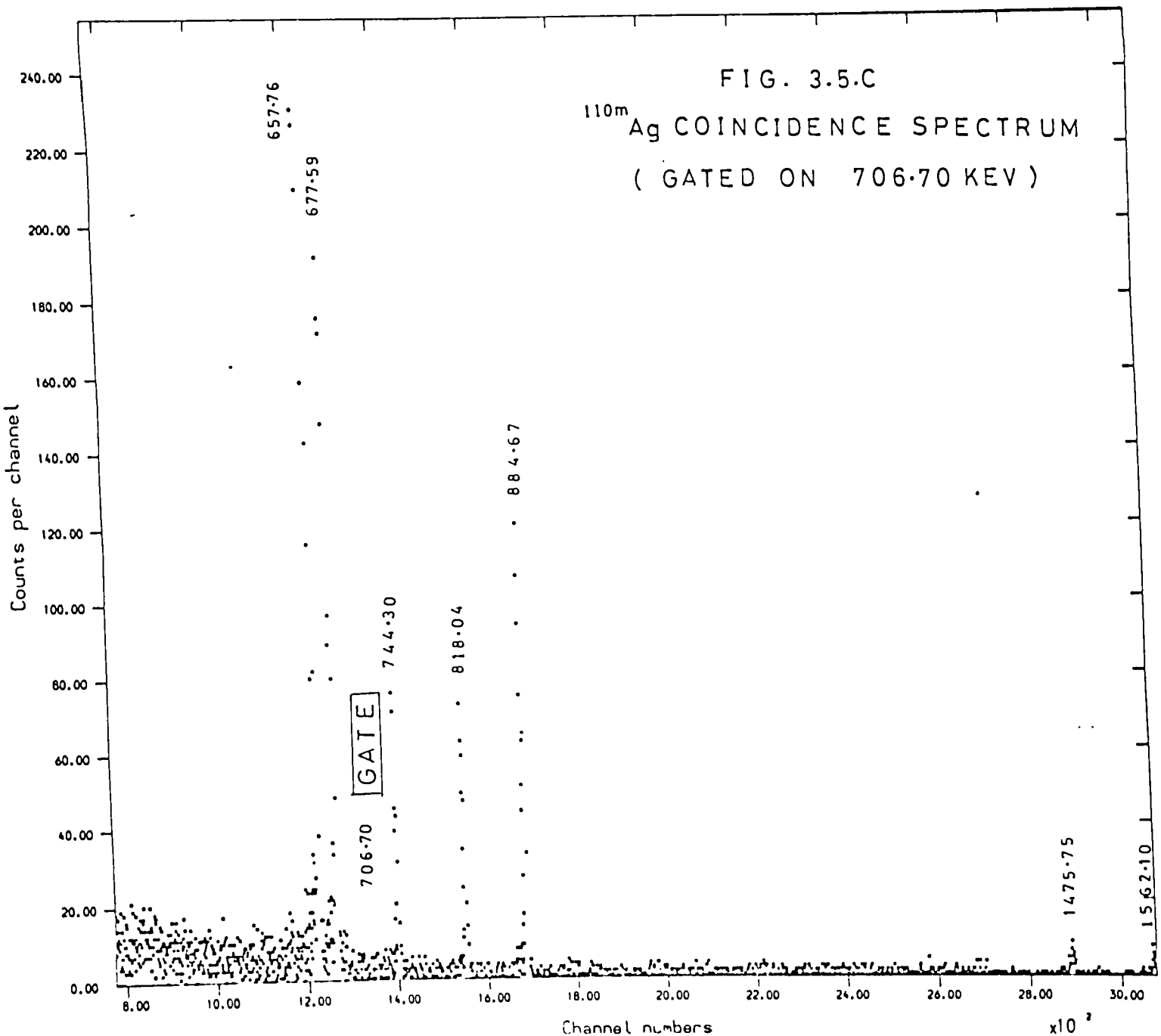


FIG.3.4 ^{110m}Ag Decay Scheme (Transitions per 100 decays)


FIG . 3.5.A
110m Ag COINCIDENCE SPECTRUM
(UNGATED+BACKGROUND-CORRECTED)
Counts per channel
x10 3
Channel numbers
x10 2
657·76
446·80
620·33
677·59
686·96
706·70
744·30
763·91
818·04
884·67
937·45
1384·32
1475·75
1504·95
1562·10


FIG. 3.5.B
110m Ag COINCIDENCE SPECTRUM
(GATED ON 657·76 KEV)
Counts per channel
x10 ²
Channel numbers
x10 ²
GATE
446·80
620·33
657·76
677·59
686·96
706·70
744·30
763·90
818·04
884·67
937·45
1384·32
1504·95
1562·10
0.00
2.00
4.00
6.00
8.00
10.00
12.00
14.00
8.00
10.00
12.00
14.00
16.00
18.00
20.00
22.00
24.00
26.00
28.00
30.00


FIG. 3.5.C
110m Ag COINCIDENCE SPECTRUM
(GATED ON 706·70 KEV)
Counts per channel
Channel numbers
x10 2
GATE
657·76
677·59
706·70
744·30
818·04
884·67
1475·75
1562·10
0.00
20.00
40.00
60.00
80.00
100.00
120.00
140.00
160.00
180.00
200.00
220.00
240.00
8.00
10.00
12.00
14.00
16.00
18.00
20.00
22.00
24.00
26.00
28.00
30.00

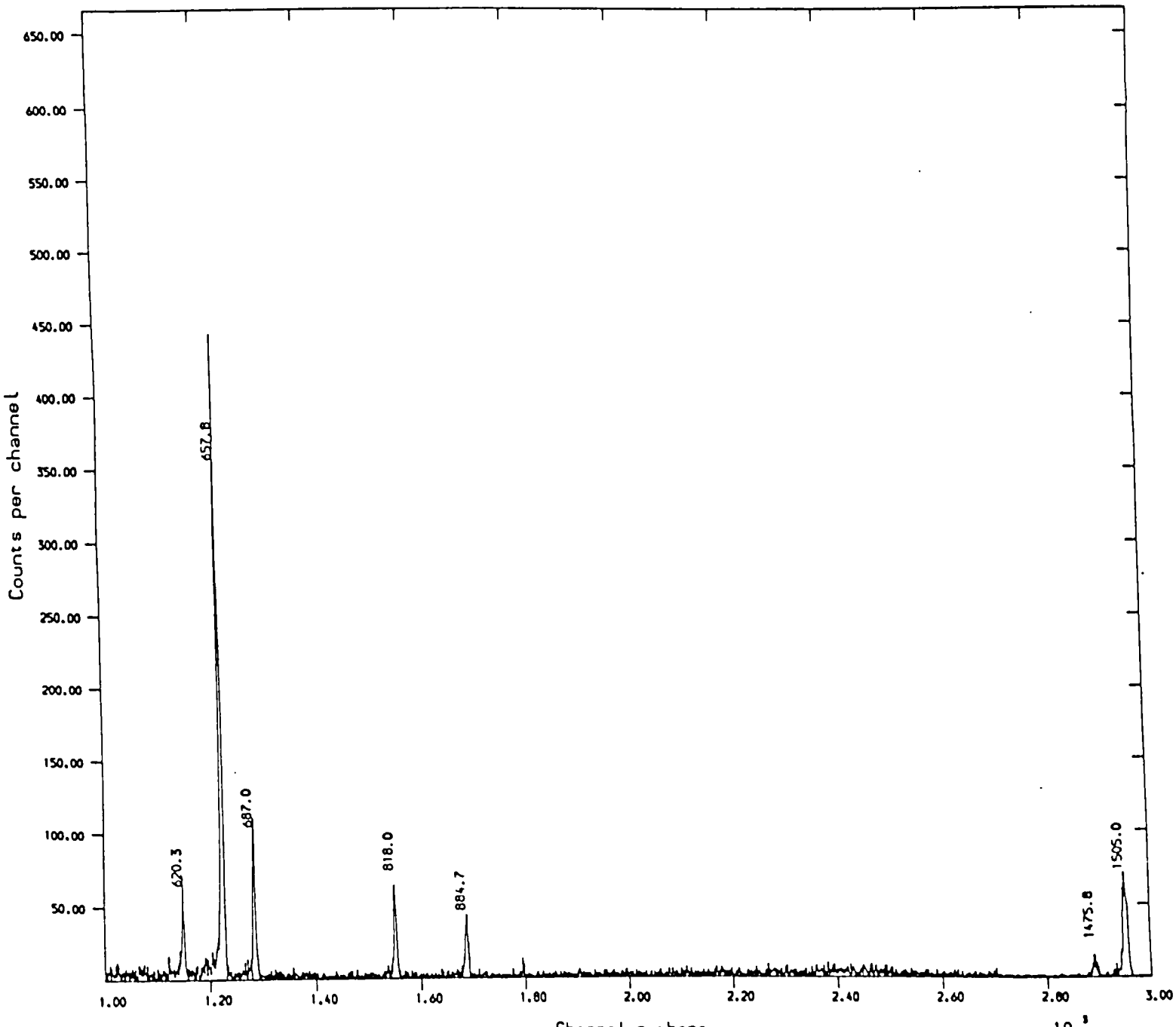


Fig. 3.5.D Corrected spectrum of Ag^{110m} in coincidence with 764 keV

4. DESCRIPTION OF (n,γ) EXPERIMENT APPARATUS

4.1. Thermal Neutron Beam Facility

4.1.1 Thermal Neutron Beam Tube

The (n,γ) experiment utilizes the 0^{o} - 180^{o} through tube which passes through the graphite of the 270^{o} thermal column at a distance of approximately 50 cm. from the centre of the reactor core. The general layout of the 0^{o} face is shown in Fig. 4.1 . A high density polythene scattering block is placed in the tube at its highest flux position where the measured thermal flux is approximately 1.5×10^{11} n-cm^{-2}sec^{-1} with a gold cadmium ratio of 6:1. The measured gamma dose rate at this point is approximately 0.6 Mr.hr^{-1}. The scattering block is contained in a vented aluminium container for which handling tools are available for removal from the reactor. The experimental tube itself is connected to the reactor ventilation system. The ambient temperature in this tube was determined by the reactor coolant outlet temperature and was less than 45^{o}C.[97)]

4.1.2 Beam Tube Collimator

The beam tube is fitted with a circular collimator consisting of eight sections. The first four sections (each 30 cm long) are made from a low carbon (type En1A) mild

steel circular collimator. The next three sections (each 40 cm long) are filled with a composite of nonantimonial lead (BS 3909/1) (10 cm long) for gamma shielding and boron-loaded polythene (5% boron by weight) (30 cm long) for neutron shielding. The last section (20 cm long) is filled with nonantimonial lead. The length of the whole collimator is approximatel 260 cm, and the internal diameter of the collimator ranges from 8.9 cm at the internal end to 2.54 cm at the point where the beam emerges from the monolithic shield of the reactor. The innermost end of the collimator is covered with an annulus of cadmium 0.5 mm thick to reduce its thermal neutron induced activity.

4.1.3 Shutter Assembly

A shutter assembly[97,98] is attached to the outermost section of the collimator and consists of a tungsten alloy (G.E.C. heavy alloy) beam stop 5 cm in diamter and 17.8 cm long, held in a rotating steel block driven by an electric motor with a flexible gear belt. The position of the rotating shutter is controlled by two micro switches in the motor drive circuit. A further micro switch controls the "beam open" and "beam closed" indicator lights and the shutter movement is enabled by a key. It takes approximately 33 secs. to open (close) fully the beam.

4.1.4 Shielding

There is a wall of 10 cm thick lead bricks and cadmium sheet outside the monolithic shield of the reactor. On the outer face of this wall, a shield of "Jabroc" resin-impregnated wood laminate of thickness 30 cm is placed extending from floor level to a height of 180 cm. In future, the outer face of the "Jabroc" will be covered with "Boroflex" B_4C/PVC sheet.

There is another experiment which makes use of another tangential tube on the 0^o face of the reactor. This neutron scattering experiment beam tube and the neutron-capture experiment beam tube are approximately 100 cm apart. A wall of 30 cm thick concrete blocks is used to provide a shield between the two experiments.

4.1.5 Neutron Beam Stop

The neutron beam stop is shown in Fig. 4.2. It consists of a 25 cm x 25 cm x 60 cm block of borated polythene in which there is a 15 cm diamter x 50 cm long hole. The borated polythene is surrounded on all sides by 10 cm thick lead bricks.

4.1.6 Thermal Neutron Beam Profiles

The thermal neutron beam profiles at the target position and beam stop position are shown in Fig. 4.3A & 4.3 B respectively. The target in the (n,γ) experiment is situated at a distance of approximately 76 cm from the outside of the reactor monolithic shield and the front face of the beam stop is about 213 cm distant from the latter position.

The thermal neutron beam flux at the target position may be described by the gaussian distribution

$$\phi(r) = \phi_o \exp(-r^2/0.36\ d_{\frac{1}{2}}^2)$$

where the radial distance r from the beam axis is given in cm,

$\phi_o \simeq 2 \times 10^6 n\text{-}cm^{-2}sec^{-1}$ with a gold cadmium ratio of 30 ± 5 at the reactor power of 100 kW, and the full width at half maximum (FWHM) amounts to $d_{\frac{1}{2}} \simeq 3$ cm. Assuming Gaussian distribution the total external thermal neutron flux value is

$$\phi = 2\pi\phi_o \int_o^\infty \exp(-r^2/0.36 d_{\frac{1}{2}}^2)\ r.dr$$

$$= 1.9 \times 10^7 \text{ per sec.}$$

The thermal neutron beam flux at the front face of the beam stop can also be described as

$$\phi(r) = \phi_o \exp(-r^2/10.8)$$

4.2. Detector Assembly

A typical arrangement of target and detectors for the neutron capture gamma ray measurements is shown in Fig.4.4 . The target is placed in the neutron beam and is viewed by two Ge(Li) detectors one of which is vertically below the target, and the other is to one side as shown. The latter Ge(Li) detector (Horizontal Detector) is surrounded with a 20 cm diameter x 20 cm length NaI shield. This system is used for the suppression of the Compton events in low energy gamma ray spectra. The NaI detector is split into two optically isolated halves to enable it to be used with the Ge(Li) detector as a three-crystal pair spectrometer for high energy spectra (> 3 MeV).

4.2.1 Ge(Li) Detector Specifications

	Vertical Detector	Horizontal Detector
Type	Coaxial	Coaxial
Active Volume	86 cc	72 cc
Diameter	48 mm	45 mm
Length	48 mm	45 mm
P-Core diameter	10 mm	8 mm
Diffusion Depth	0.6 mm	0.5 mm
E H T	+ 4000 volts	+ 3000 volts
Current	50 pA/4000 V	50 pA/3000 V
Capacitance	27 pF/4000 V	18 pF/3000 V
Resolution: F W H M	2.1 keV/1.332 MeV	2.1 keV/1.332 MeV
F W T M	4.2 keV/1.332 MeV	4.2 keV/1.332 MeV
Efficiency: Relative to 3" x 3" NaI(Tl)	12.5%	11%
Peak to Compton Ratio	38:1	35:1

4.2.2 Resolution of the Horizontal Ge(Li) Detectors

The resolution, or ability of a nuclear spectrometer to separate different radiation energies, is usually expressed in terms of the full width of the spectral lines measured at half their maximum height. The resolution obtained in any particular measurement is the result of several factors: preamplifier noise, detector characteristics, count rate, radiation energy, overall system stability, proper interfacing between instruments within the system, etc. If the count rate is low enough so that the pulse shape can be adjusted for the best signal-to-noise ratio without being distorted by pile-up or baseline shift but high enough so that effects due to long-term drifts can be neglected, and if it is assumed that the different components of the system are properly matched, the intrinsic resolution R (total resolution) of the system may be given as

R^2 = (Detector Resolution)^2 + (Electronic Noise)^2

$(FWHM)_D = 2.355 \sqrt{F.E.\ \varepsilon}$

F = Fano Factor = 0.13 (Reference 99)

E = Radiation Energy in MeV

ε = Energy in eV needed to create an electron-positron pair in germanium

= 2.98 eV/pair (Reference 100)

Usually, the main factor in line-width broadening is count rate. Count rate can have a deleterious effect in spectral resolution through several mechanisms. The three most commonly found being pulse pile-up, baseline shifts and thermal effects in components.

4.3. Compton-Suppression Spectrometer System

The Compton-suppression spectrometer incorporates a 45 mm diameter x 45 mm length true coaxial Ge(Li) detector (horizontal type) located in the middle of a 20 cm diameter x 20 cm height NaI(Tl) annulus. Both Ge(Li) detector and NaI(Tl) guard detector were manufactured by Harshaw Chemical Company. Details of the NaI(Tl) annulus are shown in Fig. 4.5. The whole system was surrounded by 10 cm thick lead blocks. During normal use the central detector is illuminated by a 2 cm diameter collimated beam of gamma rays obtained from neutron capture in targets placed within the thermal neutron beam (or radioactive sources). The NaI(Tl) guard detector cannot see the samples (or sources) directly. The distance between the centre of Ge(Li) crystal and the samples is approximately 23 cm. A LiF packet (5 mm thickness) contained in polythene is placed at the entrance of the collimator to shield the detector from scattered neutrons.

4.3.1 Electronics and NC26 Time Analyser[101]

The circuit diagram for the Compton Suppression Spectrometer System is shown in Fig. 4.6. The bisected NaI(Tl) guard detector has four photomultiplier tubes whose anodes are connected in parallel and they share the same anode voltage. Each photomultiplier tube gain is individually adjustable by changing the potential between the anode and the last dynode. The 4 photomultiplier signals are summed before going to the input of the Harshaw NC26 Time Analyser, which also receives the negative tail pulse output from the Ge(Li) pre-amplifier.

The NC26 Time Analyser is a two width NIM unit designed to measure time relationships between a primary Ge(Li) detector and a NaI(Tl) guard detector in Compton suppression spectrometers. A simplified NC26 internal block diagram is shown in Fig. 4.7. NC26 generates gate signals when appropriate coincidence/anticoincidence conditions are met. In addition to timing functions, it contains a linear amplifier for NaI(Tl) signals to provide for energy analysis. Extrapolated leading edge timing (ELET) is used to measure the arrival time of the events. A composite dual time-to-amplitude converter (TAC) generates a signal proportional to the time separation of the Ge(Li) and NaI(Tl) events. Fig. 4.8 illustrates the operation of TAC.

The timing capacitor is normally clamped at zero volts in a Robinson type baseline restorer circuit. The clamp is released when either the NaI(Tl) or Ge(Li) lower threshold is exceeded. When the lower Ge(Li) threshold is passed, two positive current sources of equal magnitude are gated on and the capacitor begins to charge positively. When the upper Ge(Li) threshold is exceeded, one current source is turned off. Since the Ge(Li) amplifier provides an essentially linear rise time signal, the charge (and thus the voltage) on the timing capacitor (after the upper threshold is crossed) is independent of pulse amplitude (ELET) but is proportional to the time since the event occurred. Similarly, the NaI(Tl) threshold discriminators control equal but negative sources. If both NaI(Tl) and Ge(Li) events occur simultaneously, the time signal will be zero after both of the upper thresholds have been crossed. When a NaI(Tl) event occurs earlier than a Ge(Li) event, the final time signal voltage is constant but negative. Conversely, an early Ge(Li) event will produce a positive signal.

Three discriminators are driven by the time signal. The thresholds are set by front panel screwdriver adjustment controls. Two of these (T and ΔT) form a single channel analyser for the time signal normally centred around zero volts. This SCA is strobed about 1.5 μs after the NaI(Tl) upper threshold is crossed by a delayed upper threshold signal. If the time signal is within the SCA window at this time, both NaI(Tl) and Ge(Li) events occurred in coincidence. A Coincidence Output is then generated and all TAC current sources are momentarily shut off.

The time signal is sampled through a biased stage with negative full scale as the reference voltage and buffered to the Linear Time Output connector. If the time signal was not in the SCA window, no Coincidence Output pulse is generated but the sampled output is still produced for possible external use. Approximately 2 μs after a NaI(Tl) event, the TAC clamp is re-enabled, discharging the timing capacitor. If the time signal increases positively above the third discriminator (T Max), which is normally set at about 1.5 μs equivalent, an Anti-coincidence Output is generated. The TAC current sources are shut off and the time signal is sampled. The time signal will be terminated by the end of the Ge(Li) lower threshold multivibrator pulse approximately 2 μs after a Ge(Li) event whether T Max threshold passed or not. The T Max setting must therefore be exceeded within this time to produce an Anticoincidence Output pulse. This can only happen if no NaI(Tl) event occurred within ± 1.5 μs of a Ge(Li) event. A NaI(Tl) event closer than this will contribute some negative charge to the TAC and thus prevent the time signal from reaching the T Max threshold.

A coincidence Output is generated only for those events which fall within the narrow (30 - 50 ns) time window while an Anticoincidence Output occurs only if a Ge(Li) signal is separated by more than ± 1.5 μs from a NaI(Tl) signal. This assures that any time walk (perhaps due to over-load pulses or pile-up) will not mistakenly permit an Anticoincidence Output pulse to be generated.

The Anticoincidence Output of the NC26 Time Analyser was applied to the delayed coincidence gate input of the multichannel analyser for all subsequent measurements. The linear Ge(Li) energy signal was preamplified by a Harshaw NB21 Preamplifier and amplified by a Ortec Spectroscopy Amplifier before being analyzed by a Laben 8000 Multichannel Analyser.

4.3.2. Performance of the Compton Suppression Spectrometer System

Several parameters have been used in the past in evaluating Compton Suppression Spectrometer Systems. These usually include such measurements as peak-to-Compton ratio, the natural background spectrum, resolution, Compton interference reduction factors, figures of merit and the response of the system to real problems. Although some of these factors are more meaningful than others, all are useful in evaluating the design and application of these spectrometers.

The normal and Compton suppressed spectra of ^{137}Cs are shown in Fig. 4.9 to provide important information on the system's basic performance. The resolution of the system remains the same after the Compton suppression. As shown in the figure, the anticoincidence mode of operation reduces the Compton continuum by a factor of 6.5 to provide a peak-to-Compton ratio of 270:1. Although the Compton edge (CE) is not completely absent from the anticoincidence spectrum, the CE is reduced by a factor of 3.5. The CE is due to a gamma ray depositing the maximum amount of energy possible in a single interaction and

escaping the active position of the Ge(Li) detector by scattering back through about 180^{o} and thus escaping through the NaI entrance hole. On the other hand the back scatter peak, which is due to gamma rays scattered through about 130^{o} to 180^{o} into the active portion of the Ge(Li) detector, is notably reduced. The rather high effectiveness of the anticoincidence shield at the low energy end of the spectrum is due to the special design of the NaI(Tl) guard detector.

Recently Camp and Van Hise[102] reported the new weak gamma transitions at 346.93, 467.4, 826.28, 1293.7 and 2158.77 keV in addition to 1173.22 and 1332.49 keV gamma rays in the decay of ^{60}Co. The 4-day low-count rate Compton-suppressed spectrum of ^{60}Co is shown in two halves in Fig. 4.10. Compton distribution suppression reached a maximum of 6.5 at about 450 keV. This yields a 1332.5 keV peak height to a minimum Compton continuum ratio of about 210:1 at 2.2 keV FWHM. The peak height to Compton edge ratio for both 1173 and 1332 keV is approximately 100:1. The energies and intensities of ^{60}Co observed in present work are given in Table 4.1. 467.4 and 1293.7 keV gamma rays are not observed.

To demonstrate the performance of the Compton Suppression Spectrometer System for a complicated decay scheme, the spectra of ^{152g}Eu decay with and without Compton suppression are shown in Fig. 4.11.

TABLE 4.1.

^{60}Co gamma-ray energies and intensities

E_γ (keV)	$I_\gamma \pm \Delta I_\gamma$	
	Present Work	Reference (102)
346.98 ± 0.08	80.3 ± 4.3	75.8 ± 5.0
467.4*	-	< 2.3, (-5.9 ± 4.1)
826.34 ± 0.10	71.4 ± 6.9	76.2 ± 8.0
1173.216± 0.021*	≡ 10^6*	≡ 10^6
1293.7*	-	< 1.1
1332.486± 0.022*	10^6 +*	10^6 +
2158.64 ± 0.11	12.5 ± 1.3	11.1 ± 1.8

*These values are adopted from Reference 102.

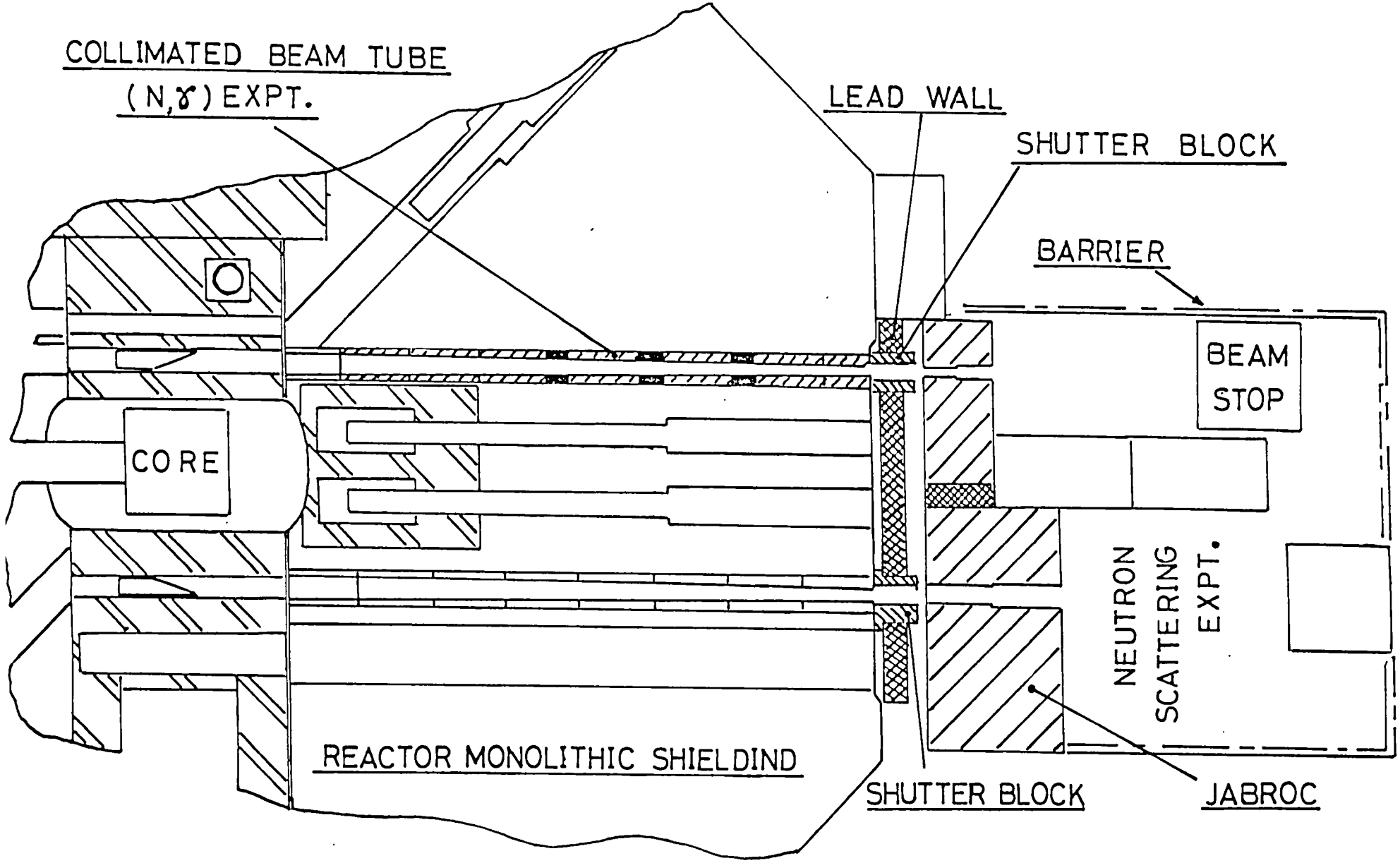


FIG. 4·1 GENERAL LAYOUT OF 0° FACE AT U.L.R.C

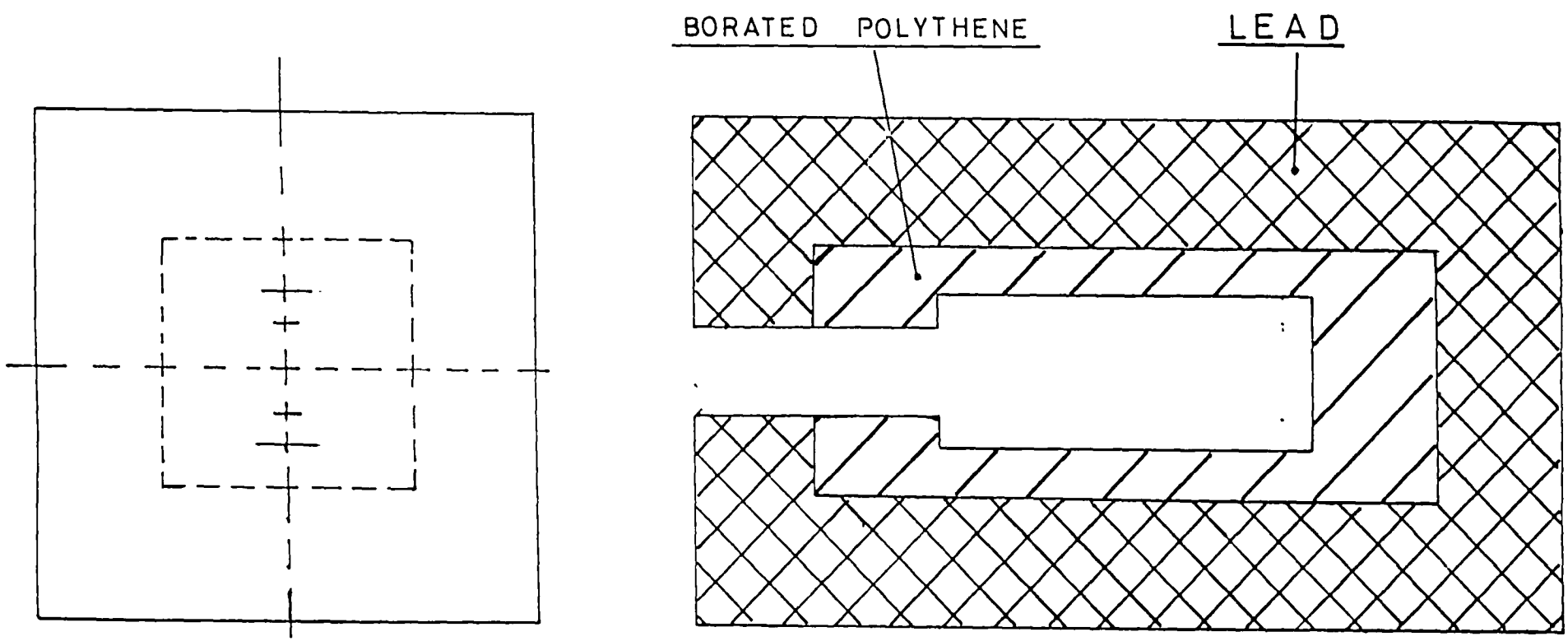
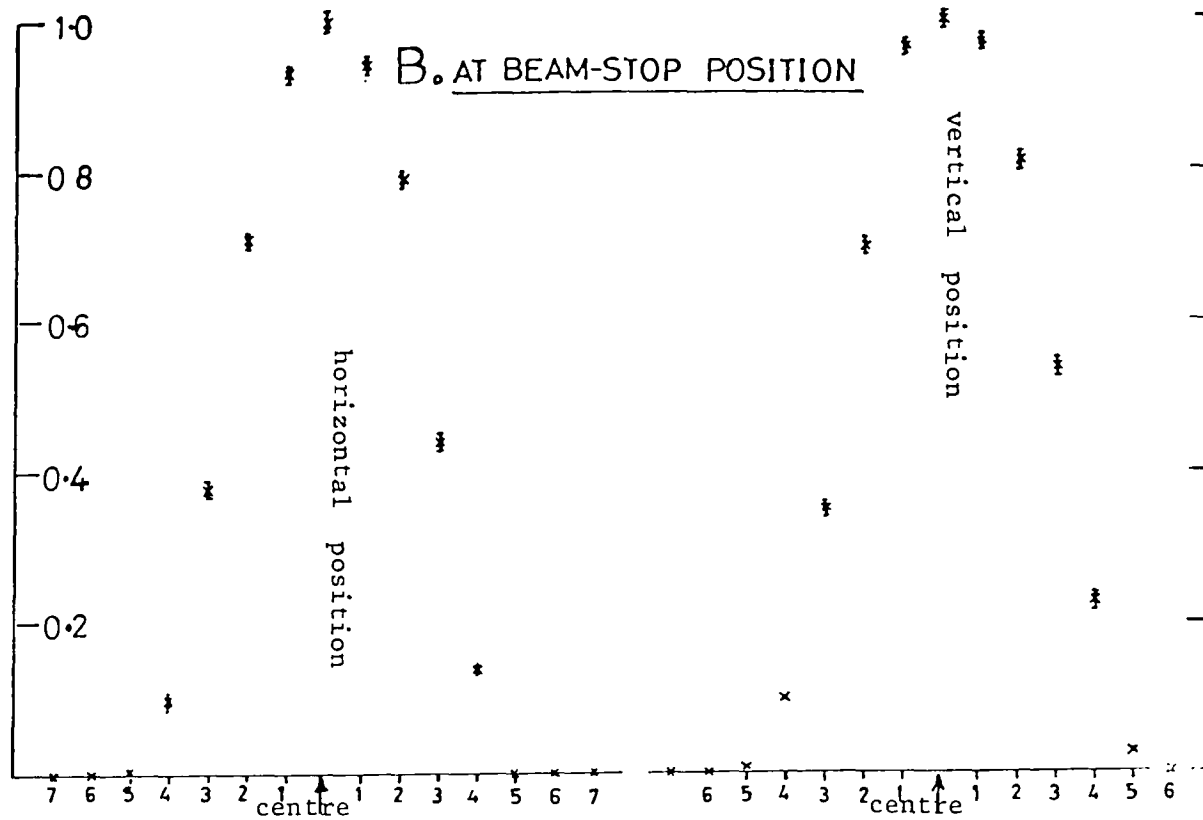


FIG. 4·2. NEUTRON BEAM STOP



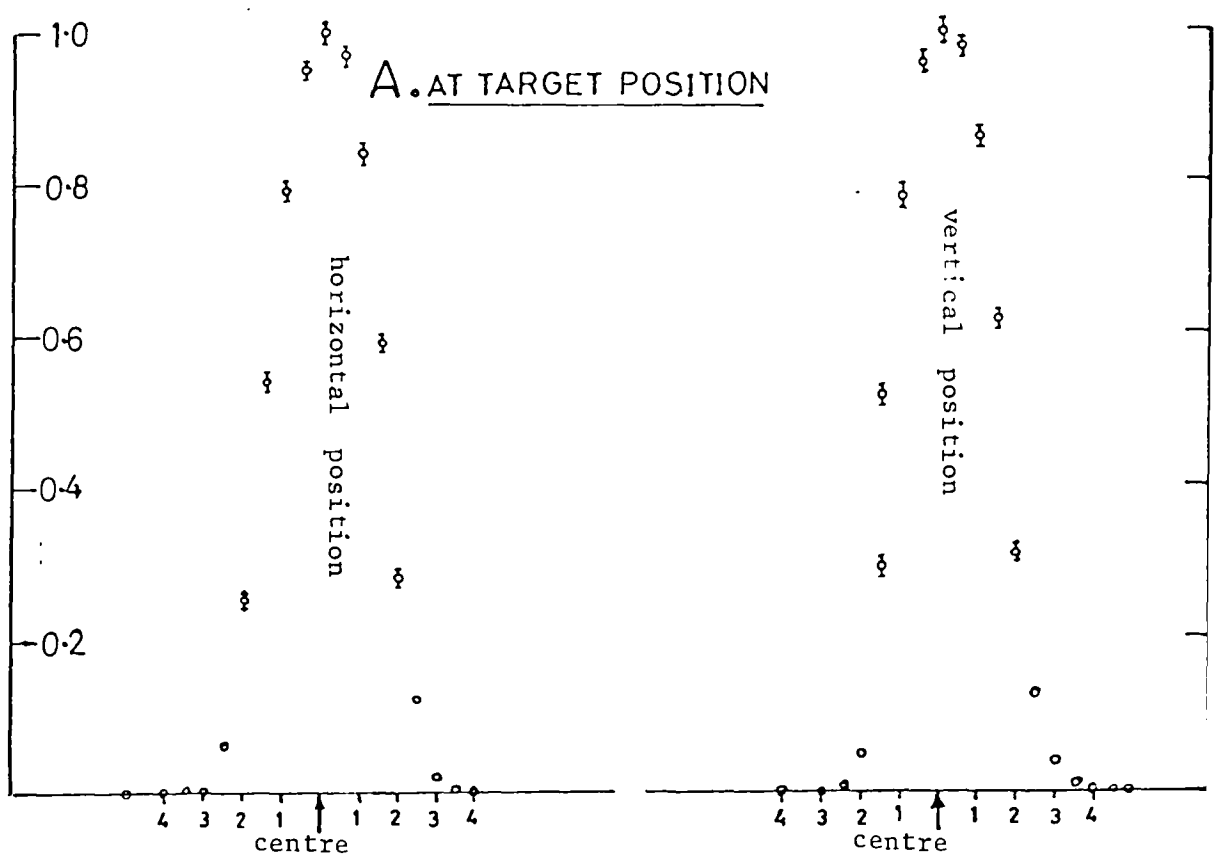
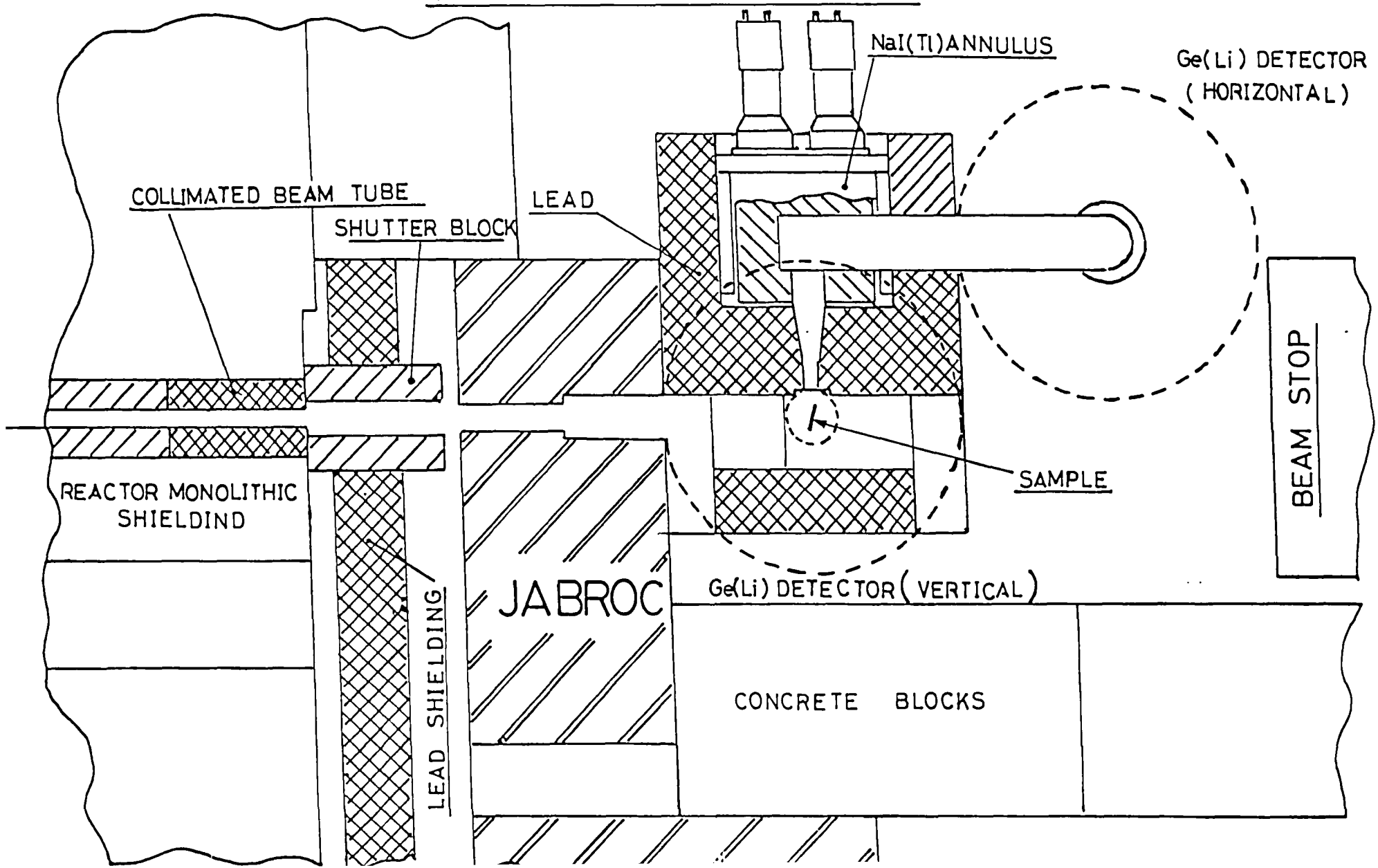


FIG. 4·3 THERMAL NEUTRON BEAM PROFILE

FIG.4-4 (n,γ) APPARATUS WITH SHIELDINDS



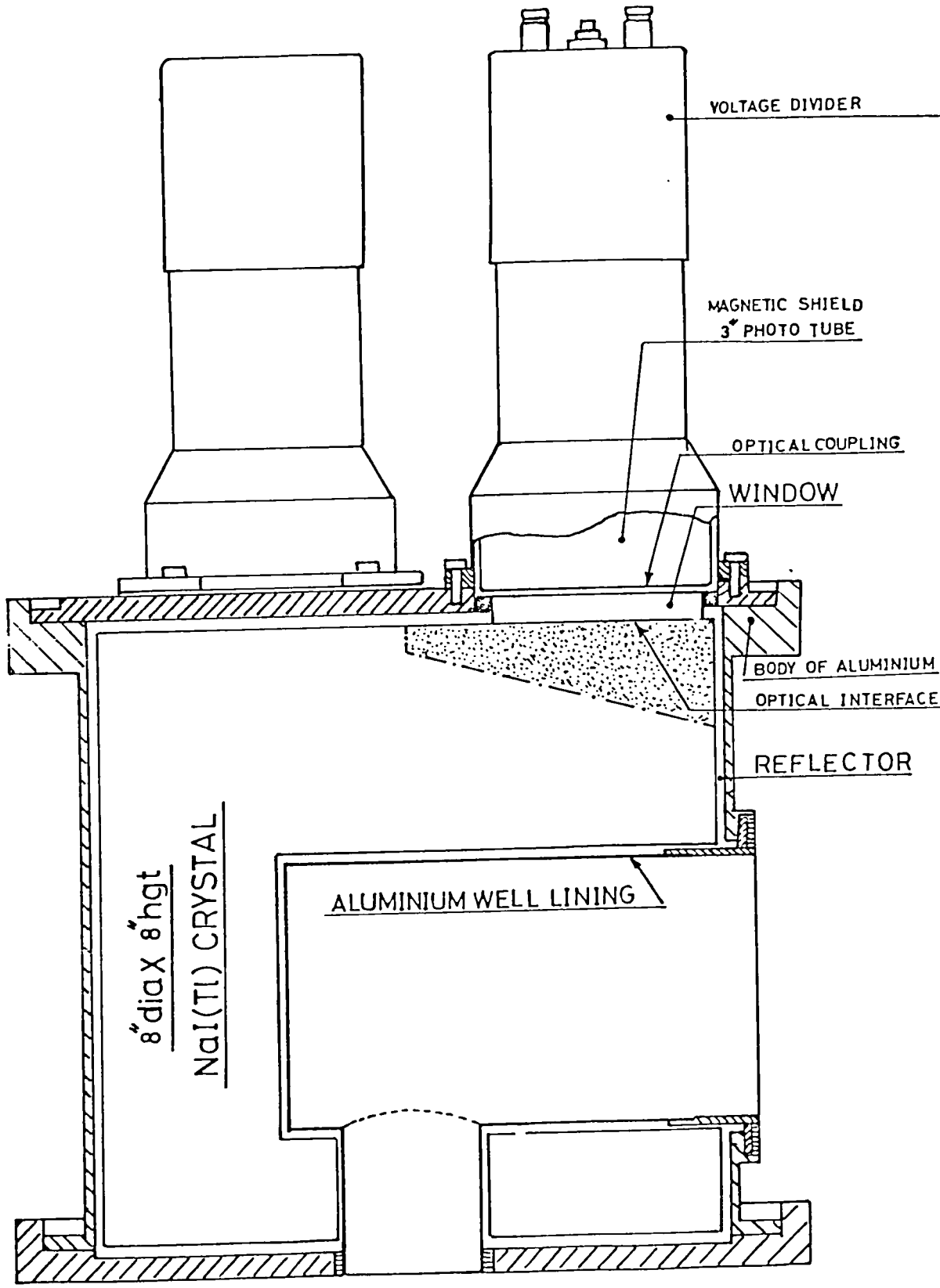


FIG.4·5 NaI(Tl) ANNULUS RING

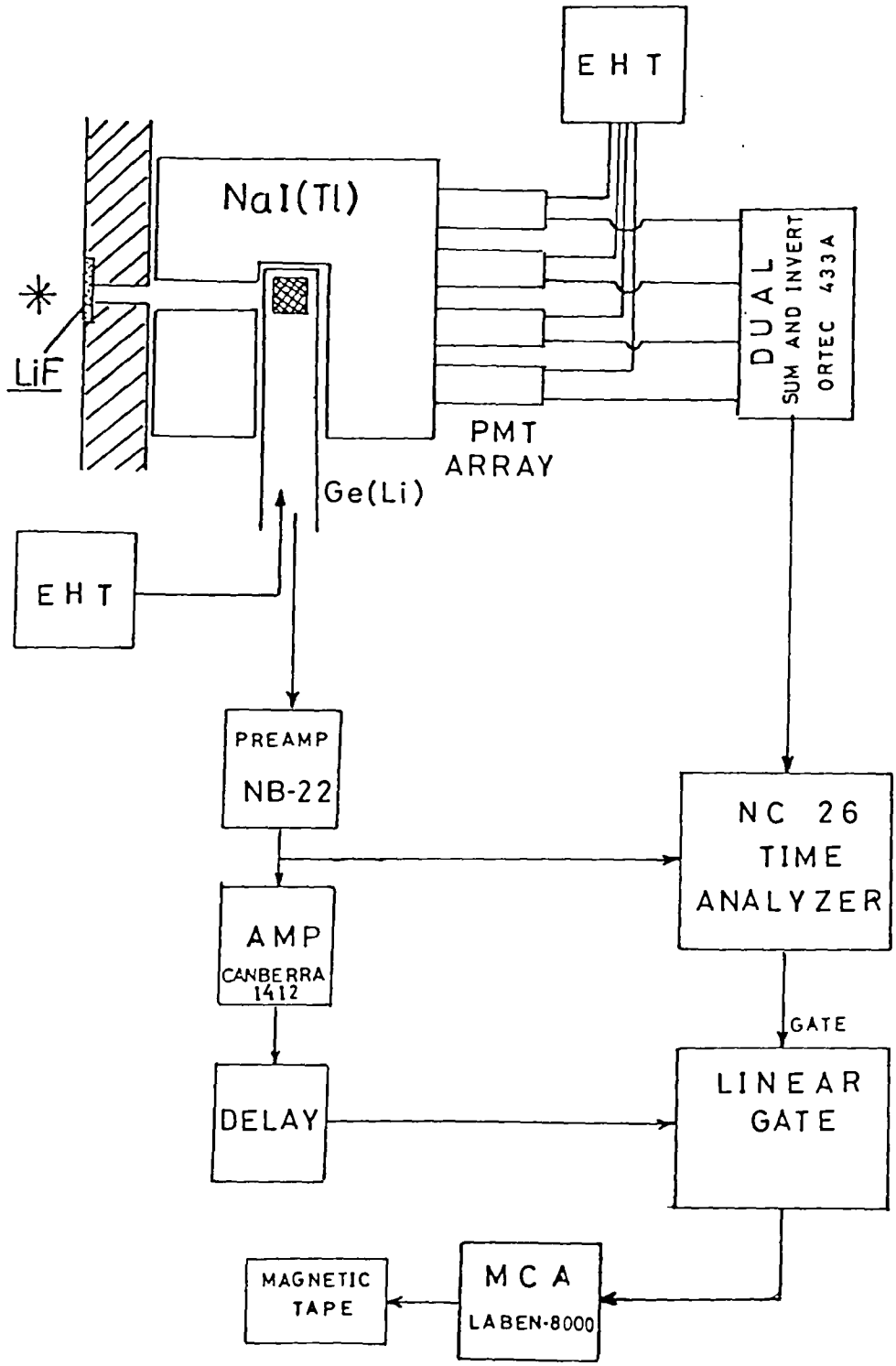


FIG. 4.6 BLOCK DIAGR. FOR COMPTON SPECTROMETER.

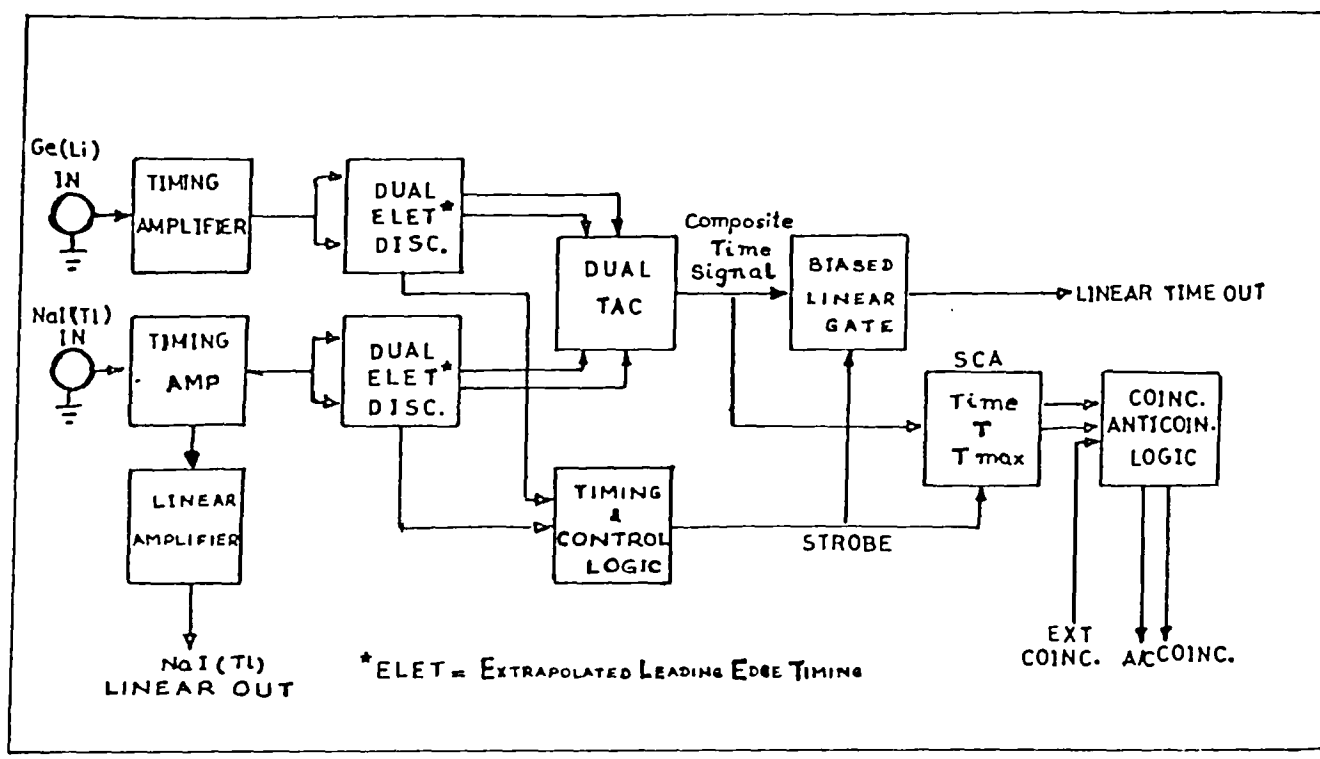


FIG.(4·7) SIMPLIFIED NC 26 INTERNAL BLOCK DIAGRAM

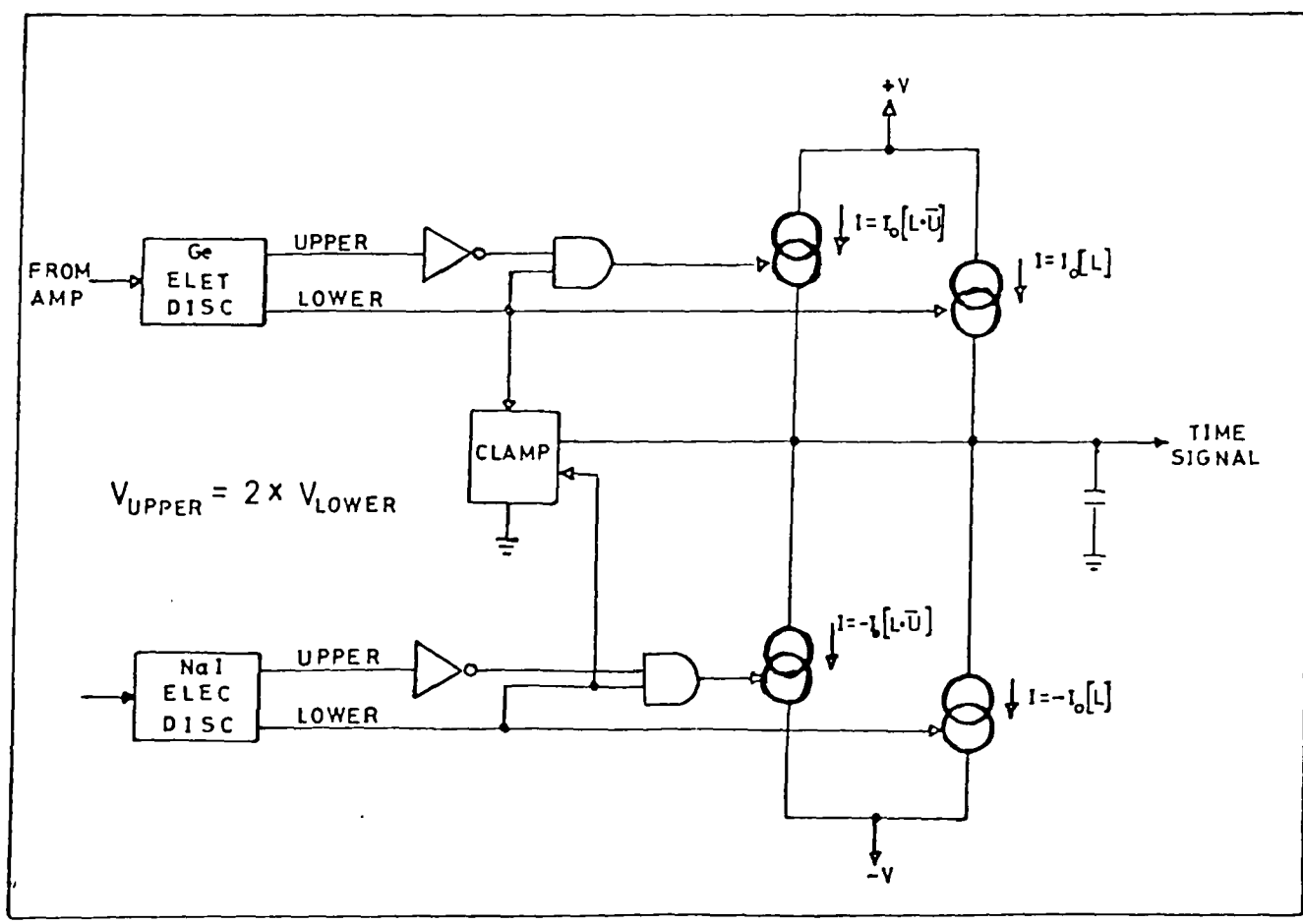


FIG.(4·8) TIME TO AMPLITUDE CONVERTER LOGIC DIAGRAM

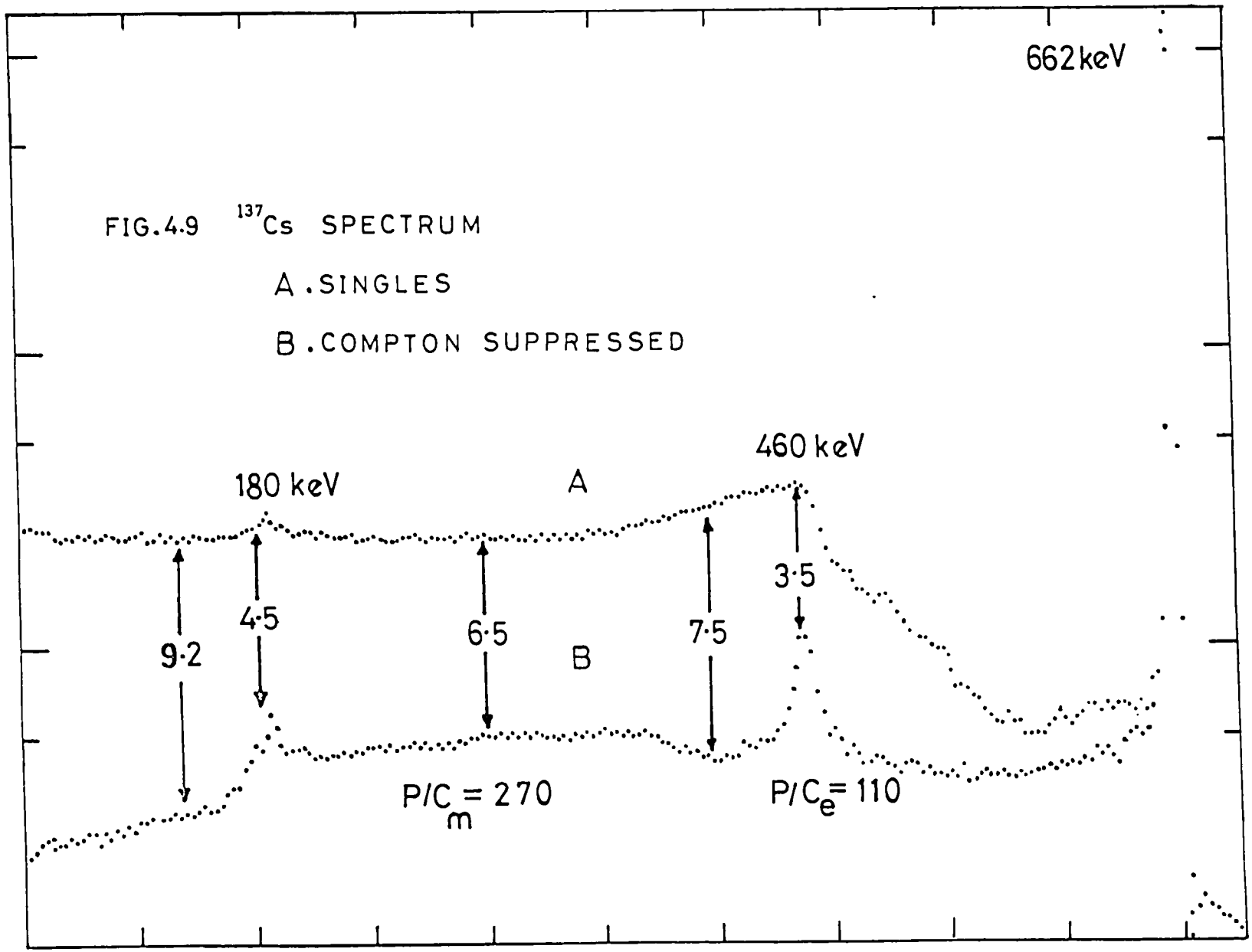


FIG.4.9 ^{137}Cs SPECTRUM

A. SINGLES

B. COMPTON SUPPRESSED

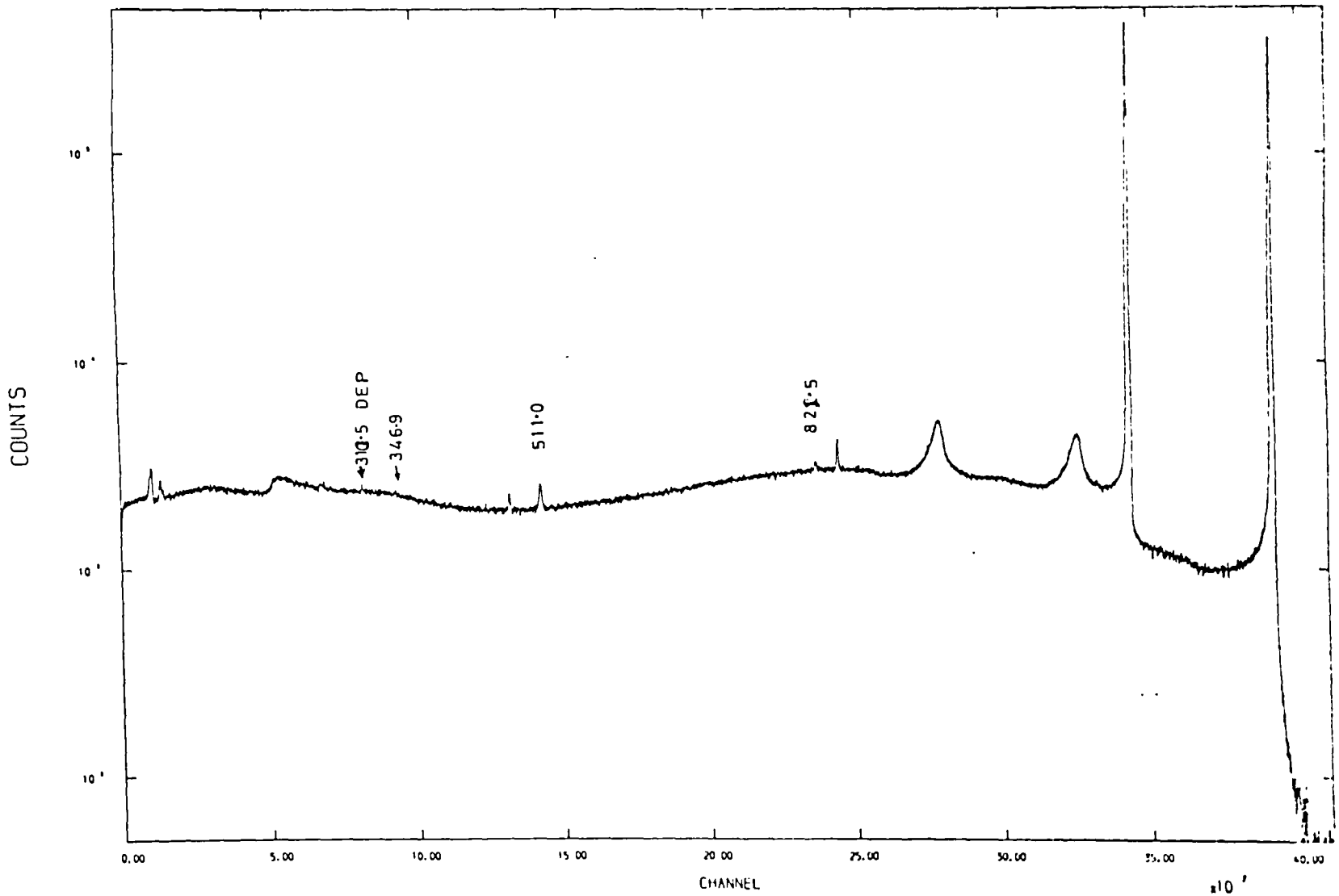


FIG.4.10.A ••••• COBALT 60 DECAY FIRST SECTION 60002 SECS •••••

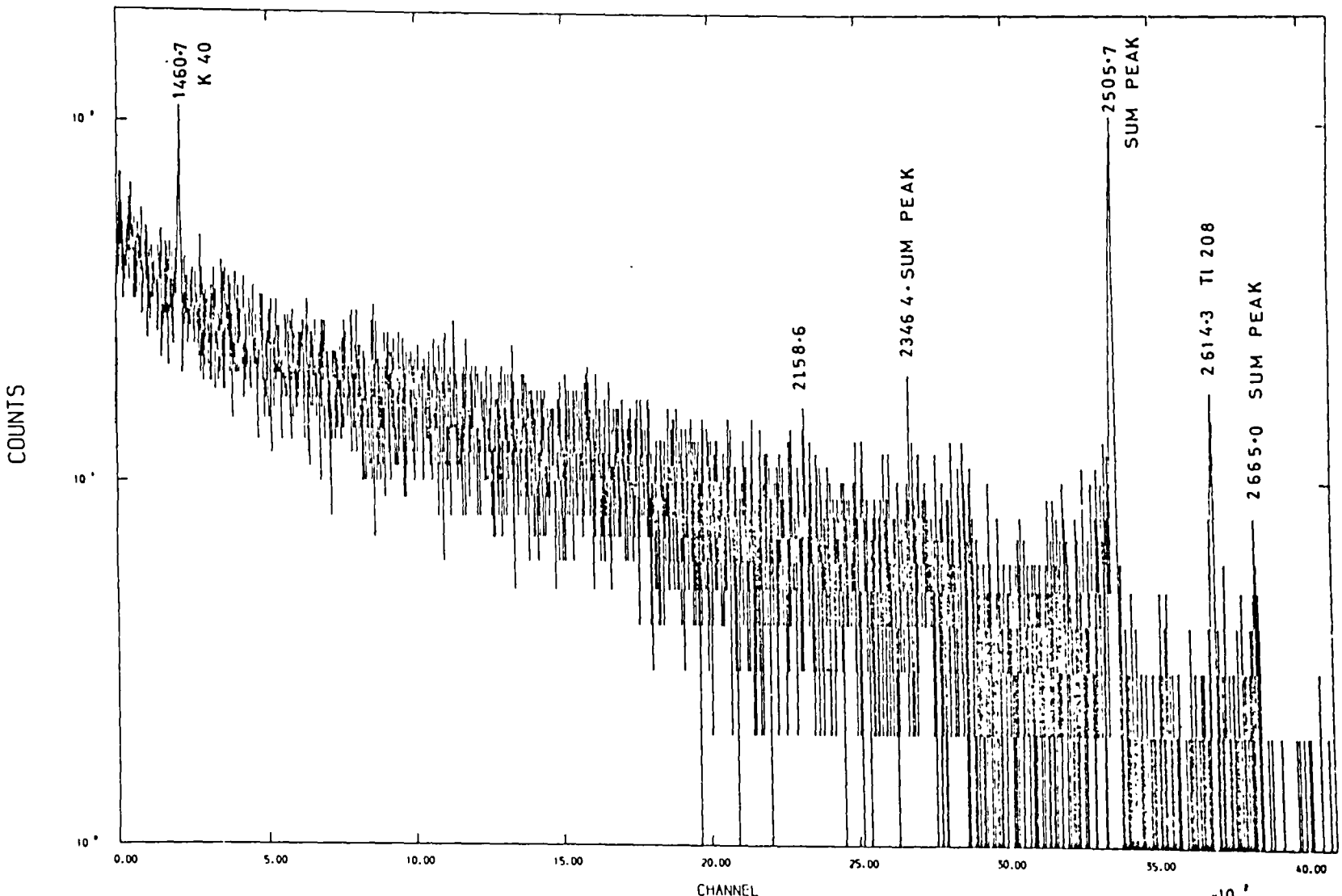


FIG.4.10.B••••• COBALT 60 DECAY SECOND SECTION 90000 SECS •••••

FIG.4.11.A ••••• EUROPIUM 152G DECAY SPECTRUM WITH COMPTON SUPPRESSION •••••

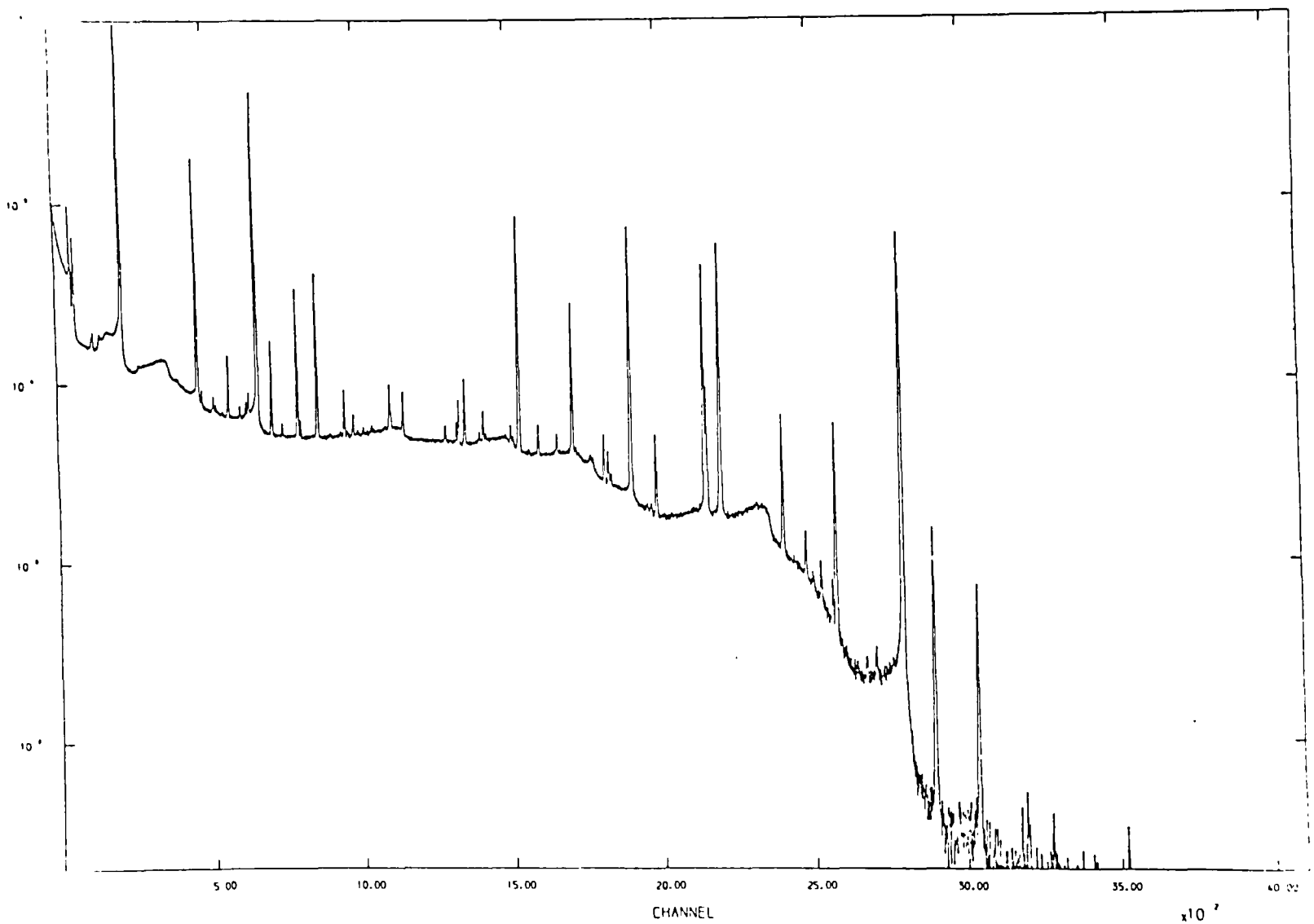


FIG.4.11.B ••••• EUROPIUM 152G DECAY SPECTRUM WITHOUT COMPTON SUPPRESSION •••••

5. GAMMA RAYS FROM THERMAL-NEUTRON CAPTURE IN NATURAL AND ^{107}Ag ENRICHED SILVER

.5.1 Low Energy (n,γ) Measurements ($E_\gamma \leq 1.5$ MeV)

The experiments have been performed at the University of London Reactor Centre 100 kW Consort II reactor and the vertical beam tube facility of the Julich FRJ-2 reactor. At ULRC the targets were placed in a thermal neutron beam with a flux of about 2×10^6 $cm^{-2}s^{-1}$. At Julich the thermal neutron beam flux is about $4 \times 10^8 s^{-1}$ with beam diameter of 16 mm. The samples used were 400 mg of natural silver (99.999% purity) metallic foil and 400 mg silver metalic foil enriched to 99.6% in ^{107}Ag (50 mg/cm^2). The enriched sample was purchased from A E R E, Harwell. Detailed descriptions of the two experimental set-ups are given in Chapters 4 and 6 .

At ULRC the low-energy γ-rays ($E_\gamma < 1.5$ MeV) were detected with high resolution Ge(Li) detectors and the Compton-Suppression Spectrometer System (CSSS), described in Chapter 4 . The spectra were analysed using a Laben 8000 Multichannel analyser and recorded on magnetic tape. With CSSS, the (n,γ) spectra were measured in three separate energy regions (0 - 0.5, 0.5 - 1.0 and 1.0 - 1.5 MeV) to resolve the multiplets. Under actual experimental operation the resolutions of the detector systems were about 25% worse than those under normal counting conditions using the standard sources. The

poor resolution is probably due to a number of factors which include high counting-rate, temperature drifts and slow but continuous activation of the Ge(Li) detectors by the scattered neutrons. Separate runs covering the same energy regions were also performed under the different conditions (such as neutron beam closed but reactor operating, neutron beam closed and reactor shut down, and neutron beam open and reactor operating) to investigate the background radiations.

At Julich a high resolution pencil-shaped Ge(Li) detector with sensitive volume 2.32 cc (27 mm in length and 86 mm^2 cross-sectional area) was used. The details of the target holder and neutron beam are described in Figures 5.1 and 6.1 . This detector is specially designed to detect double-escape peaks in the energy range > 3 MeV. The background spectrum was also measured under the same conditions (target holder inside the beam).

5.2 Analysis of the low-energy measurements

5.2.1 Energy and Efficiency Calibration

The standard sources ^{22}Na, ^{54}Mn, ^{57}Co, ^{60}Co, ^{88}Y, ^{241}Am (Martin and Blichert-Toft 1970)[39], ^{137}Cs, ^{203}Hg (Valivaara et al 1970)[45], ^{152g}Eu (Aubin et al 1969)[46], ^{56}Co (Martin et al 1970; Aubin et al 1969), ^{110m}Ag (see Chapter 3) together with $^{39}K(n,\gamma)^{40}K$, $^{45}Sc(n,\gamma)^{46}Sc$, $^{53}Cr(n,\gamma)^{54}Cr$ (Seyfarth et al 1972[103]; White and Howe 1972[104]; Kamp and

Spits 1972)[105] and nat Zn(n,γ)reaction (Rasmussen et al 1969;[9] Ottmar et al 1971)[106] were used for energy and efficiency calibrations of the detectors. The efficiency values are shown in Figures 5.2 and 5.3.

The SAMPO computer program (Routti and Prussin 1969)[48] is used throughout the experiment to determine the peak positions and areas under the peaks.

5.2.2 Gamma Energies (< 1.5 MeV) and Relative Intensities and $^{107}Ag(n,\gamma)^{108}Ag$ and $^{109}Ag(n,\gamma)^{110}Ag$ reactions

With the aid of the precisely known energies of the calibration lines and the SAMPO computer program, the energy calibration for each spectrum was obtained by fitting a third-order polynomial.

The positions and the areas of the peaks in $^{107}Ag(n,\gamma)^{108}Ag$ and $^{109}Ag(n,\gamma)^{110}Ag$ reactions were determined using SAMPO program. The fitting parameter values were obtained from (n,γ) reactions. In addition, a few of the known lines in the spectra with previously determined precise energies (Breitig et al 1974)[74,75] were used not only as internal calibrations but also to check the linearity of the system. (Table 5.6)

Figures 5.4 and 5.5 display the typical singles γ-ray spectra obtained for the reactions $^{107}Ag(n,\gamma)^{108}Ag$ and natural Ag(n,γ) with Compton-Suppressed Spectrometer System. The Ag(n,γ) spectra were found to be rather complex and it became necessary to analyse part of the data by hand to improve intensity determinations. All intensities were corrected for self-absorption by assuming a half-thickness attenuation factor. Because of the high enrichment of the sample (99.6% in ^{107}Ag), all transitions in $^{107}Ag(n,\gamma)^{108}Ag$ reaction have been unambiguously assigned to ^{108}Ag. This spectrum showed no evidence for any of the lines observed in the study of the $^{109}Ag(n,\gamma)^{110}Ag$ reaction (Hattori et al 1975;[107] Gujarathi et al 1970;[108] Kane and Scharff-Goldhaber 1970).[109] Precise energies and intensities of the gamma transitions in ^{110}Ag can be established by comparing $^{107}Ag(n,\gamma)^{108}Ag$ and natural Ag(n,γ) reactions.

The weighted average values of energy and intensities in $^{107}Ag(n,\gamma)^{108}Ag$ and $^{109}Ag(n,\gamma)^{110}Ag$ reactions are given in Tables 5.2 and 5.3 .

5.2.3. Background Radiations at U.L.R.C.

The background radiations observed with three different systems are listed in Table 5.4 . Most of the prominent background lines could be identified as transitions in Ge(n,γ) and Pb(n,γ)

reactions. Also gamma radiations from Al(n,γ) are observed with the Vertical detector and those from Na(n,γ) with Horizontal detector and the Compton Suppression Spectrometer. Therefore the following suggestions may be advisable for future operation.

(a) Lower the vertical Ge(Li) detector away from the neutron beam. At present this Ge(Li) detector is about 6 cm away from the centre of the circular neutron beam with beam diameter ≈ 6 cm.

(b) Use LiF to protect the Ge(Li) detectors from scattered neutrons.

(c) Cover the outer and inner faces of the Jabroc with "Boroflex" B_4C/PVC sheet.

(d) Move the Pb blocks, which are used as gamma shield for the Compton Spectrometer, a few more cm (2-3 cm) away from the neutron beam, although Pb(n,γ) lines may be useful as calibration lines, these lines are rather strong.

(e) It would be advantageous to remove the atmospheric nitrogen from the target position. Because some of the strong gamma radiations from the N(n,γ) reaction are about double the intensity of the strongest gamma radiations from the $^{107}Ag(n,\gamma)$ reaction in the high energy region.

.5.3 High Energy $^{107}Ag(n,\gamma)^{108}Ag$ Measurements (E_γ > 1.5 MeV)

400 mg of metallic target enriched to 99.6% in ^{107}Ag was employed. The measurements were carried out at Julich FRJ-2 reactor using the pencil-shaped Ge(Li) detector mentioned above. The performance of the Ge(Li) detector at high energies can be described by the separation achieved on the well-known 14 keV doublet of 7.646 and 7.632 MeV in the capture gamma spectrum of $^{56}Fe(n,\gamma)^{57}Fe$. The ratio of the peak to valley is about 5 for the double escape peak (dep) of the doublet. The full energy peak (fep) was not observed. The intensities of the double escape are approximately in the following ratio: dep:sep = 20:1. The resolution at 7.646 MeV on the double escape peak is 5.5 keV (FWHM). At the double escape peak of the 6018.5 keV gamma of $^{56}Fe(n,\gamma)^{57}Fe$, the FWHM resolution is 4.8 keV. At the double escape peak of the 4945.2 keV gamma of $^{12}C(n,\gamma)^{13}C$, the FWHM resolution is 4.5 keV. The intensity ratio of dep:sep:fep = 22:1:1.2 .

The gamma rays from natural Zn(n,γ) reaction (Rasmussen et al 1969[9]; Ottmar et al 1971[106]) and the background radiations mainly from $^{56}Fe(n,\gamma)^{57}Fe$, $^{207}Pb(n,\gamma)^{208}Pb$ and $^{12}C(n,\gamma)^{13}C$ (Rasmussen et al 1969[9]; Spits et al 1970[110]; Spilling et al 1968[111]) were used for energy and efficiency calibrations of the detector.

All (n,γ) spectra and background radiation spectrum (E_γ = 0-8 MeV) were measured under the same conditions. The SAMPO computer program was used to analyse the data. The relative double escape peak efficiency of the detector is shown in Fig. 5.6. Figure 5.7 displays a typical singles γ-ray spectrum obtained for the $^{107}Ag(n,\gamma)^{108}Ag$. This spectrum was obtained in a run lasting 20h. The γ-ray energies (MeV) and relative intensities of the high energy transitions (E_γ > 3 MeV) identified in ^{108}Ag are listed in Table 5.5. Because of the high enrichment of the sample (99.6% in ^{107}Ag) all transitions listed have been unambiguously assigned to ^{108}Ag. This spectrum showed no evidence of any of the lines observed in the study of the $^{109}Ag(n,\gamma)$ reaction (Bolotin and Namenson 1967: Bertrand and Raman 1971).

TABLE 5.1.

Isotopic Compositions and Relative Contributions of the Ag and Ge Samples

Isotope		Product	Atomic %	Capture cross section for thermal neutrons*	Rel. contribution to spectrum %
natural Ag		^{108g}Ag		34.2 ± 1.2	27.56 ± 0.97
	^{107}Ag	^{108m}Ag	51.83	3.0 ± 1.5	2.42 ± 1.21
		^{110g}Ag		89 ± 4	66.65 ± 3.00
	^{109}Ag	^{110m}Ag	48.17	4.5 ± 0.2	3.37 ± 0.15
enriched ^{107}Ag		^{108g}Ag			91.02 ± 3.19
	^{107}Ag	^{108m}Ag	99.6		7.98 ± 3.99
		^{110g}Ag			0.95 ± 0.04
	^{109}Ag	^{110m}Ag	0.4		0.048± 0.002
natural Ge		^{71g}Ge		3.15 ± 0.16	28.54 ± 1.45
	^{70}Ge	^{71m}Ge	20.7	0.28 ± 0.07	2.54 ± 0.63
	^{72}Ge	^{73}Ge	27.5	0.98 ± 0.09	11.80 ± 1.08
	^{73}Ge	^{74}Ge	7.7	15 ± 2	50.55 ± 6.74
		^{75g}Ge		0.24 ± 0.06	3.82 ± 0.96
	^{74}Ge	^{75m}Ge	36.4	0.143 ± 0.014	2.28 ± 0.22
		^{77g}Ge		0.05 ± 0.02	0.17 ± 0.07
	^{76}Ge	^{77m}Ge	7.7	0.092 ± 0.010	0.31 ± 0.03

*Reference 134.

TABLE 5.2.

Low Energy Gamma Rays and Relative Intensities in $^{107}Ag(n,\gamma)^{108}Ag$

$E_\gamma \pm \Delta E_\gamma$	$(I_\gamma \pm \Delta I_\gamma)\%$	$E_\gamma \pm \Delta E_\gamma$	$(I_\gamma \pm \Delta I_\gamma)\%$
46.53 ± 0.12	5.75 ± 1.11	364.45 ± 0.21	0.72 ± 0.18
74.77 ± 0.07	0.96 ± 0.22	370.94 ± 0.09	1.19 ± 0.18
79.15 ± 0.07	100	380.76 ± 0.13	1.35 ± 0.25
87.80 ± 0.06	0.98 ± 0.31	385.03 ± 0.23	1.35 ± 0.27
101.64 ± 0.13	7.98 ± 0.49	391.72 ± 0.19	1.09 ± 0.25
113.83 ± 0.16	0.98 ± 0.27	396.43 ± 0.12	1.03 ± 0.21
117.89 ± 0.12	20.82 ± 1.45	399.93 ± 0.13	1.10 ± 0.23
129.28 ± 0.10	0.97 ± 0.24	409.18 ± 0.37	0.82 ± 0.21
133.92 ± 0.10	1.05 ± 0.25	419.80 ± 0.28	0.61 ± 0.28
140.02 ± 0.08	0.64 ± 0.27	429.44 ± 0.15	4.09 ± 0.47
147.28 ± 0.11	3.24 ± 0.21	433.96 ± 0.15	1.13 ± 0.31
148.68 ± 0.13	2.85 ± 0.21	437.72 ± 0.16	1.49 ± 0.27
155.43 ± 0.18	1.27 ± 0.15	439.17 ± 0.22	4.17 ± 0.46
159.94 ± 0.21	0.82 ± 0.34	441.52 ± 0.24	0.72 ± 0.28
170.12 ± 0.15	1.41 ± 0.23	456.92 ± 0.24	0.93 ± 0.24
174.65 ± 0.19	0.61 ± 0.13	463.50 ± 0.15	1.25 ± 0.29
178.49 ± 0.12	3.42 ± 0.24	465.48 ± 0.17	2.55 ± 0.62
186.12 ± 0.14	0.40 ± 0.20	472.34 ± 0.21	0.75 ± 0.37
193.12 ± 0.09	32.47 ± 1.95	479.50 ± 0.27	1.19 ± 0.38
198.62 ± 0.15	1.11 ± 0.30	493.17 ± 0.42	0.95 ± 0.38
201.49 ± 0.11	9.82 ± 0.80	500.03 ± 0.12	0.85 ± 0.35
206.60 ± 0.11	49.38 ± 3.92	508.49 ± 0.18	5.06 ± 0.82
212.12 ± 0.09	2.63 ± 0.71	527.45 ± 0.14	3.55 ± 0.54
215.31 ± 0.08	19.42 ± 2.12	533.92 ± 0.08	0.87 ± 0.42
227.03 ± 0.14	0.34 ± 0.13	537.63 ± 0.23	1.58 ± 0.30
239.23 ± 0.13	5.38 ± 1.22	542.49 ± 0.38	0.80 ± 0.29
248.40 ± 0.11	1.20 ± 0.30	559.08 ± 0.38	0.66 ± 0.32
252.94 ± 0.13	0.40 ± 0.16	563.93 ± 0.28	1.54 ± 0.33
259.31 ± 0.11	21.79 ± 1.47	572.38 ± 0.21	1.24 ± 0.34
269.27 ± 0.16	2.45 ± 0.33	574.69 ± 0.15	0.71 ± 0.23
278.03 ± 0.28	1.00 ± 0.19	579.69 ± 0.18	1.30 ± 0.20
282.99 ± 0.31	1.16 ± 0.34	595.78 ± 0.17	2.32 ± 0.45
294.55 ± 0.10	27.46 ± 2.98	600.03 ± 0.18	1.92 ± 0.25
300.12 ± 0.11	14.88 ± 1.98	608.36 ± 0.19	2.21 ± 0.37
316.97 ± 0.23	2.34 ± 0.88	616.95 ± 0.27	1.79 ± 0.37
329.03 ± 0.15	10.57 ± 1.27	626.51 ± 0.21	3.88 ± 0.39
341.43 ± 0.28	1.39 ± 0.39	633.09 ± 0.17	3.56 ± 0.38
350.72 ± 0.22	1.52 ± 0.60	636.55 ± 0.16	3.07 ± 0.39

TABLE 5.2.

Low Energy Gamma Rays and Relative Intensities in $^{107}Ag(n,\gamma)^{108}Ag$ (continued)

$E_\gamma \pm \Delta E_\gamma$	$(I_\gamma \pm \Delta I_\gamma)\%$	$E_\gamma \pm \Delta E_\gamma$	$(I_\gamma \pm \Delta I_\gamma)\%$
640.05 ± 0.23	2.89 ± 0.29	975.79 ± 0.16	0.61 ± 0.14
646.76 ± 0.29	0.93 ± 0.35	1013.16 ± 0.16	1.41 ± 0.15
656.46 ± 0.20	1.32 ± 0.40	1020.15 ± 0.20	1.60 ± 0.19
662.35 ± 0.33	1.70 ± 0.32	1026.66 ± 0.22	0.56 ± 0.16
671.14 ± 0.19	1.19 ± 0.30	1034.09 ± 0.17	0.74 ± 0.13
674.29 ± 0.32	0.48 ± 0.10	1051.31 ± 0.16	1.08 ± 0.14
687.39 ± 0.24	1.82 ± 0.13	1057.33 ± 0.31	0.92 ± 0.19
700.19 ± 0.20	0.84 ± 0.24	1080.19 ± 0.27	1.38 ± 0.14
708.27 ± 0.13	0.62 ± 0.15	1095.26 ± 0.16	1.11 ± 0.16
714.85 ± 0.45	1.09 ± 0.25	1112.37 ± 0.27	0.73 ± 0.12
724.55 ± 0.16	1.64 ± 0.20	1137.74 ± 0.13	1.02 ± 0.16
739.98 ± 0.26	0.53 ± 0.14	1140.83 ± 0.15	1.02 ± 0.16
744.62 ± 0.30	0.52 ± 0.13	1231.61 ± 0.22	0.88 ± 0.16
747.84 ± 0.27	0.52 ± 0.15	1310.75 ± 0.29	0.58 ± 0.29
757.33 ± 0.32	0.88 ± 0.15	1355.44 ± 0.15	0.70 ± 0.14
763.32 ± 0.34	0.50 ± 0.23	1462.64 ± 0.15	0.89 ± 0.15
782.21 ± 0.30	0.55 ± 0.24	1568.30 ± 0.23	0.69 ± 0.19
789.16 ± 0.30	0.72 ± 0.18		
796.17 ± 0.25	1.43 ± 0.18		
802.82 ± 0.25	0.90 ± 0.23		
808.08 ± 0.17	0.92 ± 0.24		
817.98 ± 0.11	0.76 ± 0.13		
820.12 ± 0.24	1.38 ± 0.20		
831.28 ± 0.15	0		
845.08 ± 0.18	0.89 ± 0.19		
867.83 ± 0.14	0.75 ± 0.24		
879.81 ± 0.15	0.78 ± 0.19		
886.34 ± 0.33	0.61 ± 0.19		
890.18 ± 0.08	0.50 ± 0.25		
895.16 ± 0.28	1.04 ± 0.15		
919.08 ± 0.15	1.89 ± 0.16		
923.70 ± 0.17	0.68 ± 0.13		
931.77 ± 0.42	0.62 ± 0.10		
937.33 ± 0.23	0.82 ± 0.15		
950.72 ± 0.73	0.48 ± 0.33		
960.87 ± 0.22	0.82 ± 0.13		
969.91 ± 0.20	0.68 ± 0.11		
972.67 ± 0.25	0.76 ± 0.13		

TABLE (5.3)

The γ-ray energies (E_γ < 700 keV) and relative intensities in the $^{109}Ag(n,\gamma)^{110}Ag$ reaction

E_γ (keV)			Relative Intensity	
Present Work	Ref (108)	Ref (109)	Present Work	Ref(108)*
68.51 ± 0.12	68.47 ± 0.10	68.58	7.3 ± 1.0	7.4
72.68 ± 0.11	72.7 ± 0.3	72.83	18.3 ± 1.8	22
80.18 ± 0.10	80.24 ± 0.10	80	20.5 ± 1.9	23.8
93.30 ± 0.12	93.25 ± 0.10	93.27	10.8 ± 1.0	12.5
105.68 ± 0.10	105.67 ± 0.10	105.59	32.1 ± 2.5	26.5
110.29 ± 0.13	110.45 ± 0.10	110.30	8.9 ± 0.8	10.0
117.43 ± 0.08	117.47 ± 0.10	117.37	100	100
124.79 ± 0.15	124.99 ± 0.10	-	3.9 ± 0.9	3.5
132.70 ± 0.14	132.82 ± 0.10	-	4.8 ± 1.0	3.6
152.65 ± 0.13	152.55 ± 0.20	152.50	6.8 ± 1.0	6.2
161.89 ± 0.15	161.82 ± 0.20	161.74	2.9 ± 0.8	3.2
191.30 ± 0.11	191.45 ± 0.10	191.27	45.1 ± 3.5	42.1
195.08 ± 0.12	195.52 ± 0.20	195.16	10.2 ± 0.9	10.0
198.40 ± 0.10	198.47 ± 0.10	198.39	153 ±10	185
235.60 ± 0.20	235.78 ± 0.10	235.47	99.5 ± 7.8	105
236.88 ± 0.27	236.62 ± 0.10	236.75	39.5 ± 3.3	30.0
266.89 ± 0.10	266.95 ± 0.10	266.86	41.3 ± 3.5	57
338.58 ± 0.09		338.6	12.3 ± 1.0	
360.29 ± 0.09		360.3	33.5 ± 2.7	
380.56 ± 0.11		≈ 379.7	40.3 ± 3.2	
423.68 ± 0.12		423.3	12.0 ± 0.9	
431.90 ± 0.15		431.0	5.8 ± 0.6	
535.89 ± 0.11			35.8 ± 2.8	
549.33 ± 0.11			41.3 ± 3.3	
586.70 ± 0.12			23.2 ± 2.1	
614.55 + 0.15			6.1 + 0.7	
620.24 ± 0.10			9.8 ± 1.0	
654.61 ± 0.09			39.1 ± 3.2	

*Error in the reported intensities is 10%

TABLE (5.4)

Background Radition at ULRC (Low Energy)

keV	Source (n,γ)*	keV	Source (n,γ)*
55	Ge72	527	Ge70
68	Ge72	572	Ge70
76	Pb K_α X-ray	596	Ge73
86	Pb K_β X-ray	608	Ge73
140	? (Ge 75m)	635	Ge70
160	? (Ge 77m)	701	Ge73
175	Ge70	708	Ge70
200	?	747	Ge70
253	Ge72	809	Ge73
284	Ge72	831	Ge70
297	Ge72	868	Ge73
303	I	961	Ge73
326	Ge70, Ge72	976	Ge72
345	Cu	1096	Ge70
353	Fe, Pb214	1101	Ge73
374	Fe; Cu; Pb	1105	Ge73
391	Ge70	1139	Ge70
421	I	1201	H
431	Ge72	1205	Ge73
443	I, Tl †	1299	Ge70
458	?	1379	Ge70
472	F; Na †	1461	K40 (Background)
493	Ge73	1472	Ge73
500	Ge70	1631	F decay
511	Annihilation	1698	Ge73
		1779	Al 28 (decay)

*References : 81, 112, 113, 114

†Only observed with Compton Spectrometer

TABLE 5.5.

High-Energy Gamma Rays and Relative Intensities (%) in $^{107}Ag(n,\gamma)^{108}Ag$

keV	I_γ	keV	I_γ
7269.30 ± 0.11	114.04 ± 3.01	6027.85 ± 0.32	13.97 ± 1.16
7190.6 ± 0.5	2.20 ± 0.81	5997.87 ± 0.14	2.84 ± 0.40
7076.27 ± 0.12	100	5958.54 ± 0.27	8.54 ± 0.91
7062.73 ± 0.16	36.52 ± 2.54	5944.04 ± 0.25	8.86 ± 0.91
6974.93 ± 0.13	47.18 ± 1.44	5913.97 ± 0.23	15.38 ± 1.20
6939.9 ± 0.7	2.50 ± 0.79	5863.92 ± 0.39	5.06 ± 0.65
6931.4 ± 0.6	3.74 ± 0.80	5831.25 ± 0.42	15.78 ± 1.93
6899.6 ± 0.5	1.36 ± 0.58	5806.79 ± 0.66	7.58 ± 1.95
6890.51 ± 0.11	22.98 ± 0.88	5796.58 ± 0.24	44.77 ± 2.34
6818.9 ± 0.5	1.37 ± 0.58	5787.08 ± 0.25	43.37 ± 2.30
6809.36 ± 0.14	4.08 ± 1.02	5772.98 ± 0.26	10.76 ± 1.84
6804.05 ± 0.08	4.38 ± 0.57	5728.93 ± 0.31	14.21 ± 1.58
6761.3 ± 0.4	3.19 ± 1.10	5720.55 ± 0.35	10.48 ± 1.56
6726.9 ± 0.8	1.10 ± 0.30	5701.11 ± 0.30	12.28 ± 1.63
6705.96 ± 0.14	34.85 ± 0.99	5685.74 ± 0.25	14.49 ± 1.65
6690.31 ± 0.51	2.60 ± 0.70	5675.90 ± 0.20	22.46 ± 1.72
6663.50 ± 0.41	2.13 ± 0.55	5639.76 ± 0.10	27.26 ± 1.04
6653.0 ± 0.50	1.61 ± 0.40	5633.89 ± 0.16	17.54 ± 1.00
6569.2 ± 0.5	1.73 ± 0.43	5614.23 ± 0.15	8.69 ± 0.93
6563.53 ± 0.48	7.59 ± 0.80	5606.03 ± 0.22	9.14 ± 0.94
6466.0 ± 0.5	2.01 ± 0.51	5568.43 ± 0.34	7.75 ± 1.38
6389.12 ± 0.18	5.38 ± 0.34	5557.65 ± 0.72	2.63 ± 1.40
6372.8 ± 0.6	1.01 ± 0.30	5547.86 ± 0.10	66.43 ± 1.74
6296.27 ± 0.45	5.34 ± 0.58	5498.74 ± 0.12	52.10 ± 1.55
6267.40 ± 0.20	24.32 ± 0.84	5482.31 ± 0.51	3.84 ± 0.99
6256.81 ± 0.27	11.85 ± 0.76	5442.40 ± 0.36	10.23 ± 2.23
6218.48 ± 0.17	17.15 ± 0.89	5308.96 ± 0.51	5.54 ± 1.86
6164.00 ± 0.18	16.30 ± 2.25	5296.37 ± 0.23	35.64 ± 2.38
6158.07 ± 0.26	48.10 ± 3.09	5283.47 ± 0.45	12.22 ± 2.01
6133.0 ± 0.4	2.21 ± 0.56	5278.42 ± 0.34	12.99 ± 1.99
6125.97 ± 0.15	2.74 ± 0.40	5248.52 ± 0.12	28.62 ± 1.31
6112.9 ± 0.5	2.12 ± 0.53	5233.50 ± 0.36	4.55 ± 1.10
6069.4 ± 0.5	1.93 ± 0.46	5211.54 ± 0.15	10.00 ± 1.03
6056.56 ± 0.42	12.28 ± 1.12	5172.23 ± 0.14	11.80 ± 1.26
6038.48 ± 0.52	4.29 ± 1.11	5139.24 ± 0.27	18.48 ± 1.60

TABLE 5.5.

High-Energy Gamma Rays and Relative Intensities (%) in $^{107}Ag(n,\gamma)^{108}Ag$ (continued)

keV	I_γ	keV	I_γ
5115.24 ± 0.38	7.04 ± 1.48	4628.43 ± 0.33	18.75 ± 2.53
5095.05 ± 0.25	20.86 ± 1.67	4617.58 ± 0.49	8.23 ± 2.44
5075.53 ± 0.23	31.28 ± 1.83	4589.52 ± 0.45	6.30 ± 1.53
5059.90 ± 0.33	10.54 ± 1.54	4577.97 ± 0.61	11.11 ± 1.55
5043.75 ± 0.65	3.38 ± 1.51	4562.99 ± 0.29	13.64 ± 1.59
5017.59 ± 0.33	5.14 ± 0.66	4554.35 ± 0.30	21.25 ± 1.69
5006.29 ± 0.20	12.03 ± 1.19	4537.06 ± 0.30	20.45 ± 1.66
4983.47 ± 0.24	12.49 ± 1.17	4520.76 ± 0.40	12.08 ± 1.59
4903.27 ± 0.45	18.80 ± 2.93	4450.56 ± 0.41	11.72 ± 1.71
4893.62 ± 0.42	15.49 ± 3.18	4436.48 ± 0.45	11.10 ± 1.72
4858.99 ± 0.30	24.45 ± 1.83	4396.17 ± 0.18	14.52 ± 1.62
4838.46 ± 0.50	7.55 ± 1.67	4348.08 ± 0.16	18.01 ± 1.68
4816.60 ± 0.36	28.09 ± 2.27	4308.74 ± 0.66	5.25 ± 2.09
4794.99 ± 0.50	9.62 ± 2.13	4290.25 ± 0.40	6.74 ± 2.15
4784.62 ± 0.45	23.91 ± 2.29	4273.14 ± 0.45	12.32 ± 2.21
4771.12 ± 0.44	10.93 ± 2.11	4250.32 ± 0.30	17.69 ± 2.26
4762.71 ± 0.34	12.97 ± 2.13	4027.89 ± 0.30	13.79 ± 1.45
4716.58 ± 0.25	24.39 ± 2.25	3883.31 ± 0.37	15.95 ± 1.96
4696.20 ± 0.53	7.93 ± 2.13	3861.31 ± 0.33	15.02 ± 1.98
4673.52 ± 0.35	12.83 ± 2.16	3584.92 ± 0.35	15.91 ± 2.88

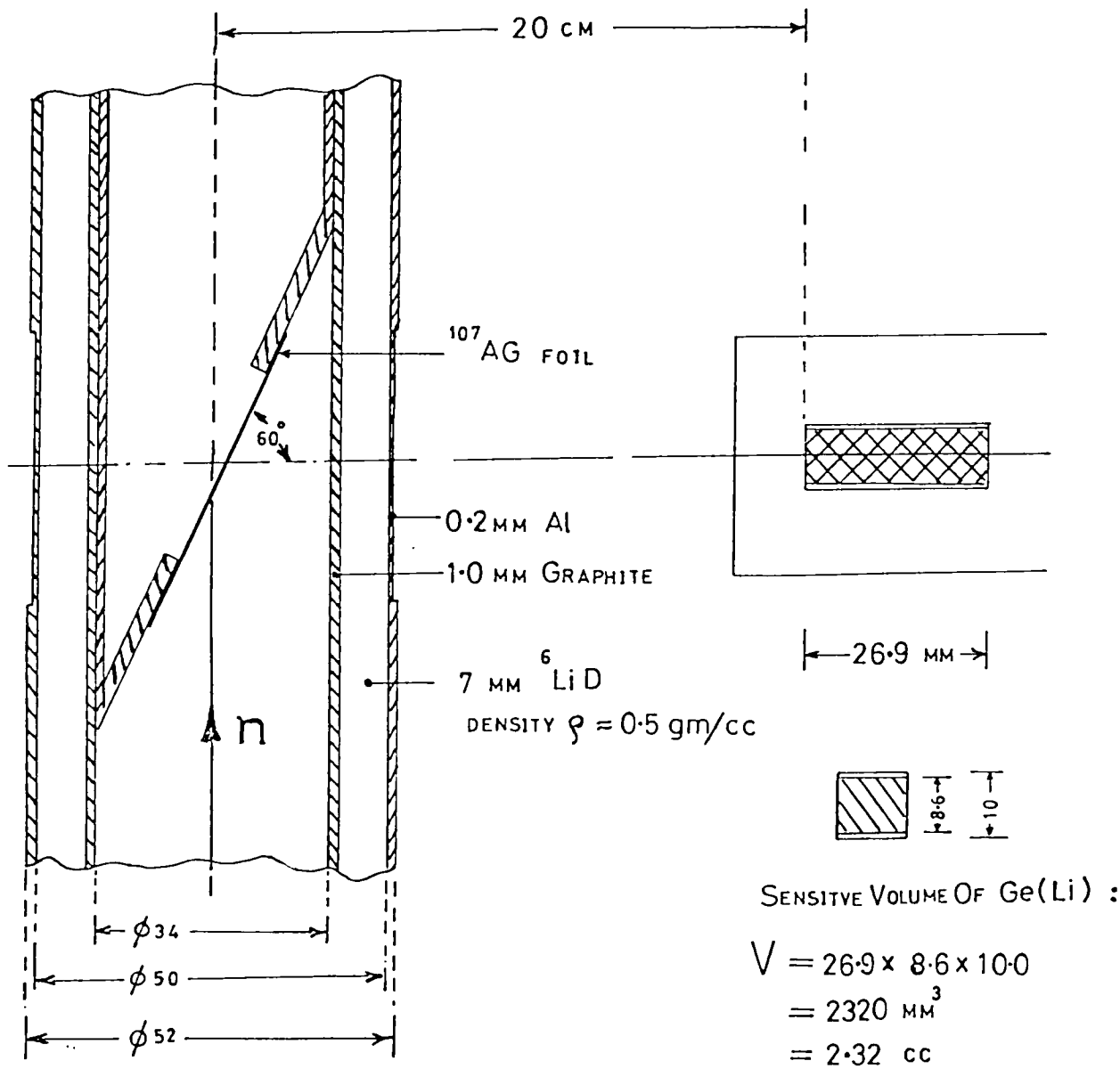


FIG.5.1 SAMPLE HOLDER AND PENCIL-SHAPE Ge(Li) DETECTOR [JÜLICH]

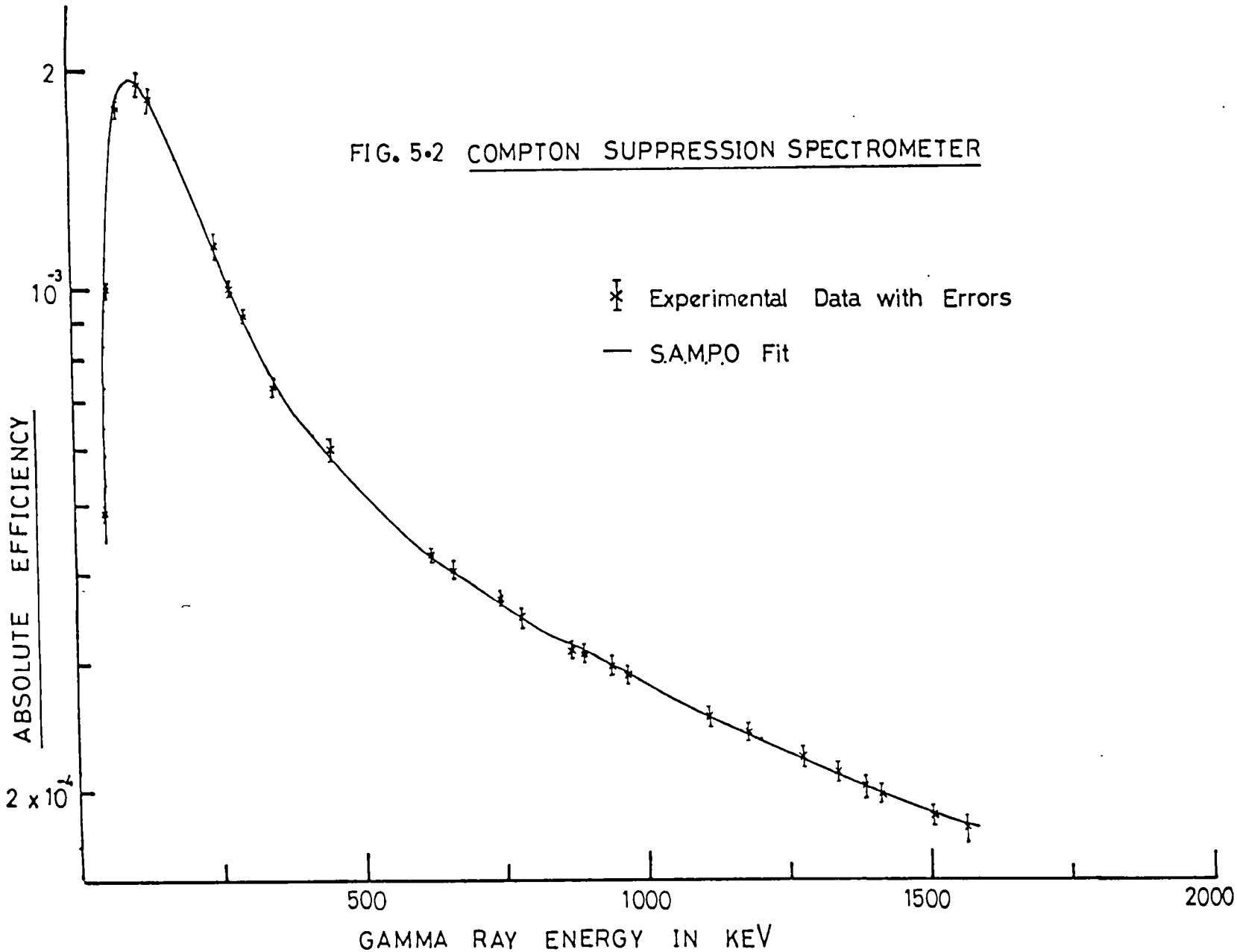


FIG. 5.2 COMPTON SUPPRESSION SPECTROMETER

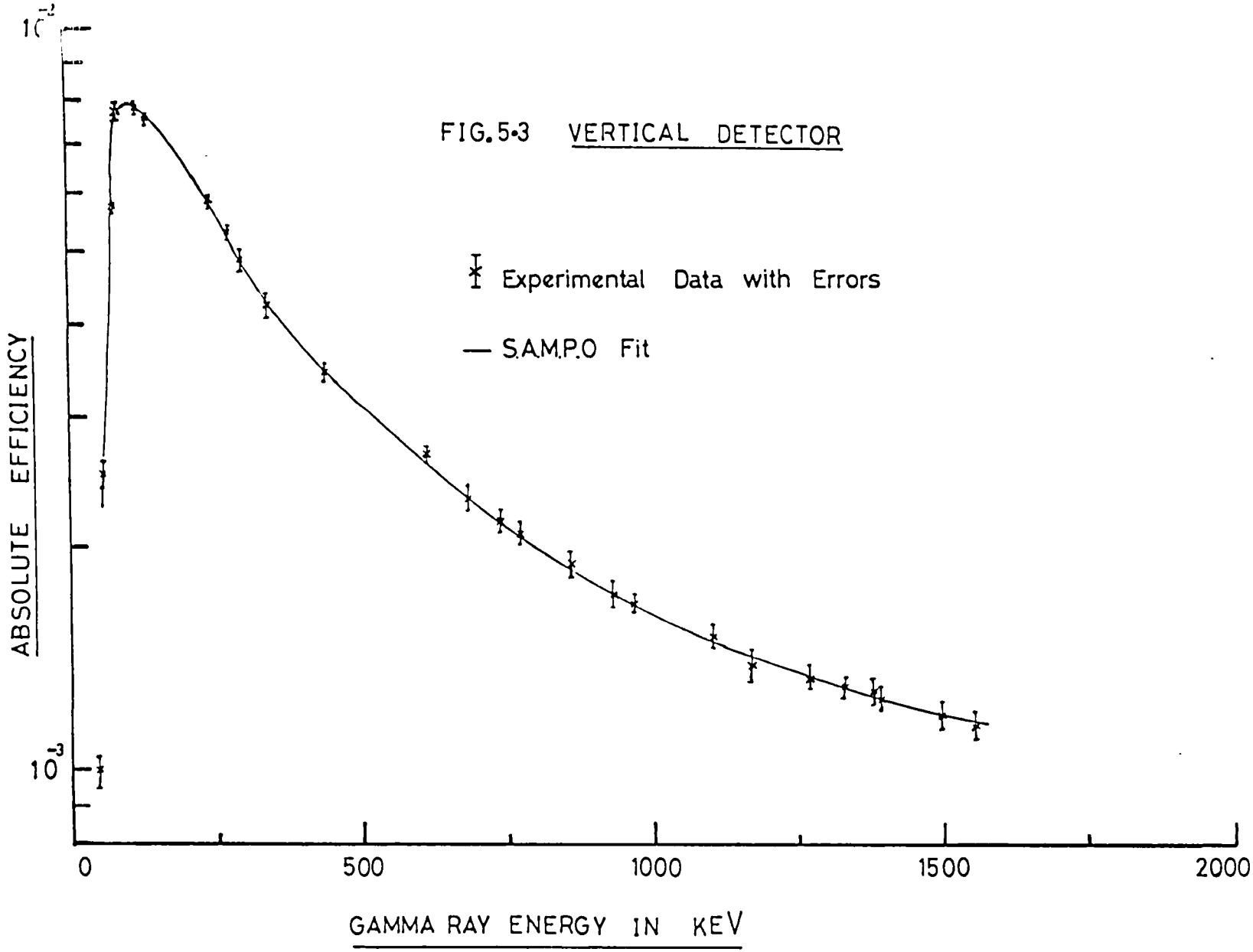


FIG. 5·3 VERTICAL DETECTOR

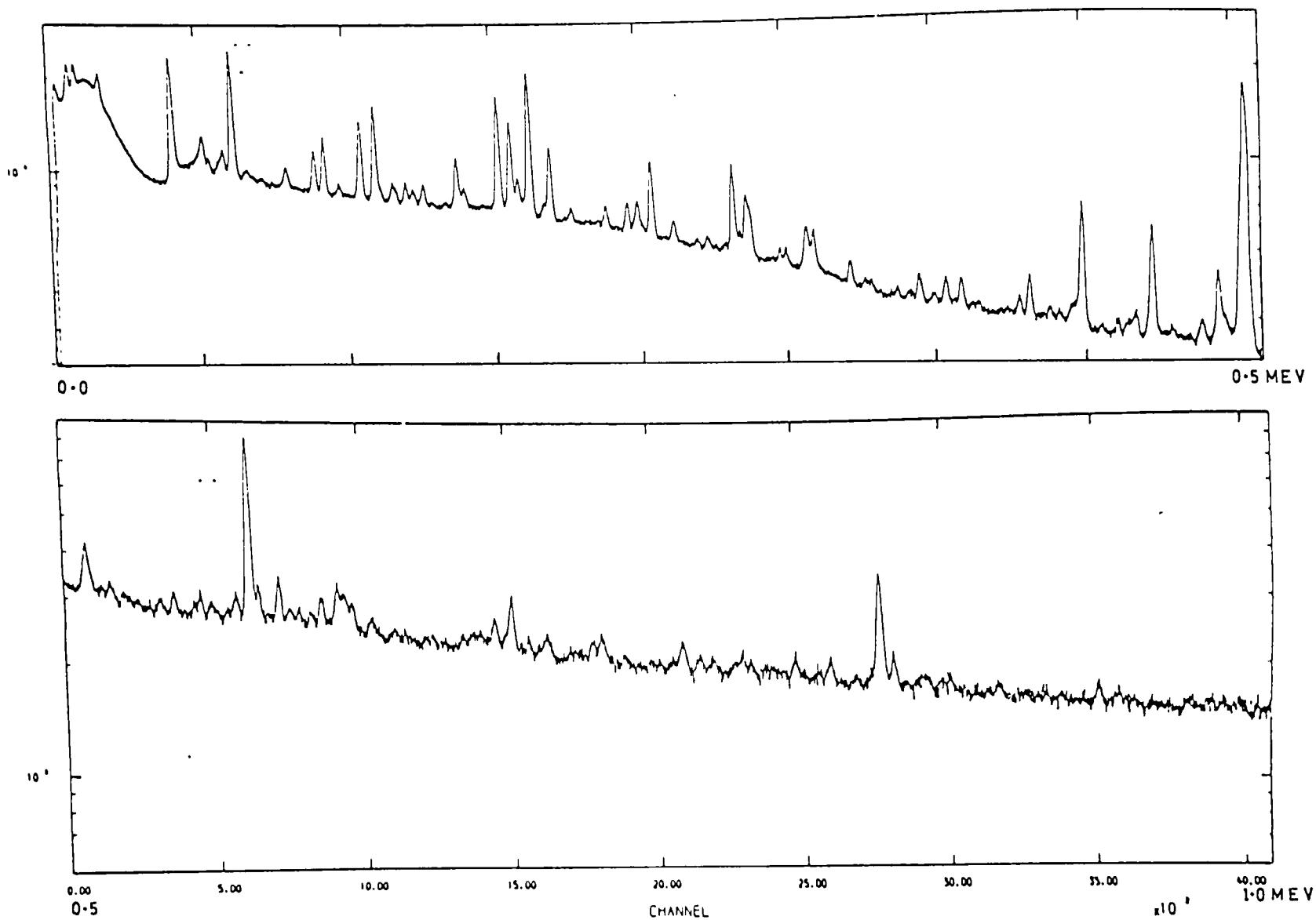


FIG.5.4 ••••• SILVER 107 (N,GAMMA) 0.0-1·0 MEV •••••

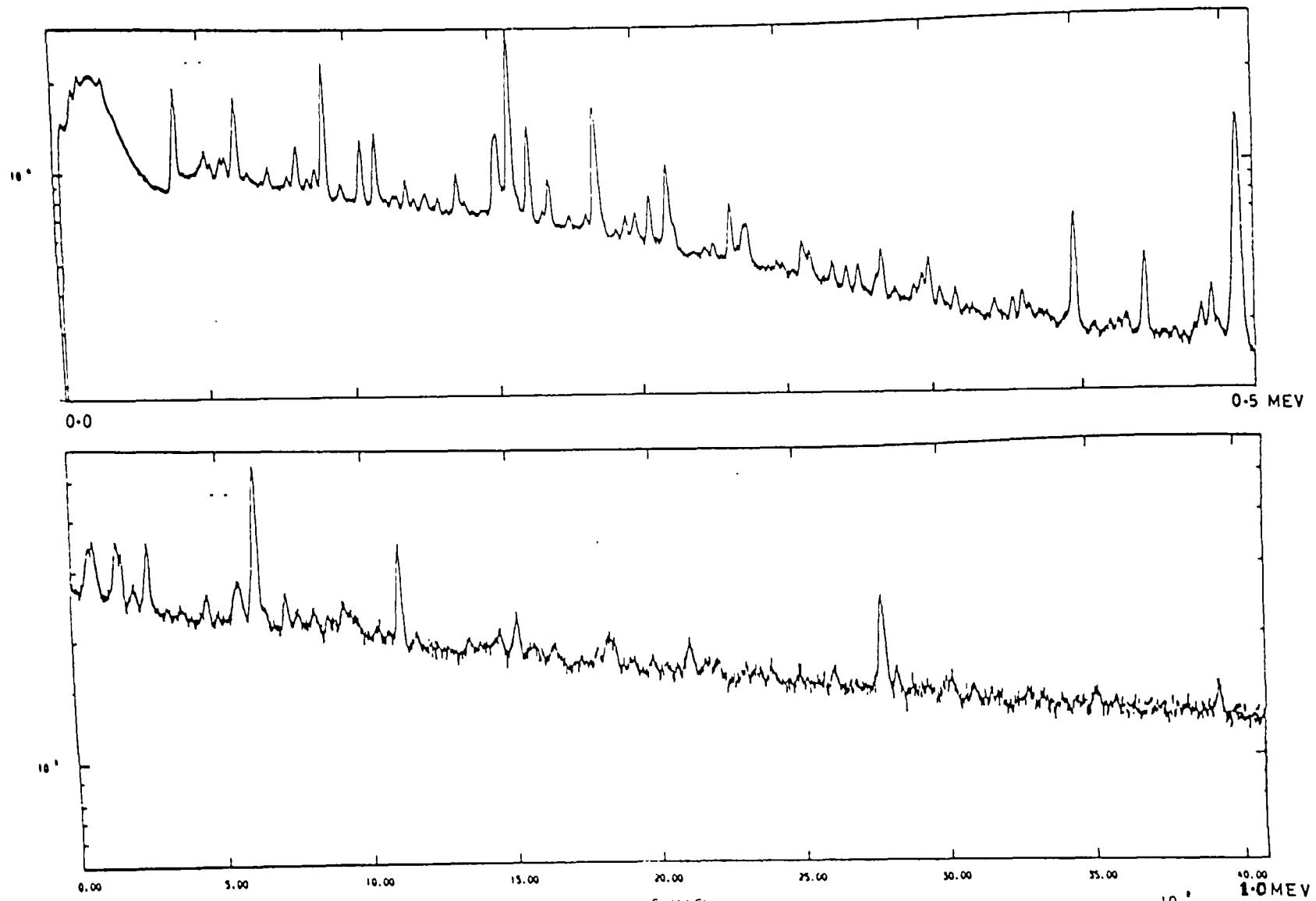


FIG. 5.5 ••••• NAT SILVER (N, GAMMA) 0.0-1.0 MEV •••••

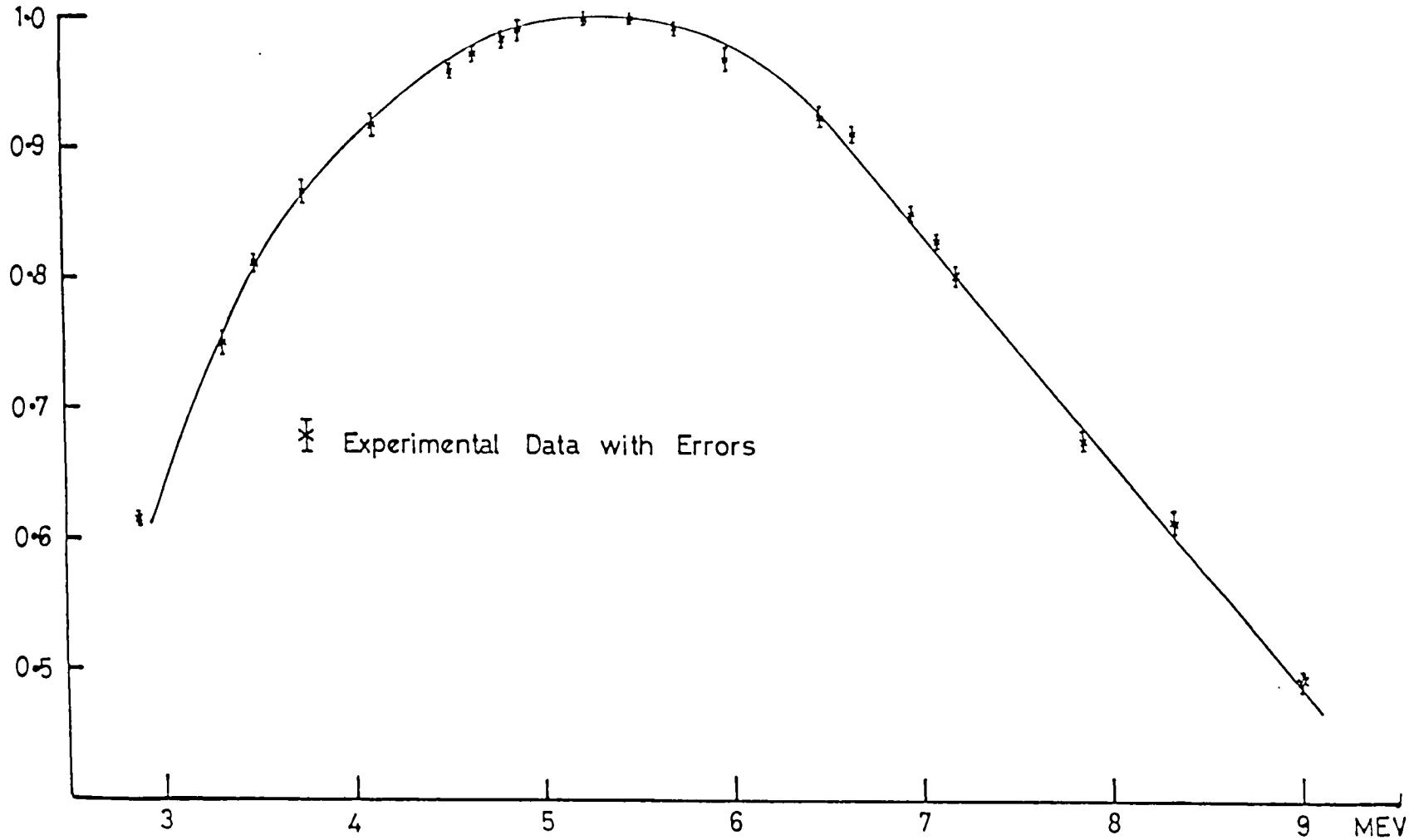


FIG. 5.6 DOUBLE ESCAPE PEAK EFFICIENCY (RELATIVE)

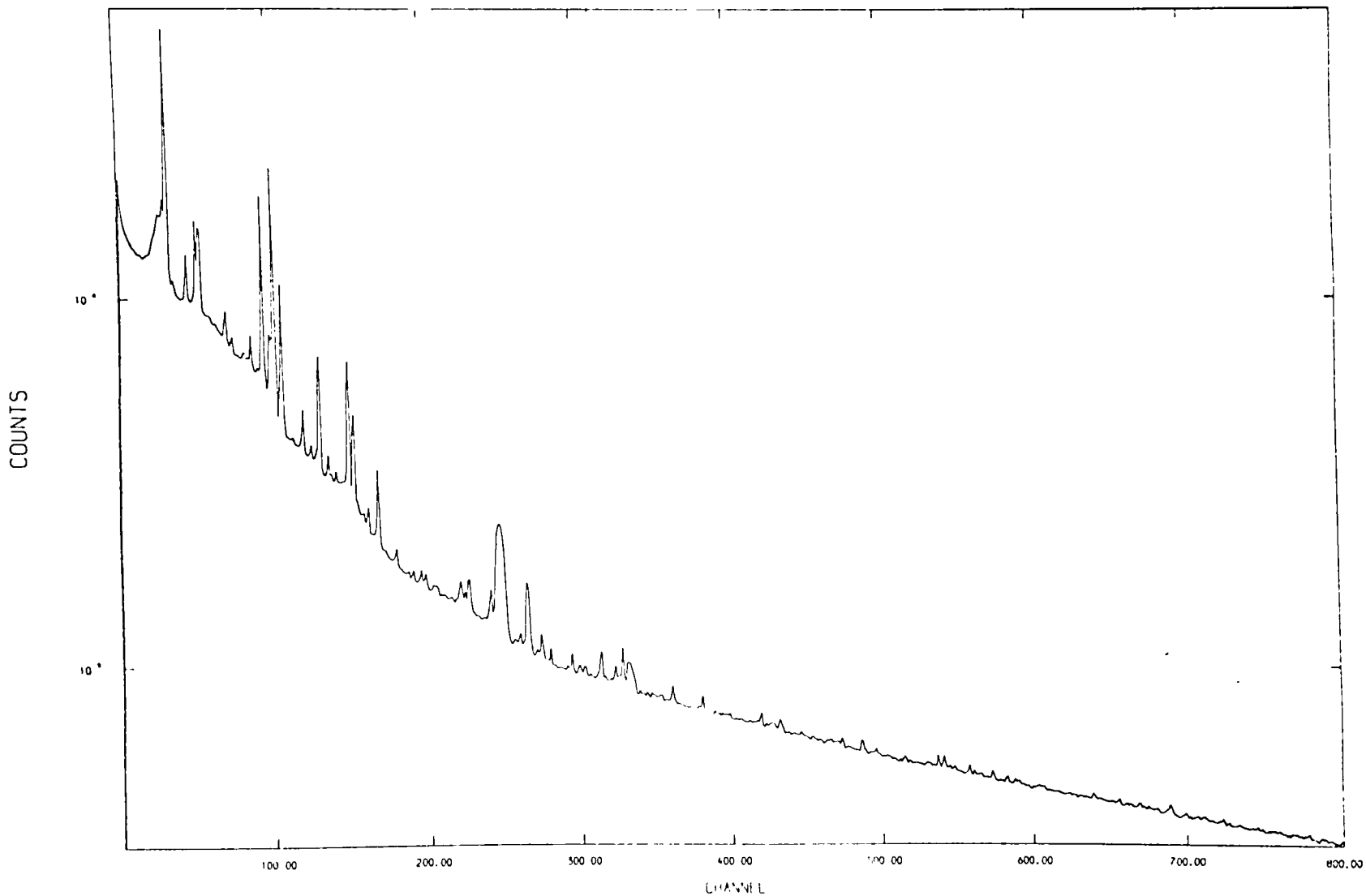


FIG.5.7.A ..... AG 107 (N,GAMMA) SINGLES SPECTRUM AT JULICH ..... (0.0 - 1.5 MEV)

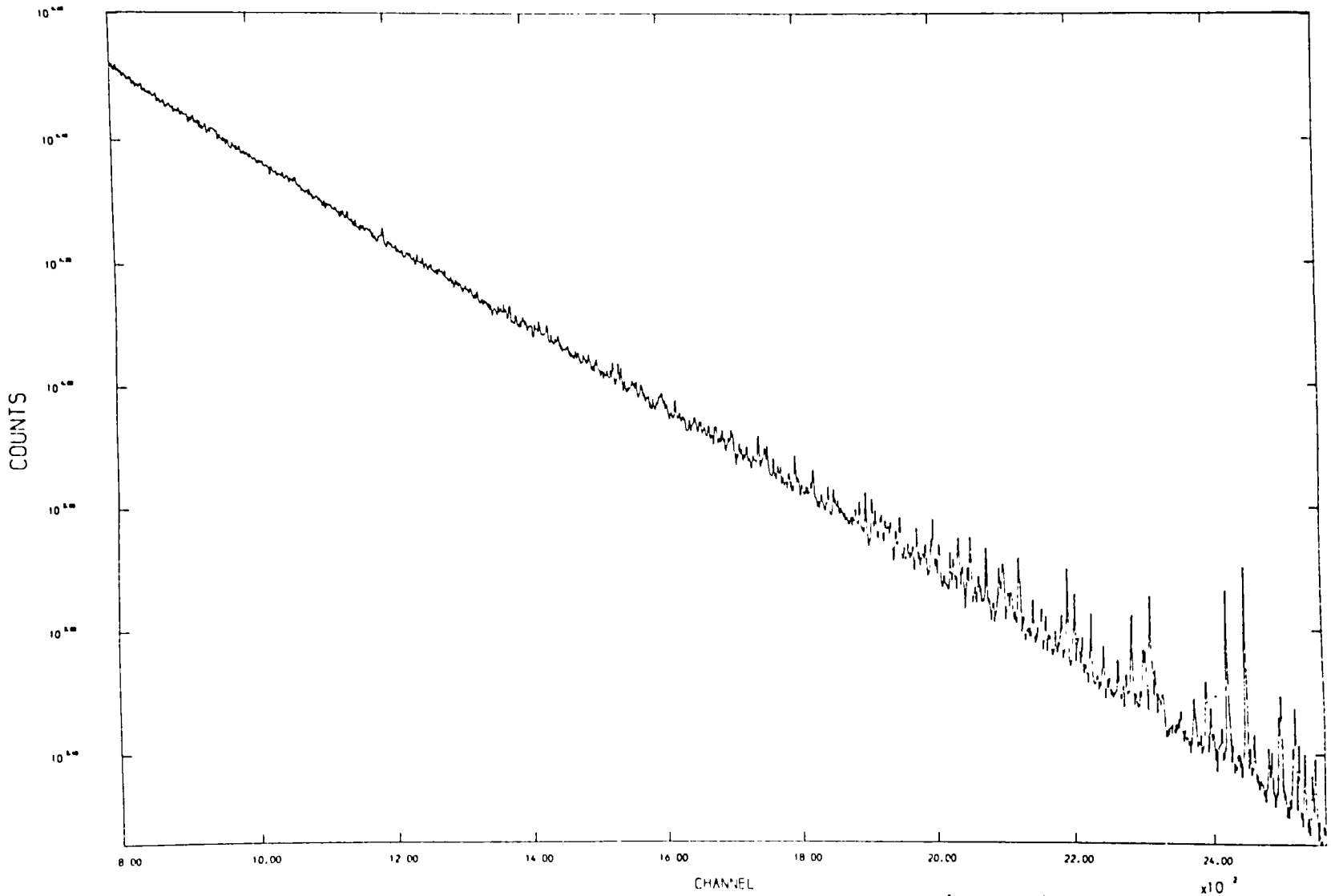


FIG.5.7.B ••••• AG 107 (N, GAMMA) SINGLES SPECTRUM AT JULICH ••••• (1·5 – 4·5 MEV)

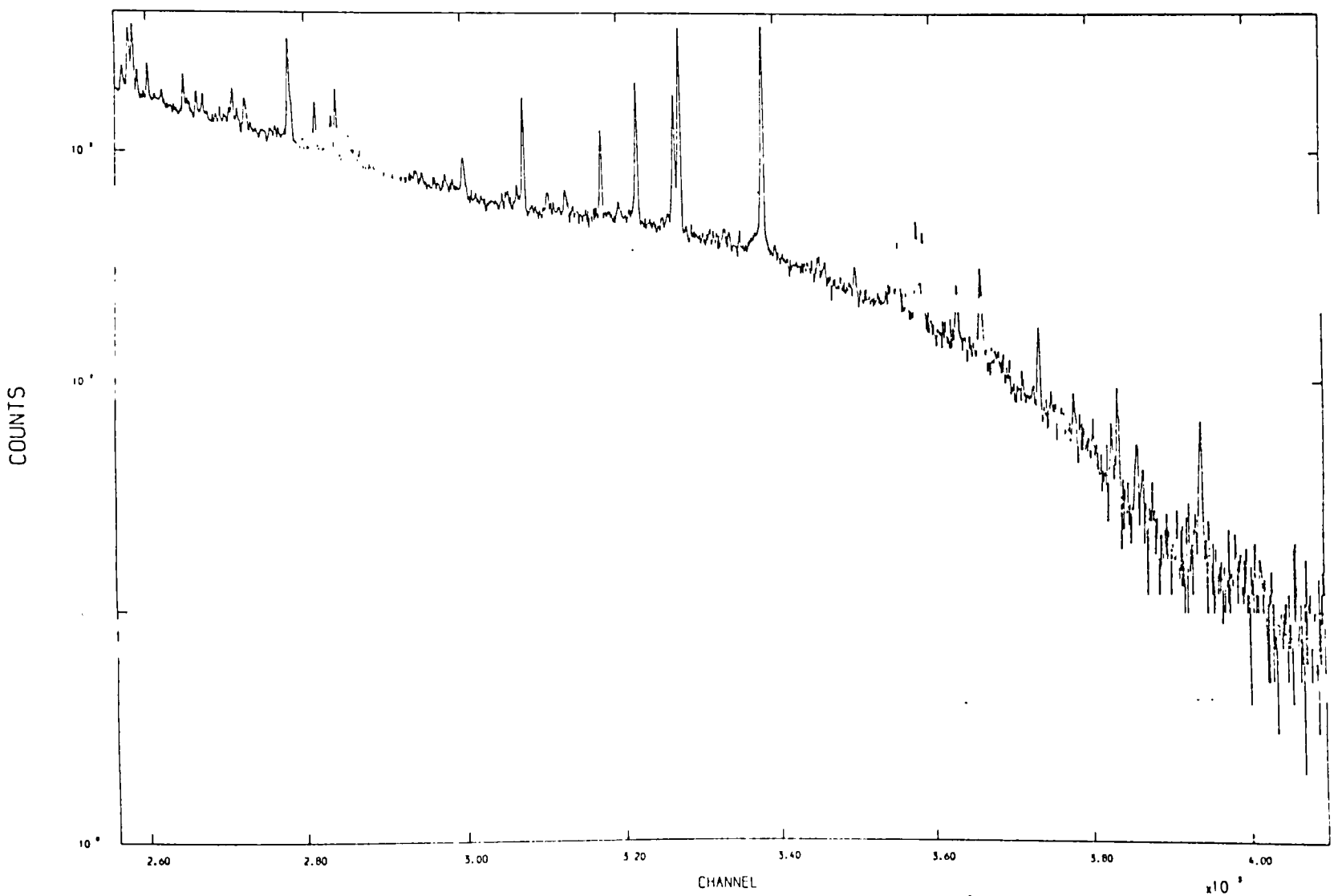


FIG.5.7.C ••••• AG 107(N,GAMMA) SINGLES SPECTRUM AT JULICH ••••• (4.5-7.5 MEV)

TABLE 5.6

Thermal Neutron Capture Gamma Rays From the $^{107}Ag(n,\gamma)^{108}Ag$ Reaction Obtained with the Curved Crystal Spectrometer and Transitions in ^{108}Ag Levels.

Energy (keV)	Error (eV)	Relative Intensity	Error (%)	Transitions in ^{108}Ag	Remarks
1140.7164	536.5	1330.879	31.3	1549.23 - 408.36	*
1136.7175	280.9	1453.548	18.8	1137.06 - 0.0	E
1112.2708	570.2	1019.970	38.5	1112.03 - 0.0	E
1079.5584	222.5	1699.838	16.9	1079.77 - 0.0	E
1051.6130	174.1	1550.341	14.6	1051.62 - 0.0	E
1034.1540	387.0	872.096	29.0	1241.00 - 206.61	CE
1031.2446	888.0	680.670	70.5	1325.24 - 294.57	*
1020.3023	160.8	2045.861	12.9	1213.35 - 193.08	CE
1013.2158	159.0	2032.510	14.8	1012.87 - 0.0	E
972.6546	149.3	1002.580	14.2	972.65 - 0.0	E
970.2224	393.0	681.197	32.4	1549.23 - 579.10	*
960.5374	314.3	746.554	32.1		
953.8066	245.4	587.421	25.3	1496.57 - 542.84	*
950.8253	301.6	701.189	27.1	1143.92 - 193.08	CE
937.3429	113.1	1378.683	10.5	1143.92 - 206.61	CE
933.2495	249.3	632.392	23.3	1012.87 - 79.14	CE
930.5014	426.4	521.180	40.4	1137.06 - 206.61	CE
[illegible]23.7051	191.7	[illegible]303.357	17.3	1540.67 - 616.94	*
920.2443	709.3	845.649	80.2	1463.10 - 542.86	*
918.8830	220.1	2207.792	33.0	1112.03 - 193.08	CE
902.6659	301.1	437.046	30.0	1231.71 - 329.18	CE
895.1877	88.7	1529.029	9.0	1355.30 - 460.08	*
890.3025	129.1	863.159	13.8	1105.82 - 215.38	CE
886.9585	307.8	388.092	31.6	1071.77 - 193.08	CE
880.8559	152.4	708.631	15.9	880.73 - 0.0	CE
876.2451	529.0	267.739	40.7	1200.38 - 324.50	CE
869.0781	483.4	262.953	52.0		
867.7842	406.5	245.275	41.0	1568.26 - 700.51	*
862.5493	388.6	416.496	44.7	1157.05 - 294.57	CE
858.7074	300.8	426.711	26.8	1051.62 - 193.08	CE
857.0735	586.3	223.671	61.4	857.34 - 0.0	CE
849.9154	219.7	359.812	21.9		
845.0110	77.4	1009.012	11.6	1051.62 - 206.61	CE
821.2367	116.8	945.130	12.6	1200.38 - 379.24	CE
820.2416	176.3	654.632	33.9	1701.25 - 880.73	*
819.0356	136.0	843.548	19.9	819.14 - 0.0	CE
817.9146	93.6	1076.797	12.0	897.11 - 79.14	CE
812.0794	116.1	851.955	15.0	1137.06 - 324.50	CE
809.5963	211.0	355.682	25.7	1002.57 - 193.08	CE
807.9302	123.5	608.911	15.6	1137.06 - 329.18	CE
802.7271	128.6	470.938	19.3	1568.26 - 765.50	*
797.0190	447.6	415.387	63.5	1012.87 - 215.38	CE
795.9587	49.9	1882.200	10.7	1002.57 - 206.61	CE
793.8407	244.7	319.864	40.7	1310.95 - 516.85	*
790.7881	173.2	366.932	24.3	1496.57 - 705.62	*
782.1680	217.3	366.681	28.3	1482.68 - 700.51	*
779.4921	316.4	204.807	43.7	972.65 - 193.08	CE
773.4941	542.1	221.619	73.7	1112.02 - 338.42	CE
772.2547	117.0	371.860	17.1	1629.77 - 857.33	*
766.8670	725.1	147.946	73.8	972.65 - 206.61	CE

TABLE 5.6 (Continued)

Energy (keV)	Error (eV)	Relative Intensity	Error (%)	Transitions in ^{108}Ag	Remarks
765.7832	172.8	241.645	25.5	765.50 - 0.0	CE
760.8357	250.9	225.641	36.5		
757.8037	135.6	594.317	26.7	1137.06 - 379.24	CE
756.9850	200.0	422.823	35.5	1051.62 - 294.57	CE
753.4438	118.5	419.958	16.9	1213.35 - 460.08	CE
749.5918	150.0	310.806	21.5	1200.38 - 451.05	CE
747.9739	127.1	359.191	18.5	1213.35 - 465.65	CE
744.4895	76.3	603.301	10.8	1985.59 - 1241.00	*
739.9825	68.6	671.177	9.5	1200.38 - 460.08	E
735.2963	151.5	193.773	26.7	1105.82 - 370.40	CE
732.5757	05.7	424.943	13.1	1112.03 - 379.24	CE
727.0331	244.8	190.885	41.0	1051.62 - 324.50	CE
724.6281	28.3	2599.938	5.7	803.70 - 79.14	CE
723.1900	201.9	224.431	30.6	1231.71 - 508.47	CE
722.0500	122.8	293.414	18.0	1438.13 - 715.80	*
719.8924	312.4	245.253	47.6		
718.6760	107.0	452.816	17.8	1325.24 - 606.53	*
715.8974	129.4	247.728	18.7	715.80 - 0.0	CE
713.5950	169.1	222.144	21.7	1325.24 - 611.66	*
709.3257	173.2	160.265	25.4	1079.77 - 370.40	E
708.1290	161.9	184.152	26.2	1002.57 - 294.57	E
701.0771	165.4	173.510	27.4		
698.1844	595.6	110.631	101.1	1105.82 - 408.38	E
695.6311	73.5	378.439	13.6		
693.2777	163.9	171.869	28.5	1272.28 - 579.10	CE
690.8163	112.4	403.179	14.1	897.11 - 206.61	CE
688.6136	75.2	555.599	16.4	1231.71 - 542.84	E
687.4906	26.0	2168.060	6.8	880.73 - 193.08	CE
686.3112	75.8	505.720	16.5	765.50 - 79.14	CE
680.5635	171.8	220.401	29.7		
679.1610	73.0	437.094	11.6	679.08 - 0.0	CE
675.3246	76.1	234.827	27.2	1787.06 - 1112.03	*
674.1838	55.7	726.187	7.7	880.73 - 206.61	CE
672.9332	117.1	254.412	22.4	1438.13 - 765.50	*
671.4482	69.3	445.059	12.1	1137.06 - 465.65	CE
668.0204	60.2	404.928	9.6	1231.71 - 563.82	CE
665.2910	66.3	360.356	10.2	880.73 - 215.38	CE
662.6700	51.9	645.593	9.7	1635.31 - 972.65	*
661.9448	117.8	253.987	35.1	1241.00 - 579.10	CE
657.5415	164.8	184.452	32.0	1200.38 - 542.84	CE
656.3314	48.5	578.081	10.2	656.33 - 0.0	CE
651.8268	51.0	401.484	9.0	1112.03 - 460.08	CE
646.2593	82.5	223.920	19.0	972.65 - 324.80	CE
647.5831	80.7	280.414	18.3	1972.88 - 1325.24	*
646.7147	64.6	333.328	13.7	1112.03 - 465.65	CE
642.1071	139.3	204.733	29.4	857.34 - 215.38	CE
641.2084	476.6	133.656	83.4	1721.45 - 1079.77	*
640.2320	17.9	3161.634	5.3	1105.82 - 465.65	CE
637.5353	69.6	339.145	16.3	1012.87 - 375.62	CE
636.6660	17.0	4212.138	6.0	1200.38 - 563.81	CE

TABLE 5.6 (Continued)

Energy (keV)	Error (eV)	Relative Intensity	Error (%)	Transitions in ^{108}Ag	Remarks
635.9141	37.7	695.391	10.7	1991.18 - 1355.30	*
633.0674	15.7	5469.479	5.1		^{108}Ag decay
629.6916	27.1	960.887	8.4	1787.06 - 1157.05	*
628.6287	101.0	270.353	20.5	1137.06 - 508.47	CE
626.5570	16.0	5905.698	4.8	705.62 - 79.14	CE
626.0147	44.1	469.080	36.6	819.14 - 193.08	CE
624.4271	45.7	486.203	11.5	1231.71 - 606.53	CE
622.4327	50.8	407.057	15.8	1635.31 - 1012.87	*
621.7587	23.6	1098.574	8.1	1701.25 - 1079.77	*
620.3521	291.5	165.803	66.8	1231.71 - 611.66	E
618.9127	26.6	775.819	8.1		^{108}Ag decay
616.9408	18.3	2480.503	6.0	616.94 - 0.0	CE
615.2940	161.8	159.599	36.3	1721.45 - 1105.82	*
613.8126	121.1	178.898	26.8	1770.86 - 1157.05	*
612.3364	64.7	278.600	15.7	819.04 - 206.61	CE
611.7587	54.0	353.729	12.7	611.66 - 0.0	CE
606.4749	73.0	277.907	14.7	606.53 - 0.0	CE
606.0047	192.3	181.046	43.5	1711.82 - 1105.82	*
603.9106	27.5	648.745	9.4	819.04 - 215.38	CE
602.8933	81.7	225.837	20.3	897.11 - 294.57	CE
599.9646	13.2	2700.851	7.7	679.08 - 79.14	CE
597.3720	41.3	392.277	10.0	803.70 - 206.61	E
595.0849	34.4	420.850	8.7	1241.00 - 645.51	CE
594.1920	114.0	159.623	26.0	1002.57 - 408.36	CE
585.9975	21.6	551.782	6.7	880.73 - 294.57	CE
583.9322	138.5	96.636	33.7		
580.8966	41.4	348.591	11.0	1438.13 - 857.34	*
580.1014	39.5	443.394	11.2	1143.92 - 563.81	CE
579.1927	19.5	1407.211	6.9	579.10 - 0.0	CE
576.3337	86.8	126.367	20.6	1473.34 - 897.11	*
574.7580	24.0	567.260	6.6	1711.82 - 1137.06	*
573.0854	79.3	146.421	21.6	1137.06 - 563.81	CE
572.3740	20.6	1144.289	7.3	765.50 - 193.08	CE
571.2570	57.8	185.970	15.8	1079.77 - 508.47	E
569.3217	173.9	83.592	45.4	1112.03 - 542.84	E
566.1886	102.0	125.800	23.8	645.51 - 79.14	CE
563.8198	13.0	2633.928	5.3	563.81 - 0.0	CE
558.8602	21.3	696.506	6.9	765.50 - 206.61	CE
552.4987	39.1	277.734	9.6	1231.71 - 679.08	E
550.2250	70.6	146.184	20.5	765.50 - 215.38	CE
542.6047	33.8	341.968	8.8	1002.57 - 460.08	CE
537.7904	13.1	2084.073	5.1	616.94 - 79.14	CE
536.2086	83.4	117.289	24.2	1355.30 - 819.14	*
533.9416	40.4	239.275	14.1	1213.35 - 679.08	CE
533.0032	25.4	503.472	8.9	1584.07 - 1051.62	*
530.6107	22.1	517.259	6.7	1137.06 - 606.53	CE
527.3909	11.1	4402.611	4.8	606.53 - 79.14	CE
526.5873	67.9	209.262	30.7	897.11 - 370.40	E
525.9020	313.6	126.542	90.7	1231.71 - 705.62	E
524.6018	77.9	215.309	26.4	819.14 - 294.57	CE

TABLE 5.6 (Continued)

Energy (keV)	Error (eV)	Relative Intensity	Error (%)	Transitions in ^{108}Ag	Remarks
524.1157	17.8	803.635	6.5	1496.57 - 972.65	*
522.9290	461.6	84.192	138.3		
522.7066	221.7	106.959	95.4	715.80 - 193.08	CE
521.7004	23.2	492.182	8.6	972.65 - 451.05	CE
520.7068	25.3	558.445	7.8	1137.06 - 616.94	CE
520.0352	47.6	272.030	19.4		
519.5195	30.9	363.585	14.9	1663.44 - 1143.92	*
517.0396	95.9	139.743	50.1	516.85 - 0.0	CE
514.8521	194.4	131.511	58.0	1787.06 - 1272.23	*
511.5418	64.0	313.185	19.5	1157.05 - 645.51	E
509.2673	32.8	540.650	27.0	803.70 - 294.57	CE
508.4665	10.6	4901.957	7.4	508.47 - 0.0	CE
504.3019	25.6	337.988	10.8	1584.07 - 1079.77	*
502.2441	26.8	363.464	8.7	1827.22 - 1325.24	*
500.5814	22.0	592.381	8.7	1473.34 - 972.65	*
500.2559	50.0	351.844	45.9	1200.38 - 700.51	CE
499.9520	14.2	1626.712	8.6	579.10 - 79.14	CE
497.6602	23.2	322.316	8.4	1549.23 - 1051.62	*
495.1440	37.2	304.346	14.7	1112.03 - 616.94	CE
494.6963	18.4	600.905	7.6	1200.28 - 705.62	CE
494.1156	47.8	166.369	19.5	1002.57 - 508.47	E
493.4258	28.4	302.429	10.1		
492.5682	86.8	180.537	19.3	1629.77 - 1137.06	*
491.9870	77.3	113.787	26.6	1310.95 - 819.14	*
490.6122	30.6	176.634	12.6	1463.10 - 972.65	*
488.2263	38.1	144.129	22.4		
487.7454	18.2	470.431	9.0	1051.62 - 563.81	CE
486.1819	52.6	306.742	50.9	1629.77 - 1143.92	*
485.9840	23.2	602.730	11.0	679.08 - 193.08	CE
485.1696	39.3	184.029	16.5	700.51 - 215.38	CE
484.1978	93.8	139.563	34.0		
482.3727	16.5	409.063	7.8	1593.20 - 1112.03	*
480.7343	59.8	163.012	20.6	819.14 - 338.42	CE
479.1561	17.1	450.067	7.8	803.70 - 324.50	CE
478.3804	101.2	87.775	51.2		
473.2629	59.3	204.555	24.2	1079.77 - 606.53	CE
472.5030	33.0	334.083	19.0	679.08 - 206.61	CE
472.2240	24.7	434.391	16.0	880.73 - 408.37	CE
471.4542	25.8	137.914	22.1	1584.07 - 1112.03	*
466.1220	50.9	215.275	32.4	1231.71 - 765.50	CE
465.6502	8.0	3819.976	5.3	465.65 - 0.0	CE
465.3134	16.9	480.169	21.7	803.70 - 338.42	CE
463.7187	9.0	1618.096	5.1	542.84 - 79.14	CE
462.8264	81.5	142.134	26.4	1079.77 - 616.94	E
462.1981	120.0	85.360	49.1		
460.9213	29.7	227.054	12.9	1540.69 - 1079.77	*
458.0150	42.1	185.000	17.8	1137.06 - 679.08	CE
457.4956	42.1	173.166	18.8		
456.1403	30.3	262.583	9.3	1593.20 - 1137.06	*
452.9787	43.1	132.152	13.5	1272.23 - 819.14	E

TABLE 5.6 (Continued)

Energy (keV)	Error (eV)	Relative Intensity	Error (%)	Transitions in ^{108}Ag	Remarks
451.1467	112.0	84.737	32.3	451.05 - 0.0	E
449.6580	42.2	194.955	15.1	656.33 - 206.61	CE
449.1761	150.9	73.079	54.1	857.34 - 408.36	E
448.7265	57.1	70.089	24.7	819.14 - 370.40	E
446.1627	37.5	102.356	16.2		
445.5754	15.0	303.573	6.8		
443.3989	63.3	98.360	20.3	1143.92 - 700.51	E
442.8332	58.0	73.005	31.7		
441.5819	48.0	171.336	30.1		
441.3135	11.7	545.501	7.7	1157.05 - 715.80	CE
440.6935	13.1	644.497	8.6		
439.8658	9.3	1828.452	6.7	819.14 - 379.24	CE
438.8990	10.9	2791.329	8.7	645.51 - 206.61	CE
438.7686	20.0	752.888	33.2	1002.57 - 563.81	CE
437.7156	7.4	2108.058	4.7	516.85 - 79.14	CE
437.0810	90.4	119.561	56.2		
436.1679	35.0	120.190	19.2		
435.2686	15.3	[illegible]	7.4	1200.38 - 765.50	E
434.2761	33.8	174.157	21.9	1079.77 - 645.51	CE
433.9852	7.6	1676.503	5.1		^{108}Ag decay
433.2154	83.1	64.313	38.6	803.70 - 370.40	E
432.2116	27.7	166.415	13.1		
431.8631	27.9	181.258	12.3		
431.3681	13.9	334.679.	8.2	897.11 - 465.65	CE
430.0857	51.4	116.528	27.2	645.51 - 215.38	CE
429.3522	6.6	3854.257	6.6	508.47 - 79.14	CE
428.7985	82.1	135.598	36.1		
427.0535	6.9	1835.845	4.6	765.50 - 338.42	CE
425.5625	52.7	65.484	24.4		
423.8792	8.1	699.107	4.9	616.94 - 193.08	CE
422.7076	44.2	56.883	27.8		
420.9789	46.6	77.943	17.0		
419.7860	24.1	111.275	12.9		
419.0057	19.0	188.659	8.8		
418.5776	89.1	93.937	40.7	611.66 - 193.08	E
417.1698	60.8	55.523	28.3		
416.7384	65.6	54.498	31.2		
414.3060	20.0	129.369	11.5		
413.4879	34.8	129.756	17.1	606.53 - 193.08	CE
412.4369	38.1	95.059	24.4	1231.71 - 819.14	E
411.8562	31.3	65.597	22.8		
410.7306	86.9	57.203	47.5	819.14 - 408.37	E
410.3275	11.6	358.832	7.3	616.94 - 206.61	CE
408.3694	9.2	504.918	5.9	408.37 - 0.0	CE
406.1736	27.7	114.035	13.1	1051.62 - 645.51	E
405.2761	37.3	119.357	25.9	1105.82 - 700.51	E
405.0702	15.1	320.406	10.1	611.66 - 206.61	CE
403.5039	74.1	64.058	27.2		
401.5802	49.9	71.916	23.1	616.94 - 215.38	E
401.0807	54.8	77.449	46.8	1012.87 - 611.66	E

TABLE 5.6 (Continued)

Energy (keV)	Error (eV)	Relative Intensity	Error (%)	Transitions in ^{108}Ag	Remarks
400.2413	18.6	206.613	14.5	1105.82 - 705.62	CE
399.9229	7.0	1481.977	5.9	606.53 - 206.61	CE
399.2410	23.8	105.300	16.3		
397.4182	14.6	202.365	7.8		
396.2800	7.0	1093.269	5.3	1200.38 - 803.70	CE
395.8863	19.2	128.906	14.1		
395.3047	25.2	105.284	16.6	803.70 - 408.37	E
393.4773	9.5	287.062	6.7		
391.4581	18.2	126.520	10.9	1157.05 - 765.50	E
389.4027	18.6	92.062	12.4		
388.1949	17.3	146.366	12.0		
388.0601	37.7	185.004	31.1		
387.6968	32.3	102.976	21.4		
386.5048	6.5	851.536	5.4	465.65 - 79.14	CE
386.2185	9.7	449.419	9.8	765.50 - 379.24	CE
386.0336	10.3	360.374	11.9	579.10 - 193.08	CE
384.3546	8.1	533.271	5.2		
381.7630	23.2	83.038	14.7		
381.1513	19.8	143.345	19.5	705.62 - 324.50	CE
380.9442	5.9	1446.601	5.9		
379.7996	35.9	47.875	44.4		
379.2500	7.7	397.472	5.9	379.24 - 0.0	CE
377.6793	16.7	133.071	9.1		
375.6206	11.9	144.201	8.9	375.61 - 0.0	CE
372.4338	9.4	271.452	6.7	880.73 - 508.47	CE
370.7440	5.5	1085.870	4.7	563.81 - 79.14	CE
370.4163	11.8	166.440	10.7	370.40 - 0.0	CE
368.5534	26.6	64.978	15.1		
366.0433	39.4	34.328	34.8		
365.1661	5.9	738.872	5.0		
364.0320	29.1	157.215	1001.0		
362.4403	10.1	168.194	8.2		
361.2418	28.6	41.198	28.3		
360.6267	14.0	98.376	9.4		^{109}Ag (n,γ)
359.9940	24.8	111.129	26.8	1241.00 - 880.73	CE
358.3645	37.0	53.269	33.5		
357.4105	11.3	154.090	9.7		
357.1601	16.2	111.540	12.7	765.50 - 408.37	CE
355.5960	23.3	51.248	16.7		
353.4819	16.6	97.804	10.0	1157.05 - 803.70	E
351.9051	62.8	41.693	41.5		
351.4970	95.1	121.457	27.7		
351.3057	15.2	130.438	12.0	1051.62 - 700.51	E
350.9413	5.1	1549.582	6.6	645.51 - 294.57	CE
350.5221	18.4	82.699	16.0		
349.9076	15.2	112.102	12.2	679.08 - 329.18	CE
349.2691	10.6	130.357	9.7		
348.4241	6.7	416.861	5.5	563.81 - 215.38	CE
346.4268	8.1	221.916	6.2	1112.03 - 765.50	CE
345.7531	103.0	40.643	34.4		

TABLE 5.6 (Continued)

Energy (keV)	Error (eV)	Relative Intensity	Error (%)	Transitions in ^{108}Ag	Remarks
343.2331	70.8	26.928	48.6		
342.4210	14.0	104.695	12.9		
341.7220	7.7	238.317	6.2		
339.5150	32.7	43.943	29.2		
338.4896	22.9	53.384	22.9	338.42 - 0.0	E(?)
337.9777	14.1	89.920	12.2	880.73 - 542.84	E
337.3824	11.3	90.308	12.4		
336.8813	31.7	53.425	30.1		
336.5551	10.3	139.072	9.2	715.80 - 379.24	CE
332.1584	5.7	512.978	5.5	1213.35 - 880.73	CE
329.1751	4.8	11456.818	4.7	329.18 - 0.0	CE
328.9741	33.2	159.461	40.2		
327.4569	5.2	585.349	5.0	542.84 - 215.38	CE
326.9504	16.0	70.841	13.9		
326.4528	36.6	54.112	21.2	705.62 - 379.24	E
325.4228	28.3	41.878	24.3		
324.4935	6.4	366.498	5.6	324.49 - 0.0	CE
323.1894	46.8	71.163	56.6		
322.7086	7.0	207.951	7.3		
322.3770	20.4	67.774	17.3	616.94 - 294.57	E
320.9993	9.2	122.496	8.4	645.51 - 324.50	CE
319.2787	32.0	39.144	22.4	1200.38 - 880.73	E
317.9234	33.6	41.984	27.3	897.11 - 579.10	E
317.1062	4.0	3119.974	4.6	880.73 - 563.82	CE
315.4144	8.1	230.289	6.9	508.47 - 193.08	CE
313.2242	16.4	74.323	15.0		
311.9617	5.0	771.635	5.5	606.53 - 294.57	CE
310.8177	10.9	175.159	9.1		
310.2233	13.3	125.952	11.2	516.85 - 206.61	CE
309.8766	23.1	136.604	33.1		
309.2999	46.6	51.131	28.9		
307.9142	40.5	57.488	29.9		
305.4178	16.1	86.850	15.7	765.50 - 460.08	E
304.9282	36.3	74.582	22.7		
304.1130	38.4	56.598	52.9		
303.8783	4.9	798.817	5.6		
302.2213	9.1	161.441	9.9	1105.82 - 803.70	CE
301.8413	5.2	515.646	6.1	508.47 - 206.61	CE
300.9068	11.0	115.997	14.1		
300.4264	15.0	90.534	22.1		
300.0815	4.1	19625.618	5.2	379.24 - 79.14	CE
299.8924	21.2	224.204	31.9	765.50 - 465.65	CE
298.7994	15.8	97.979	16.6		
296.0602	9.3	109.827	12.9		
295.2458	10.5	96.932	11.9	803.70 - 508.47	E
294.5672	3.7	34112.394	5.0	294.57 - 0.0	CE
292.4310	7.3	140.829	8.3	616.94 - 324.50	E
292.1044	34.0	39.573	31.0	700.51 - 408.36	E
291.2136	4.1	700.966	4.7	370.40 - 79.14	CE
290.2267	5.9	197.634	6.5		

TABLE 5.6 (Continued)

Energy (keV)	Error (eV)	Relative Intensity	Error (%)	Transitions in ^{108}Ag	Remarks
287.1653	4.1	515.874	5.4		
286.8914	5.2	302.311	6.3	803.70 - 516.85	CE
286.6687	9.0	111.488	11.2	1105.82 - 819.14	E
285.9769	7.5	153.935	8.1	656.33 - 370.40	E
285.7564	14.0	59.680	17.8		
283.0048	3.8	759.279	4.2		
279.8307	6.8	118.824	9.2	1137.06 - 819.14	E
279.5295	4.2	700.938	5.0		
278.9418	34.6	63.181	37.7		
278.5283	3.7	1158.002	4.8	616.94 - 329.18	CE
278.2391	11.5	110.865	11.8		
277.3205	40.6	40.162	29.8	606.53 - 329.18	E
275.2271	4.3	303.138	5.4	645.51 - 370.40	CE
274.6588	40.1	50.122	45.5		
274.1734	8.2	84.889	10.6	880.73 - 606.53	E
272.5647	4.3	670.198	4.7	465.65 - 193.08	CE
270.9996	5.5	175.558	6.4		
270.1396	10.1	63.823	12.8		^{109}Ag (n,γ)
269.2534	3.9	3319.640	4.3	563.81 - 294.57	CE
268.9934	31.6	66.103	35.9	880.73 - 611.66	E
268.6419	8.1	93.823	10.7		
268.3350	39.5	49.255	46.2	1241.00 - 972.65	CE
267.2079	5.3	266.433	5.6		^{109}Ag (n,γ)
266.0752	8.0	88.163	10.0	645.51 - 379.24	E
265.1700	15.5	74.869	14.7		
262.8820	4.7	313.431	5.3		
262.4013	20.8	47.261	25.1		
261.7564	8.7	69.168	13.9		
260.8760	37.9	45.723	43.3	803.70 - 606.53	E
260.2396	4.6	388.046	5.9		
259.8432	44.8	53.974	47.6		
259.7115	3.9	851.102	5.2	1157.05 - 897.11	CE
259.2771	3.7	28887.095	4.7	338.42 - 79.14	CE
257.1372	6.5	116.735	9.9	765.50 - 508.47	E
256.9872	4.2	311.593	5.9		
256.7670	16.9	53.804	22.1		
255.2920	4.1	831.758	4.8	819.14 - 563.81	CE
254.7333	23.9	63.481	38.5	1112.03 - 857.34	E
254.4447	5.5	194.869	7.6	705.62 - 451.05	CE
253.5260	11.0	43.317	21.7		
252.9314	6.1	149.207	7.7		
251.4701	8.1	93.130	10.4	897.11 - 645.51	E
251.0067	17.4	52.474	29.9		
250.1374	20.5	48.615	32.5	715.80 - 465.65	E
248.9374	3.9	926.286	4.9		
248.6280	8.3	87.947	12.4	765.50 - 516.85	E
248.2876	4.5	1156.462	4.9	542.84 - 294.57	CE
244.6836	15.5	69.357	16.7		
244.3374	5.4	173.399	7.3	451.05 - 215.38	E
241.4421	15.6	51.125	22.9	616.94 - 375.62	E

TABLE 5.6 (Continued)

Energy (keV)	Error (eV)	Relative Intensity	Error (%)	Transitions in ^{108}Ag	Remarks
240.7846	6.4	97.912	10.2	1213.35 - 972.65	CE
240.0535	7.6	80.237	10.0	705.62 - 465.65	E
239.3162	3.2	6584.246	4.1	563.81 - 324.50	CE
238.9753	9.8	70.030	15.2		
237.7235	16.5	42.291	27.1	616.94 - 379.24	E
237.2855	19.6	46.997	26.5		^{109}Ag (n,γ)
237.1329	10.2	95.421	22.0	645.51 - 408.37	E
237.0519	6.2	176.241	11.1	1002.57 - 765.50	CE
236.8790	5.7	140.526	9.7		
235.9374	6.0	130.454	9.1		^{109}Ag (n,γ)
235.7380	4.0	386.570	6.3		^{109}Ag (n,γ)
233.5144	8.6	70.578	12.9		
233.0081	28.9	42.825	36.6		
232.7216	11.7	50.391	23.8		
231.6929	13.5	40.195	25.0		
231.4447	11.8	52.906	19.0	1112.03 - 880.73	E
230.6800	6.9	61.081	15.2		
229.8040	9.2	43.777	22.4		
229.2326	20.2	42.819	29.7	1231.71 - 1002.57	E
227.9600	11.0	57.317	18.3	1200.38 - 1051.62	E
227.2890	3.4	674.939	5.2	606.53 - 379.24	CE
226.4616	5.4	109.455	9.0		
225.3882	4.0	213.108	5.9	563.81 - 338.42	CE
223.7331	36.2	31.595	54.6		
222.9897	4.1	160.202	6.4		
222.6066	11.0	51.157	18.9	765.50 - 542.86	E
220.8904	4.6	245.754	6.1	1272.23 - 1112.03	CE
218.7419	12.4	62.221	29.3	1231.71 - 1012.87	E
218.5243	9.6	68.471	13.9		
215.5429	3.8	386.620	8.9		
215.3825	2.8	28280.226	5.7	215.38 - 0.0	CE
213.9106	4.0	203.691	7.2	508.47 - 294.57	CE
213.4103	4.3	259.087	7.5	679.08 - 465.65	CE
213.0487	3.3	1398.609	5.8	1325.24 - 1112.03	*
212.5530	4.4	338.303	6.2	819.14 - 606.53	CE
212.3096	2.9	2062.054	5.2		
208.5661	6.5	80.202	11.8	616.94 - 408.37	E
207.3398	3.1	1119.878	5.6	972.65 - 765.50	CE
206.6082	3.0	74555.548	5.1	206.61 - 0.0	CE
204.4276	3.0	2084.891	5.2	542.84 - 338.42	CE
203.4556	4.5	153.617	9.0	579.10 - 375.62	CE
203.2904	3.0	903.250	5.5	611.66 - 408.36	CE
202.9479	20.6	57.270	39.4		
202.5070	5.5	123.025	8.5		
202.1452	4.6	220.359	7.6	819.14 - 616.94	CE
201.7488	3.8	6134.836	5.2	408.36 - 206.61	CE
201.0130	3.8	5841.197	5.2	857.34 - 656.33	CE
200.3578	7.7	70.206	13.7	1213.35 - 1012.87	E
199.8700	5.1	150.200	8.5	579.10 - 379.24	CE
198.676	3.8	836.175	5.3		^{109}Ag (n,γ)

TABLE 5.6 (Continued)

Energy (keV)	Error (eV)	Relative Intensity	Error (%)	Transitions in ^{108}Ag	Remarks
197.1992	10.6	52.492	19.2	705.62 - 508.47	E
196.4490	23.1	66.547	49.5	897.11 - 700.51	E
195.507	5.9	69.145	12.0		^{109}Ag (n,γ)
193.0777	3.1	49870.598	4.8	193.08 - 0.0	CE
192.3564	7.4	51.708	17.9	516.85 - 324.50	E
192.0028	3.4	333.378	5.5	700.51 - 508.47	CE
191.5577	3.7	201.606	6.9		^{109}Ag (n,γ)
190.8581	7.4	57.881	14.1		
186.1664	3.9	483.865	5.3	379.24 - 193.08	CE
185.9215	9.0	57.518	16.1		
182.3912	10.4	53.274	23.3		
180.5816	10.5	57.964	21.4		
180.2521	4.4	119.044	8.9	880.73 - 700.51	E
179.0405	8.9	54.490	23.0		
178.6136	10.4	47.918	29.7		
178.4249	2.7	5146.956	4.6	516.85 - 338.42	CE
175.9303	15.2	51.719	34.8		
174.6583	2.7	612.861	4.9		
174.3368	21.2	54.054	55.1		
173.6479	5.1	72.825	12.6	819.14 - 645.51	E
172.6255	4.2	99.858	10.6	379.24 - 206.61	E
172.1070	6.5	64.601	17.1		
170.6153	5.5	70.187	15.0	679.08 - 508.47	E
170.0582	2.5	1339.820	4.7	508.47 - 338.42	CE
165.9966	3.8	150.111	9.4	616.94 - 451.05	E(?)
165.2903	9.9	57.734	35.3		
164.0633	6.1	62.799	20.1		
161.9162	12.6	70.899	29.6	1213.35 - 1051.62	E
160.4594	9.4	57.606	21.4	611.66 - 451.05	E
159.2908	5.3	163.216	13.5		
155.4496	2.3	2241.507	5.3	563.81 - 408.36	CE
149.1589	3.9	115.723	10.9		
148.8551	2.4	3077.408	4.8	1200.38 - 1051.62	CE
148.5240	3.9	107.146	10.8	765.50 - 616.94	CE
147.3497	3.0	2738.409	7.0	802.70 - 656.33	CE
143.9112	12.4	48.233	41.2	1157.05 - 1012.87	E
140.8950	4.6	164.683	11.4	606.53 - 465.65	E
137.4978	11.3	69.664	27.8		
136.9039	25.2	96.203	46.8	645.51 - 508.47	E
136.2433	3.0	645.325	6.3	215.38 - 79.14	CE
134.4725	3.1	405.477	7.1	542.84 - 408.36	CE
131.8064	3.9	185.948	10.6	338.42 - 206.61	CE
129.8928	20.2	125.254	42.1		
129.2323	2.7	659.754	6.2	508.47 - 379.24	CE
127.4740	3.2	160.741	10.9	206.61 - 79.14	CE
126.3667	4.1	167.425	11.8	705.62 - 579.10	CE
121.4486	3.1	393.223	9.7	700.51 - 579.10	CE
117.8862	2.1	25484.187	5.4	324.49 - 206.61	CE
117.6046	2.4	714.707	6.7		^{109}Ag (n,γ)
113.9300	2.1	1161.651	6.1	193.08 - 79.14	CE

TABLE 5.6 (Continued)

Energy (keV)	Error (eV)	Relative Intensity	Error (%)	Transitions in ^{108}Ag	Remarks
113.7988	2.0	8132.832	5.4	408.36 - 294.56	CE
113.5932	2.0	9393.645	5.4	819.14 - 705.62	CE
110.1788	2.9	297.921	10.8		
105.8291	4.4	207.172	17.0		^{109}Ag (n,γ)
103.0158	2.3	573.225	9.2	803.70 - 700.51	CE
102.3100	1.7	2940.546	6.7		
101.4816	1.7	7342.478	6.5	294.57 - 193.08	CE
91.8927	7.9	254.404	29.5	542.84 - 451.05	E
87.9472	4.4	397.039	17.1	294.57 - 206.61	CE
79.1386	1.8	147644.994	8.3	79.14 - 0.0	CE
74.8308	4.9	841.078	24.9	1231.71 - 1157.05	CE
46.430	5	17200.	40.	375.61 - 329.18	CE

CE - These have been assigned according to coincidence results.

E - These are assigned only by energy combination.

* - These are assigned in extra suggested levels above 1.3 MeV.

6. MEASUREMENT OF γ-γ COINCIDENCES IN THE REACTION $^{107}Ag(n,\gamma)^{108}Ag$

6.1 Introduction

To construct a dependable level scheme the results obtained from high precision γ-ray measurements are required to combine with the complementary information obtained from other types of studies such as γ-γ coincidence studies, (d,p) reaction studies, conversion electron measurements, and the lifetime studies of the excited states. The level scheme of ^{108}Ag is not well established due to few low-energy, high-energy and conversion electron measurements. In addition to early studies of singles spectra in $^{107}Ag(n,\gamma)$ reaction[66], the conversion electron spectrum and γ-γ coincidences were investigated by Estulin et al[115] and Bondarenko et al[116] using a two-crystal scintillation spectrometer.

To extend our knowledge of the ^{108}Ag level scheme a γ-γ coincidence measurement was carried out at the 23 MW research reactor FRJ-2 (Dido) of the Kernforschungsanlage Julich, F.R. Germany.

6.2 Apparatus

A schematic drawing of the main elements of the beam tube facility and the apparatus is shown in Fig.6.1 . The apparatus is situated at a vertical beam tube on the top of the reactor. The thermal neutron beam profile at the target position is well des-

cribed by the gaussian distribution.

$$\phi(r) = \phi_o \exp\left|-r^2/0.36\ d_{\frac{1}{2}}^2\right|$$

where the radial distance from the beam axis is given in mm, ϕ_o = 1.3×10^6 $mm^{-2}sec^{-1}$ at the reactor power of 23 MW and with the Bi-filter cooled to 77^oK, and the FWHM amounts to $d_{\frac{1}{2}}$ = 16 mm. The mean neutron wavelength is $2.4A^o$. The total external neutron flux values are

ϕ(thermal) = 3.8×10^8/sec

ϕ(epithermal) = 6.0×10^4/sec.1nE

and $\phi(E_n > 0.1$ MeV) = 5.0×10^5/sec.

Properties of the single crystal filtered beam are published elsewhere[117]. Details of the target holder and the shielding around the beam at the height of the Ge(Li) detectors are shown in Fig. 6.2 . The neutron beam is screened by a double walled tube between the reactor shielding and the beam catcher which is situated at the top of the coincidence apparatus. This tube is fitted with ^6LiD in the target region and B_4C elsewhere. To minimize the number and intensity of background γ-ray lines high-purity graphite is used for the target capsule and the holder, additionally CO_2 flows through the interior of the shielding tube to avoid neutron capture in the N_2 of the air.

The source consisted of a 400mg silver foil (50 mg/cm^2) enriched to 99.6% ^{107}Ag. The detectors used in the present coincidence measurement were true coaxial Ge(Li) detectors with an active volume of 58cm and 50cm , energy resolutions of 2.4 keV and 2.2 keV at 1.33 MeV, and peak-to-Compton ratios of 28 and 30 respectively. The first detector covered the energy range 20 keV to 8 MeV and the second detector 15 keV to 4 MeV. Singles spectra of ^{107}Ag(n,γ)^{108}Ag and natural Zn(n,γ) were also measured using a pencil-shaped Ge(Li) detector of 27 mm in length and 86 mm cross section (see chapter 5). The neutron capture gamma radiations emitted from Zn, shielding material (Fe, H, C, etc.) and ^{60}Co decay were used for energy calibration.

6.3 Electronics

Details of the two-dimensional data-acquisition system have been published elsewhere[118]. In order to cover all cascades contained in the spectrum in a single coincidence measurement, the following method was used. The output pulses of both Ge(Li) detectors were converted into 12 bit binary numbers by two A.D.C.'s. The two addresses of a coincident event were stored together with a 12 bit tagword on magnetic tape. Additional information on singles count rates of the two detectors, prompt and delayed coincidence count rates were taken with four scalers for day to day checks.

A block diagram of the electronics is shown in Fig. 6.4 . These perform the following three functions:

(i) detection and selection of events

(ii) reduction and storage of data

(iii) controlling and monitoring the measurement.

6.3.1 Detection and Selection of Events

This includes all steps from the detection of the γ-ray by the Ge(Li) detectors to the representation of coincident or single events as three 12 bit words. From each preamplifier of the two Ge(Li) detectors, a time signal was taken by a timing filter amplifier and a constant fraction discriminator. The output pulses from each of the two discriminators, one of them through 100 n secs delay, were fed into a time-to-pulse height converter. The TPHC output was then fed into two timing-single-channel-analysers. Output from one of the timing SCA was then taken into TAGWORD control through a delay time and it gives the information for delayed coincidence and marked by '0'. The output signals of both SCA's passed through an OR-gate and delay to the gate inputs of the two A.D.C.'s. An energy signal from each preamplifier was taken by a linear amplifier. The energy signals were then digitized by the two A.D.C.'s. The time resolution for coincidence (2τ) was measured as 100 n secs.

The first bit of the tagword was used to distinguish between the two coincidence conditions as '1' for prompt coincidence and '0' for delayed coincidence.

6.3.2 Reduction and Storage of the Data

For each event which fulfilled one of the gate conditions, a 36 bit word was kept ready for storage and collected in a buffer before being recorded. The buffer was divided into two sections, each of which contained 128 events. When one section was filled, its content was written as one record on the tape. At the same time further events were stored into the other section of the buffer, so that there was minimum loss of information by dead time during the run. A part of a PDP 8/L computer memory was used as buffer and the memory contained a program which controlled the data storage.

6.3.3 Controlling and Monitoring the Measurement

The prompt and the delayed (accidental) coincidence counting rates as well as the singles counting rates of the Ge(Li) detectors were registered by decimal counters and printed by teleprinter after every 20 minutes of counting period. In this way possible disturbances of the measurement may be detected for the later evaluation of the magnetic tapes.

In addition each spectrum behind the two A.D.C.'s or the digital windows were collected alternatively in 2048 channels of a 4K-memory. The contents of this memory can be displayed at any time without interrupting the measurement. By doing this the stability of the system (such as channel drifting, energy gain, etc.) was

checked every day. In this way all functions except the storage itself could be monitored.

6.4 Evaluation of the Data

The counting rates for the singles spectra in the two Ge(Li) detectors were $1.3 \times 10^4 sec^{-1}$ and $1.1 \times 10^4 sec^{-1}$. The average prompt coincidence and delayed coincidence counting rates were 180 sec^{-1} and 8 sec^{-1}. Energy discrimination and pulse shape inspection reduced the final coincidence rate to 128 sec^{-1}. As mentioned before, one section of the buffer could store 128 events and when it was full, the buffer memory was recorded on magnetic tape (one record). The data from three of these magnetic tapes were transferred to one high density magnetic tape for convenience of use with the computer. The actual coincidence experiment has taken 17 days of reactor time operating at full power 23 MW, and filled 29 high density magnetic tapes. A total of 1.6×10^8 coincidence events were recorded on magnetic tapes with a 4K x 4K two-dimensional data acquisition system[118] and handled off-line at the central IBM 370/168 computer of the KFA, Julich.[119]

A closed representation of a 4K x 4K coincidence matrix in one computer run leads to considerable difficulties due to the requirements of core memory space. However, in most cases not all possible coincidence combinations are needed and it is sufficient to take different sections of this matrix in order to remove possible ambiguities from Ritz combination. A computer program has been developed and in which up to 60

coincidence sections in vertical and horizontal directions can be analysed with simultaneous correction for accidental and background coincidences .

In thermal neutron capture highly excited nuclei are generated and those lose their energy mainly by gamma de-excitation. With high resolution Ge(Li) detectors hundreds of gamma transitions with various intensity values may be detected in the de-excitation spectra. To be able to evaluate the coincidence spectra of these nuclei, an exact and quantitative knowledge of the background is essential. The regions selected to assess the background subtracted area under the peak are shown in Fig.6.3 . The regions II and VIII contain coincident contributions between the line in X-direction and the Compton background in Y-direction, while the regions IV and VI contain the corresponding contributions between the Y-line and X-Compton background. The regions I, III, VII and IX contain background coincidences exclusively. The number of coincidences in these different areas is normalized to the peak area. The background corrected area under the peak is calculated using the following equation:

$$P = N_V + \frac{1}{4}(N_I+N_{III}+N_{VII}+N_{IX}) - \frac{1}{2}(N_{II}+N_{IV}+N_{VI}+N_{VIII})$$

where N_i = the number of coincidences in these corresponding normalised area (i).

Three coincidence matrices are constructed in such a way that all possible coincidences are included. The first matrix contains the coincidence between 0 - 1.5 MeV (low energy detector X-branch) and 0 - 2.0 MeV (high energy detector Y-branch). The second matrix includes the coincidences between 0 - 1.5 MeV (X-branch) and 0 - 8 MeV (Y-branch). Finally, the coincidences between 1.3 - 4 MeV (X-branch) and 0 - 6.5 MeV (Y-branch) are included in the third matrix.

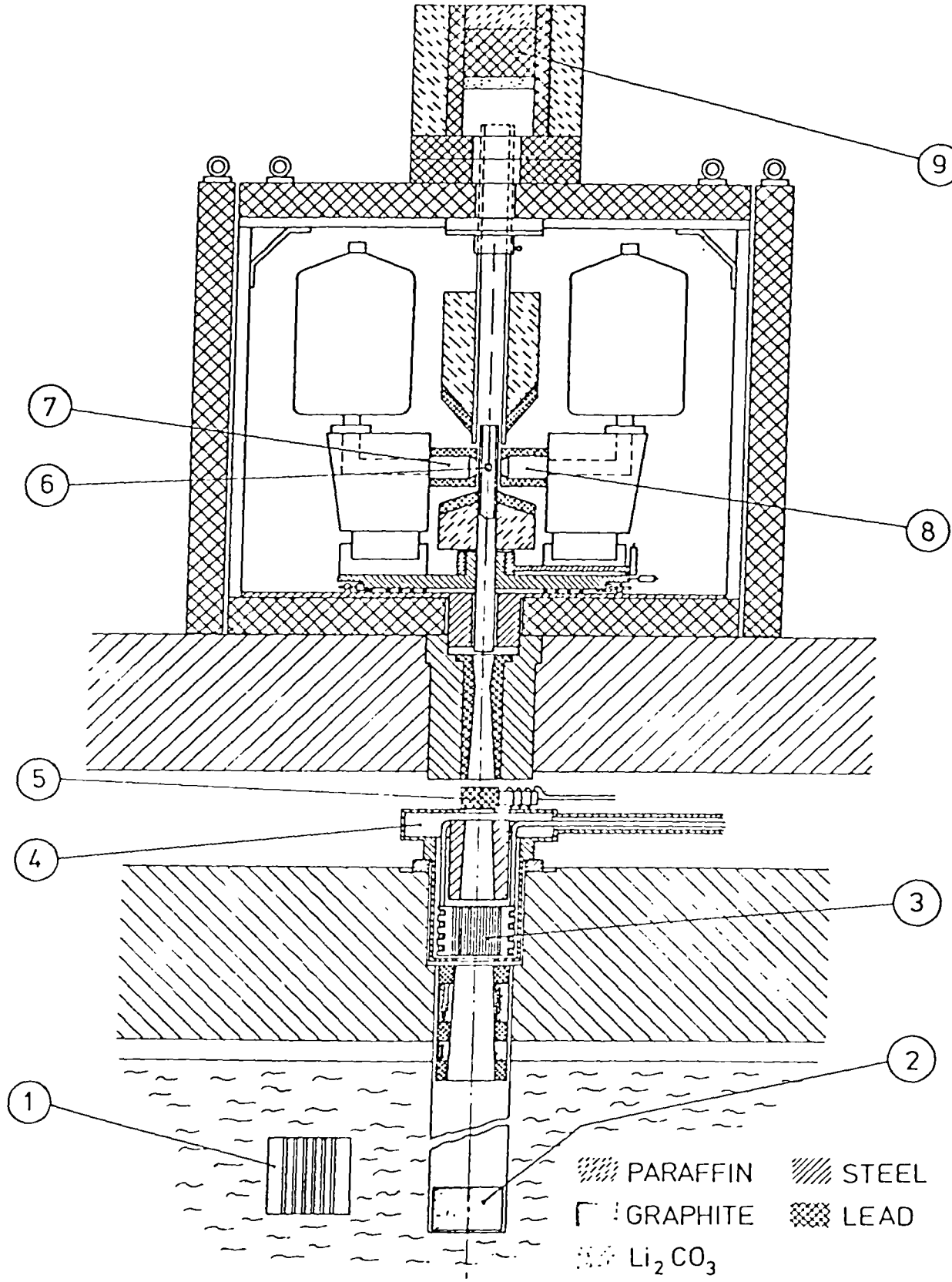


FIGURE 6.1

Beam tube system and measuring equipment on the top of the FRJ-2 research reactor at Jülich (not in correct scale, 1: reactor core, 2: graphite scatterer, 3: Bi-single crystal (20 cm in length, 77°K), 4: vacuum chamber, 5: beam shutter, 6: target, 7 and 8: Ge(Li) detectors, 9: beam catcher).

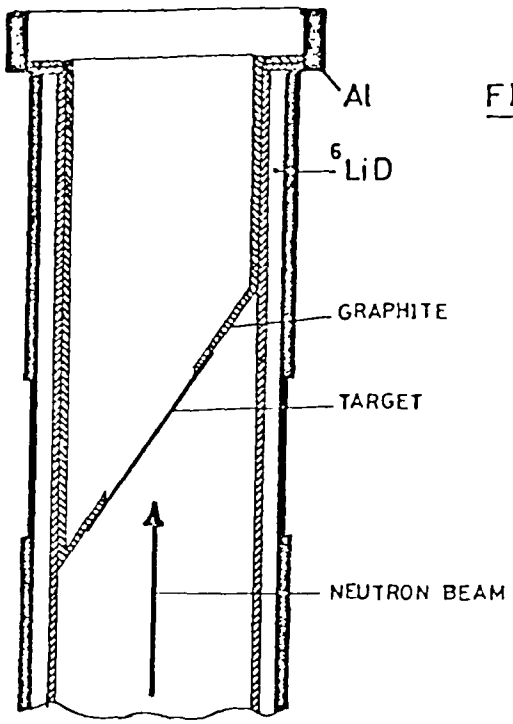


FIG.6·2 Target holder and shielding of the external beam in the height of the detector.
Inner diameter of the shielding tube = 36 mm
Outer diameter = 52 mm

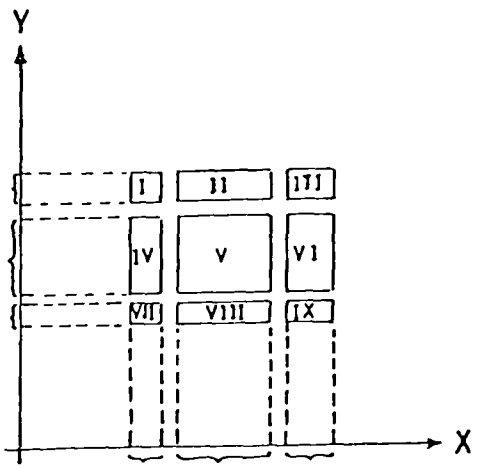


FIG. 6·3 PEAK AND BACKGROUND REGIONS IN COINCIDENCE-MATRIX

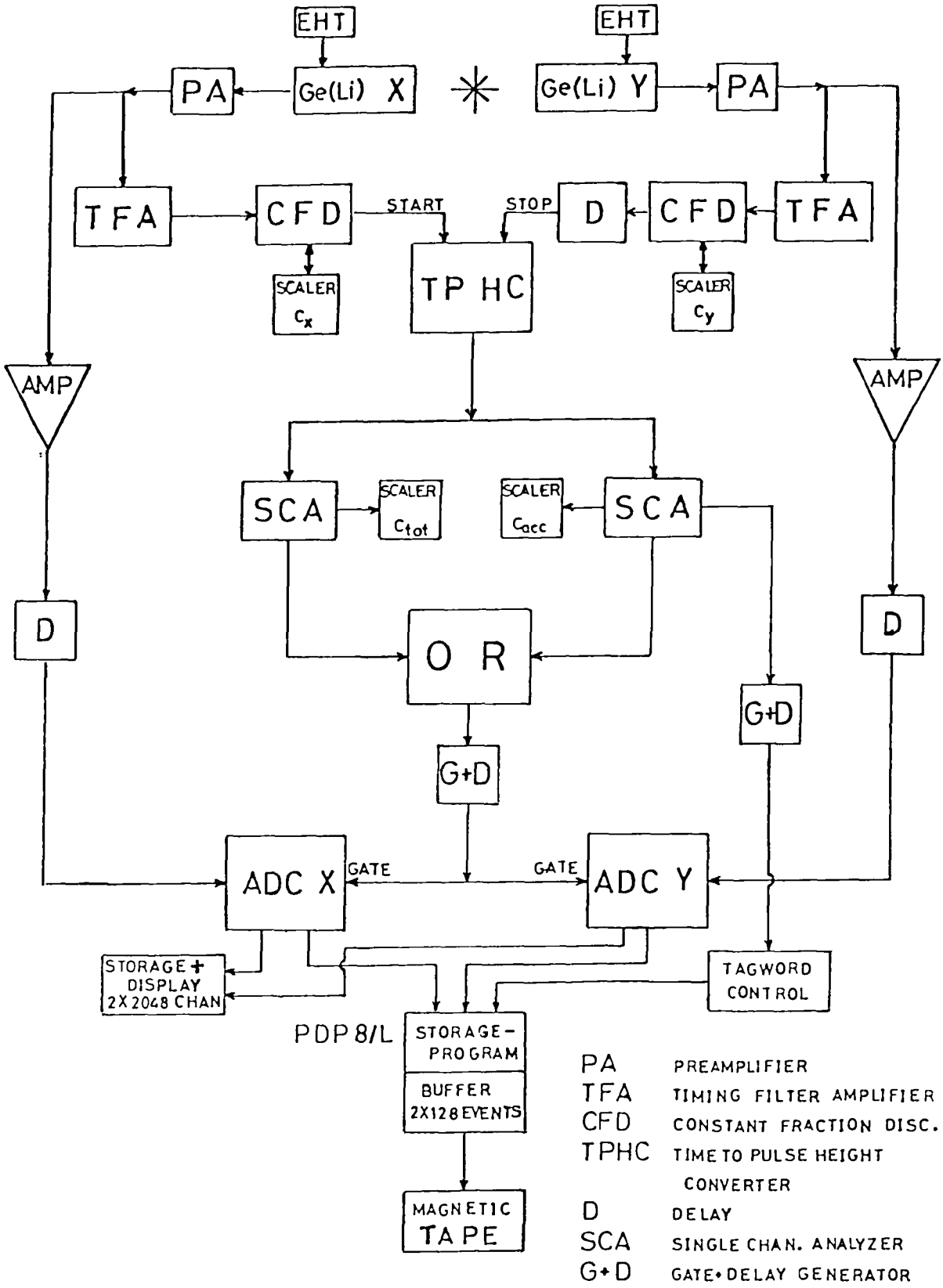


FIG. 6.4 BLOCK DIAGRAM OF ELECTRONICS

7. RESULTS AND DISCUSSION

7.1. LEVEL SCHEME OF ^{108}Ag

A simultaneous study of the level structures of ^{108}Ag and ^{110}Ag is an interesting subject since both nuclei seem to have certain common features from the previously available data (Bertrand[66] and Horen 1974[81]; Bertrand and Raman 1971[80]). The odd-odd nuclei $^{108}_{47}$Ag and $^{110}_{47}$Ag are situated between the vibrational nuclei of $_{46}$Pd and $_{48}$Cd. Therefore it would be of considerable interest to study the vibrational motion and its coupling to the particle motion in these odd-odd nuclei.[74] In view of the very complicated level schemes expected for odd-odd nuclei, this is quite a difficult task which requires first of all a detailed knowledge about the nuclear level schemes of ^{108}Ag and ^{110}Ag. Although extensive studies of ^{110}Ag have been carried out during the past years, the ^{108}Ag level scheme is relatively less well-known. In addition to the earliest studies[*] the primary (n,γ) spectrum was measured by Bolotin and Namenson.[120] A few low-energy transitions were observed by Gujrathi et al (1970)[108] (E_γ < 388 keV) and Hattori et al (1976)[107] (E_γ < 675 keV). Recently a low-energy ^{107}Ag(n,γ)^{108}Ag reaction measurement was performed with the diffractometer at Risø (Breitig et al 1974)[74,75], and precise gamma energies (E_γ < 1.14 MeV) and relative intensities were presented. The conversion electron spectra and γ-γ coincidences with a magnetic γ-spectrograph and Ge(Li) detectors (45 cc, resolution 4.8 keV at 661.5 keV) respectively were investigated by Bondarenko et al (1972).[116]

[*] REFERENCES: 63,66,116,121,122

Recently the (d,p) reaction was studied by Brient et al (1972)[65] and orbital angular momentum transfer (l) values and spectroscopic factors (s) have been extracted for 19 states in ^{108}Ag. A decay scheme of ^{108}Ag was proposed on the basis of the older results. A rather detailed preliminary low-energy level scheme was also proposed by Breitig et al (1974)[74]. But it is clear that the best possible qualitative data are essential for the extension of the level scheme of this odd-odd ^{108}Ag isotope.

It is the aim of the present work to provide the most detailed and precise information on the high-energy (n,γ) spectrum of ^{108}Ag (E_γ > 3 MeV) and the data on the γ-γ coincidence measurements. These results will complement the existing low-energy (n,γ) and (d,p) data and will provide the basis for high-resolution (n,$\bar{e}$) and γ-γ angular correlation studies.

By combining the present precise high-energy data, precise low-energy data of Breitig et al[74] and the present γ-γ coincidence data, a level scheme for ^{108}Ag is proposed which accounts for most of the observed transitions, such a level scheme is displayed in Figures 7.1. and 7.2. The level schemes proposed by Breitig et al and Bertrand[66] and (d,p) data[65] were used as a basic guide in constructing the level scheme. The energies and spin-parity assignments are given in Table 7.1.

As far as the spins and parities are concerned, only those of the ground state (1^+), the first excited state (2^-) and the second excited state (6^+) are definitely known.* Recently Hattori et al (1976)[107] have assigned the spins for a few low-lying states by comparing the measured γ-ray angular distribution and excitation functions in $^{108}Pd(p,n\gamma)^{108}Ag$ reaction with predictions of the statistical compound-nucleaus model. Within the framework of shell-model configurations, the low-lying states in ^{108}Ag would lead to (d,p) population of only the negative parity states - the positive-parity levels close to the ground state are expected to arise from excited-proton configurations that (d,p) reactions do not populate, or at most populate extremely weakly. Therefore primary transitions from the negative-parity capture state $(0,1)^-$ to low-lying levels that are also observed in the (d,p) reaction would be expected to be M1. Since the average probability for primary E1 transitions to low-lying excited states is expected to be $\approx$100 times that for the corresponding M1 transitions (see Chapter 1. section 1.3), ^{108}Ag provides a means of examining the ratio of E1 to M1 transition probability for many transitions in a single nuclide.

A comparison with the decay scheme presented in Ref.66 shows that the present coincidence data do not give evidence for a level at 45·46 keV and this agrees with Breitig et al. The 46·43 keV gamma is

* REFERENCES : 53,66,115,116.

strongly coincident with 329.18 keV and 114 keV gamma rays, the last two are also in coincidence with each other. There are three possible gammas with energy about 114 keV, i.e. 113.93, 113.80 and 113.59 keV. Since the first two gammas are already assigned in the existing level scheme and cannot be in coincidence with the 329.18 keV gamma, the last one, 113.59 keV, is taken as the one in question.

Breitig et al[74] pointed out that there are no transitions with reasonable intensities, which could account for the depopulation of a level at 287.47 keV which was suggested only because of the high-energy (n,γ) data of Bolotin and Namenson.[120] In the present high-energy $^{107}Ag(n,\gamma)^{108}Ag$ spectrum no evidence was found for the existence of a primary gamma transition with energy about 6982 keV, which could result in a level at 287 keV. On the other hand the transition to this level would have an energy which is only 7 keV higher than the 15 times stronger line to the 294 keV level. Since the FWHM resolution of the Ge(Li) detector is about 6 keV at this energy, the line in question may be due to a poor computer fit.

Most of the levels shown result from the present primary (n,γ) data. Since primary gamma transitions are mainly E1 and a few M1 ($\Delta I = \pm 1$), the capture of s-wave neutrons by the target nucleus ^{107}Ag (spin and parity $I^{\pi} = \frac{1}{2}^{-}$) allows primary population

of levels with $I \leq 2$. Several of these and additional levels follow from the (d,p) data. The knowledge of the angular momentum transfer ℓ values 0, 2 and 4 (Brient et al 1972) requires negative parity for these levels and I = 0,1 ; 1,2,3 and 1,2,3,4,5 respectively. Additional information is obtained from the present γ-γ coincidence work and conversion electron measurements of Bondarenko et al. The energy combination principle and simple intensity considerations are also applied to the location of the transitions in the level scheme.

To discuss the possible states of the unpaired nucleons in the odd-odd nucleus $^{108}_{47}Ag_{61}$, it should be compared with neighbouring nuclei. The odd-even nuclei $^{107}_{47}Ag_{60}$ and $^{109}_{47}Ag_{62}$ both have ground states with spin and parity $\frac{1}{2}^-$ and first excited states $\frac{7}{2}^+$. According to this the unpaired protons in these isotopes are in states $P_{\frac{1}{2}}$ and $(g^{-3}_{9/2})_{7/2}$. The ground states of the neighbouring even-odd nuclei (with 61 neutrons) $^{107}_{46}Pd$ and $^{109}_{48}Cd$ have spin and parity $\frac{5}{2}^+$ (i.e. $d_{5/2}$ shells). On the other hand, Cohen[123] has experimentally observed the lowering of the $g_{7/2}$ level with the increasing number of neutrons in the unfilled shell due to strong n-p interaction. Therefore one would expect the unpaired neutrons to be mainly in states $d_{5/2}$ and $g_{7/2}$. But $d_{3/2}$, $S_{1/2}$ and $h_{11/2}$ neutron states cannot be neglected completely. For odd-odd Ag isotopes, the proton configurations ($1g_{9/2}$ and $2p_{1/2}$) and the neutron configurations ($1g_{7/2}$, $2d_{5/2}$, $2d_{3/2}$, $3s_{1/2}$ and $1h_{11/2}$) are available to play a major role in the low-lying states. Hattori et al[107] has given the possible p-n con-

figuration for several I^{π} values in ^{108}Ag and these are shown in Table 7.2 .

Thermal Neutron Capture State

^{107}Ag has an unpaired proton in the $2p_{\frac{1}{2}}$ orbital and consequently has ground-state spin and parity values of $\frac{1}{2}^-$. The capture of s-wave neutrons by the $\frac{1}{2}^-$ ground state of ^{107}Ag allows the population of a capture state with $I^{\pi} = (0,1)^-$. The neutron separation energy of ^{108}Ag is determined to be (7269.85 ± 0.32) keV (see Table 7.3). This agrees with the previous values of (7270 ± 20) keV and (7269 ±1) keV obtained by Bartholomew et al[124,125] and Bertrand[66] respectively in their study of the same reaction, but is higher than the value of 7267 ± 1 keV obtained by Bolotin and Namenson.[120] It agrees with the mass-adjusted value (7275 ± 7) keV listed in the compilation of Mattauch et al.[126] The ground-state Q value of 5044 keV (deuteron reaction binding energy = 2223 keV) in the $^{107}Ag(d,p)^{108}Ag$ reaction by Wapstra and Gove[127] also supports the present value.

Ground State of ^{108}Ag

The highest-energy gamma ray (7269.3 keV) is taken as the transition from the capture state to the ground-state of ^{108}Ag. It

could be identified as E1 since it is one of the strongest lines in the high energy (n,γ) spectrum.

The ground-state configuration of ^{108}Ag is either $|\pi(g_{9/2}^{-3})_{7/2}, \nu(d_{5/2}^{-1})|_{1^+}$ or $|\pi\, g_{9/2}^{-1}, \nu\, g_{7/2}^{-1}|_{1^+}$ as inferred from allowed decay to even parity levels in ^{108}Cd (Koteh and Yoshizawa 1962)[128] and from nuclear magnetic dipole moment measurements (Cussens et al 1969).[129] The decay scheme of ^{108g}Ag is mentioned in Chapter 3.

In ^{108}Ag the primary population to the 1^+ ground-state is one of the strongest observed while in ^{110}Ag the transition to the 1^+ ground-state appears as one of the weaker transitions seen (Bolotin and Namenson).[120] Bolotin and Namenson also pointed out that lines of considerable strength populate low-lying levels in ^{108}Ag while there is a lack of any strong transitions to levels below an excitation energy of $\sim$ 700 keV in ^{110}Ag. This lack of similarity agrees with the wide fluctuations in the strengths of particular primary transitions predicted by Porter and Thomas[29] on the basis of the statistically complex and independent nature of the capture states which gives rise to virtually randomly-constituted matrix elements connecting these states and low-lying excited states.

The ground-state group in ^{108}Ag was not observed in the (d,p) reaction by Brient et al[65] as is to be expected from the assignment of positive parity to the ground state.

The 79.14 keV level

The spin and parity of this level were previously assigned to be 2^- (Kistner and Sunyar 1966)[58]. In the (d,p) reaction, this level was populated with $\ell = 2$. Since ^{107}Ag contains one extra odd $P_{\frac{1}{2}}$ proton outside the ^{106}Pd and ^{108}Pd cores respectively, the possible p-n configuration is $|\pi(P_{\frac{1}{2}}), \nu(d_{5/2})|_{2^-}$. The half-life was measured and given as < 0.7 ns (Bondarenko et al)[116].

The 7190 keV transition from the capture state $(0,1^-)$ to this level (2^-) has been established as M1. The intensity (strength) of this transition is only $\sim$ 2% of that of the E1 transition (7269.3 keV) to the 1^+ ground-state, and this is consistent with the expected dominance of transition of E1 type. The established negative parity of this level leads to an E1 assignment for 79 keV transition to the positive parity ground state. The experimental conversion coefficient ($\alpha_k = 0.21$) and the theoretical value ($\alpha_k = 0.26$) confirm the above assignment (Bondarenko et al)[116].

The First Isomeric State in ^{108}Ag

The de-excitation of the 127 y isomer in ^{108}Ag was studied by Kistner and Sunyar.[58] They observed that the isomer is located at 109.43 and decays 90% by electron capture and 10% by isomeric transition via the 79 keV level to the ground state. The 30.38 keV (M4) and the 79.05 (E1) gamma rays make up the isomeric cascade. The known multipolarities (M4 and E1) of the transitions in the isomeric cascade, the lack of a crossover transition from the isomeric state, together with the life time of order 10^2 y, enable the spin and parity of this isomeric state to be assigned as 6^+. The possible p-n configuration is $|\pi(g_{9/2}^{-3})_{7/2},\ \nu(d_{5/2})|$. The decay of ^{108m}Ag is described in Chapter 3.

The 193.07 keV Level

The primary population to this level, which is not observed in (d,p) from the capture state $(0,1)^-$ is one of the strongest observed in high-energy (n,γ) data, so that this 7076 keV transition will be E1 type. Therefore the spin and parity may be limited to $(0,1,2)^+$. Bondarenko[116] has shown that it depopulates to the ground-state (1^+) via a 193 keV gamma transition which is an admixture of M1 + E2. But the mode of de-excitation of this level to the 79 keV (2^-) level excludes spin 0. Recently Hattori et al[107] has assigned the spin and parity of this level to be $|1^+,\ (2)^+|$ in their (p,n) studies. The p-n configuration

of this level may be $|\pi(g_{9/2}^{-3})_{7/2}, \nu(d_{5/2})|$.

The 206.61 keV level

The primary gamma transition to this level, not observed in (d,p) reaction, from the capture state should be identified as E1 type due to the strong intensity. The gamma transition from this level to the ground-state is an admixture of M1 and E2. The mode of de-excitation of this level to 79 keV level excludes spin 0. This restricts the spin and parity to be $(1,2)^+$. Later Hattori et al[107] adopted the 2^+ value according to measured function and angular correlation measurements The p-n configuration for this level is likely to be $|\pi(g_{9/2}^{-3})_{7/2}, \nu(d_{5/2})|$

The Second Isomeric State (215.38 keV)

A rather detailed discussion for this level is given by Hattori.[107] They have assigned the spin and parity to be 3^+ according to the excitation function and the measured g-factor. This is consistent with the facts that this level is not directly populated in (d,p) reaction and there is no direct primary gamma transition from the capture state to this level. With this spin assignment the 215 keV transition to ground state must be that of a pure $E2(3^+ \rightarrow 1^+)$. Although Bondarenko et al[116] have shown that this transition is $|E1 + M2(E2)|$ type, the measured half-life of 45.8 ± 0.7 ns (Hattori et al) and 48 ns (Bondarenko et al) are fairly close to that for single particle E2 transition (order of 40 ns),[130] 1×10^3 times smaller than that for single particle M2 transition

(order of $10^{-6}/10^{-5}$ s)[130] and 5 x 10^5 times greater than that for E1 transition (order of 10^{-13}s).[130] A 3^+ assignment is made more plausible by the fact that the second isomeric state in ^{110}Ag(118.7 keV, $T_{\frac{1}{2}}$ = 36.7 ± 0.7 ns) has a measured spin and parity of 3^+ (refs. 107 and 122 131). The n-p configuration of this level is likely to be $|\pi(g_{9/2}^{-3})_{7/2}, \nu(d_{5/2})|$.

The 294.56 keV level

The spin of this level is assigned by Hattori et al to be 2 from the measured excitation function, angular distribution and large M2/E1 mixing ratio in (p,nγ) reaction. In addition this level is populated strongly by a primary transition (6974.9 keV, relative intensity = 47.18%), which could be identified as E1 type, from the neutron capture state and this level is not populated in (d,p) reaction where negative parity states are mainly populated. Furthermore, no gamma transition is observed to the negative parity 79 keV level in de-excitation of this level. From these facts, it is fair to assign spin and parity to be 2^+ with p-n configuration $|\pi(g_{9/2}^{-3})_{7/2}, \nu(d_{5/2})|$. Half-life was given as < 0.7 ns.[122]

The 324.50 keV level

Although there are some conflicting views on this level, the present γ-γ coincidence data support the existence of this level from

from the observed 117.89 - 206.61 cascade. There is no primary gamma transition to this level from the capture state and this level is not populated in the (d,p) reaction. Bondarenko[116] has measured the K-internal conversion coefficient α_k and identified this 117.9 keV transition to be an admixture of M1 + E2. In addition, based on the measured excitation function and angular distribution in (p,nγ) reaction, Hattori et al has suggested the spin and parity of this level to be 3^+.

The 329.18 keV level

There are some conflicting views on the existence of this level. Gujrathi et al[108] proposed a level at 331.0 keV mainly on the basis of the 331.04 keV (relative intensity 15%) observed in low-energy (n,γ) data. Bolotin and Namenson[120] proposed a level at 333 keV due to the primary transition (6934 ± 2 keV, relative intensity 1.2 ± 0.2%) in high-energy (n,γ) data. Later Breitig et al[74] again proposed a level at 329.18 keV due to 329.18 keV gamma ray and a possible 113.80 - 215.38 keV gamma cascade. But the present γ-γ coincidence data shows that there is no coincidence between 113.80 keV and 215.38 keV gamma rays. Instead, very strong coincidences are observed among 329.18, 113.59 and 46.43 keV gamma rays. As discussed previously there is no evidence for the existence of the level at 45.46 keV, 113.59 keV is also strongly coincident with 259 keV gamma, and there are no transitions with reasonable intensities which could account for the depopulation of levels at 331 keV and 333 keV. Since there

is only one gamma ray with energy 329.175 keV and reasonable intensity (taking into account the high resolution of the curved crystal spectrometer and simple intensity considerations) to fulfil that condition in low energy (n,γ) data and a primary transition (6939.9 ± 0.7 keV, relative intensity 2.5%) is observed in present high-energy (n,γ) data, 329.18 keV level is taken as the one in question.

The negative parity state 79 keV (2^-) is weakly populated by a direct M1 transition from the capture-state $(0,1)^-$. On the other hand positive parity states are strongly populated by direct E1 transitions. Therefore the primary transition (with very weak intensity) could be taken as M1 or (E2) type. There is no population of this level in (d,p) reaction. The mode of de-excitation to the ground-state should exclude spin 3. From these facts, the spin and parity of the 329.18 keV could only be restricted to $(0,1,2)^+$.

The 338.42 keV level

This level is directly populated in the (d,p) reaction with angular momentum transfer $\ell=2$ and neutron orbital $d_{5/2}$, the same as the 79 keV level. The primary gamma transition to this level in the present high-energy (n,γ) data could be identified as M1 type due to its weak intensity value. Due to the coupling of an odd $P_{\frac{1}{2}}$ proton and an odd $d_{5/2}$ neutron, two spin - parity values of 2^- and 3^- are

obtained Talmi[132] has shown that the energy splitting of the doublet levels $|\pi(P_{\frac{1}{2}}), \nu(d_{5/2})|_{2^-,3^-}$ depends little on the number of neutrons in the shell. By analogy with other nuclei, this value can be 200-240 keV. Therefore 338.42 keV and 79 keV levels can be taken as a doublet of this kind. Since 79 keV level is known to be a 2^- state, one would expect the 338 keV level to have spin and parity 3^-. The data on the measured excitation function and angular distribution in (p,nγ) experiment by Hattori et al confirms this assignment.

The 370.40 keV level

This new level is proposed according to high-energy (n,γ) data, (primary gamma 6899.6 keV, relative intensity 1.36%, M1(E2) type) γ-γ coincidence results and energy combination principle. This level is not directly populated in the (d,p) reaction, but there is an observed level at 378 keV, and since the experimental resolution is about 20 keV the 370 keV level could have been masked by the 378 keV level. The mode of de-excitation of this level to 79 keV (2^-) excludes the spin 0. Therefore its spin and parity value may be limited to $(1,2)^-$.

The 375.61 keV level

This new level is proposed mainly due to the strong coincidence observed between the 46.43 and 329.18 keV gamma rays,

the energy combination principle and simple intensity considerations. The modes of de-excitation of this level to 329 keV levels ($\lesssim 2^+$) and ground state (1^+) suggest the spin and parity values to be $\lesssim 3^+$.

The 379.24 keV level

There has been some uncertainty concerning the existence of the 6890.51 ± 0.11 keV primary gamma transition which populates 379 keV level. Bolotin and Namenson[120] have somehow omitted this gamma ray from their high-energy (n,γ) data. This gamma ray is definitely observed in their (n,γ) spectrum. When their spectra of $^{107}Ag(n,\gamma)^{108}Ag$ and $^{109}Ag(n,\gamma)^{110}Ag$ are compared, there is no evidence for the existence of this gamma ray in the latter spectrum. In addition, the separation energy of ^{110}Ag is 6805.6 ± 1.0 keV. This shows that the gamma ray in question is neither background radiation nor a transition from the $^{109}Ag(n,\gamma)^{110}Ag$ reaction. On the other hand, Rasmussen et al[9] has observed this gamma ray with relative intensity 18% (the intensity of 7269 keV gamma taken as 100%) in their natural Ag(n,γ) experiment. This agrees with the present result. Therefore, this 6890.51 ± 0.11 keV (relative intensity 22.98 ± 0.88%) is assigned to be the primary transition which populates the 379.24 keV level in ^{108}Ag.

This 379.24 keV level is populated in the (d,p) reaction with angular momentum transfer value $\ell=0$. This suggests that the spin and parity are $(0,1)^-$. The data on the measured excitation function and

angular distribution in the (p,nγ) reaction (Hattori et al)[107] suggest that the spin value is 1,(2). Therefore the spin and parity of 379.24 keV level can be adopted as 1^-, which in turn implies that the primary transition is M1. However, the intensity of the primary transition is 2 to 5 times stronger than that expected for M1. Unless the primary gamma transition is strong M1 (or perhaps strongly enhanced E2 type; or mixture of M1 and E2), 1^- level, observed in the (d,p) reaction, may not be the level populated by the 6890 keV primary gamma transition. Improved (d,p) studies with higher resolutions would be of considerable interest. Complete angular correlation of outgoing protons will also conclusively establish the parities of these levels. And this, when coupled with present data would allow the desired qualitative comparison between E1 and M1 transition probabilities.

Although the spin-parity assignment is still open to question, it is adopted as 1^- with the p-n configuration of $|\pi(P_{\frac{1}{2}}), \nu(S_{\frac{1}{2}})|_{1^-}$.

The 465.64 keV level

This level is populated by a primary transition (M1 type) in the (n,γ) reaction from the neutron capture state as well as in the (d,p) reaction with angular momentum transfer values $\ell=0$ and neutron orbital $s_{\frac{1}{2}}$. The coupling of the $P_{\frac{1}{2}}$ proton with an odd-neutron in the single-particle orbital $S_{\frac{1}{2}}$, should give rise to two possible spin states $(0,1)^-$. The energy splitting of the doublet levels 0^- and 1^- suggest that one may take the 379 keV and 465 keV levels as the most

likely components of the doublet under consideration arising in the (d,p) reaction. Since the 379 keV level is adopted as 1^-, the assignment 0^- to 465 keV may be a reasonable choice although 1^- cannot be completely omitted.

The 606.53 and 679.08 keV levels

Both levels are populated in the (d,p) reaction with angular momentum transfer value $\ell=0$ and neutron orbital $9_{\frac{1}{2}}$. The 606.53 keV level is also populated by the primary gamma transition of M1 type in the (n,γ) reaction. The energy splitting of these levels suggest that they are probably components of the doublet with p-n configuration $|\pi(p_{\frac{1}{2}}), \nu(s_{\frac{1}{2}})|_{0^-,1^-}$. The large (d,p) cross section of the 606 keV level suggests $I^\pi = 1^-$, although 0^- cannot be completely neglected. The small (d,p) cross section of the 679 keV level suggests $I^\pi = 0^-$, although 1^- cannot be completely omitted.

The 1002.57 keV level

This level is populated by the primary gamma transition (6267.40 keV, relative intensity 24.32%) and $\gamma-\gamma$ coincidence data. This transition may be E1 transition in accordance with the general E1/M1 intensity ratio. This suggests positive parity value for the level in question. In the (d,p) reaction measurements the 993 keV

(Brient et al)[65] and 996 keV (Lopez)[133] are populated. If the FWHM resolution (20 keV) in (d,p) is taken into consideration, the 1002.57 keV may represent the 993 (or 996) keV level in the (d,p) reaction. The (d,p) data suggest negative parity states. Therefore unless the primary gamma transition is a strong M1, the 1002.57 keV may not be the level populated in (d,p) data. The spin can be restricted to be $\lesssim 2$.

Spin and Parity Assignments for the other levels

For the other levels which are established through the primary transition in (n,γ) reaction, γ-γ coincidence results, (d,p) reaction data or combinations of these, spin and parity are assigned (or limited rather) on the basis of the arguments similar to those already discussed.

Further suggested levels (E > 1.3 MeV) in ^{108}Ag

The results of the present high energy and low energy (n,γ) measurements with Ge(Li) detectors together with the Risø results have established the position of 43 levels (above 1.3 MeV) in ^{108}Ag. The first low-lying 27 levels (energy region 1.3 - 2.0 MeV) are checked by the energy combination principle (see Table 7.4). These results are compared with existing (d,p) data (Brient et al[65]; Lopez[133]) (see in Table 7.5). Spin and parity assignments are based on arguments similar to those already discussed. Although the γ-γ coincidence

measurements (high energy γs vs low energy γs, high energy γs vs high energy γs) have been carried out, the data-analysis has not yet been carried out due to lack of time available.

The qualitative interpretation of these levels must be postponed until the level-scheme has been completed through detailed (n,e^-), γ-γ coincidence and angular correlation data in (n,γ) and (d,p) reactions so that unique spin and parity assignments can be made.

7.2. LEVEL SCHEME OF ^{110}Ag

The energy level scheme of ^{110}Ag, although it has been the subject of many investigations*, is still incomplete in many respects. The high-energy gamma rays from the ^{109}Ag(n,γ)^{110}Ag reaction have been studied by Freund (1968)[135], Bolotin et al (1967)[120] and Winkler (1967)[87], and Gujrathi et al (1970)[108], Kane and Scharff-Goldhaber (1970)[109] and Elze et al (1968)[131] have presented the energies and intensities for gamma rays in the energy region below 300 keV. Only Winkler (1967)[87] has measured low-energy gamma spectra as high as 1·3 MeV, but with poor energy resolution and not very precise intensity determination. It is thus necessary to study the low-energy ^{109}Ag(n,γ)^{110}Ag reaction more precisely.

The gamma-transitions in ^{110}Ag were identified from the comparison of the spectra obtained by using enriched ^{107}Ag and natural silver targets (see Chapter 5). The weighted average values from the various measurements for the energy and intensity determinations are presented in Table 5.3. The present energy and intensity values are in reasonable agreement with the previously published results within two standard deviations. Since the present work is not a comprehensive study of the ^{109}Ag(n,γ) reaction, no attempt was made to identify the weak transitions.

*References : 80, 81, 87, 88, 107-120, 128, 131, 135.

A rather tentative level scheme of ^{110}Ag below 655 keV excitation energy has been constructed with the present data and Bertrand and Raman (1972)[80] Figure 7.3 displays such a level scheme. Spin and parity assignments are based on the previous investigations* and the arguments similar to those already discussed.

The interpretation of the levels must be postponed until the level scheme has been completed through detailed low-energy (n,γ) (n,e^-), γ-γ coincidence, (d,p) and angular correlation data.

*References : 80, 81, 87, 88, 107, 109, 135.

TABLE 7.1.

Energy-Levels in ^{108}Ag (E_x < 1300 keV)

Level No.	(n,γ) data		(d,p) data		I^π
	Present Work	Ref. ( )	Brient et al	Lopez	
1	0	0	-	-	1^+
2	79.139 ± 0.002	79.05	79(ℓ_n=2)	80.8	2^-
3	109.43*	109.43	-	-	6^+
4	193.073 ± 0.006	192.75	-	-	$1^+, (2)^+$
5	206.610 ± 0.004	206.23	-	-	2^+
6	215.383 ± 0.004	-	-	-	3^+
7	294.560 ± 0.007	294.80	-	-	2^+
8	324.495 ± 0.006	-	-	-	3^+
9	329.180 ± 0.005	331.04	-	-	$\leqslant 3^+$
10	338.416 ± 0.006	338.10	338(ℓ_n=2)	339	3^-
11	370.40 ± 0.05	-	-	-	$\leqslant 2^+$
12	375.62 ± 0.05	-	-	-	$\leqslant 3^+$
13	379.24 ± 0.008	378.55	378(ℓ_n=0)	379	1^-
14	408.36 ± 0.009	-	-	-	$(1-3)^+$
15	451.05 ± 0.15	451.18	-	-	$\leqslant 3^-$
16	460.08 ± 0.009	460	-	-	$\leqslant 2^-$
17	465.65 ± 0.001	465	465(ℓ_n=0)	467	$(0,1)^-$
18	508.47 ± 0.01	509.55	-	-	$\leqslant 2^-$
19	516.85 ± 0.05	-	518(ℓ_n=2,4)	512	$(1,2)^-$
20	542.84 ± 0.01	542.93	543(ℓ_n=2)	541	$(1-3)^-$
21	563.81 ± 0.02	563.93	-	-	$(1,2)^+$
22	579.10 ± 0.02	578	-	588	$\leqslant 2^-$
23	606.53 ± 0.08	606	607(ℓ_n=0)	608	$(0)^-, 1^-$
24	611.66 ± 0.08	-	-	-	$(2,3)^-$
25	616.94 ± 0.05	-	-	-	$\leqslant 2^-$
26	645.51 ± 0.10	) 650	655(ℓ_n=4)	655	$\leqslant 3^-$
27	656.33 ± 0.10	)			$(3,4)^-$
28	679.08 ± 0.10	675	676(ℓ_n=0)	679	$(0,1)^-$
29	700.51 ± 0.20	699	-	-	$\leqslant 2^-$
30	705.62 ± 0.11	706	-	-	$\leqslant 2^-$

TABLE 7.1.

Energy-Levels in ^{108}Ag (E_x < 1300 keV) (continued)

Level No.	(n,γ) data		(d,p) data		I^π
	Present Work	Ref. ( )	Brient et al	Lopez	
31	715.80 ± 0.12	-	713(ℓ_n=2,4)	713	$(1,2)^-$
32	765.50 ± 0.07	763	765(ℓ_n=2)	767	$(2,3)^-$
33	803.70 ± 0.15	-	804(ℓ_n=2)	804	$(2,3)^-$
34	819.14 ± 0.08	-	-	819	$\leq 3^+$
35	857.34 ± 0.10	-	856(ℓ_n=2)	861	$(2,3)^-$
36	880.73 ± 0.14	879	-	-	$\leq 3^-$
37	897.11 ± 0.21	897	898(ℓ_n=0)	901	$(0,1)^-$
38	972.65 ± 0.17	975		973	$\leq 2^-$
39	1002.57 ± 0.10	1002	993(ℓ_n=0,2)	996	$\leq 3^+$
40	1012.87 ± 0.35+	1012	-	-	$\leq 3^+$
41	1051.62 ± 0.11	1047	1048(ℓ_n=2)	1052	$\leq 2^-$
42	1079.77 ± 0.10	-	1084(ℓ_n=2)	1085	$\leq 3^+$
43	1105.82 ± 0.14	1105)	1109	1108	$\leq 3^+$
44	1112.03 ± 0.19	1111)			$\leq 2^+$
45	1137.06 ± 0.10	1136	1137	1136	$\leq 3^+$
46	1143.92 ± 0.10	-	-	-	$\leq 3^+$
47	1157.05 ± 0.14	1157	-	-	$\leq 3^+$
48	1200.38 ± 0.35	1200	1198(ℓ_n=0)	1199	$\leq 3^+$
49	1213.35 ± 0.27	1214	-	-	$\leq 3^-$
50	1231.71 ± 0.18	1231	1229	1230	$\leq 3^+$
51	1241.00 ± 0.08	1242	-	-	$\leq 3^+$
52	1272.23 ± 0.15	1271	-	-	≤ 3

* - adopted from Reference 81

\+ - this level may be a doublet of 1013.25 ± 0.10 and 1012.51 ± 0.09 keV levels. If this is the case, then 6256.81 keV primary gamma will populate the latter level.

TABLE (7.2)

Possible p-n configurations of the ^{108}Ag and ^{110}Ag levels (Ref. 107)

p-n Configuration	I^{π}
$\pi(P_{\frac{1}{2}})$, $\nu(d_{5/2})$	$2^- - 3^-$
$\pi(P_{\frac{1}{2}})$, $\nu(g_{7/2})$	$3^- - 4^-$
$\pi(g^{-3}_{9/2})_{7/2}$, $\nu(d_{5/2})$	$1^+ - 6^+$
$\pi(g^{-3}_{9/2})_{7/2}$, $\nu(g_{7/2})$	$0^+ - 7^+$
$\pi(g^{-3}_{9/2})_{9/2}$, $\nu(g_{7/2})$	$1^+ - 8^+$

TABLE 7.3.

Binding Energy of ^{108}Ag

Primary Gamma	Recoil Energy	Level Energy	B.E.
7269.30 ± 0.11	0.28	0	7269.58 ± 0.11
7076.27 ± 0.12	0.27	193.07	7269.61 ± 0.12
7062.73 ± 0.16	0.27	206.61	7269.61 ± 0.16
6974.93 ± 0.12	0.26	294.56	7269.75 ± 0.12
6890.51 ± 0.11	0.25	379.24 ± 0.03	7270.00 ± 0.12
6804.05 ± 0.08	0.25	465.64	7269.89 ± 0.08
6705.96 ± 0.14	0.24	563.81 ± 0.01	7270.02 ± 0.14
6690.33 ± 0.53	0.24	579.10 ± 0.10	7269.67 ± 0.54
6563.53 ± 0.48	0.23	705.62 ± 0.10	7269.15 ± 0.49
6389.12 ± 0.18	0.22	880.73 ± 0.14	7270.07 ± 0.23
6296.27 ± 0.45	0.21	972.65 ± 0.16	7269.16 ± 0.48
6267.40 ± 0.20	0.21	1002.57 ± 0.02	7270.18 ± 0.20
6256.81 ± 0.27	0.21	1012.87 ± 0.35	7269.89 ± 0.44
6218.48 ± 0.17	0.21	1051.62 ± 0.17	7270.31 ± 0.24
6164.00 ± 0.18	0.20	1105.82 ± 0.14	7270.02 ± 0.23
6158.07 ± 0.26	0.20	1112.03 ± 0.19	7270.90 ± 0.32
6125.97 ± 0.15	0.20	1143.92 ± 0.05	7270.09 ± 0.16
6056.56 ± 0.42	0.20	1213.35 ± 0.26	7270.11 ± 0.49
6038.48 ± 0.52	0.19	1231.71 ± 0.16	7270.38 ± 0.54
6027.85 ± 0.32	0.19	1241.00 ± 0.05	7269.04 ± 0.33
5997.87 ± 0.14	0.19	1272.23 ± 0.15	7270.29 ± 0.21
	Weighted Average B.E. =		7269.85 ± 0.32

TABLE 7.4.

Further suggested levels (1.3 MeV < E_x < 2.0 MeV)

Level Energy E_x (keV)	Primary Transition E_γ (I_γ%)	(d,p) data		I^π
		Brient et al	Lopez	
1310.95 ± 0.22	5958.54 (8.54)	1309	1307	$\leqslant 3^-$
1325.24 ± 0.17	5944.04 (8.86)	1335	1335	$\leqslant 3^-$
1355.30 ± 0.15	5913.97 (15.38)	1352	1353	$\leqslant 3^-$
1405.41 ± 0.20	5863.92 (5.06)	-	1394	$\leqslant 3^-$
1438.13 ± 0.26	5831.25 (15.78)	1429	1430	$\leqslant 2^-$
1463.10 ± 0.35	5806.79 (7.58)	1468	1467	$\leqslant 3^-$
1473.34 ± 0.15	5796.60 (44.77)	-	-	$\leqslant 2^+$
1482.68 ± 0.22	5787.08 (43.37)	-	-	$\leqslant 2^+$
1496.57 ± 0.16	5772.98 (10.76)	1494	1490	$\leqslant 3^-$
1540.67 ± 0.20	5728.93 (14.21)	1542	1538	$\leqslant 2^-$
1549.23 ± 0.23	5720.55 (10.48)	-	-	
1568.26 ± 0.25	5701.11 (12.28)	1568(ℓ_n=2)	1566	$(2,3)^-$
1584.07 ± 0.23	5685.74 (14.49)	-	-	$\leqslant 2^+$
1593.20 ± 0.22	5675.90 (22.46)	-	-	$\leqslant 2^+$
1629.77 ± 0.29	5639.76 (27.26)	1624	1616	$\leqslant 2^+$
1635.31 ± 0.15	5633.89 (17.54)	1644	1638	$\leqslant 3^+$
1655.13 ± 0.20	5614.23 (8.69)	-	-	$\leqslant 2^+$
1663.44 ± 0.22	5606.03 (9.14)	-	-	$\leqslant 2^+$
1701.25 ± 0.30	5568.43 (7.76)	-	-	$\leqslant 2^-$
1711.82 ± 0.11	5557.65 (2.63)	1711	1705	$\leqslant 3^+$
1721.45 ± 0.20	5547.86 (66.43)	-	1739	$\leqslant 2^+$
1770.86 ± 0.17	5498.74 (52.10)	1779	1762	$\leqslant 2^-$
1787.06 ± 0.31	5482.31 (3.84)	-	1788	$\leqslant 3^+$
1827.22 ± 0.36	5442.40 (10.23)	-	1823	$\leqslant 2^+$
1972.88 ± 0.23	5296.37 (35.64)	-	-	$\leqslant 2^+$
1985.59 ± 0.45	5283.47 (12.22)	1988		
1991.18 ± 0.25	5278.42 (12.99)	2005		

The level energies are determined according to primary gamma transitions together with low energy gamma rays and energy combination principles.

TABLE 7.5.

Further suggested levels above 2 MeV

Level Energy E_x (keV)	Primary Transition E_γ (I_γ%)	(d,p) data Brient et al	I^π
2021.1	5248.52 (28.62)	2022	$\lesssim 2^+$
2036.1	5233.50 (4.55)	-	$\lesssim 3^-$
2058.1	5211.54 (10.00)	2083	$\lesssim 3^-$
2097.4	5172.23 (11.80)	2096	$\lesssim 3^+$
2130.4	5139.24 (18.48)	2119	$\lesssim 2^+$
2154.4	5115.24 (7.04)	2165	
2174.6	5095.05 (20.86)		
2194.1	5075.53 (31.28)	2201	$\lesssim 2^+$
2209.7	5059.90 (10.54)		
2226.9	5043.75 (3.38)	2240	$\lesssim 3^-$
2252.1	5017.59 (5.14)		$\lesssim 3^-$
2263.3	5006.29 (12.03)	2261	$\lesssim 2^+$
2286.1	4983.47 (12.49)	2289	
2366.3	4903.27 (18.80)	2362	
2477.0	4893.62 (15.49)	-	$\lesssim 2^+$
2410.7	4858.99 (24.45)	-	$\lesssim 2^+$
2431.1	4838.46 (7.55)	2429	$\lesssim 3^-$
2453.1	4816.60 (28.09)	-	$\lesssim 2^+$
2474.7	4794.99 (9.62)	-	
2485.0	4784.62 (23.91)	-	$\lesssim 2^+$
2498.5	4771.12 (10.93)	2499	$\lesssim 3^-$
2506.9	4762.71 (12.97)	-	
2553.1	4716.58 (24.39)	-	$\lesssim 2^+$
2573.5	4696.20 (7.93)		
2596.2	4673.52 (12.83)	2618	
2641.3	4628.43 (18.75)		
2652.1	4617.58 (8.23)		
2680.1	4589.52 (6.30)		
2691.7	4577.97 (11.11)		
2706.6	4562.99 (13.64)	2707	$\lesssim 3^-$
2715.3	4554.35 (21.25)	2728	
2732.5	4537.06 (20.45)		

Level energies are determined by taking the binding energy and nuclear recoil energy as 7269.65 and 0.2 keV respectively.

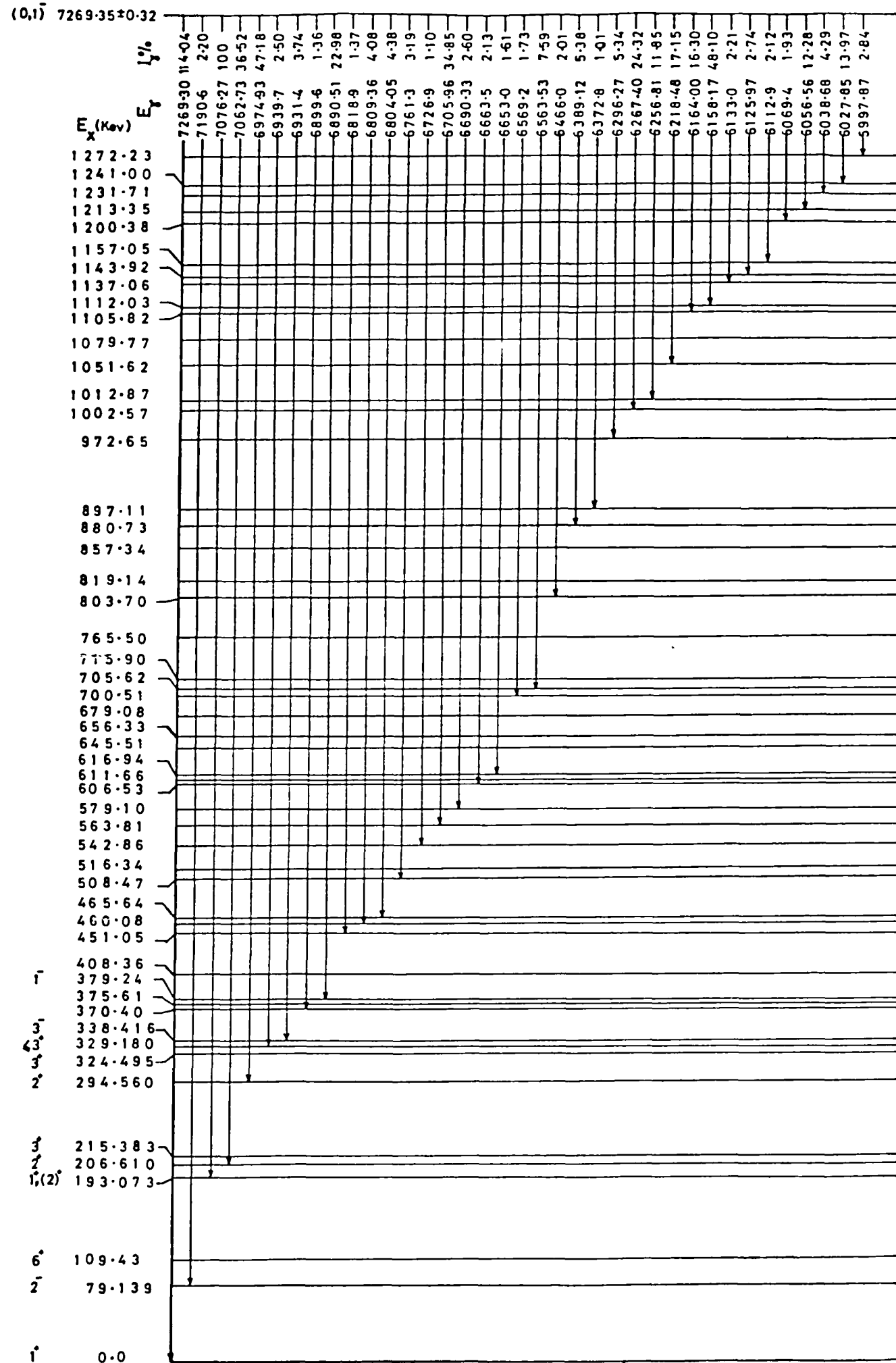
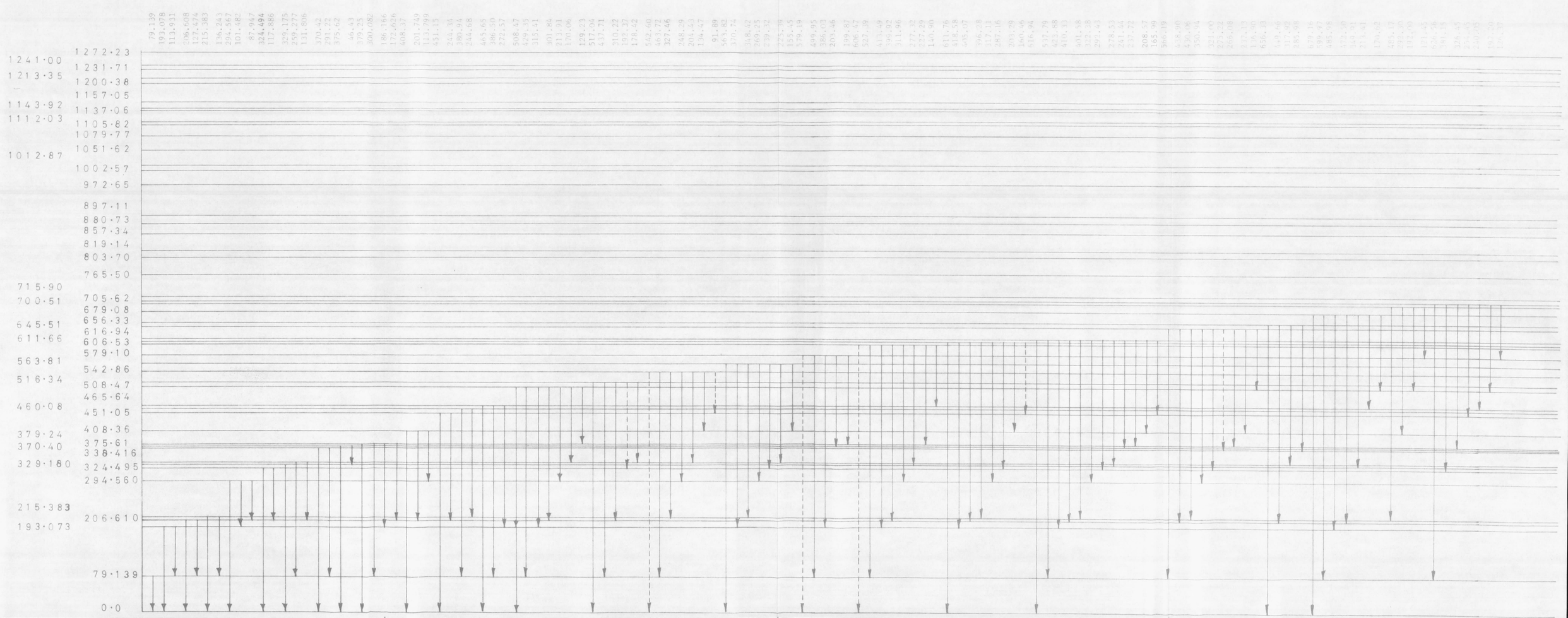
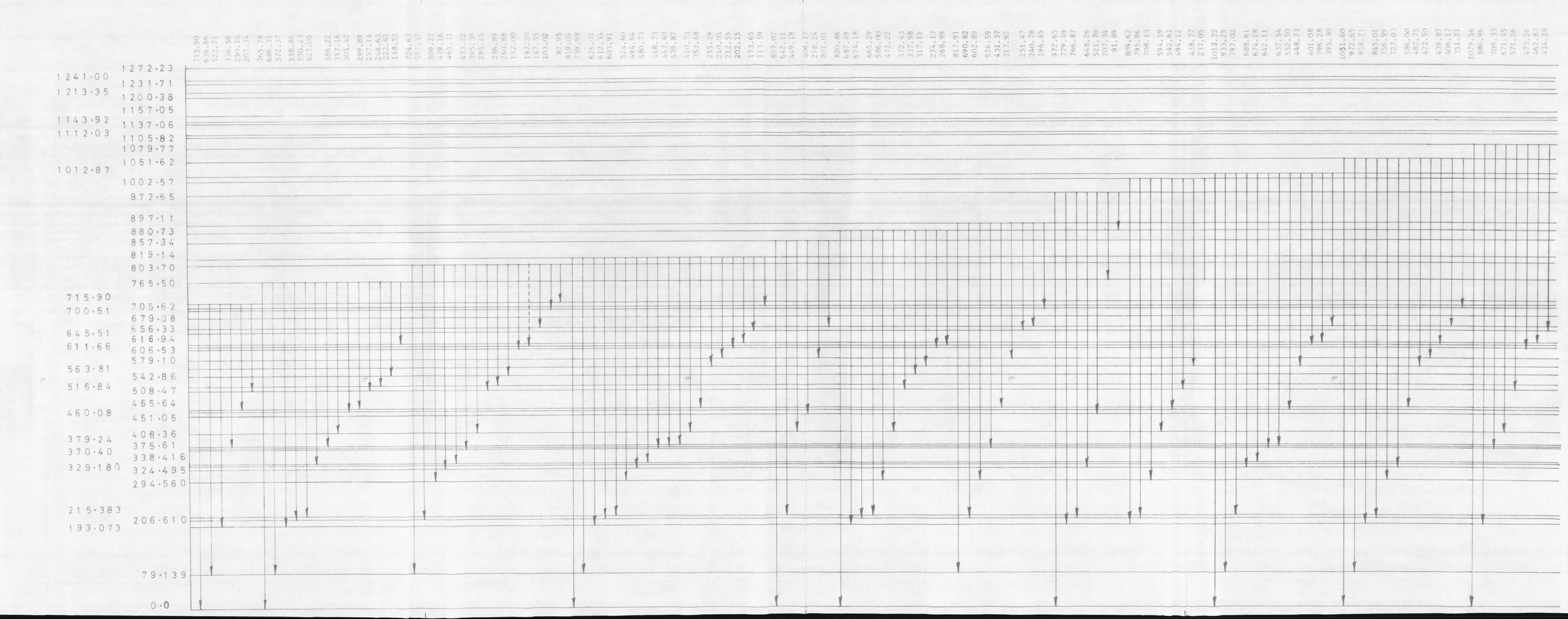


FIG.7.1 PRIMARY GAMMA TRANSITIONS IN $^{107}Ag(n,\gamma)^{108}Ag$ REACTION


1241·00
1213·35
1143·92
1112·03
1012·87
715·90
700·51
645·51
611·66
563·81
516·34
460·08
379·24
370·40
329·180
215·383
193·073
1272·23
1231·71
1200·38
1157·05
1137·06
1105·82
1079·77
1051·62
1002·57
972·65
897·11
880·73
857·34
819·14
803·70
765·50
705·62
679·08
656·33
616·94
606·53
579·10
542·86
508·47
465·64
451·05
408·36
375·61
338·416
324·495
294·560
206·610
79·139
0·0
79.139
193.078
113.931
296.608
127.474
215.383
136.243
204.567
101.482
87.947
324.494
117.886
329.175
259.277
131.806
370.42
291.22
375.62
46.43
379.25
300.082
186.166
172.626
408.37
201.749
113.799
451.15
244.34
380.94
244.68
465.65
386.50
272.57
508.47
429.35
315.41
301.84
213.91
170.06
129.23
517.04
437.71
310.22
192.37
178.42
542.60
463.72
327.46
248.29
204.43
134.47
91.89
563.82
370.74
348.42
269.25
239.32
725.79
655.45
379.19
499.95
386.03
209.46
199.87
606.47
522.39
415.49
299.92
311.96
277.30
227.29
140.90
611.76
418.58
405.07
396.28
317.11
287.16
283.29
340.46
616.94
517.79
423.88
410.50
591.58
322.38
291.43
278.53
241.44
237.72
208.57
165.99
566.89
428.90
440.08
550.54
321.00
273.52
266.04
317.13
1A.90
656.43
149.46
117.98
285.98
179.35
199.42
145.54
173.30
344.61
213.43
170.04
305.12
293.20
197.90
171.5
524.56
391.15
324.55
2.5
260.15
197.50
177.87


1241·00
1213·35
1143·92
1112·03
1012·87
715·90
700·51
645·51
611·66
563·81
516·84
460·08
379·24
370·40
329·180
215·383
193·073
1272·23
1231·71
1200·38
1157·05
1137·06
1105·82
1079·77
1051·62
1002·57
972·65
897·11
880·73
857·34
819·14
803·70
765·50
705·62
679·08
656·33
616·94
606·53
579·10
542·86
508·47
465·64
451·05
408·36
375·61
338·416
324·495
294·560
206·610
79·139
0·0
715.90 636.66 522.71
336.56 250.14 207.34
765.78 686.31 572.37
558.86 550.23 427.05
386.22 357.16 305.42
299.89 257.14 248.63 222.61 148.52
724.62 597.37
509.27 479.16 465.31
433.22 395.30 295.25
286.89 260.88 192.00
197.20 147.35 103.02
87.95 819.04 739.98
626.01 612.34 603.91
524.60 494.64 480.73
448.73 443.40 439.87
410.73 353.48
255.29 240.05 212.55 202.15
173.65 113.59
857.07 642.11 449.18
406.17 278.24 201.01
880.86 687.49 674.18
665.29 586.00 472.22
372.43 337.98 317.11
274.17 268.99
817.91 690.82 602.89
526.59 431.37 317.92
251.47 240.78 196.45
972.65 779.49 766.87
648.26 521.70 207.34 91.89
809.62 795.96 708.13
594.19 542.61 494.12
438.77 237.05
1013.22 933.25 797.02
688.61 674.18 642.11
637.54 532.50 448.73
401.08 396.28 395.30
1051.60 972.65 858.71
845.01 756.99 727.03
586.00 487.75 472.50
439.87 406.17 351.21
1079.56 886.96
709.33 671.45 571.26
473.26 462.83 434.28

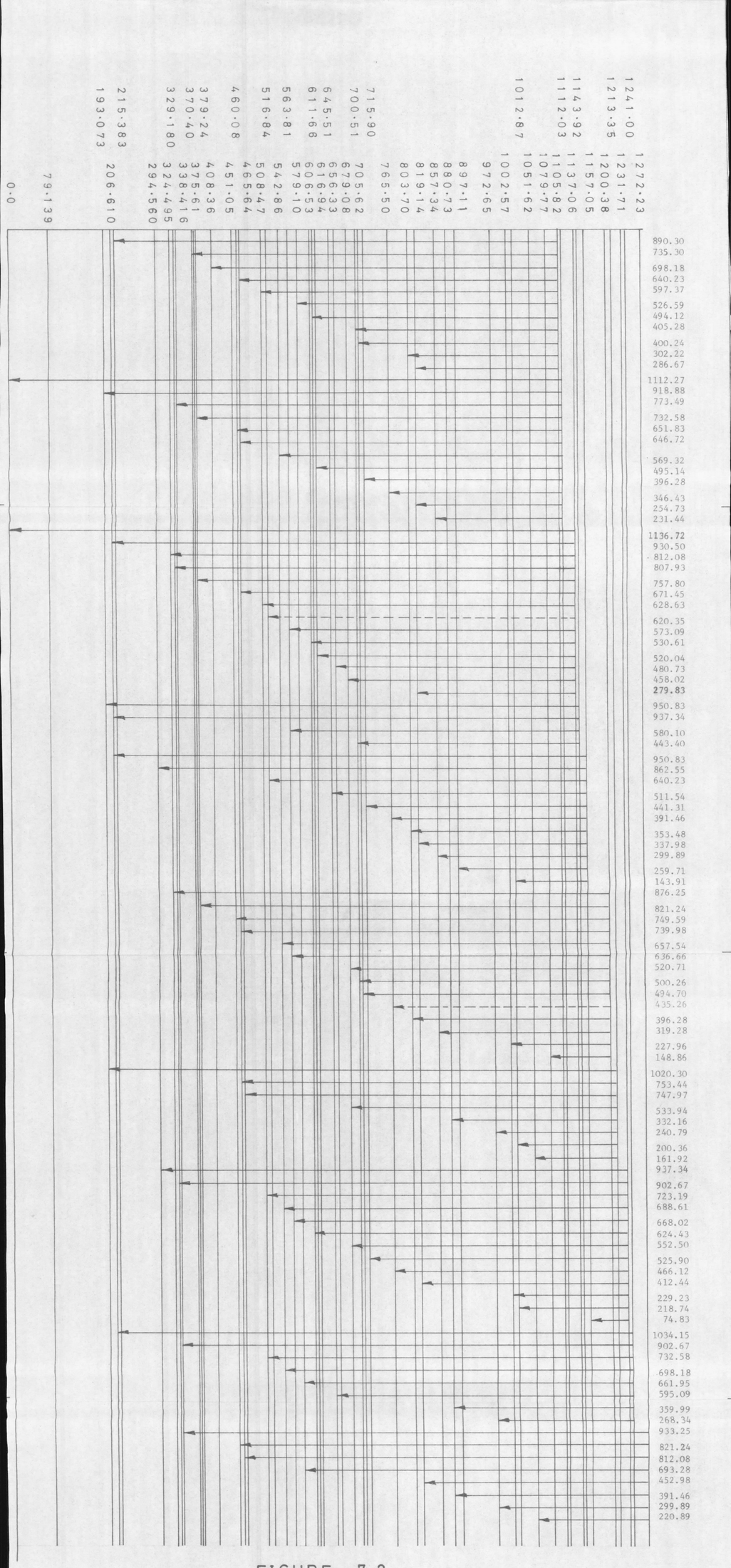


FIGURE 7.2

PARTIAL LEVEL SCHEME OF ^{108}Ag

BECAUSE OF THE LARGE NUMBER OF AVAILABLE LEVELS AND TRANSITIONS, ONLY THE ENERGY VALUES (IN KEV) ARE GIVEN TO TWO DECIMAL PLACES.

FOR DETAILS, SEE ALSO TABLE 5.6 (ENERGY, INTENSITY, COINCIDENCE DATA), TABLE 7.1 (SPIN AND PARITY) AND FIGURE 7.1 (PRIMARY TRANSITIONS).

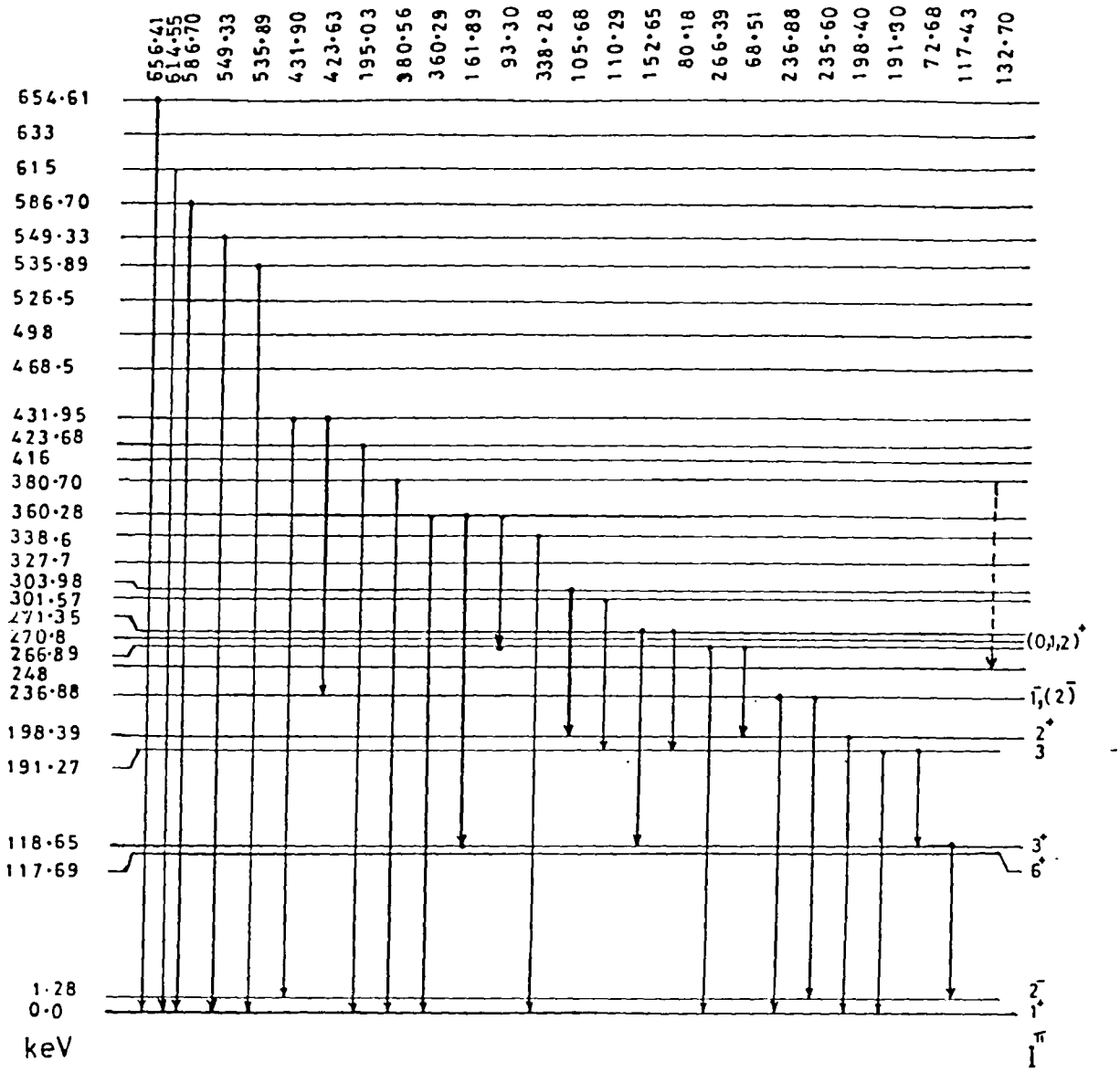


FIG. 7.3 PRELIMINARY LEVEL SCHEME OF ^{110}Ag .

REFERENCES

1. MOTZ, H.T. Annual Review of Nuclear Science, Vol. 20 (1970) p. 1 - 38.
2. LANE, A.M. Atomic Energy Research Establishment Report AERE T/R 1289 (1954).
3. KINSEY, B.B. α, β and γ-Ray Spectroscopy (Ed. K. Siegbahn), Chapter XXY. Amsterdam: North-Holland.
4. MOTZ, H., BACKSTROM, G. α, β and γ-Ray Spectroscopy (Ed. K. Siegbahn) Vol. 1 (1965) p. 769-804 Amsterdam: North-Holland.
5. IAEA, Vienna. Proc. Int. Symp. Neutron Capture Gamma Ray Spectroscopy, Studsvik, Aug. 1969.
6. Proc. Second Int. Symp. on Neutron Capture Gamma Ray Spectroscopy, Petten - the Netherlands, September 1974.
7. BARTHOLOMEW, G.A., Ann. Rev. Nucl. Sci. Vol. 11 (1961) p. 259-302.
8. BARTHOLOMEW, G.A., Nuclear Spectroscopy (Ed. F.Ajzenberg Selove) Part A (1960) p. 304-332. New York and London, Academic.
9. RASMUSSEN, N.C. et al., Thermal Neutron Capture Gamma-Ray Spectra of the elemtns (1969) M I T N E-85 (AF-688, 955).
10. BOLLINGER, L.M. Particles and Nuclei (Ed. N.N. Bogolyubov) Vol. 2, Part 4 (1973) p. 47-64, Consultants Bureau. New York-London.

11. SUMBRAEV, O.I., SMIROV, A.I., Nucl. Instr. Meths., 22, 125 (1963).

12. KOCH, H.R. et al., in Neutron Capture Gamma-Ray Spectroscopy, IAEA, Vienna (1969) p. 55.

13. SMITHER, R.K., BUSS, D.J. in Neutron Capture Gamma-Ray Spectroscopy, IAEA, Vienna (1969). p. 55-63.

14. BAADER, H.A. et al, in Neutron Capture Gamma-Ray Spectroscopy, IAEA, Vienna (1969). p.363-369.

15. BURSON, S.B., in Argonne National Laboratory Report ANL-7436 (1968), p.3.

16. T. von EGIDY, in Neutron Capture Gamma-Ray Spectroscopy, IAEA, Vienna (1968), p. 127-139.

17. SCHULT, O.W.B., in Neutron Capture Gamma-Ray Spectroscopy, Petten, Netherlands (September 1974) p. 505-519.

18. CAMP, D.C. in Radioactivity in Nuclear Spectroscopy (Ed. Hamilton and Manthuruthil) Vol. 1 (1972), p. 135-205 : Gordon & Breach. New York, London, Paris.

19. SHIPILOV. : Instr. Exp. Tech. 15 (2) (1972) p. 305-318.

20. EVANS, R.D. The Atomic Nucleus, McGraw-Hill (1955), p. 677.

21. BIRKETT, R.E. A Study of Gamma Rays Following Thermal Neutron Capture in ^{42}Ca and ^{44}Ca. (Ph.D. Thesis 1971) UCRL-51060.

22. BURCHAM, W.E. An Introduction to Nuclear Physics, Longman (1973) p. 267.

23 PAUL, E.B. Nuclear and Particle Physics, North-Holland, (1969) p. 227-230.

24. BOLLINGER, L.M. "Radiative Transitions from Highly Excited Nuclear States", Nuclear Structure, IAEA, Vienna, (1968), p. 317.

25. MOSZKOWSKI, S.A. α-, β- and γ-Ray Spectroscopy (Ed. K. Siegbahn) Vol. 2 (1966) p. 863-886. Amsterdam, North-Holland.

26. BLATT, J.M. and WEISSKOPF, V.F. Theoretical Nuclear Physics, (John Wiley & Sons, New York, 1952).

27. VARSHALOVICH, D.A. Soviet Phys. JETP, 11, 125 (1960).

28. OBI, ISHIDZU, HORIE, YANAGAWA, TANABE and SATO. Ann. Tokyo Astronom. Observatory, II ser. 4, No. 1 and 2 (1954).

29. PORTER, C.E. and THOMAS, R.G. Phys. Rev. 104 (1956) p. 483.

30. BOLLINGER, L.M. and THOMAS, G.E. Phys. Rev. Letters 18 (1967) p. 1143.

31. BOLLINGER, L.M. and THOMAS, G.E. Phys. Rev. Letters 21 (1968) p.233.

32. GRANT, P.J. Elementary Reactor Physics 1966 (Pergamon Press) Chap. III.

33. BECKURTS, K.H. and WIRTZ, K. Neutron Physics (Springer-Verlag, New York, 1964) Chapter 6.

34. HENRY, E.A. Nucl. Data. Sheets 11 (1974) p. 495-548.

35. SCHMIDT-OTT, W.D. and FINK, R.W. Z. Physik 249 (1972) p. 286-293.

36. BOSCH, H.E. et al Nucl. Phys. A108 (1968) p. 209-220.

37. ALEXANDER, P. and LAU, J.P. Nucl. Phys. A121 (1968) p. 612-624.

38. NOTEA, A. and GURFINKEL, Y. Nucl. Phys. A107 (1968) p. 193-208.

39. MARTIN, M.J. and BLICHERT-TOFT, P.H. Nucl. Data Tables A8 (1970) p. 126-132.

40. DZELEPOW, B.S. and ZHUKOVSKY, N.N. Nucl. Phys. 8 (1958) p. 250.

41. EWAN, G.T. and TAVENDALE, A.J. Can. J. Phys. 42 (1964) p. 2286.

42. WALFORD, G. and DOUST, C.E. Nucl. Instr. and Meth. 62 (1968) p. 353.

43. ROBERT, M. CEA-R-3692 (1968).

44. WALLACE, G. and COOTE, G.E. Nucl. Instr. and Meth. 74 (1969) p. 353-354.

45. VALIVAARA, K.G. et al Phys. Scripta 2 (1970) p. 19-22.

46. AUBIN, G. et al Nucl. Instr. and Meth. 76 (1969) p. 93-99.

47. ROUTTI, J.T. UCRL-1952 (1969).

48. ROUTTI, J.T. and PRUSSIN, S.G. Nucl. Instr. and Meth. 72 (1969) p. 125-142.

49. PARADELLIS, T. et al Bull. Am. Phys. Soc. 13 (1968) p. 69.

50. LEDERER, C.M. et al Table of Isotopes, 6th edition (1967) (John Wiley and Sons: New York).

51. WINN, W.G. and SARANTITES, D.G. Phys. Rev. C1 (1970) p. 215.

52. HACHEM, A. C.R. Acad. Sci. SER. B. 279 (1974) p. 677-680.

53. ZOBEL, V. et al Nucl. Instr. and Meth. 141 (1977) p. 329-336

54. TOTH, K.S. Nucl. Data Sheets, 20, No. 2 (Feb. 1977).

55. WAHLGREN, M.A. and MEINKE, Phys. Rev. 118 (1960) p. 181.

56. FUNK, E.G. et al Bull. Am. Phys. Soc. 6 (1961) p. 428.

57. KISTNER, O.C. and SUNYAR, A.W. Bull. Am. Phys. Soc. 7 (1962) p. 342.

58. KISTNER, O.C. and SUNYAR, A.W. Phys. Rev. 143 No. 3 (March 1966) p. 918-922.

59. HARBOTTLE, G. Radiochem. Acta. 13 (1970) p. 132-138.

60. HAMILTON, J.H. et al Nucl. Phys. A172 (1971) p. 139.

61. KRACIKOVA, T.I. and KRACIK, B. Czech. J. Phys. 18B (1968) p. 143.

62. ROSE, M.E. Internal Conversion Coefficients (North-Holland Publishing Company, Amsterdam, 1958).

63. ESTULIN, I.V. Soviet J. Nucl. Phys. 4 (1967) p. 16-19.

64. ROCHESTER, C.K. and SMITH, K.G. Phys. Lett. 8 (1964) p. 266.

65. BRIENT, C.E. et al Phys. Rev. C6 (1972) p. 1837-1847.

66. BERTRAND, F.E. Nucl. Data Sheets 7 No. 1 (January 1972) p. 33.

67. FREVERT, L. Z. Physik 169 (1962) p. 456.

68. FREVERT, L. et al Z. Physik 182 (1965) p. 439.

69. PERLMAN, M.L. et al Phys. Rev. 92 (1953) p. 1236-1240.

70. JOHNSON, N.D. and HAMILTON, J.H. Z. Physik 243 (1971) p. 395-401.

71. OKANO, K. et al Nucl. Phys. A164 (1971) p. 545-551.

72. TAYLOR, H.W. and EASTWOOD, T.A. Can. J. Phys. 42 (1964) p. 2173.

73. MILNER, W.T. et al Nucl. Phys. A129 (1969) p. 687.

74. BREITIG, D. et al in Neutron Capture Gamma-Ray Spectroscopy, Petten, Netherlands (September 1974) p. 549-551.

75. SCHULT, O.W.B. Institut fur Kernphysik, KFA-Julich, private communication.

76. BOLEY, F.I. Phys. Rev. 94 (1954) p. 1078.

77. MARAGUES, J.A. et al Nucl. Phys. A99 (1967) p. 652.

78. VAN HISE, J.R. et al Phys. Rev. C1 (1970) p. 1861-1865.

79. NEWBOLT, W.B. and HAMILTON, J.H. Nucl. Phys. 53 (1964) p. 353.

80. BERTRAND, F.E. and RAMAN, S. Nucl. Data Sheets 5 No. 5 (May 1971).

81. HOREN, D.J. et al Nuclear Level Schemes A=45 through A=257 from Nucl. Data Sheets (Academic Press, New York and London, 1973).

82. KRACIKOVA, T.I. and KRACIK, B. Czech. J. Phys. 17B (1967) p. 483.

83. BRAHMAVAR, S.M. et al Nucl. Phys. A125 (1969) p. 217.

84. KRACIKOVA, T.I. Czech. J. Phys. B20 (1970) p. 1138-1148.

85. PHILLIPS, G.B. et al Nucl. Phys. A182 (1972) p. 606-618.

86. AUBLE, R.L. et al Phys. Rev. C6 (1972) p. 2223-2231.

87. WINKLER, P. ZfK-126 (1967).

88. GROSHEV, L.V., BARTHOLOMEW, G.A. et al Nucl. Data Tables A5, 1 (1968).

89. PRATT, W.W. J. Inorg. Nucl. Chem. 36 (1974) p. 1199-1200.

90. HAGER, R.S. and SELTZER, E.C. Internal Conversion Tables, Nucl. Data A4 (1968) Nos. 1 and 2.

91. YUSOF-SULAIMAN and THOMAS, R.N. private communication.

92. LAVI, N. Nucl. Instr. and Meth. 107 (1973) p. 197-198.

93. LEGRAND, J. and BOULANGER, J. Compt. Rend. 265 (1967) B 697.

94. KRANE, K.S. and STEFFEN, R.M. Phys. Rev. C2 (1970) p. 724.

95. SUNYAR, A.W. et al Bull. Am. Phys. Soc. 16 (1971) p. 642.

96. SARANTILES, D.G. Nucl. Phys. A142 (1970) p. 649.

97. WILLIAMS, J.G. and LINDSTROM, D.G. ULRC Experiment No. 51 (May 1973).

98. BURHOLT, G.D. ULRC Experiment No. 59 (March 1976).

99. ANTMAN, S.D.W. et al Nucl. Instr. and Meth. 40 (1966) p. 272.

100. BILGER, H.R. Phys. Rev. 163 (1967) p.238.

101. SHOFFNER, B.M. An Analog Signal Processor for Compton Suppression (The Second ISPRA Nuclear Electronics Symposium, Stresa, Italy, May 1975).

102. CAMP, D.C. and VAN HISE, J.R. Phys. Rev. C14 (1976) p. 261-263.

103. SEYFARTH, H. et al Nucl. Instr. and Meth. 105 (1972) p. 301-310.

104. WHITE, D.H. and HOWE, R.E. Nucl. Phys. A187 (1972) p. 12-20.

105. KAMP, A.M.F. OP DEN and SPITS. Nucl. Phys. A180 (1972) p. 569-586.

106. OTTMAR, H. et al Nucl. Phys. A164 (1971) p. 69-96.

107. HATTORI, T. et al Journal of the Physical Society of Japan 41 No. 6, Dec 1976, p. 1830-1842.

108. GUJRATHI, S.C. et al Can. J. Phys. 49 (1972) p. 747-755.

109. KANE, W.R. and SCHARFF-GOLDHABER, G. Phys. Rev. C2 (1970) p. 314-319.

110. SPITS, A.M.J. et al Nucl. Phys. A145 (1970) p. 449.

111. SPILLING, S. et al Nucl. Phys. A113 (1968) p. 395-411.

112. ALVAR, K.R. Nuclear Data Sheets 13 No. 3 (Nov 1974).

113. KOCHER, D.C. Nuclear Data Sheets 17 No. 4 (Apr 1976).

114. HOREN, D.J. and LEWIS, M.B. Nuclear Data Sheets 16 No. 1 (Sept 1975).

115. ESTULIN, I.V. et al Soviet Physics JETP, 16 No. 4 (April 1963) p. 978-982.

116. BONDARENKO, V.A. et al Bull. Acad. Sci. USSR, Phys. Ser. 36 (1972) p. 561.

117. BAUER, G. and SEYFARTH, H. Atomkernenergie, 18 (1971) p. 236.

118. DELANG, W. et al Nucl. Instr. and Meth. 99 (1972) p. 13-17.

119. SEYFARTH, H. private communication.

120. BOLOTIN, H.H. and NAMENSON, A.I. Phys. Rev. 157 (1967) p. 1131-1136.

121. ESTULIN, I.V., KALINKIN, L.F. and MELIORANSKII, A.S. Soviet Phys.-JETP 16 (1963) p. 978.

122. ESTULIN, I.V. et al Soviet J. Nucl. Phys. 5 (1967) p. 819.

123. COHEN, B.L. Phys. Rev. 127 (1962) p. 127.

124. BARTHOLOMEW, G.A. and KINSEY, B.B. Can. J. Phys. 31 (1953) p. 1025.

125. GROSHEV, L.V. et al Atlas of Thermal Neutron Capture Gamma Rays, translated by J.B. Sykes (Pergamon Press, Inc., New York, 1959) p. 115.

126. MATTAUCH, J.H.E., THIELE, W. and WAPSTRA, A.H. Nucl. Phys. 67 (1965) p. 32.

127. WAPSTRA, A.H. and GOVE, N.B. Nucl Data Tables 9 (1971) p. 403.

128. KATOH, T. and YOSHIZAWA, Y. Nucl. Phys. 32 (1962) p.5.

129. CUSSENS, C.J. et al J. Phys. A (London) 2 (1969) p. 658.

130. LOBNER, K.E.G. in The Electromagnetic Interaction in Nuclear Spectroscopy (Ed. Hamilton, North-Holland 1975) p. 141-169.

131. ELZE, Th.W. et al Z. Phys. 209 (1968) p. 497.

132. TALMI, Y. Phys. Rev. 126 (1962) p. 2116.

133. LOPEZ, M.E. de. see reference 65.

134. MUGHABGHAB, S.F. and GARBER, D.I. Nuetron Cross Sections, BNL 325, June 1973.

135. FREUND, H. Thesis, Technische Hochschule, Munich (1968).